

DTIC FILE COPY

1

AD-A202 760



REMOTE ORBITAL CAPTURE USING AN ORBITAL  
MANEUVERING VEHICLE EQUIPPED WITH  
A MULTIBODY GRAPPLING ARM ASSEMBLY

THESIS

F. Joseph Bishop  
Captain, USAF

AFIT/GA/AA/88D-02



DTIC  
SELECTED  
JAN 18 1989  
S D  
8 D

DISTRIBUTION STATEMENT A

Approved for public release  
Distribution Unlimited

DEPARTMENT OF THE AIR FORCE

AIR UNIVERSITY

**AIR FORCE INSTITUTE OF TECHNOLOGY**

Wright-Patterson Air Force Base, Ohio

89 1 17 01

AFIT/GA/AA/88D-02

(1)

DTIC  
S E L E C T  
JAN 18 1989  
S & D  
D

REMOTE ORBITAL CAPTURE USING AN ORBITAL  
MANEUVERING VEHICLE EQUIPPED WITH  
A MULTIBODY GRAPPLING ARM ASSEMBLY

THESIS

F. Joseph Bishop  
Captain, USAF

AFIT/GA/AA/88D-02



ACCESSION FOR	J
NTIS	00000
DTIC	00000
UNCLASSIFIED	00000
DATE	00000
BY	00000
DATA	00000
DOC	00000
UNIT	00000
A-1	

Approved for public release; distribution unlimited

**REMOTE ORBITAL CAPTURE USING AN ORBITAL  
MANEUVERING VEHICLE EQUIPPED WITH  
A MULTIBODY GRAPPLING ARM ASSEMBLY**

**THESIS**

Presented to the Faculty of the School of Engineering  
of the Air Force Institute of Technology  
Air University  
In Partial Fulfillment of the  
Requirements for the Degree of  
Master of Science in Astronautical Engineering

**F. Joseph Bishop, M.S.  
Captain, USAF**

**December 1988**

**Approved for public release; distribution unlimited**

### Preface

The purpose of this study was to develop a computer model of the dynamics and controls for a robot spacecraft used to capture a tumbling and spinning satellite. The robot spacecraft is to detumble and despin the other spacecraft so it can be repaired and returned to useful service. I would like to acknowledge the help of Lt Col Joseph W. Widhalm in getting me started on this endeavor, which was a follow-on to his previous work. I would also like to acknowledge the help of Dr. Curtis H. Spenny who later filled in as my thesis advisor after Lt Col Widhalm's departure in July of this year.

## Table of Contents

	Page
Preface	ii
List of Figures	iv
List of Tables	viii
Notation	ix
Abstract	xi
1. Introduction	1
2. Problem Formulation	4
System Configuration	4
Body 2 Requirements	12
The Hooker-Margulies Equations	13
Application of the Hooker-Margulies Equations	15
3. Control Laws	21
Deployment Phase	24
Spin-Up Phase	27
Nonlinear Feedback Control - Detumble/Despin Phase	27
4. Results	32
Docking Configuration	34
Deployment Phase	35
Case 1 - Deployment Without External Thrusters	39
Case 2 - Nominal Deployment	41
Case 3 - Deployment Without Body 2 Compensation	41
Spin-up Phase	42
Case 4 - Nominal Spin-up	42
Detumble/Despin Phase	43
Case 5 - With Widhalm/Conway Gain Settings	45
Case 6 - Reduced Grappling Arm Length	47
Case 7 - Increased Target Coning Angle	48
Case 8 - Decreased Target Coning Angle	48
Case 9 - Nominal Detumble/Despin	49
5. Conclusion	146
6. Recommendations	148
References	149
Vita	150

### List of Figures

	Page
1. The Widhalm and Conway Model for the Two-Body System	2
2. The Five-Body OMV Model With Grappling Arm Assembly	5
3. The Five-Body OMV Model Docked with Target	8
4. The Five-Body Satellite/Target System in Spin-Stabilized State of Equilibrium	11
5. Docking Configuration	37
 <b>Deployment Phase / Case 1</b>	
6. Joint 1 Position	52
7. Joint 1 Relative Velocity	53
8. Joint 1 Relative Acceleration	54
9. Body 1 $\gamma_1$ History	55
10. Body 1 $\dot{\gamma}_1$ History	56
11. Body 2 $\gamma_2$ History	57
12. Body 2 $\dot{\gamma}_2$ History	58
13. Internal Motor Torque TG1	59
14. Internal Motor Torque TG2	60
15. Internal Motor Torque TG3	61
16. Internal Motor Torque TG4	62
17. Internal Motor Torque TG5	63
18. Internal Motor Torque TG6	64
19. Constraint Torque at Joint 1	65
20. Constraint Torque at Joint 2	66
21. Constraint Torque at Joint 3	67
22. Body 0 $\omega_{03}$	68
23. Angular Momentum Component HX	69
24. Angular Momentum Component HY	70
25. Angular Momentum Component HZ	71
26. Total System Angular Momentum	72
27. Vertical Translation of OMV	73

<b>Deployment Phase / Case 2</b>	
28. Body 0 $\omega_0$ History	74
29. External Torque T1	75
30. External Torque T2	76
31. External Torque T3	77
<b>Deployment Phase / Case 3</b>	
32. External Torque T1	78
33. External Torque T2	79
34. External Torque T3	80
<b>Spin-up Phase / Case 4</b>	
35. Body 3 $\dot{\gamma}_s$ History	81
36. Body 4 $\dot{\gamma}_s$ History	82
37. Internal Motor Torque TG5	83
38. Internal Motor Torque TG6	84
39. Angular Momentum Component HX	85
40. Angular Momentum Component HY	86
41. Angular Momentum Component HZ	87
42. Total System Angular Momentum	88
<b>Detumble/Despin Phase / Case 5</b>	
43. Body 1 $\gamma_s$ History	89
44. Body 1 $\dot{\gamma}_s$ History	90
45. Body 2 $\gamma_s$ History	91
46. Body 2 $\dot{\gamma}_s$ History	92
47. Body 3/4 $\gamma_s$ History	93
48. Body 3/4 $\dot{\gamma}_s$ History	94
49. Body 3 $\dot{\gamma}_s$ History	95
50. Body 4 $\dot{\gamma}_s$ History	96
51. Joint 1 Position	97
52. Joint 1 Relative Velocity	98
53. Joint 1 Relative Acceleration	99

54.	<b>External Torque T1</b>	100
55.	<b>External Torque T2</b>	101
56.	<b>External Torque T3</b>	102
57.	<b>Internal Motor Torque TG1</b>	103
58.	<b>Internal Motor Torque TG2</b>	104
59.	<b>Internal Motor Torque TG3</b>	105
60.	<b>Internal Motor Torque TG4</b>	106
61.	<b>Internal Motor Torque TG5</b>	107
62.	<b>Internal Motor Torque TG6</b>	108
63.	<b>Constraint Torque at Joint 1</b>	109
64.	<b>Constraint Torque at Joint 2</b>	110
65.	<b>Constraint Torque at Joint 3</b>	111
66.	<b>Joint 1 Constraint Force in Y-Direction</b>	112
 <b>Detumble/Despin Phase / Case 6</b>		
67.	<b>External Torque T1</b>	113
68.	<b>Internal Motor Torque TG1</b>	114
69.	<b>Internal Motor Torque TG4</b>	115
 <b>Detumble/Despin Phase / Case 7</b>		
70.	<b>External Torque T1</b>	116
71.	<b>Internal Motor Torque TG1</b>	117
72.	<b>Internal Motor Torque TG4</b>	118
 <b>Detumble/Despin Phase / Case 8</b>		
73.	<b>External Torque T1</b>	119
74.	<b>Internal Motor Torque TG1</b>	120
75.	<b>Internal Motor Torque TG4</b>	121
 <b>Detumble/Despin Phase / Case 9</b>		
76.	<b>Body 1 <math>\gamma</math>, History</b>	122
77.	<b>Body 1 <math>\dot{\gamma}</math>, History</b>	123
78.	<b>Body 2 <math>\gamma</math>, History</b>	124
79.	<b>Body 2 <math>\dot{\gamma}</math>, History</b>	125

80.	<b>Body 3/4 <math>\gamma</math>, History</b>	126
81.	<b>Body 3/4 <math>\dot{\gamma}</math>, History</b>	127
82.	<b>Body 3 <math>\gamma</math>, History</b>	128
83.	<b>Body 4 <math>\gamma</math>, History</b>	129
84.	<b>Joint 1 Position</b>	130
85.	<b>Joint 1 Relative Velocity</b>	131
86.	<b>Joint 1 Relative Acceleration</b>	132
87.	<b>External Torque T1</b>	133
88.	<b>External Torque T2</b>	134
89.	<b>External Torque T3</b>	135
90.	<b>Internal Motor Torque TG1</b>	136
91.	<b>Internal Motor Torque TG2</b>	137
92.	<b>Internal Motor Torque TG3</b>	138
93.	<b>Internal Motor Torque TG4</b>	139
94.	<b>Internal Motor Torque TG5</b>	140
95.	<b>Internal Motor Torque TG6</b>	141
96.	<b>Constraint Torque at Joint 1</b>	142
97.	<b>Constraint Torque at Joint 2</b>	143
98.	<b>Constraint Torque at Joint 3</b>	144
99.	<b>Joint 1 Constraint Force in Y-Direction</b>	145

List of Tables

	Page
I. Nominal Mass Properties	33
II. Nominal Dimensions (Constants)	34
III. Nominal Target	35
IV. Deployment Phase Initial Conditions	38
V. Detumble/Despin Phase Initial Conditions	44
VI. Effect of Decay Rate on Final Equilibrium Position	50

### Notation

Symbol	Definition
$\hat{e}_1, \hat{e}_2, \hat{e}_3$	= unit vector set arbitrarily fixed at the center of mass of Body 0 (OMV) and aligned with its principal axes
$F_\lambda^1$	= nongravitational external force on body $\lambda$
$F_{\lambda j}^H$	= interaction force on body $\lambda$ transmitted through joint $j$
$\hat{g}_i$	= unit vectors representing the axes at the joints of an n-body system about which rotation is possible
$i, j, k$	= unit vector set representing inertial planetocentric coordinate system
$J_\lambda$	= set of joints on body $\lambda$
$L_{\lambda\mu}$	= vector from the center of mass of body $\lambda$ to the joint on body $\lambda$ leading to a body $\mu$
$m$	= total mass of the n-body system
$m_\lambda$	= mass of a component body $\lambda$
$n$	= number of bodies in the multibody system
$\hat{n}_1, \hat{n}_2, \hat{n}_3$	= unit vector set arbitrarily fixed at the center of mass of the target satellite and aligned with its principal axes
$r$	= number of rotational degrees of freedom in the n-body system
$r_\lambda$	= vector from the system center of mass to the center of mass of body $\lambda$
$T_\lambda^1$	= nongravitational external torque on body $\lambda$
$T_{\lambda j}^C$	= constraint torque on body $\lambda$ at joint $j$
$T_{\lambda j}^{SD}$	= spring damper torque on body $\lambda$ at joint $j$
$t$	= time
$u$	= nine-element control vector

$\bar{x}$	=	nine-element state vector
$\bar{x}_{13}^*$	=	augmented thirteen-element state vector
$\bar{Y}$	=	three-element joint translational vector
$l$	=	unit dyadic
$\gamma$	=	planet's gravitational constant
$y_t$	=	angle of rotation about axis $\theta_t$
$y_\lambda$	=	coning angle of the target satellite
$\bar{\rho}$	=	planetocentric position vector of n-body system center of mass
$\hat{\rho}$	=	unit vector in the direction of $\bar{\rho}$
$\bar{\rho}_\lambda$	=	planetocentric position vector to the center of mass of body $\lambda$
$\phi_\lambda$	=	inertia dyadic of body $\lambda$
$\dot{\phi}_t$	=	pure spin rate of target satellite
$\dot{\psi}_t$	=	precession rate of the target satellite
$\bar{\omega}_0$	=	angular velocity of body 0
$\bar{\omega}_\lambda$	=	angular velocity of body $\lambda$

Abstract

The problem of detumbling and despinning a freely spinning and precessing axisymmetric target satellite using an orbital maneuvering vehicle is considered. The axisymmetric orbital maneuvering vehicle is equipped with a multibody grappling arm assembly to capture the target. Counter-masses are used to maintain dynamic balancing and stability throughout the deployment of the arm and the subsequent spin-up of the grappling device prior to docking. The five-body system is modeled using Eulerian-based equations of motion developed by Hooker and Margulies. Open-loop control laws are formulated to deploy the grappling arm assembly and spin-up the grappling device using internal motor torques. A Liapunov technique is applied to derive a nonlinear feedback control law that drives the docked system to a final spin-stabilized state of equilibrium. External thrusters are used to maintain the absolute motion of the system during this process. Variations in grappling arm length, target coning angle, and response times are examined for design purposes. State and control histories are presented and the results from this five-body model are compared with the Widhalm and Conway two-body study. The simulation indicates that the required control magnitudes are higher for the five-body model but are still quite reasonable. The addition of the grappling arm assembly adds both realism and flexibility to the capture problem.

REMOTE ORBITAL CAPTURE USING AN ORBITAL MANEUVERING VEHICLE  
EQUIPPED WITH A MULTIBODY GRAPPLING ARM ASSEMBLY

I. Introduction

The servicing and repair of satellites in orbits beyond the direct reach of the Space Shuttle requires a teleoperator spacecraft or orbital maneuvering vehicle (OMV) to dock with these target satellites and, if necessary, return them to an accessible orbit. If the target has experienced a control system failure, it may be necessary to detumble it. If the target satellite is spin stabilized it may be necessary to despin it. Docking followed by despining or detumbling is defined here as remote orbital capture.

Previous work by Widhalm and Conway (9) considered both the detumbling and despining aspects of remote orbital capture, and the requirement to control the absolute motion of the two-body system using feedback control. In their model (Fig. 1), an axisymmetric OMV was docked with a freely spinning and precessing axisymmetric target. The OMV was equipped with a two rotational degree of freedom joint that connected with a fixed appendage on the target body. This joint was free to translate along the surface of the OMV to provide positioning adjustments during docking. Despining and detumbling were accomplished using feedback control by driving the joint to the OMV's axis of symmetry and applying internal motor torques to the target through the connecting joint. While this was being done, the OMV external thrusters were fired to control the absolute motion of the two-body system. It was shown that this "detumbling process is quite benign and that the required control magnitudes are small" (9:657).

One key assumption made in the Widhalm and Conway model was that the target had a fixed appendage that the OMV's joint connected with to form the two-body docked configuration. In reality, however, a target satellite would probably not have this convenient appendage to serve as a docking point. What would really be required is for the OMV to be equipped with a grappling arm assembly which it could deploy to capture and detumble the target satellite.

This thesis extends the Widhalm and Conway two-body model by taking into account the requirement for a grappling arm assembly attached to the OMV. The new model consists of five constant mass rigid bodies. Simulation of the capture process now

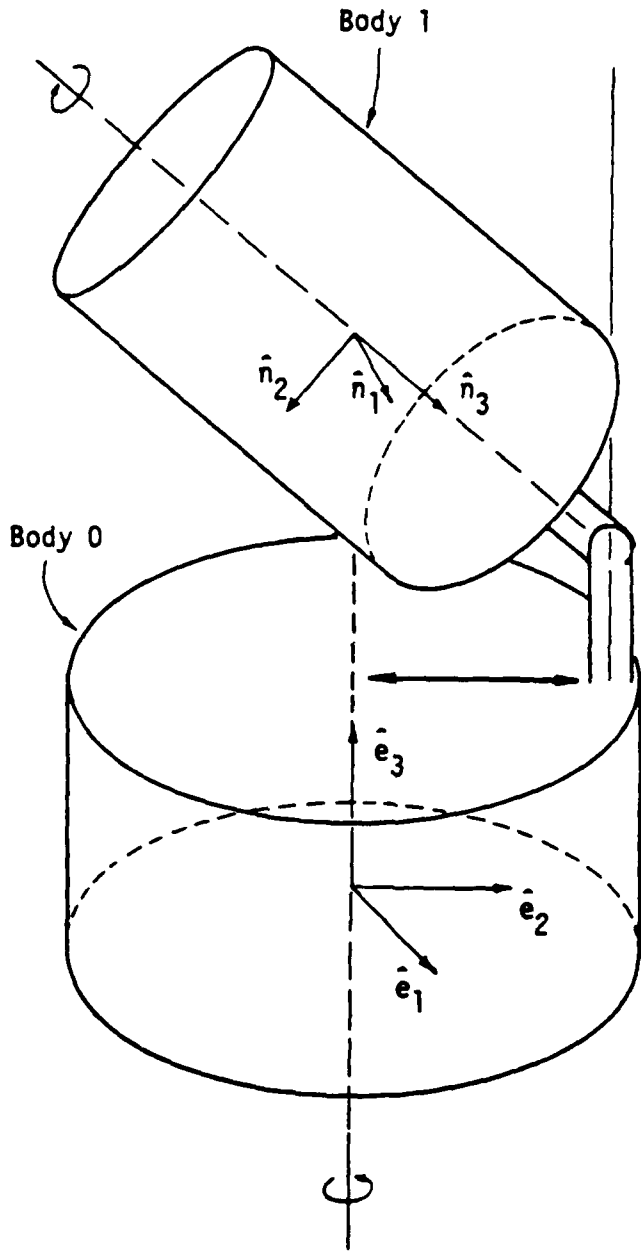


Fig 1. The Widhalm and Conway Model for the Two-Body System

becomes a three step rather than a single step process. The first step is the deployment of the grappling arm assembly up to but not including docking with the target vehicle. The deployment of the grappling arm significantly alters the dynamics of the system, and one important aspect of the problem is to maintain dynamic balancing and stability throughout the process. The second step is the spin-up of the grappling device to match the pure spin rate of the target , just prior to docking. The actual docking process itself is not treated in this thesis, and is handled as a discrete event. The final step once the target satellite is joined with the OMV is to apply the required internal motor torques and OMV thruster firings using feedback control to detumble and despin the target and drive the entire system to a spin-stabilized state of equilibrium.

Both the system initial configuration and the desired final state are defined. The applicable equations of motion for the five body system are then derived, and the required control laws are formulated for each of the three steps in the capture process. The results of the simulation show the magnitude of both the internal and external control torques required to achieve the desired outcome. This information would be necessary in eventual hardware design for sizing motors and thrusters, and in performing structural analysis of the system.

## II. Problem Formulation

### **System Configuration**

The OMV model for this thesis consists of five rigid bodies as depicted in Fig. 2. These five bodies are; the original axisymmetric reference or base body used in the Widhalm and Conway model, the grappling arm, the counter-mass, and the grappling device with its corresponding counter-mass. The  $e_1, e_2, e_3$  coordinate system used here is a rotating system fixed at the center of mass of Body 0, not at the center of mass of the system. The  $e_2$  axis is aligned along the direction of the translating joint and the the grappling arm assembly, and the  $e_3$  axis is the axis of symmetry for the reference body. There is no specified coordinate system fixed at the center of mass of the system and all equations are eventually expressed in the  $e_1, e_2, e_3$  system.

Body 0, the reference or base body, has angular velocity components  $w_{01}, w_{02}, w_{03}$  corresponding to its three principal axes,  $e_1, e_2, e_3$ . Also, Body 0 contains the three external variable control thrusters. The three external control torques generated ,  $T_1, T_2, T_3$ , again correspond to the  $e_1, e_2, e_3$  principal axes. To simplify the problem, it is assumed that firing the thrusters does not affect the mass properties of the OMV and the entire model is assumed to be a constant mass system.

There are six additional rotational degrees of freedom for the overall OMV system, specified by their respective axes of rotation,  $g_1, g_2, g_3, g_4, g_5, g_6$ , for a total of nine rotational degrees of freedom. The amount of rotation about each axis is specified by  $\gamma_1, \gamma_2, \gamma_3, \gamma_4, \gamma_5, \gamma_6$ , respectively. There are also six internal motor torques,  $TG_1, TG_2, TG_3, TG_4, TG_5, TG_6$  , again corresponding to the six axes of rotation.

Body 1 is connected to the reference body by Joint 1 which is the same type of translating joint used in the Widhalm and Conway model. Joint 1 has two rotational degrees of freedom, one about  $g_1$  which is parallel to the  $e_1$  axis, and one about  $g_2$  which is aligned with the grappling arm. The amount of rotation of Body 1 relative to Body 0 in the positive  $e_1$  direction is measured by the angle  $\gamma_1$ . Body 1 is the grappling arm itself, and does not include the two end masses, Body 3 and Body 4, which represent the

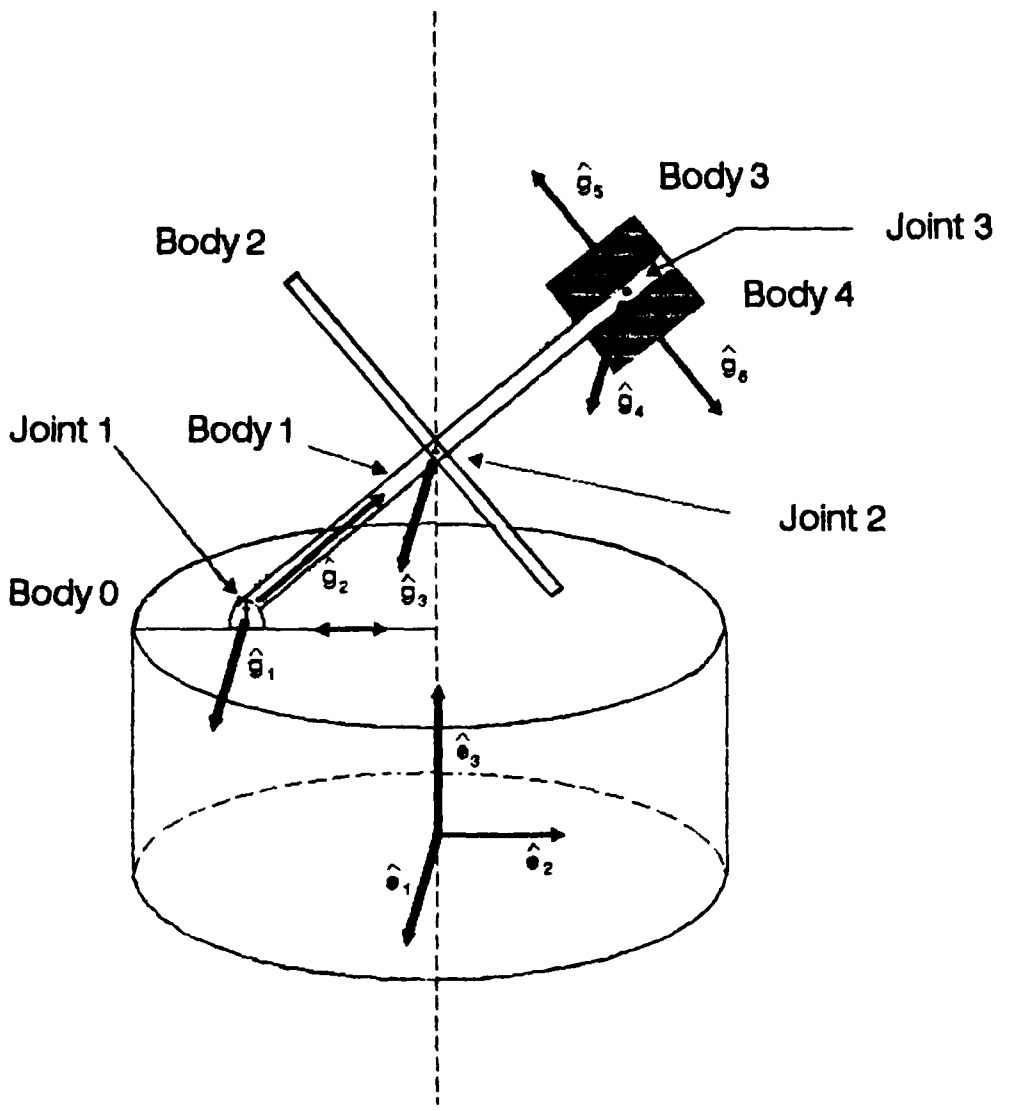


Fig 2. The Five-Body OMV Model With Grappling Arm Assembly

grappling device assembly. However, Body 1 does include the mass of the translating joint assembly, Joint 1.

Body 2 is the counter-mass which is designed to balance out the combined effects of Body 1, Body 3, and Body 4 so that no cross products of inertia terms are generated during the deployment phase. Body 2 is connected to Body 1 with Joint 2. Its only degree of freedom is about the  $g_3$  axis which is parallel to the  $e_1$  axis. The amount of this rotation relative to Body 1 is measured by  $\gamma_3$  and is in the negative  $e_1$  direction.

Body 3 is the grappling device. Note that it is not the scope of this thesis to design or specify an actual hardware device. Body 3 is merely a mathematical representation of the grappling device. Similarly, the actual docking process is not part of this simulation, and is merely a discrete event. The system is still undocked at the end of the deployment and spin-up phases and already docked at the start of the detumble/despin phase.

Body 4 is another counter-mass with exactly the same mass and inertia properties as Body 3. Its purpose is to spin at an equal but opposite rate as Body 3 during the spin-up phase. This will cancel out the moment created by spinning up Body 3.

Body 3 and Body 4 are both attached to Body 1 by Joint 3 which must allow for three rotational degrees of freedom. It allows Body 3 and Body 4 to rotate as one body about the  $g_4$  axis which is parallel to the  $e_1$  axis. The amount of this rotation is measured by the angle  $\gamma_4$  and the direction is in the negative  $e_1$  direction. Note that  $\gamma_4$  is defined to be in the  $0^\circ$  position when the  $g_5$  and  $g_6$  axes are perpendicular to Body 1, as shown in Fig. 2. In addition there is the spin rotation of Body 3 about the  $g_5$  axis, and the spin rotation of Body 4 about the  $g_6$  axis. Note that  $g_5$  and  $g_6$  are the same axis, with the spin of Body 3 in the positive direction and the spin of Body 4 in the negative direction. Note also that Body 3 and Body 4 have axisymmetric inertia properties with their axis of symmetry being this  $g_5/g_6$  axis.

In the initial configuration prior to deployment of the arm, the OMV is positioned relative to the target satellite such that the OMV's axis of symmetry,  $e_3$ , is parallel to the target's angular momentum vector. The target satellite is both tumbling and spinning, where

$$\gamma_T, \psi_T, \phi_T$$

correspond to the target's coning angle, precession rate, and spin rate (about its  $n_3$  axis), respectively. These three properties are related as shown by Greenwood (5:386) and repeated here:

$$\dot{\phi}_T = \left( \frac{I_{zz} - I_{xx}}{I_{zz}} \right) \dot{\psi}_T \cos \gamma_T \quad (1)$$

where  $I_{xx}$  is the target's moment of inertia about the  $n_1$  and  $n_2$  axes, and  $I_{zz}$  is the target's moment of inertia about its axis of symmetry,  $n_3$ . The OMV is positioned such that the target's center of mass is lined up on the OMV's  $e_3$  axis. The OMV is spun-up so that its angular velocity component  $w_{03}$  about the  $e_3$  axis exactly matches the target's precession rate, while the  $w_{01}$  and  $w_{02}$  components remain zero. The OMV is therefore in a state of pure spin. Besides the target's pure spin rate, the OMV and the target will have zero relative motion. The OMV is also positioned at a pre-determined stand-off distance from the target, such that when Joint 1 translates a specified amount in the  $e_2$  direction and the grappling arm is raised by a corresponding angle  $\gamma_1$ , the grappling device will be able to successfully dock with the target as shown in Fig. 3. This stand-off distance depends on the target's length and coning angle, the length of the grappling arm, and the allowable amount of joint translation. It is assumed that the complete initial state of the target has been accurately determined by the OMV's computer, that the OMV has been properly placed into the required position, and has already been spun-up to match the target's precession rate. It is with this initial configuration that this thesis begins.

The first phase of the simulation is the deployment of the grappling arm assembly. In the initial state Bodies 1, 2, 3, and 4 are stored horizontally on the surface of the OMV so that  $\gamma_1$ ,  $\gamma_3$ ,  $\gamma_4$  are all zero. Joint 1 is commanded to begin translating in the  $e_2$  direction toward the  $e_3$  axis of symmetry, and internal motor torques are applied to begin erecting the grappling arm assembly. It is the intent of this thesis to perform the entire deployment process and still maintain the OMV in a state of pure spin at the constant initial rate with a minimum application of external control torques, if any. It is desired not to fire these external thrusters unless absolutely necessary in order to conserve the attitude maneuvering fuel.

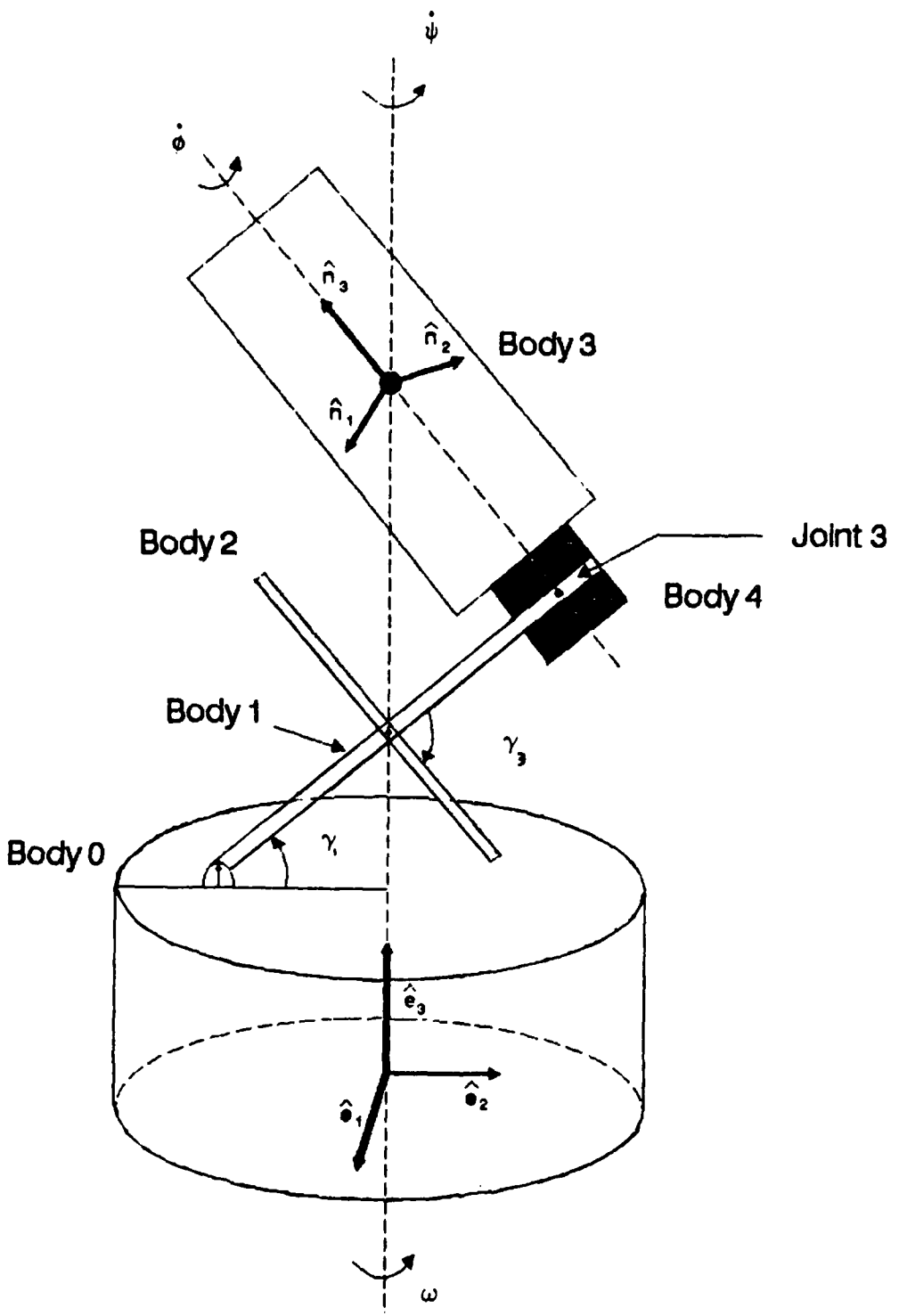


Fig. 3. The Five-Body OMV Model Docked with Target

It is therefore critical in order to maintain dynamic balancing and stability, that; 1) the combined center of mass of Bodies 1, 2, 3, and 4 always lies on the  $e_3$  axis, and 2) the inertia properties of the counter-mass Body 2 are such that, when combined with the inertia properties of Bodies 1, 3, and 4, the  $e_3$  axis is always the axis of symmetry for all five bodies so no cross products of inertia terms are generated. To solve this problem, the mass properties of Body 1, Body 3, and Body 4 must be such that the total mass center of these three masses is at Joint 2 , which is located at the geometric center of the grappling arm and is also the center of mass of Body 2. Therefore, the combined center of mass of Bodies 1, 2, 3, and 4 is located at Joint 2 and the control problem now is to maintain Joint 2 always along the  $e_3$  axis during the deployment process. This is achieved with the use of an open-loop control algorithm and the application of internal motor torques. It is also desired to lock the rotations about  $g_2$ ,  $g_4$ ,  $g_5$ , and  $g_6$  fixed during this process, since they are not required. As for the cross product of inertia problem, Body 2 should maintain a constant relationship with Body 1 such that  $\gamma_3$  is always exactly twice as much as  $\gamma_1$ , but in the opposite direction. Again, this is handled with the appropriate open-loop algorithm and the application of the required internal motor torques.

Throughout this process if the thrusters are not fired the OMV's system mass center will not move in inertial space since no external forces or torques are being applied. However, the system mass center will be moving "upward" relative to the OMV's base and so the center of mass of the OMV's base, the reference Body 0, will translate "downward" in inertial space along the vertical  $e_3$  axis. The reference body's position relative to the target will therefore be changing during the process. Although this translation can easily be calculated, it will be assumed for the purposes of this thesis that the OMV has a separate control system that will compensate for it by applying the appropriate translational thrusters, thereby maintaining zero relative motion between the base of the OMV and the target.

The arm will be deployed up to but not including docking. Body 3 will then be assumed to be at an infinitely small distance away from the target. In reality, this would probably be the best opportunity to measure the spin rate of the target accurately using a sensor on Body 3. At this point the second phase of the simulation begins. Body 3 will be spun-up, from rest, to the same rate as the pre-determined spin rate of the target. At

the same time, Body 4 will be spun-up at an equal and opposite rate , cancelling out the moment created by Body 3, in order to maintain dynamic balance and stability. Body 3 will now have zero relative velocity in relation to the target, and will be ready to grab hold of it. Prior to docking, the entire OMV system should be in a state of pure spin about the  $e_3$  axis without the application of the external thrusters.

The third and final phase of the simulation begins immediately after docking with the target. After this discrete event, the total system is still treated as a five-body problem by simply adding the mass and inertia properties of the target to Body 3, and treating the target and grappling device as one single body (still labeled Body 3 - See Figs. 2 and 3). The closed-loop feedback system is now turned on, and both internal motor torques and external thruster torques are applied to drive the system to the final desired state. This final state is that in which Joint 1 is centered at the  $e_3$  axis,  $\gamma_1 = 90^\circ$  ,  $\gamma_3 = 180^\circ$  , and  $\gamma_4 = 90^\circ$  so that Body 1, Body 2, Body 3 (including the target), and Body 4 are all in the vertical position, as shown in Fig. 4 and the entire system is in a spin-stabilized state of equilibrium.

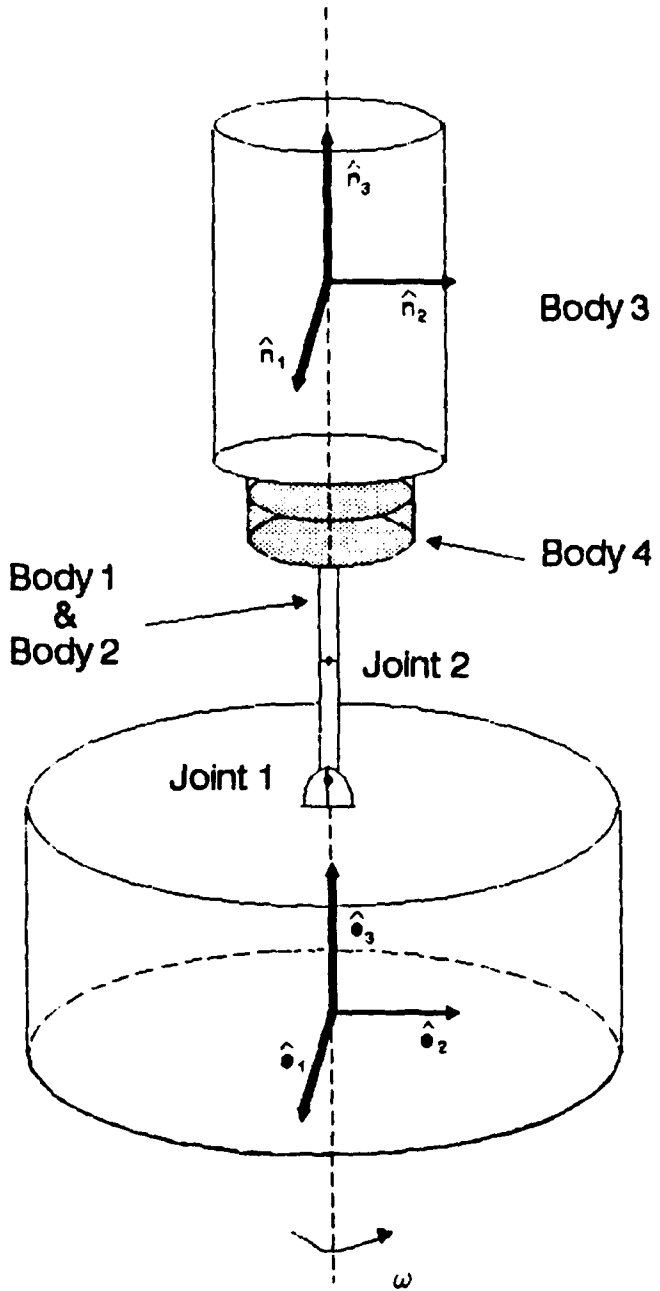


Fig. 4. The Five-Body OMV /Target System in Spin-Stabilized State of Equilibrium

## Body 2 Requirements

As discussed in the previous section, Body 2 with its center of mass at Joint 2 must have the equivalent inertia properties as Body 1, Body 3, and Body 4 with their combined mass center also at Joint 2. Body 2's inertia requirements can be determined by a simple application of the parallel axis theorem.

$$\begin{aligned} I_{xx}(2) &= I_{xx}(1) + m_1(L_{12})^2 + \\ &I_{xx}(3) + m_3[(L_{13} - L_{12})^2 + (L_{31})^2] + \\ &I_{xx}(4) + m_4[(L_{14} - L_{12})^2 + (L_{41})^2] \end{aligned} \quad (2)$$

$$\begin{aligned} I_{yy}(2) &= I_{yy}(1) + I_{yy}(3) + m_3(L_{31})^2 + \\ &I_{yy}(4) + m_4(L_{41})^2 \end{aligned} \quad (3)$$

$$\begin{aligned} I_{zz}(2) &= I_{zz}(1) + m_1(L_{12})^2 + \\ &I_{zz}(3) + m_3(L_{13} - L_{12})^2 + \\ &I_{zz}(4) + m_4(L_{14} - L_{12})^2 \end{aligned} \quad (4)$$

$I_{xx}$  (i),  $I_{yy}$  (i),  $I_{zz}$  (i) refer to the principal mass moments of inertia of each body. Note that when all bodies are initially in the stored position, these principal moments of inertia are parallel to the  $e_1$ ,  $e_2$ ,  $e_3$  axes, respectively. Note that  $L_{12}$  is the length from the center of mass of Body 1 to Joint 2, and  $L_{13}$ ,  $L_{14}$  are both the length from the center of mass of Body 1 to Joint 3. Also,  $L_{31}$  is the length from the center of mass of Body 3 to Joint 3 which, prior to docking, is equal to  $L_{41}$ .

### The Hooker-Margulies Equations

The appropriate equations of motion now need to be developed to describe the five-body model. Fletcher, Rongved, and Yu (4) derived the dynamical attitude equations for a two-body satellite. Hooker and Margulies (7) then generalized these equations for an n-body satellite. They used Newton's equations to eliminate the moments of the unknown interaction forces (i.e. the moments of the reactive forces transmitted through the joints) from the Euler equations. They therefore derived a complete set of  $3n$  scalar equations for an n-body system that are free of unknown joint constraint forces but still contain the unknown constraint torques. There are, however, two restrictions placed on these equations. First of all, the topology of the overall configuration of bodies and interconnecting joints must be equivalent to a topological tree (i.e. no closed loops). Second, the relative motion about a joint is assumed to be rotational and does not allow translation of either body relative to the joint. (7:123)

Hooker (6) in a follow-on paper showed that the the constraint torques could also be eliminated. This reduces the number of dynamical attitude equations from  $3n$  to  $r$  where  $r$  is the number of rotation degrees of freedom for the system. The number of dependent variables is also reduced from the set of  $3n$  angular velocity components to 3 angular velocity components of the reference body and an additional  $r-3$  relative angular rotational rates. The original Hooker-Margulies equations are written for all the bodies lying on one side of a selected joint and subsequently added. The interaction torques all cancel in pairs with the exception of the constraint torque at the selected joint. If this particular joint has a rotational degree of freedom about an axis  $g$ , then the dot product of  $g$  and the expression for the constraint torque is zero, and so writing the dot product and setting it to zero yields an equation that is free of the constraint torque. This process can then be repeated for each degree of freedom at each joint to eliminate all the unknown constraint torques from the equations. (6:1205-1207) This subsequent set of  $r$  equations for an n-body system with  $r$  rotational degrees of freedom is called the modified Hooker-Marquilles equations.

An equivalent set of dynamical attitude equations of motion could be derived using the Lagrangian method. The Lagrange approach to deriving the equations of motion has the advantage that the constraint torques never appear, and that the number of equations

is  $r$ , the number of rotational degrees of freedom for the system. However, the resulting equations would not be written in terms of physical body axes, as are the HM and modified HM equations. As a result, it would be exceeding difficult to modify the Lagrange equations in order to adapt them to an active control system and to include the effects of joint motion. (6:1205)

One other important advantage of the modified HM equations is that they significantly reduce the amount of computer time by only having to integrate numerically  $r$  equations rather than  $3n$  equations. (6:1205)

As previously mentioned, neither the HM equations nor the modified HM equations account for translation of the joints relative to the bodies adjacent to the joint. In this thesis, as in the Widhalm and Conway model, Joint 1 connecting Body 0 and Body 1 translates relative to Body 0, the reference body. This was dealt with by Conway and Widhalm (1) with an extension of the modified HM equations that permits the translation of the joint. It is therefore this extended version of the modified HM equations that can now be applied to this thesis.

Even though the modified HM equations eliminate both the constraint forces and the constraint torques, this information may later be needed in performing a structural analysis of the system. Fortunately, it is relatively easy to recover this information as shown in references (6) and (7).

### Application of the Hooker-Margulies Equations

The dynamical attitude equations for the 5-Body OMV system ( $n=5$ ) with its 9 rotational degrees of freedom ( $r=9$ ) can be derived directly using the modified Hooker-Margulies Equations (6) extended by Widhalm and Conway (1) to take into account the translation of Joint 1 relative to Body 0.

$$\begin{bmatrix} a_{00} & a_{01} & \cdot & \cdot & \cdot & \cdot & \cdot & a_{06} \\ a_{10} & a_{11} & \cdot & \cdot & \cdot & \cdot & \cdot & \\ \cdot & & & & & & & \\ \cdot & & & & & & & \\ a_{60} & \cdot & \cdot & \cdot & \cdot & \cdot & \cdot & a_{66} \end{bmatrix} \begin{bmatrix} \dot{\omega}_0 \\ \ddot{y}_1 \\ \ddot{y}_2 \\ -\ddot{y}_3 \\ -\ddot{y}_4 \\ \ddot{y}_5 \\ -\ddot{y}_6 \end{bmatrix} =$$

$$\begin{bmatrix} E_0^+ + E_1^+ + E_2^+ + E_3^+ + E_4^+ \\ -m_1 L_{01}^- \times \bar{G} - m_2 L_{02}^- \times \bar{G} - m_3 L_{03}^- \times \bar{G} \\ -m_4 L_{04}^- \times \bar{G} + D_{10}^- \times m \bar{G} + D_{30}^- \times m \bar{G} \\ + D_{40}^- \times m \bar{G} \\ \hat{g}_1 \cdot \bar{B}_1 \\ \hat{g}_2 \cdot \bar{B}_2 \\ \hat{g}_3 \cdot \bar{B}_3 \\ \hat{g}_4 \cdot \bar{B}_4 \\ \hat{g}_5 \cdot \bar{B}_5 \\ \hat{g}_6 \cdot \bar{B}_6 \end{bmatrix} \quad (5)$$

where

$$a_{00} = \sum_{\lambda} \sum_{\mu} \Phi_{\lambda\mu} , \quad a \text{ dyadic} \quad (6)$$

$$a_{0k} = \sum_{\lambda} \sum_{\mu} \epsilon_{k\mu} \Phi_{\lambda\mu} \cdot \hat{g}_k , \quad a \text{ vector} \quad (7)$$

$$a_{i0} = \hat{g}_i \cdot \sum_{\lambda} \sum_{\mu} \epsilon_{i\lambda} \Phi_{\lambda\mu} , \quad a \text{ vector} \quad (8)$$

$$a_{ik} = \hat{g}_i \cdot \sum_{\lambda} \sum_{\mu} \epsilon_{i\lambda} \epsilon_{k\mu} \Phi_{\lambda\mu} \cdot \hat{g}_k , \quad a \text{ scalar} \quad (9)$$

and

$\epsilon_{i\mu} = 1$ , if  $g_i$  belongs to a joint anywhere on the chain

of bodies connecting  $\mu$  with the reference body

0, otherwise (e.g. if  $\mu = 0$ )

and

$$\begin{aligned}\bar{B}_1 &= \bar{E}_1^* + \bar{E}_2^* + \bar{E}_3^* + \bar{E}_4^* \\ &\quad + \bar{D}_{10} \times m\bar{G} + \bar{D}_{30} \times m\bar{G} + \bar{D}_{40} \times m\bar{G} \\ &= \bar{B}_2\end{aligned}\tag{10}$$

$$\bar{B}_3 = \bar{E}_2^* \tag{11}$$

$$\bar{B}_4 = \bar{E}_3^* + \bar{E}_4^* + \bar{D}_{30} \times m\bar{G} + \bar{D}_{40} \times m\bar{G} \tag{12}$$

$$\bar{B}_5 = \bar{E}_3^* + \bar{D}_{30} \times m\bar{G} \tag{13}$$

$$\bar{B}_6 = \bar{E}_4^* + \bar{D}_{40} \times m\bar{G} \tag{14}$$

and

$$\mathcal{G} = \mathcal{D}_{01}^R + 2\bar{\omega}_0 \times \mathcal{D}_{01}^R \quad (15)$$

$$\Phi_{\lambda\lambda} = \phi_\lambda + m_\lambda [\mathcal{D}_\lambda^2 I - \mathcal{D}_\lambda \mathcal{D}_\lambda] + \sum_{\mu \neq \lambda} m_\mu [\mathcal{D}_{\lambda\mu}^2 I - \mathcal{D}_{\lambda\mu} \mathcal{D}_{\lambda\mu}] \quad (16)$$

$$\Phi_{\lambda\mu} = -m [\mathcal{D}_{\mu\lambda} \cdot \mathcal{D}_{\lambda\mu} I - \mathcal{D}_{\mu\lambda} \mathcal{D}_{\lambda\mu}] \quad (17)$$

$$\mathcal{D}_\lambda = -\sum_{\mu \neq \lambda} m_\mu m^{-1} L_{\lambda\mu} \quad (18)$$

$$\mathcal{D}_{\lambda\mu} = \mathcal{D}_\lambda + L_{\lambda\mu} \quad (19)$$

where  $L_{\lambda\mu}$  is the vector from the mass center of a body  $\lambda$  to the joint on body  $\lambda$  leading to a body  $\mu$ ,  $m_\lambda$  and  $\phi_\lambda$  are the mass and the inertia dyadic of body  $\lambda$ , and  $m$  is the total mass of the five-body system. The actual values for the masses, lengths, and inertia properties used in the model are specified in Chapter IV.  $E_\lambda^*$  is determined from

$$E_\lambda^* = E_\lambda - \sum_\mu \Phi_{\lambda\mu} \cdot \sum_k \epsilon_{k\mu} \dot{y}_k \dot{g}_k \quad (20)$$

and  $E_\lambda$  is the vector

$$\begin{aligned}
 E_\lambda = & 3\gamma\bar{\rho}^{-3}\hat{\rho}\times\phi_{\lambda\lambda}\cdot\hat{\rho} - \bar{\omega}_\lambda\times\phi_{\lambda\lambda}\cdot\bar{\omega}_\lambda + T_\lambda^1 + \sum_{j\in J_\lambda} T_{\lambda j}^{SD} \\
 & + D_\lambda\times F_\lambda^1 + \sum_{\mu\neq\lambda} D_{\lambda\mu}\times[F_\mu^1 + m\bar{\omega}_\mu\times(\bar{\omega}_\mu\times D_{\mu\lambda})] \\
 & + my\bar{\rho}^{-3}(1 - 3\hat{\rho}\hat{\rho})\cdot D_{\mu\lambda}
 \end{aligned} \tag{21}$$

In Eq (5),

$$\bar{\omega}_0 = \omega_{01}\hat{e}_1 + \omega_{02}\hat{e}_2 + \omega_{03}\hat{e}_3$$

and the  $\gamma_i$  terms again refer to the rotation about the  $g_i$  axes of rotation. Note that

$$\bar{L}_{01} = \bar{L}_{02} = \bar{L}_{03} = \bar{L}_{04}$$

since all of these terms represent the vector from the center of mass of the reference body to Joint 1, the translating joint. Note also, superscript R in Eq (15) refers to the fact that the time derivatives are taken relative to the rotating  $e_1, e_2, e_3$  reference frame.

Therefore, the  $D_{01}^R, D_{01}^A$  terms refer to the translational velocity and acceleration of Joint 1 relative to the surface of the OMV. The spring and damper torques  $T_{SD}$  refer to the six internal motor control torques TG1, TG2, TG3, TG4, TG5, and TG6. The external torques  $T'$  refer to the three external thruster control torques, T1, T2, T3, located on the reference body. All external forces are assumed zero. In addition, all gravity gradient terms are assumed negligible (all terms containing the planetocentric position vector  $\bar{\rho}$ ). The joint translational motion and the internal and external control torques need to be specified in the equations of motion, which is the topic of next chapter.

As mentioned earlier, the constraint forces and torques at the joints have been eliminated from the equations of motion. These terms can easily be recovered as described in references (6) and (7). The equation for the constraint torques is as follows, where the subscript i refers to the particular joint; Joint 1, Joint 2, or Joint 3:

$$T_i^c = \sum_{\lambda} \epsilon_{i\mu} \left\{ \sum_{\mu} \phi_{\lambda\mu} \cdot \left( \dot{\omega}_0 + \sum_k \epsilon_{k\mu} \ddot{\gamma}_k g_k \right) - E_{\lambda}^* \right\} \quad (22)$$

and the constraint force at the translating joint can be found with

$$F_{01}^H = m_0 \bar{r}_0 \quad (23)$$

where  $\bar{r}_0$  is the position vector from the system mass center to the center of mass of the reference body, Body 0.

### III. Control Laws

There are two types of control schemes required in this thesis. The first involves maintaining dynamic balancing and stability throughout the deployment of the grappling arm and the subsequent spin-up of the grappling device prior to docking. The second control problem involves the detumbling and despinning of the OMV/Target docked system to a spin-stabilized state of equilibrium. The first problem incorporates a rather simple set of open-loop control laws. The second control problem is more complex and involves applying a Liapunov analysis to the system in order to derive the feedback control laws.

Before specifying either the open-loop or the closed-loop control laws, a quick analysis should be performed in order to express the equations of motion in a form more convenient to work with. The following analysis closely parallels the formulation performed by Widhalm and Conway (9:659-661).

Eq (5) can first be written in the form

$$A\vec{x} = F^* \quad (24)$$

where A is defined as the 9 X 9 matrix on the left-hand side of Eq (5). The vector  $F^*$  is defined as the nine element vector on the right-hand side of Eq (5), and

$$\begin{aligned} \vec{x} &= [\dot{x}_1 \ \dot{x}_2 \ \dot{x}_3 \ \dot{x}_4 \ \dot{x}_5 \ \dot{x}_6 \ \dot{x}_7 \ \dot{x}_8 \ \dot{x}_9]^T \\ &= [\dot{\omega}_{01} \ \dot{\omega}_{02} \ \dot{\omega}_{03} \ \ddot{y}_1 \ \ddot{y}_2 \ -\ddot{y}_3 \ -\ddot{y}_4 \ \ddot{y}_5 \ -\ddot{y}_6]^T \end{aligned} \quad (25)$$

where Eq (25) is derived from the state variables

$$\begin{aligned} \vec{x} &= [x_1 \ x_2 \ x_3 \ x_4 \ x_5 \ x_6 \ x_7 \ x_8 \ x_9]^T \\ &= [\omega_{01} \ \omega_{02} \ \omega_{03} \ \dot{y}_1 \ \dot{y}_2 \ -\dot{y}_3 \ -\dot{y}_4 \ \dot{y}_5 \ -\dot{y}_6]^T \end{aligned} \quad (26)$$

Due to the convenient form of the modified Hooker-Margulies equations, the control vector,  $u$ , can easily be extracted from the right-hand side so that Eq (24) can now be written as

$$A\vec{x} = F + \bar{u} \quad (27)$$

where

$$\begin{aligned}\bar{u} &= [u_1 \ u_2 \ u_3 \ u_4 \ u_5 \ u_6 \ u_7 \ u_8 \ u_9]^T \\ &= [T_1 \ T_2 \ T_3 \ TG_1 \ TG_2 \ TG_3 \ TG_4 \ TG_5 \ TG_6]^T\end{aligned}\quad (28)$$

$T_1, T_2, T_3$  are the three external thrusters and  $TG_1, TG_2, TG_3, TG_4, TG_5, TG_6$  are the six internal motor torques corresponding to the six axes of rotation  $g_1, g_2, g_3, g_4, g_5, g_6$ .

The symmetric matrix  $A$  is always invertible for physical systems, and pre-multiplying Eq (27) by the inverse of matrix  $A$  yields

$$\dot{\bar{x}} = A^{-1} F + A^{-1} \bar{u} \quad (29)$$

This system of equations of motion can then be augmented with the kinematical equations

$$\begin{aligned}\dot{x}_{10} &= x_4 \\ \dot{x}_{11} &= x_6 \\ \dot{x}_{12} &= x_7 \\ \dot{x}_{13} &= x_5\end{aligned}\quad (30)$$

where

$$\begin{aligned}x_{10} &= \gamma_1 \\ x_{11} &= -\gamma_3 \\ x_{12} &= -\gamma_4 \\ x_{13} &= \gamma_2\end{aligned}\quad (31)$$

Therefore,  $x_{10}$  is the angle between Body 1 and Body 0,  $x_{11}$  is the angle between Body 2 and Body 1, and  $x_{12}$  is the angle between Body 3/4 and Body 1, all in the  $e_1$  direction.  $x_{13}$  is the angle of rotation about the grappling arm itself. It is used only in the coordinate transformations required to rotate the inertia matrices to the  $e_1, e_2, e_3$  system. The angles  $\gamma_3$  and  $\gamma_4$  are the angles of rotation of Body 3 and Body 4, respectively, about the  $g_5 / g_6$

axis (See Fig. 2). Since both Body 3 and Body 4 have cylindrical inertia properties, these two angles are not needed in any of the coordinate transformations and are not included in the kinematical equations.

This completes the set of attitude equations of motion. The augmented state vector is now defined as  $x_{13}^*$  and contains the original state vector  $x$  plus the additional elements  $x_{10}, x_{11}, x_{12}, x_{13}$ .

Note that Eq (5) rewritten as Eq (27) still contains the terms

$$L_{01}, \quad L_{01}^R, \quad \dot{L}_{01}^R$$

corresponding to Joint 1 position, velocity, and acceleration relative to the reference body. Since this translating joint motion is a specified function of time, Eq (27) is a nonautonomous system. It will later be shown that it is desirable to work with autonomous systems when applying the Liapunov analysis. Widhalm and Conway (9:660) suggested that the joint motion can be expressed as a third order linear system. The joint position relative to the reference body is

$$L_{01} = (Y_1 - w)\hat{e}_2 + c\hat{e}_3 \quad (32)$$

Note that  $w$  and  $c$  are both constants.  $c$  is the height from the center of mass of the base of the OMV to its top surface.  $w$  is the width from the original Joint 1 position, when the grappling arm is stored horizontally, to the  $e_3$  axis.  $w$  is also half the length of the grappling arm which is the length from Joint 1 to Joint 2 and also the length from Joint 2 to Joint 3.  $Y_1$  is the joint translation in the positive  $e_2$  direction (i.e.: towards the  $e_3$  axis). Since  $w$  and  $c$  are both constants:

$$\dot{L}_{01}^R = \dot{Y}_1 \hat{e}_2 = Y_2 \hat{e}_2 \quad (33)$$

$$\ddot{L}_{01}^R = \ddot{Y}_1 \hat{e}_2 = \dot{Y}_2 \hat{e}_2 = Y_3 \hat{e}_2 \quad (34)$$

Expressing the Joint 1 translational motion as a third order linear system and combining it with Eq (29) and (30) yields the following set of equations for the system:

$$\ddot{\bar{x}} = A^{-1}\bar{F} + A^{-1}\bar{u}$$

$$\dot{x}_{10} = x_4$$

$$\dot{x}_{11} = x_6 \quad (35)$$

$$\dot{x}_{12} = x_7$$

$$\dot{x}_{13} = x_5$$

$$\ddot{Y} = D\ddot{Y}$$

where

$$D = \begin{bmatrix} 0 & 1 & 0 \\ 0 & 0 & 1 \\ D_{31} & D_{32} & D_{33} \end{bmatrix} \quad (36)$$

The constants  $D_{31}$ ,  $D_{32}$ , and  $D_{33}$  can be specified for whatever Joint 1 motion and response time is desired.

### Open-Loop Control Laws

As previously mentioned, the purpose of the open-loop control laws is to deploy the grappling arm assembly, and to spin-up the grappling device, while the OMV system remains in a state of pure constant spin about the  $e_3$  axis. In other words,  $w_{01}$  and  $w_{02}$  should remain zero, and  $w_{03}$  should remain constant. In addition, the  $HX$  and  $HY$  components of angular momentum should also remain zero, and  $HZ$  should remain constant if the external thrusters are not applied (conservation of angular momentum). In order to maintain this state of pure spin, several relationships need to be obeyed.

### Deployment Phase

At all times throughout the deployment process, Joint 2 must remain along the  $e_3$  axis. Also, Body 2 must form a "scissors" arrangement with Body 1 so that the  $e_3$  axis remains the axis of symmetry for the five body system. Since the Joint 1 translational motion can

be arbitrarily specified, the various requirements for the dynamical attitude motion of the system need to be defined as functions of this Joint 1 motion. Since Joint 2 must always be on the  $e_3$  axis the following relationship has to be satisfied:

$$-L_{01}\hat{e}_2 = -(Y_1 - w)\hat{e}_2 = w \cos(\gamma_1)\hat{e}_2 \quad (37)$$

so that

$$\gamma_1 = \cos^{-1} \left\{ \frac{w - Y_1}{w} \right\} \quad (38)$$

Taking the first and second time derivatives yields

$$\dot{\gamma}_1 = \frac{Y_1}{w \sin(\gamma_1)} = \frac{Y_2}{w \sin(\gamma_1)} \quad (39)$$

and

$$\begin{aligned} \ddot{\gamma}_1 &= \frac{Y_2 \sin(\gamma_1) - Y_2 \dot{\gamma}_1 \cos(\gamma_1)}{w \sin^2(\gamma_1)} \\ &= \frac{Y_3 \sin(\gamma_1) - Y_2 \dot{\gamma}_1 \cos(\gamma_1)}{w \sin^2(\gamma_1)} \end{aligned} \quad (40)$$

Also, the "scissors" arrangement between Body 1 and Body 2 requires that

$$\gamma_3 = -2\gamma_1 \quad (41)$$

$$\dot{\gamma}_3 = -2\dot{\gamma}_1 \quad (42)$$

and

$$\ddot{\gamma}_3 = -2\ddot{\gamma}_1 \quad (43)$$

Finally, since the rotation about the  $g_2$ ,  $g_4$ ,  $g_5$ ,  $g_6$  axes should remain fixed;

$$\begin{aligned}\ddot{\gamma}_2 &= 0 \\ \ddot{\gamma}_4 &= 0\end{aligned}\tag{44}$$

$$\begin{aligned}\ddot{\gamma}_5 &= 0 \\ \ddot{\gamma}_6 &= 0\end{aligned}$$

Eqs (40), (43), and (44) specify the required motion of Bodies 1, 2, 3, and 4 during the deployment phase in order to maintain dynamic balancing. The required control torques now need to be calculated in order to achieve this motion.

For the case of not using any external torques, T1, T2, and T3 can be set equal to zero. Referring back to Eq (29), both the A matrix and the F vector are known. Also, the terms

$$\dot{x}_4, \dot{x}_5, \dot{x}_6, \dot{x}_7, \dot{x}_8, \dot{x}_9$$

have all been specified in Eq (40), (43), and (44). The only unknowns on either side of these six equations are the terms contained in the control vector  $\bar{u}$ . Therefore since T1, T2, and T3 are zero, the only unknown terms are TG1, TG2, TG3, TG4, TG5, and TG6. There are now six equations and six unknowns which can be solved simultaneously to yield the six required internal control torques.

If external torques are allowed to ensure the system remains in a state of pure spin, then the additional requirements that

$$\begin{aligned}\dot{\omega}_{01} &= 0 \\ \dot{\omega}_{02} &= 0 \\ \dot{\omega}_{03} &= 0\end{aligned}\tag{45}$$

can be added, and the system then solved for all nine control torques. Rather than simultaneously solving nine equations for nine unknowns, these nine control torques can be computed directly with a simple manipulation of Eq (27).

$$\bar{u} = A \bar{x} - F\tag{46}$$

It is desired that the deployment phase be accomplished without the external thrusters, if possible. For either case, once the control vector has been solved for, it can be substituted back into the original system of equations which are then numerically integrated to yield the state vector.

### Spin-up Phase

This same methodology can be applied for spinning up the grappling device after deployment of the arm and just prior to docking. Body 3 is spun-up to match the spin rate of the target satellite while Body 4 is simultaneously spun-up at an equal and opposite rate. Since Joint 1 is no longer translating and is stationary

$$\begin{aligned}\ddot{\gamma}_1 &= 0 \\ \ddot{\gamma}_3 &= 0\end{aligned}\tag{47}$$

and again

$$\begin{aligned}\ddot{\gamma}_2 &= 0 \\ \ddot{\gamma}_4 &= 0\end{aligned}\tag{48}$$

but this time

$$\ddot{\gamma}_5 = \text{constant} = -\ddot{\gamma}_6\tag{49}$$

### Nonlinear Feedback Control-Detumble/Despin Phase

Once the OMV and the satellite are docked, the next control problem is to detumble and despin the target by applying the appropriate internal motor torques while firing

external thrusters to control the absolute motion of the system. Joint 1 is driven to the center of the OMV corresponding to the  $e_3$  axis, and Bodies 1, 2, 3 (including the target) and 4 are all erected to the vertical position. The OMV should remain in a state of pure constant spin throughout the process.

In order to solve this problem, a feedback control approach, similar to that taken by Widhalm and Conway, needs to be incorporated. The complete nine element control vector,  $\bar{u}$ , is a nonlinear function of the augmented system state variables and the Joint 1 motion expressed in Eq (35). Liapunov's direct method can be applied to derive a control law which is globally asymptotically stable with respect to the spin-stabilized state of equilibrium. Eq (35) is repeated here for convenience.

$$\begin{aligned}\bar{x} &= A^{-1} \bar{F} + A^{-1} \bar{u} \\ \dot{x}_{10} &= x_4 \\ \dot{x}_{11} &= x_6 \\ \dot{x}_{12} &= x_7 \\ \dot{x}_{13} &= x_5 \\ \bar{Y} &= D\bar{Y}\end{aligned}\tag{35}$$

Recall from the previous discussion that the Joint 1 translational motion  $Y$  is expressed separately as a third order linear system so that the equations of motion form an autonomous system more suitable for Liapunov analysis. Note that  $D$  is a negative definite matrix selected to obtain the desired decay of Joint 1 to the final position at [0 0 c].

A lemma presented by Vidyasagar (8), which is valid for autonomous systems, can now be applied. It is stated as follows: "Let  $V(x_{13}^*, Y)$  be continuously differentiable and suppose that for some  $d \geq 0$  the set

$$S_d^* = [\bar{x}_{13}^*, Y : V(\bar{x}_{13}^*, Y) \leq d]$$

is bounded. Suppose that  $V$  is bounded below over the set  $S_d^*$  and that

$$\dot{V}(\bar{x}_{13}^*, Y) \leq 0$$

for all  $x_{13}^*$  and  $Y$  in  $S_d^*$ . Let  $S$  denote the subset of  $S_d^*$  defined by

$$S = \{ x_{13}^* , Y \in S_d^* : V(\bar{x}_{13}^*, Y) = 0 \}$$

and let  $M$  be the largest invariant set of a system which is contained in  $S$ . Then whenever  $x_{13}^*$  and  $Y(0)$  are members of  $S_d^*$ , the solution of the system of Eq (35) approaches  $M$  as  $t$  approaches infinity." (8:157)

Since the system of Eq (35) is autonomous, every state trajectory is an invariant set. The task, therefore, is to find the candidate Liapunov function,  $V$ , in order to "derive a nonlinear feedback control law that drives the five-body system to the spin-stabilized state of equilibrium." (9:660)

On the same lines as Widhalm and Conway (9:660), one candidate Liapunov function is

$$\begin{aligned} V = & \left( \frac{1}{2} \right) \bar{x}^T I \bar{x} + \left( \frac{1}{2} \right) K_{10}(x_{10} - 90^\circ)^2 + \left( \frac{1}{2} \right) K_{11}(x_{11} - 180^\circ)^2 \\ & + \left( \frac{1}{2} \right) K_{12}(x_{12} - 90^\circ)^2 + \left( \frac{1}{2} \right) K_{13}(x_{13})^2 + Y^T R Y \end{aligned} \quad (50)$$

where  $I$  is the identity matrix,  $K_{10}$ ,  $K_{11}$ ,  $K_{12}$ , and  $K_{13}$  are positive constants, and  $R$  is a positive definite constant matrix. The function is continuously differentiable, and taking its derivative with respect to time yields

$$\begin{aligned} \dot{V} = & \bar{x}^T I \bar{x} + K_{10}(x_{10} - 90^\circ) \dot{x}_{10} + K_{11}(x_{11} - 180^\circ) \dot{x}_{11} \\ & + K_{12}(x_{12} - 90^\circ) \dot{x}_{12} + K_{13} x_{13} \dot{x}_{13} + Y^T R Y + Y^T R Y \end{aligned} \quad (51)$$

Substituting from Eq (35) gives

$$\begin{aligned} \dot{V} = & \bar{x}^T I [ A^{-1} F + A^{-1} \bar{u} ] + K_{10}(x_{10} - 90^\circ) x_4 + K_{11}(x_{11} - 180^\circ) x_6 \\ & + K_{12}(x_{12} - 90^\circ) x_7 + K_{13} x_{13} x_5 + Y^T [ D^T R + R D ] Y \end{aligned} \quad (52)$$

However, since  $R$  is positive definite and  $D$  was specified to be negative definite, the Liapunov matrix equation can be written as

$$D^T R + RD = -Q \quad (53)$$

where  $Q$  is a positive definite matrix. Therefore,  $Y[D^T R + RD]Y$  is negative definite. To make the derivative of  $V$  at least negative semidefinite, choose (9:660):

$$\begin{aligned} \bar{u} &= -F \\ &+ A[0, 0, 0, -K_{10}(x_{10} - 90^\circ), -K_{13}x_{13}, -K_{11}(x_{11} - 180^\circ), -K_{12}(x_{12} - 90^\circ), 0, 0]^T \\ &- AB\bar{x} \end{aligned} \quad (54)$$

substituting back into (51) yields

$$\dot{V} = -\bar{x}^T I B \bar{x} + Y^T [D^T R + RD]Y \quad (55)$$

If the matrix  $B$  is positive definite, then the derivative of  $V$  is negative semidefinite in  $x_{10}$ ,  $x_{11}$ ,  $x_{12}$ . However, if  $B$  is diagonal with positive elements (except  $B_{33} = 0$ ), then the derivative of  $V$  is negative semidefinite in  $x_3$  and  $x_{10}$ ,  $x_{11}$ ,  $x_{12}$ . (9:660). Note that  $90^\circ$ ,  $180^\circ$ , and  $90^\circ$  have been subtracted from  $x_{10}$ ,  $x_{11}$ ,  $x_{12}$ , respectively, in this analysis. This is just a simple coordinate rotation. The spin-stabilized state of equilibrium is about the  $x_3$  axis ( $e_3$  axis). This state occurs when  $x_{10} = 90^\circ$ ,  $x_{11} = 180^\circ$ , and  $x_{12} = 90^\circ$ , so that the coordinate rotation is needed to express these three values in relationship to the state of equilibrium. Whenever these three values are not  $90^\circ$ ,  $180^\circ$ , and  $90^\circ$ , respectively (i.e.: when they are nonzero relative to the  $x_3$  axis), then a nonzero control  $u$  results. The control law for  $u$  in Eq (54) represents the desired nonlinear feedback control law to drive the system of Eq (35) to a spin-stabilized state of equilibrium.

Substituting Eq (54) for  $u$  into the system of Eq (35) results in the following linear system :

$$\begin{aligned} \ddot{\bar{x}} &= [0, 0, 0, -K_{10}(x_{10} - 90^\circ), -K_{13}x_{13}, -K_{11}(x_{11} - 180^\circ), -K_{12}(x_{12} - 90^\circ), 0, 0]^T \\ &- B\bar{x} \end{aligned}$$

$$\begin{aligned}
 \dot{x}_{10} &= x_4 \\
 \dot{x}_{11} &= x_6 \\
 \dot{x}_{12} &= x_7 \\
 \dot{x}_{13} &= x_5 \\
 \bar{Y} &= D\bar{Y}
 \end{aligned} \tag{56}$$

Note again that the four constants,  $K_{10}$ ,  $K_{11}$ ,  $K_{12}$ , and  $K_{13}$  are positive as are the elements of the diagonal matrix  $B$ . These values determine the motion and response times of the various bodies as they decay to the spin-stabilized state of equilibrium, just as the elements of the  $D$  matrix determine the decay of Joint 1. However, since the rotation ( $\gamma_2$ ) about the grappling arm itself is locked prior to docking,  $x_{13}$  and  $x_5$  are both initially zero. Therefore, the constants  $K_{13}$  and  $B_{55}$  will have no effect on the control law and can be chosen arbitrarily. Note also that if  $w_{01}$  and  $w_{02}$  ( $x_1$  and  $x_2$ ) are initially zero, any choice of  $B_{11}$  and  $B_{22}$  will still result in these two components of angular velocity remaining zero. Also,  $B_{33}$  should be chosen to be zero so that  $w_{03}$  remains constant. The choice of the other  $K$ ,  $B$ ,  $D$  constants should be made such that the motion of Bodies 1, 2, 3, and 4 is closely coordinated with the motion of Joint 1 so that Joint 2 and the target center of mass remain as close to the  $e_3$  axis as is practical. This will help reduce the required amount of control to maintain the absolute motion of the system.

#### **IV. Results**

In this chapter, the mass and inertia properties for the five bodies of the OMV system and for the target are presented, and the actual docking configuration is established. The initial conditions for the three phases of the simulation are specified, and the results from each phase are presented. A total of nine cases are analyzed; three cases from the deployment phase, one case from the spin-up phase, and five cases from the detumble/despin phase. The deployment phase is run without external thrusters, with external thrusters, and finally with external thrusters but without deployment of the counter-mass. The spin-up phase is only run without external thrusters. The detumble/despin phase is run with variations in response time, target coning angle, and deployment arm length.

The equations of motion formulated in this problem are rather complex, and the corresponding computer code quite lengthy. To validate the equations and computer code, a routine was added to compute both the total system angular momentum and the total system kinetic energy during each time step in the numerical integration. When no external torques were applied (i.e.  $T_1, T_2, T_3 = 0$ ) both these properties were successfully conserved, thereby verifying the validity of the equations of motion for this model.

Both the target and the OMV mass and inertia properties are presented in Table I, and the necessary dimensions are listed in Table II. The target properties are the same as those used in the Widhalm and Conway study (9). The base of the OMV, Body 0, also has the same properties as the the OMV in the Widhalm and Conway model. These values were chosen as such so that a reasonable comparison could be made between the results from the 2-body model and the 5-body model. An estimate was made for the mass and inertia properties of Body 1, the grappling arm, and for Body 3, the grappling device. The grappling arm was chosen to have a total length of 3.5 meters, with two equal halfs of 1.75 meters divided by Joint 2. Body 1 includes the mass of the translating Joint 1 assembly so its center of mass is somewhat to the left of Joint 2. Body 4 has exactly the same properties of Body 3, and together they form two equal halfs of a sphere. Body 2's required inertia properties were computed using Eqs (2), (3), and (4) in Chapter 2, and its corresponding mass was estimated given these requirements. Note that the mass and

inertia properties of Body 2 are approximately six time higher than those of Body 1. This adds considerable extra mass to the system. However, the total mass of Body 1, 2, 3, and 4 is 390 kg which is less than a 9% addition to the original OMV.

TABLE I  
Nominal Mass Properties

BODY	MASS (Kg)	$I_{xx}$ (Kg-m)	$I_{yy}$ (Kg-m)	$I_{zz}$ (Kg-m)
Target	1000	1000	1000	1100
Body 0 (Base of OMV)	4500	6400	6400	11800
Body 1 (Grappling Arm)	50	50	10	50
Body 2 (Counter-mass)	300	311.125	50.625	311.125
Body 3 (Grappling Device)	20	20	20	20.3125
Body 4 (Counter-mass)	20	20	20	20.3125

**TABLE II**  
**Nominal Dimensions (Constants)**

<b>W</b>	One Half the Length of the Grappling Arm (i.e. from Joint 1 to Joint 2 or from Joint 2 to Joint 3)	1.75 m
<b>C</b>	Vertical Length from Center of Mass of the Reference Body to Joint 1	0.62 m
<b>L<sub>10</sub></b>	Length along Grappling Arm from Center of Mass of Body 1 to Joint 1	0.35 m
<b>L<sub>12</sub></b>	Length along Grappling Arm from Center of Mass of Body 1 to Joint 2	1.40 m
<b>L<sub>13</sub>, L<sub>14</sub></b>	Length along Grappling Arm from Center of Mass of Body 1 to Joint 3	3.15 m
<b>L<sub>30</sub>, L<sub>31</sub></b>	(Pre-Docked) Length from Center of Mass of Body 3 to Joint 3	0.125 m
<b>L<sub>40</sub>, L<sub>41</sub></b>	Length from Center of Mass of Body 4 to Joint 3	0.125 m
<b>L<sub>30</sub>, L<sub>31</sub></b>	(Post-Docked) Length from Center of Mass of Body 3 (Target Satellite) to Joint 3	1.75 m

### Docking Configuration

As previously mentioned, the target used in this problem has the same characteristics as in the Widhalm and Conway problem (9). These characteristics, along with the target's length from its center of mass to Joint 3 after docking, determine the initial positioning and spin rate of the OMV prior to deployment of the grappling arm, and the necessary position of the grappling arm assembly after deployment. The target's state also determines the required pre-docking spin-up of the grappling device. Nominal motion of the target is listed in Table III and its mass and inertia properties have already been presented in Table I.

TABLE III  
Nominal Target Motion

$\gamma_T$	Coning Angle	0.349 radians
$\dot{\psi}_T$	Precession Rate	0.102 rad/sec
$\dot{\phi}_T$	Spin Rate	0.009 rad/sec

The initial spin rate of the OMV about its  $e_3$  axis of symmetry must be 0.102 rad/sec in order to match the precession rate of the target. The spin rate of Body 3 must be 0.009 rad/sec to match the target's spin rate. The docking configuration is outlined in Fig. 5. It can easily be seen that with the given lengths and coning angles, only one configuration will work. The angles,  $\gamma_1$  and  $\gamma_4$ , required for docking have to be determined. Since the lengths from Joint 2 to Joint 3 and from the target's center of mass to Joint 3 are both 1.75 meter, the triangle from Joint 2 to Joint 3 to the target's center of mass to Joint 2 is isosceles. Therefore, the angle formed between the grappling arm and the  $e_3$  axis is equal to the coning angle,  $20^\circ$  (0.3490 rads), so that  $\gamma_1$  must be  $70^\circ$  (1.2217 rads) in the docked configuration. Furthermore, the angle  $\gamma_4$ , the rotation of Body 3/Body 4 with respect to the grappling arm, must be  $50^\circ$  (0.8727 rads). The distance of Joint 1 from the  $e_3$  axis in the docked configuration determines the necessary amount of joint translation. This distance from Joint 1 to the  $e_3$  axis is a function of the target coning angle and is equal to the horizontal displacement,  $b$ , of Joint 3 from the  $e_3$  axis. This distance is calculated to be 0.5985 meters.

#### Deployment Phase

The OMV is initially pre-positioned relative to the target, and spun-up to match the target's precession rate. Initial conditions for the deployment phase are shown in Table IV. Bodies 1, 2, 3, and 4 are all stored flat on the top surface of the OMV's base. Note,

however, in the deployment open-loop control law Eq (40) there is a singularity at  $y_1 = 0^\circ$ . Body 1 is therefore stored slightly offset from the horizontal, at an initial angle of  $1^\circ$  (0.01745 rads), and Body 2 is stored at an angle of  $2^\circ$  (0.03490 rads). This is a simple work around to this singularity, since it does not lend itself to an easy removal using L'Hospital's rule. This slight offset does not in anyway detract from the analysis of the results. 250 seconds are allocated for the total deployment event. Joint motion is specified as a third order linear system, with three equal eigenvalues of -0.06, giving a joint motion of

$$Y_3 = -0.000216(Y_1 + 0.599) - 0.0108Y_2 - 0.18Y_3 \quad (57)$$

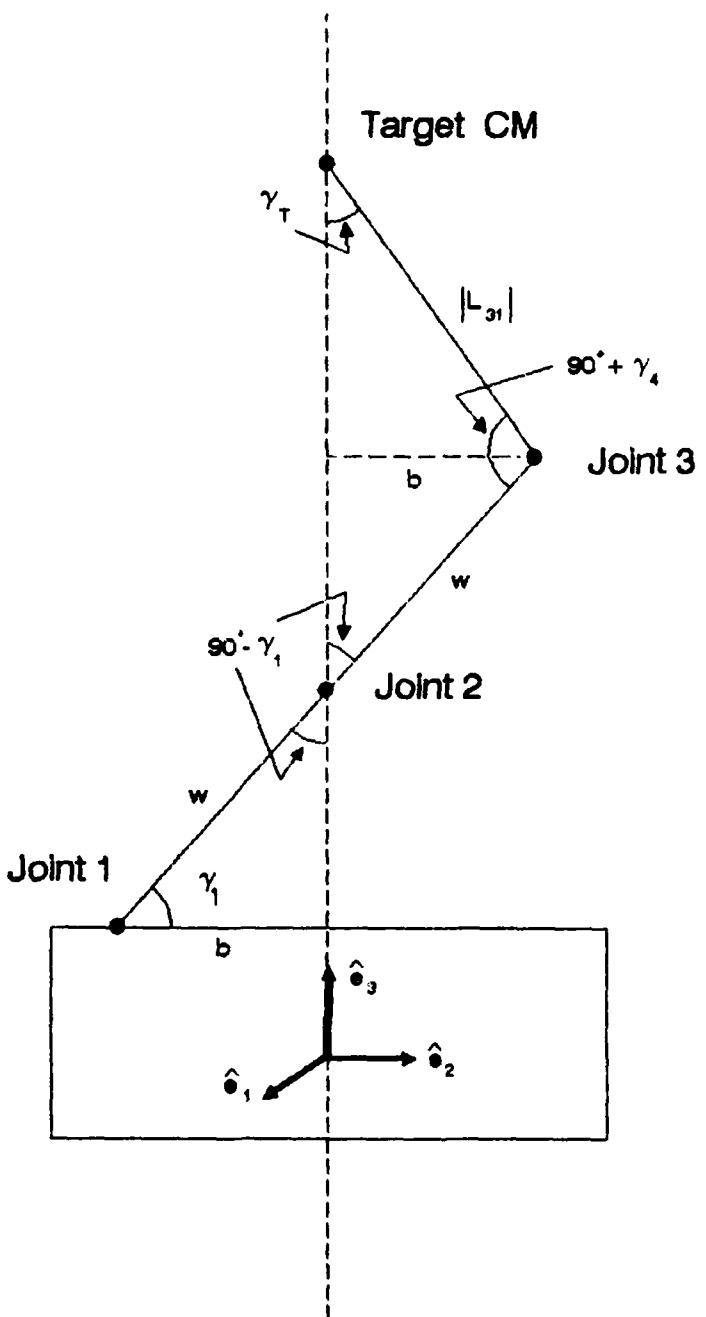


Fig. 5. Docking Configuration

TABLE IV  
Deployment Phase Initial Conditions

$\omega_{01}$	0.0	rad/sec
$\omega_{02}$	0.0	rad/sec
$\omega_{03}$	0.102	rad/sec
$\gamma_1$	0.01745	radians
$\gamma_2$	0.0	radians
$\gamma_3$	0.03490	radians
$\gamma_4$	0.0	radians
$\dot{\gamma}_1$	0.0	rad/sec
$\dot{\gamma}_2$	0.0	rad/sec
$\dot{\gamma}_3$	0.0	rad/sec
$\dot{\gamma}_4$	0.0	rad/sec
$\dot{\gamma}_5$	0.0	rad/sec
$\dot{\gamma}_6$	0.0	rad/sec
$Y_1 - W$	-1.75	meters
$Y_2$	0.0	m/sec
$Y_3$	0.0	m/sec <sup>2</sup>

**CASE 1 - DEPLOYMENT WITHOUT EXTERNAL THRUSTERS:** In this particular case, the deployment of the arm is achieved with the external thrusters turned off. It can be seen from Figs. 6, 7, and 8 that Joint 1 moves smoothly from a position of rest -1.75 meters from the  $e_3$  axis and decays down to -0.5985 meters, well within the allocated 250 seconds. Looking at  $\gamma_1$  and  $\dot{\gamma}_1$  in Figs. 9 and 10, the grappling arm is smoothly raised from  $1^\circ$  to  $70^\circ$ . Body 2 is successfully deployed (See Figs. 11 and 12) in a manner such that  $\gamma_3$  is always twice as much as  $\gamma_1$  so that Body 2 forms a scissors arrangement with Body 1. It can be seen from Fig. 13 that the internal motor torque TG1 responsible for erecting the grappling arm assembly experiences a sharp start-up transient which dies out after approximately 10 seconds. The peak required start-up torque is less than 7 N-M. A sharp transient is also present in the constraint torques at Joint 1 and Joint 2 (See Figs. 19, 20, and 21). The rest of the internal motor control torques (TG2, TG3, TG4, TG5, TG6) are very small (Figs. 14-18), since they all play minors roles, with the exception of TG3 which controls the motion of Body 2. The sharp transient control torque at TG1 is due to the fact that a large moment is initially required to raise the arm from its stored horizontal position, and get it moving.

The most important goal in the deployment phase is to maintain dynamic balance and stability throughout the process without having to fire the external thrusters. In other words, there should only be pure spin about the  $e_3$  axis, and  $w_{01}$  and  $w_{02}$  should remain zero. Also, the cross products of inertia should all be cancelled out by the deployment of Body 2, so that angular momentum exists only in the  $e_3$  direction, lined up with  $w_{03}$ . This is successfully achieved. Both  $w_{01}$  and  $w_{02}$  remain zero throughout the process. The HX and HY components (See Figs. 23 and 24) are negligible when compared with the HZ component in Fig. 25, and can be attributed to numerical round-off errors. Figs. 25 and 26 show that all the angular momentum remains completely in the  $e_3$  direction. Fig. 26 also shows that angular momentum is conserved throughout the process since no external torques are applied, thus proving that the equations of motion for the system are valid.

There is one important thing that does not work as expected, however. The initial spin rate of  $w_{03} = 0.102$  rad/sec does not remain constant, as required, but instead increases to almost 0.106 rad/sec. It is important to note again though that the  $w_{01}$  and  $w_{02}$  components remain zero and so the system is still in a state of pure , though not

constant, spin about the  $e_3$  axis. The reason that the spin rate changes is due to a simple conservation principle that was overlooked in the initial formulation stages of the problem. The angular momentum remains constant about the  $e_3$  axis throughout the deployment process. As the translating joint moves inward and the arm is erected, the individual angular momentum components of Body 1, Body 2, Body 3, and Body 4 all change, but the total system angular momentum must remain the same. Therefore, the angular momentum of Body 0 must somehow change, and since it is in a state of pure spin, its spin rate must change. This is not a problem for stability but it is a serious docking problem.

The spin rate of the OMV must match the precession rate of the target. There are two possible solutions to this problem, short of a system configuration change. The first solution merely involves applying the external thrusters during the deployment process to keep the spin rate of the OMV fixed. The other alternative is to start with a different initial spin rate and not use the external thrusters. Since the desired OMV spin rate at the end of the deployment process is known (0.102 rad/sec) and angular momentum is constant, the required spin rate at the beginning of the deployment can easily be computed. This was done, and it was found that an initial OMV spin rate of 0.0982 rad/sec will yield a final spin rate of 0.102 at the end of the deployment process (i.e. when  $\gamma_1 = 70^\circ$  and  $\gamma_3 = 140^\circ$ ). This lower initial spin-rate saves maneuvering fuel in two ways. First of all, the OMV has to be initially spun-up that much less, and second, the external thrusters don't have to be turned on at all during the deployment process. The main problem with this approach is with alignment. The grappling arm assembly is initially lined up "underneath" its intended docking point on the target. If the OMV does not have the same constant spin rate throughout the deployment process to match the constant precession rate of the target, the grappling device will not arrive at the intended point on the target. If the OMV is spun-up at the lower initial rate, an additional algorithm is required to ensure that the grappling device arrives at the intended docking point. This adds more complexity to the pre-positioning program and runs the added risk of interference with appendages on the target. Therefore, it is probably more desirable to use the external thrusters to keep the OMV's spin rate constant about the  $e_3$  axis during the deployment process, and it is this technique that is incorporated in Case 2, hereafter referred to as the Nominal Deployment Case.

One last noteworthy piece of data is gleaned from this case. During the deployment process, the total system mass center of the OMV assembly remains fixed in inertial space since no external torques or forces are applied. However, as the grappling arm assembly is deployed, the system mass center moves "upward" relative the base reference body. Since the system mass center is fixed in inertial space, the base reference body, Body 0, moves "downward," away from the target. This has to be compensated for by a translational external thruster control system on board the OMV in order to maintain a constant stand-off distance. This amount of vertical translation that needs to be compensated is computed to be 0.18 meters as shown in Fig. 27.

**CASE 2 - NOMINAL DEPLOYMENT:** The second deployment run is made using exactly the same initial conditions as Case 1 (Table IV) except this time the external thrusters are turned on in order to maintain the OMV at a constant initial spin rate of 0.102 rad/sec. Fig. 28 shows that the control scheme is successful in achieving this objective. The internal motor torques are exactly the same as in Case 1, as expected since their task remains unchanged. The required external thrusters are shown in Figs. 29, 30, and 31 . Note that T1 and T2 about the  $e_1$  and  $e_2$  axes are both negligible and can be attributed to numerical round-off error. The only external control torque required was T3 about the  $e_3$  axis, and it has a peak magnitude of less than 1 N-M. Therefore, the amount of external control required to maintain a constant spin-rate is quite reasonable

**CASE 3 - DEPLOYMENT WITHOUT BODY 2 COMPENSATION:** In both Case 1 and Case 2, Body 2 is deployed in a scissors fashion relative to Body 1. This successfully accomplishes its intended purpose of cancelling out the cross-product of inertia terms thereby maintaining stability without the use of the external thrusters. However, Body 2 adds a considerable amount of mass to the system. This extra mass has to be ferried up into orbit along with the OMV and also has to be transported each time the vehicle is boosted into higher capture orbits. This could amount to a significant fuel cost. There might also be the problem of Body 2 interfering with target appendages such as solar panels and antennas. One alternative that needs to be examined is at what maneuvering fuel cost can the deployment phase be achieved without deploying Body 2. In this case,  $\gamma_3$  is fixed at 0° throughout the process so that Body 1 and Body 2 remain coincident.

while the external thrusters are turned on to maintain a constant spin about the  $e_3$  axis only. The resulting control magnitudes are shown in Figs. 32, 33, and 34 . Most of the control is with T1 about the  $e_1$  axis in keeping the system balanced. The T2 and T3 thrusters are used to a lesser degree. Both their magnitudes are less than 1 N-M, and neither are required beyond 200 seconds where the deployment process is essentially achieved. Notice that the T1 thruster is still turned on at a constant 1.8 N-M at the end of the 250 seconds process. This appears to be the major advantage offered by Body 2. The external thruster control without using Body 2 is not unreasonable during deployment, but must be kept on continuously in the pre-docked configuration. By deploying Body 2, the system remains in a state of pure (although not constant) spin without the use of external thrusters. The advantages offered by Body 2 versus its added mass is a decision that would need to be weighed by the mission planner. This thesis merely shows that both options are feasible from a controls point of view.

### Spin-Up Phase

CASE 4 - NOMINAL SPIN-UP: Once deployment is completed, Body 3 is spun-up in order to match the spin rate of the target satellite just prior to docking. Body 4, the counter-mass, is spun-up at an equal rate but in an opposite direction in order to cancel out the moments. For this phase of the simulation Joint 1 is held fixed as are the other bodies ( $w_{03} = 0.102$  rad/sec,  $y_1 = 70^\circ$ , and  $y_3 = 140^\circ$ ). External thrusters are shut completely off. Both Body 3 and Body 4 are given a constant acceleration of 0.0009 rad/sec<sup>2</sup> for 10 seconds, and then the OMV system is left in its pre-docked pure spin configuration for an additional 40 seconds, again with no external controls. The spin-up of Body 3 and Body 4 is shown in Figs. 35 and 36 . Both bodies successfully spin-up to a constant 0.009 rad/sec. Figs. 37 and 38 show the very small internal motor torques required to accomplish this task. Figs. 39-42 show that dynamic stability is maintained throughout this process without the use of external controls, and the angular momentum vector remains aligned in the  $e_3$  direction along with the constant spin rate.

### **Detumble/Despin Phase**

The actual mating of the grappling device to the target is not within the scope of this thesis, and occurs as a discrete event in which Body 3 takes on the mass, length, and inertia properties of the target. Nonlinear feedback control is then applied, using all nine internal and external controls, to drive Joint 1 to the  $e_3$  axis, and erect all bodies in the vertical position ( $\gamma_1 = 90^\circ$ ,  $\gamma_3 = 180^\circ$ ,  $\gamma_4 = 90^\circ$ ) in a spin-stabilized state of equilibrium. Also in this process, the spin-rate of Body 3 (target) and Body 4 is reduced to zero in order to despin the target. The initial conditions for the detumble-despin phase are shown in Table V.

TABLE V  
Detumble/Despin Phase Initial Conditions

$\omega_{01}$	0.0	rad/sec
$\omega_{02}$	0.0	rad/sec
$\omega_{03}$	0.102	rad/sec
$\gamma_1$	1.2217	radians
$\gamma_2$	0.0	radians
$\gamma_3$	2.4434	radians
$\gamma_4$	0.8727	radians
$\dot{\gamma}_1$	0.0	rad/sec
$\dot{\gamma}_2$	0.0	rad/sec
$\dot{\gamma}_3$	0.0	rad/sec
$\dot{\gamma}_4$	0.0	rad/sec
$\dot{\gamma}_5$	0.009	rad/sec
$\dot{\gamma}_6$	-0.009	rad/sec
$Y_1 - W$	-0.5985	meters
$Y_2$	0.0	m/sec
$Y_3$	0.0	m/sec <sup>2</sup>

CASE 5 - DETUMBLE/DESPIN WITH WIDHALM/CONWAY GAIN SETTINGS: In this case, control values are chosen in such a fashion as to emulate the Widhalm and Conway study (9) as much as possible for comparison purposes. Feedback is applied for 300 seconds. The joint translational motion is specified using the same third order linear equation as Widhalm and Conway (9), corresponding to three equal eigenvalues of -0.04. :

$$\dot{Y}_3 = -0.000064Y_1 - 0.0048Y_2 - 0.12Y_3 \quad (58)$$

The constants  $K_{10}$ ,  $K_{11}$ ,  $K_{12}$ , and  $K_{13}$  as well as the nine elements of the positive diagonal  $B$  matrix (See Eqs (54) and (56)) have to be specified.  $B_{33}$  is set equal to 0.0 since it is desired that the OMV's spin rate about the  $e_3$  axis remains constant throughout the process.  $B_{11}$  and  $B_{22}$  are set equal to 0.046 as is done in the Widhalm study. Actually, since  $w_{01}$  and  $w_{02}$  (corresponding to  $x_1$  and  $x_2$ ) are both initially zero and remain that way, the constants  $B_{11}$  and  $B_{22}$  have no effect on the problem and can be any value. Note also that the rotation about the  $g_2$  axis (the axis coincident with the grappling arm) needs to be initially zero. Rotation about this axis after docking and prior to erection could be disastrous, since it would create stability problems and could even result in the target crashing into the base of the OMV. Therefore, since  $\gamma_2(x_{13})$  and  $\dot{\gamma}_2(x_5)$  are initially zero, the constants  $K_{13}$  and  $B_{55}$  have no influence on the problem.  $K_{13}$  is arbitrarily set equal to a value chosen for one of the other  $K$  constants, and  $B_{55}$  is set equal to  $B_{11}$  and  $B_{22}$ .

The choice of  $B_{44}$  and  $K_{10}$  determines the second order linear system which represents the motion of  $\gamma_1(x_{10})$  from  $70^\circ$  to  $90^\circ$ . Similarly,  $B_{66}$  and  $K_{11}$  determine the motion of  $\gamma_3(x_{11})$  from  $140^\circ$  to  $180^\circ$ , and  $B_{77}$  and  $K_{12}$  determine the motion of  $\gamma_4(x_{12})$  from  $50^\circ$  to  $90^\circ$ . Widhalm and Conway (9) chose to specify the erection of the target (which is similar to the erection of Body 1 in this model) as a critically damped system using two equal eigenvalues of -0.035. The equivalent motion of Body 1 in this problem needs to be closely coordinated with the decay of the translating joint in order that Joint 2 remain as close to the  $e_3$  axis as possible. The erection of Body 3 (the target) should be timed so that the center of mass of the target also remains close to the  $e_3$  axis. This

reduces the amount of external torque needed to maintain a dynamically stable system. Body 2 should decay in a fashion similar to Body 1. The motion of all three angles is chosen to be represented by the critically damped second order equation consisting of two equal eigenvalues of -0.035. Therefore  $B_{44}$ ,  $B_{66}$ , and  $B_{77}$  are all chosen to be 0.07 while  $K_{10}$ ,  $K_{11}$ ,  $K_{12}$  and are all chosen to be 0.001225.

Finally, the decay rate for the spin of Body 3 (the target) is determined by the choice for  $B_{88}$ . This again is chosen using the same decay rate as in the Widhalm and Conway model (9), an eigenvalue of -0.02, making  $B_{88}$  equal to 0.02. The decay of Body 4 (in the opposite direction) is also chosen to be -0.02 so  $B_{99}$  too is set at 0.02.

The results illustrate that the detumbling and despinning of the satellite is successfully accomplished in the allotted 300 seconds, leaving the system in the desired state of pure spin shown in Fig. 4. All motion shown in Figs. 43-48 is smooth and is such that the target center of mass is always directly above Joint 2. Body 2 has exactly twice the rate as Body 1 at all times, since it has to cover twice the angular displacement. Fig. 49 shows the successful despin of Body 3 - the target, while Fig. 50 illustrates the corresponding despin of Body 4. The smooth joint translational motion is shown in Figs. 51, 52, and 53.

The most important information from this run is the required external and internal control torques needed in the detumble and despin process. The largest control torques are clearly the internal motor torque  $TG_1$  and the external thruster  $T_1$ , both in the  $e_1$  direction.  $T_1$  starts off at approximately 18 N-M and drops down to almost -9 N-M in the opposite direction before decaying towards zero. This is an order of magnitude higher than the external torque in the results of the Widhalm and Conway study (9), which were bounded from +2 N-M to -3 N-M.

There are two probable reasons why the required  $TG_1$  and  $T_1$  and also  $TG_4$  control are so much higher than in the Widhalm and Conway model (9). First of all, this model has the additional mass and inertia of the grappling arm, the counter-mass., the grappling device, and its counter-mass. This adds 390 kg to the system, which is a 39% addition to the target mass. Second, the geometry in this problem is considerably different. In the Widhalm and Conway model (Fig. 1), the target was joined directly at the translating joint. In this model, the target is connected at Joint 3 which is linked with Joint 1 by a 3.5 meter long grappling arm. The maximum negative control torque magnitude for both  $T_1$  and  $TG_1$  occurs, just as in the Widhalm and Conway study (9) at 50 seconds, and

corresponds to when Joint 2 and the center of mass of the target both have the equal maximum displacement from the  $e_3$  axis of approximately 11.4 cm.. The second largest required internal motor torque is seen by TG4 at Joint 3, which is responsible for erecting the target itself relative to Body 1 (i.e.  $\gamma_4$ ). The amount of torque required to despin the target, TG5, is quite small due to its very small initial spin rate.

All internal and external control torques decay very close to zero within 300 seconds, implying that the system achieves a spin-stabilized state of equilibrium. The magnitude of the constraint torques at Joints 1, 2, and 3 are shown in Figs. 63, 64, and 65 . Notice that the magnitudes of these torques correspond approximately to the magnitude of the internal motor torque at the particular joints. Also, the constraint force in the  $e_2$  direction for the translating joint is shown in Fig. 66 . The force in the y-direction is the amount of force required to "push" the translating joint towards the center of the OMV.

CASE 6 - REDUCED GRAPPLING ARM LENGTH: The next case examines the effect of reducing the length of the grappling arm to see if a shorter arm reduces the large TG1 and T1 control torques seen in Case 5. The question first is how short can the grappling arm be, and still accomplish its task. Looking at Fig. 5, it is apparent that with the coning angle and the length from the target center of mass to Joint 3 fixed,  $\gamma_4$  changes as the length w from Joint 2 to Joint 3 changes. The smaller the w, the less the Body 3 and Body 4 assembly needs to be rotated in order to dock with the target. As a design constraint, it is decided to limit the minimum angle  $\gamma_4$  at  $0^\circ$  in order that the target not run the risk of interference with the grappling arm assembly or the reference body. In other words when docked at this minimum angle of rotation, the target should be perpendicular to the grappling arm so that the angle between the length from the target center of mass to Joint 3 and the length from Joint 2 to Joint 3 is  $90^\circ$ . The length w required for this can easily be computed using simple geometry , and is found to be 0.63695 meters so that the total length of the grappling arm is 1.2739 meters. This is considerably less than the original 3.5 meters. The angle  $\gamma_1$  is also found to be equal to the coning angle. Therefore, the new initial conditions are  $\gamma_1 = 20^\circ$  ,  $\gamma_2 = 40^\circ$  , and  $\gamma_4 = 0^\circ$  . Also, the joint translation and the the control values for K and B are all the same as those used in case 5.

The resulting T1, TG1, and TG4 control torques are shown in Figs. 67, 68, and 69 . These three are chosen since they have the most significant magnitudes in Case 5. Shortening the length of the grappling arm does not help reduce T1 and TG1. In fact, TG4 actually increases due to the fact that it rotates the target from 0° to 90° in the same amount of time it originally had to rotate it from 50° to 90°.

The most important piece of information gained from this run is the fact that TG1 and T1 are not reduced by significantly decreasing the length of the grappling arm and instead remain almost exactly the same. There is one thing to note here that could explain this lack of change. Even though the length of the arm changes, the length b in Fig. 5 remains exactly the same . Length b is the horizontal displacement of the end of the target at Joint 3 from its center to mass on the  $e_3$  axis, and is a function of the target's length and coning angle only. The length b is also the length that Joint 1 has to translate inward. It appears that T1 and TG1 are somehow dependent on this length b.

**CASE 7 - INCREASED TARGET CONING ANGLE:** Since altering the length of the grappling arm has little effect on T1 and TG1 , the next two cases study the effect of altering the horizontal length b mentioned above by varying the initial coning angle of the target. The length , precession rate, and mass properties of the target are all kept the same, but the coning angle is increased from 20° to 30° . This decreases the initial spin rate of the target to 0.008 rad/sec, in accordance with Eq (1). The original length of the grappling arm of 3.5 meters is used. From Fig 5 with the new coning angle of 30° it can be seen that the new initial conditions are  $\gamma_1 = 60^\circ$  ,  $\gamma_3 = 120^\circ$  , and  $\gamma_4 = 30^\circ$  . Joint translation motion and decay rates are again the same as in Case 5. This leads to a new length b of 0.875 meters and an initial Joint 1 position of -0.875 meters from the the  $e_3$  axis.

The resulting T1, TG1, and TG4 for this run are shown in Figs. 70, 71, and 72 . It is apparent that increasing the cone angle thereby increasing the required amount of Joint 1 translation has the effect of increasing the required T1 and TG1 control torques.

**Case 8 - DECREASED TARGET CONING ANGLE:** This next case examines the effect of decreasing the coning angle. A coning angle of 10° is used which results in initial conditions of  $\gamma_1 = 80^\circ$  ,  $\gamma_3 = 160^\circ$  , and  $\gamma_4 = 70^\circ$  , and an initial Joint 1 position of only

-0.30388 meters. The resulting T1, TG1, and TG4 are shown in Figs. 73, 74, and 75 . Note that the peak control magnitudes are reduced to less than 10 N-M. Therefore, reducing the coning angle significantly reduces the required control torques, TG1 and T1

Case 7 and 8 illustrate that the coning angle, which determines the required amount of Joint 1 translation, significantly affects the principal control torques T1 and TG1, while Case 6 shows that altering the length of the grappling arm has very little effect.

Case 9 - NOMINAL DETUMBLE/DESPIN: The next and final case incorporates the original grappling arm length of 3.5 meters, and the designated target coning angle of 20° . It uses all the same initial conditions as in Case 5 shown in Table V. The big difference though is the choice of control variables K<sub>10</sub>, K<sub>11</sub>, K<sub>12</sub>, and the elements of the diagonal B matrix. Joint translational motion is again kept the same as that specified in Eq (58). B<sub>11</sub>, B<sub>22</sub>, B<sub>33</sub>, K<sub>13</sub>, B<sub>55</sub>, B<sub>88</sub> and B<sub>99</sub> are also chosen to remain the same as in Case 5. The values that are manipulated are the values K<sub>10</sub>, B<sub>44</sub>, K<sub>11</sub>, B<sub>66</sub>, K<sub>12</sub>, B<sub>77</sub> that specify the decay functions of the angles  $\gamma_1$ ,  $\gamma_3$  and  $\gamma_4$ . There are three things at stake here in choosing these constants. First of all, these constants show up directly in the control laws (see Eq (54)), so that higher instructed decay rates require higher control magnitudes. Second, decay rates determine how long it takes the complete system to reach its spin-stabilized state of equilibrium ( $\gamma_1 = 90^\circ$ ,  $\gamma_3 = 180^\circ$ , and  $\gamma_4 = 90^\circ$ ). The third and final effect the choice of these control constants have is on how well both Joint 2 and the center of mass of the target are maintained as close to the  $e_3$  axis as possible. It is important to coordinate the decay of  $\gamma_1$  and  $\gamma_4$  with the Joint 1 translation. Large deviations of either Joint 2 or the target center of mass call for large control magnitudes to balance the system and keep it stable. In case 2 the largest negative external T1 (and TG1) control torque of approximately -8 N-M occurs 50 seconds into the detumble/despin phase, when both Joint 2 and the target center of mass are offset by almost 11.5 cm. to the left of the  $e_3$  axis.

Various efforts were made to reduce the large control torques T1, TG1, and to a lesser extent TG4, seen in Case 5 by altering these response values. At first, the decay rates of  $\gamma_1$  and  $\gamma_3$  (Body 1 and 2) were kept the same while the decay rate of  $\gamma_4$  (Body 3/4) was altered. Quicker response times led to higher initial values of TG1 and T1.

Slower responses, while reducing the initial control magnitudes, led to much higher negative torques in the process, due to the fact that the target's center of mass became further offset from the  $e_3$  axis. It appears that overall lower control torques are produced when Joint 2 and the target center of mass are lined up vertically as in Case 5. Therefore, the last option for lowering the control torques is to change the original response values used in the Widhalm and Conway analysis. Since Joint 2 and the target cm are offset to the left of the  $e_3$  axis, this offset can be reduced by slowing the decay rates of  $\gamma_1$ ,  $\gamma_3$  and  $\gamma_4$  while keeping the joint translation the same. The only trade-off is response time. The final values chosen are equal eigenvalues of -0.025 for all three functions. This leads to a value of 0.000625 for  $K_{10}$ ,  $K_{11}$ , and  $K_{12}$ , and a value of 0.05 for  $B_{44}$ ,  $B_{66}$ , and  $B_{77}$ . Also, due to the slower response rate, an additional 50 seconds worth of feedback is applied, allowing a total of 350 rather than 300 seconds for the detumble/despin event.

The results of this run are illustrated in Figs. 76 - 99. Body 1, Body 2 and Body 3/4 ( $\gamma_1$ ,  $\gamma_3$ ,  $\gamma_4$ ) all decay smoothly to their final designated positions within the 350 seconds. The effects of changing the response time are shown in Table VI.

TABLE VI  
Effect of Decay Rate on Final Equilibrium Position

	$\gamma_1$ (degs)	$\gamma_3$ (degs)	$\gamma_4$ (degs)
Case 5/ 300 secs	89.994	179.987	89.987
Case 9/ 300 secs	89.906	179.812	89.812
Case 9/ 350 secs	89.969	179.938	89.938

It can be seen that despite the slower response time of this case, the bodies still come very close to their equilibrium position after 300 seconds. The additional 50 seconds worth of

feedback control, although not critical, brings them even closer to the values seen in Case 5.

Joint 1 translational motion and the despin of Bodies 3 and 4 are the same as in Case 5, except they are given an additional 50 seconds to damp out any residue motion. The biggest change in the run is the very significant improvement in the TG1, T1, and TG4 control torques. The initial T1 and TG1 torques are reduced from the 18 N-M peak value seen in case 5 to a much lower peak value 9.31 N-M . Also, the negative torque is reduced from the original low of -8 N-M at the 50 seconds point to a much smaller value of -1.63 N-M at the 43 seconds point.

The reduction of the initial starting torque can be explained by the slower decay rates fed into the control laws. The much lower negative torque at 43 seconds can be explained by better coordination of these decay rates with the Joint 1 translation rate. Joint 2 and the target cm are both maintained closer to the  $e_3$  axis of symmetry. In case 5 they are displaced a maximum at the 50 seconds point of 11.5 cm to the left of the  $e_3$  axis. In this case they are only displaced a maximum at the 43 seconds point of 3.5 cm to the right of the  $e_3$  axis. This smaller displacement leads to much smaller required control torques, T1 and TG1. The TG4 torque is also reduced from the original 7 N-M to less than a 4 N-M initial torque with almost no overshoot. This new case also reduces T2 and smooths out T3. These reduced internal and external motor torques provide comparable reductions in the constraint torques

The results of this case clearly show a significant improvement in the required external and internal control torques. Reducing the response rates makes a big improvement, while only having to extend the required maneuvering time shortly.

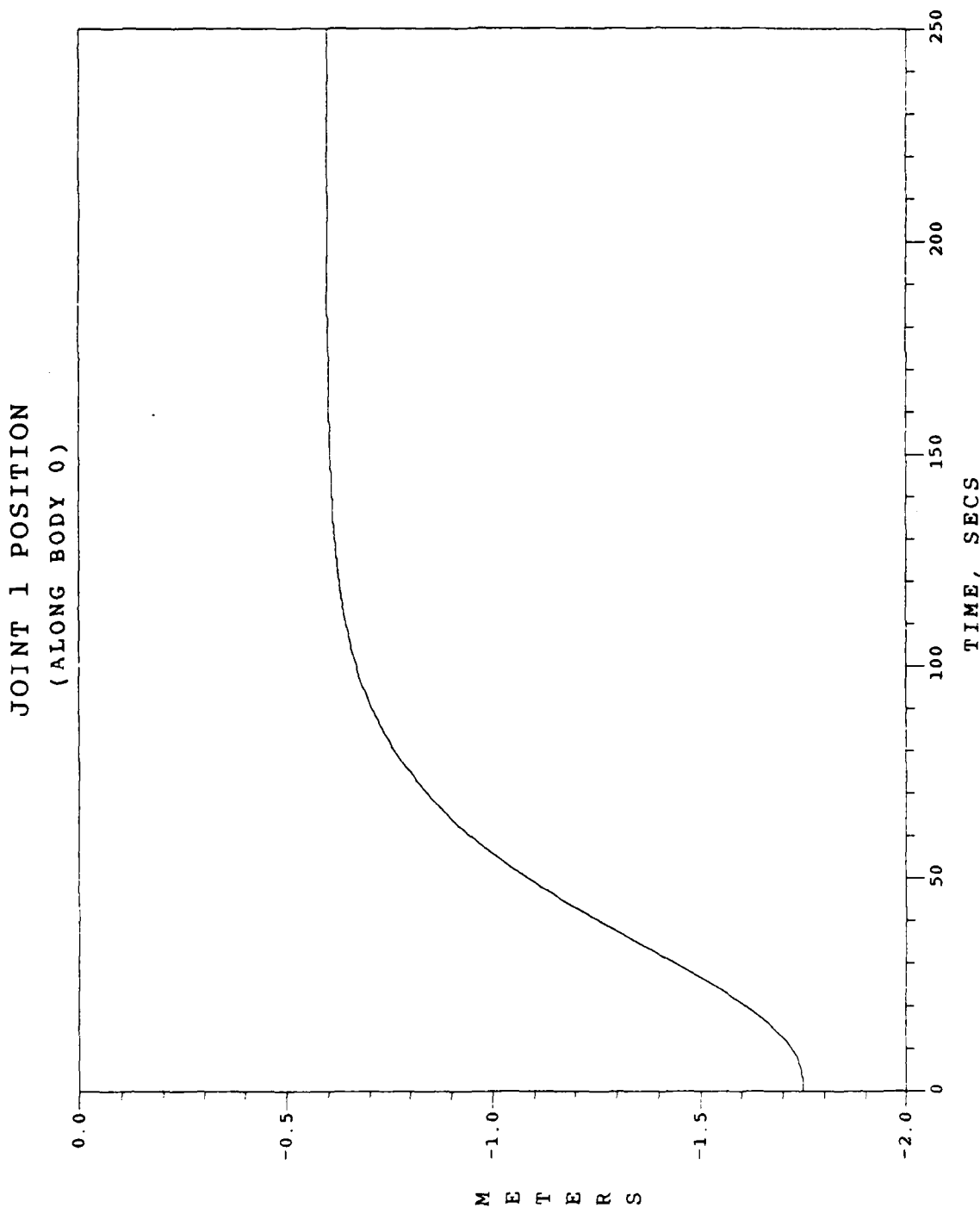


Fig. 6. Deployment Phase / Case 1  
Joint 1 Position

JOINT 1 RELATIVE VELOCITY  
(ALONG BODY 0)

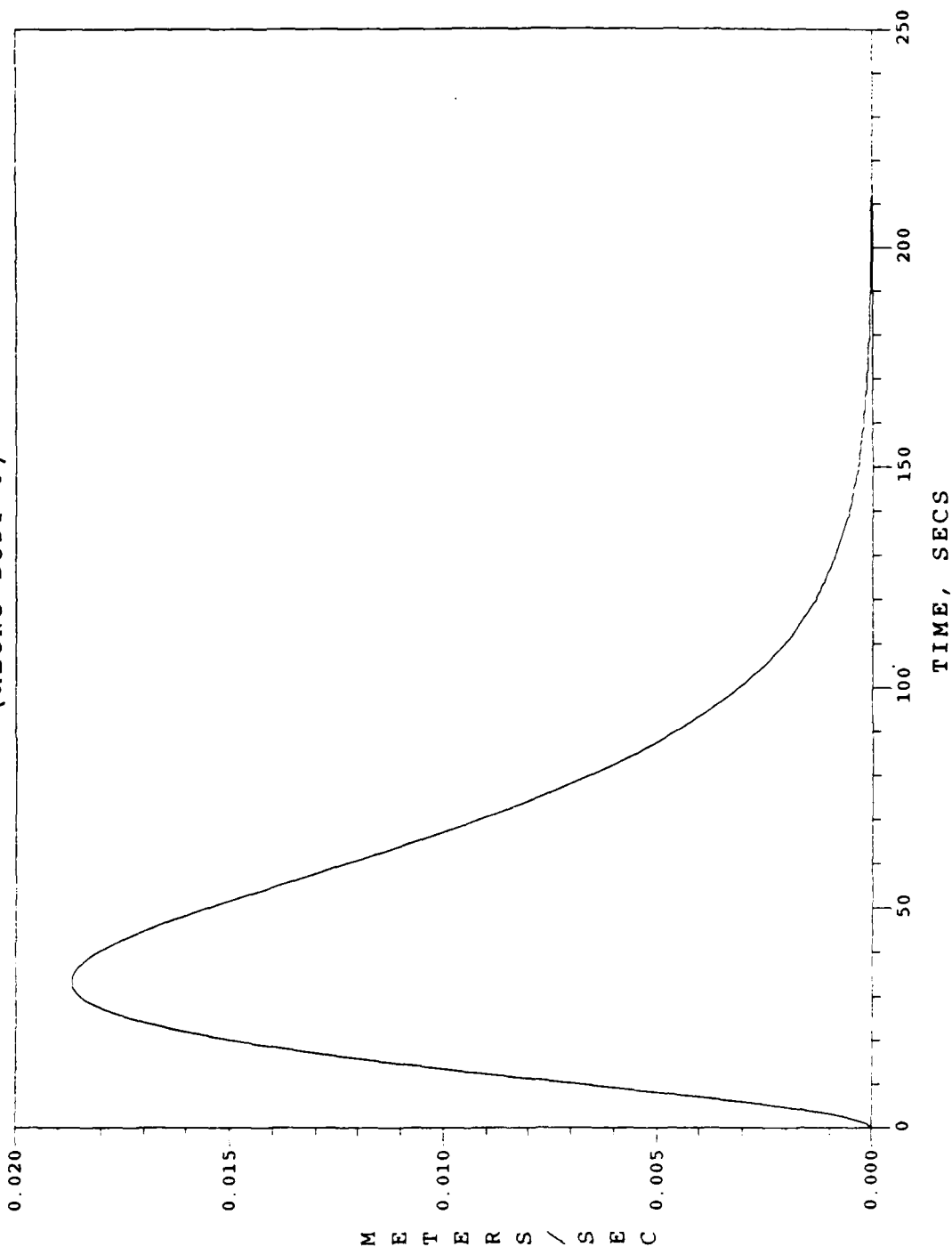


Fig 7. Deployment Phase / Case 1  
Joint 1 Relative Velocity

JOINT 1 RELATIVE ACCELERATION  
(ALONG BODY 0)

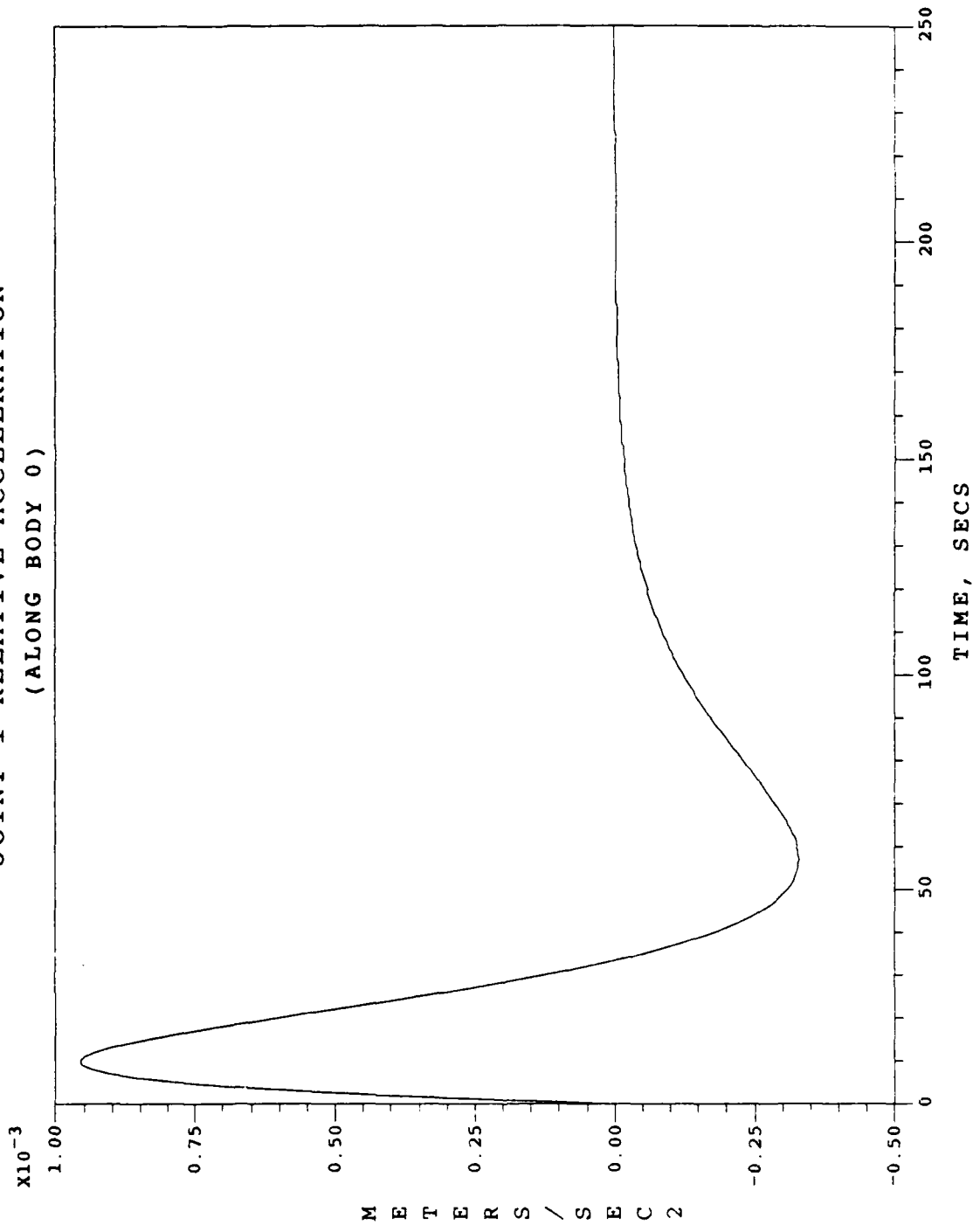


Fig. 8. Deployment Phase / Case 1  
Joint 1 Relative Acceleration

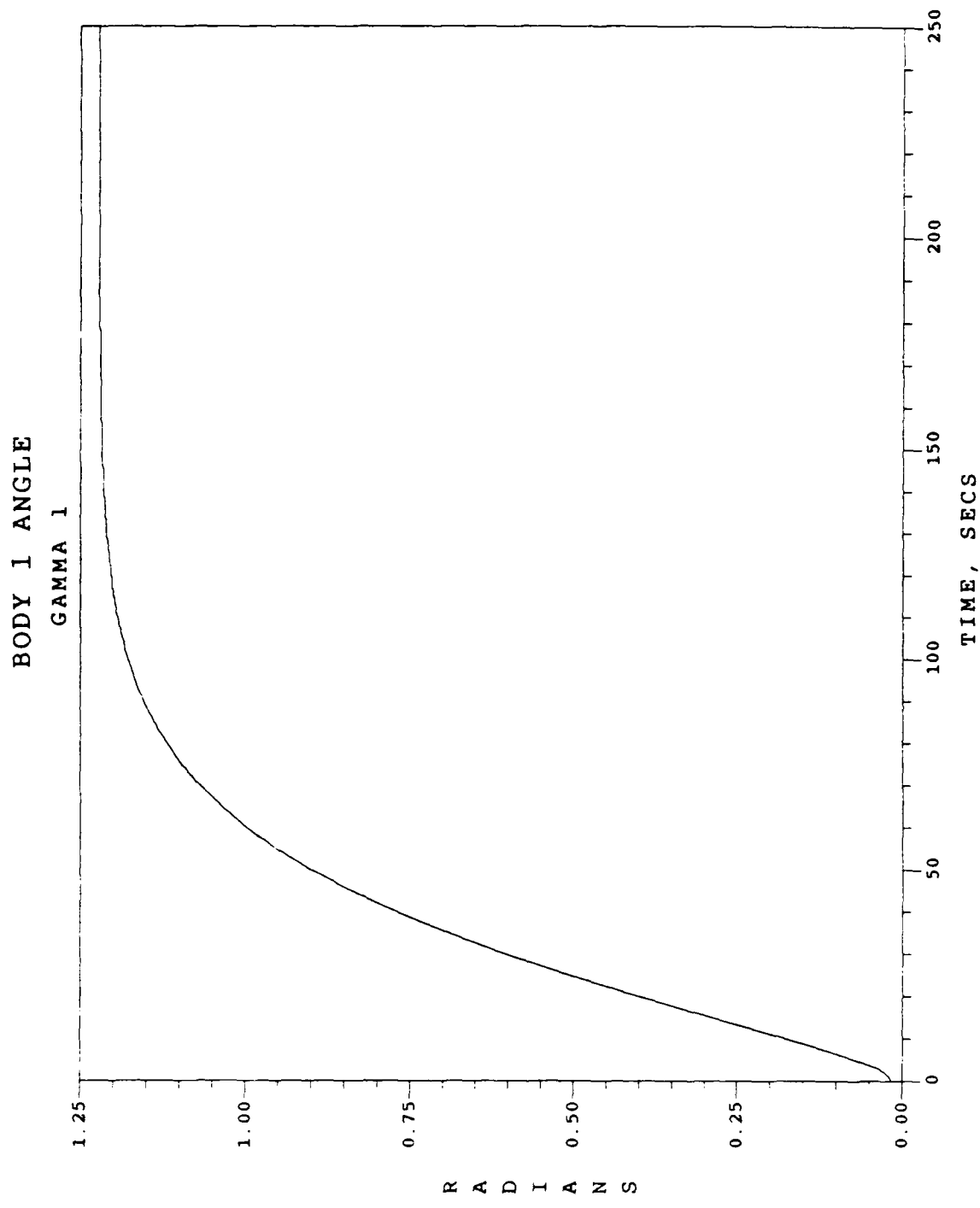


Fig. 9. Deployment Phase / Case 1  
Body 1  $\gamma_1$  History

BODY 1 RATE  
GAMMA DOT 1

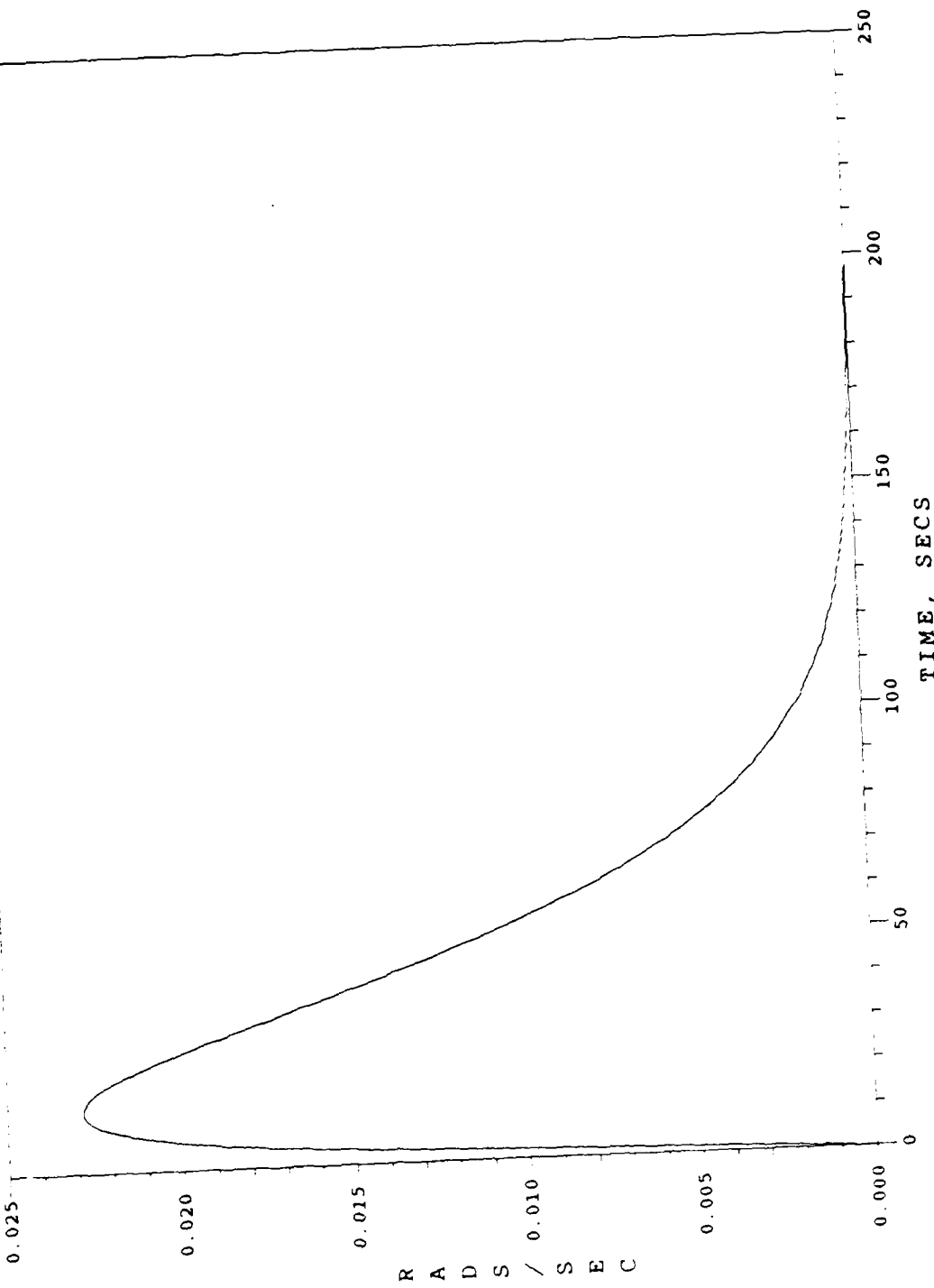


Fig. 10. Deployment Phase / Case 1  
Boay 1  $\dot{\gamma}$  History

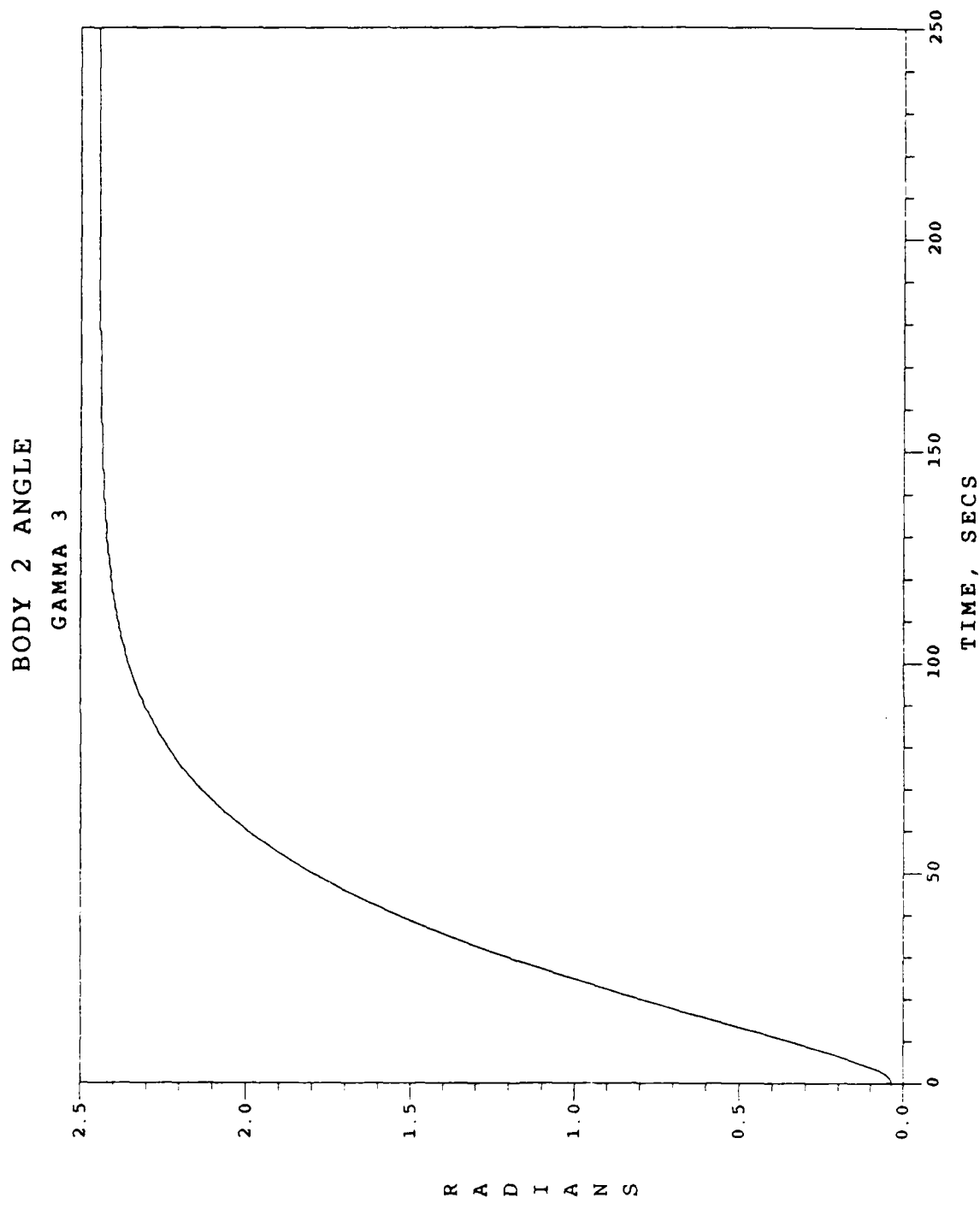


Fig. 11. Deployment Phase / Case 1  
Body 2  $\gamma_3$  History

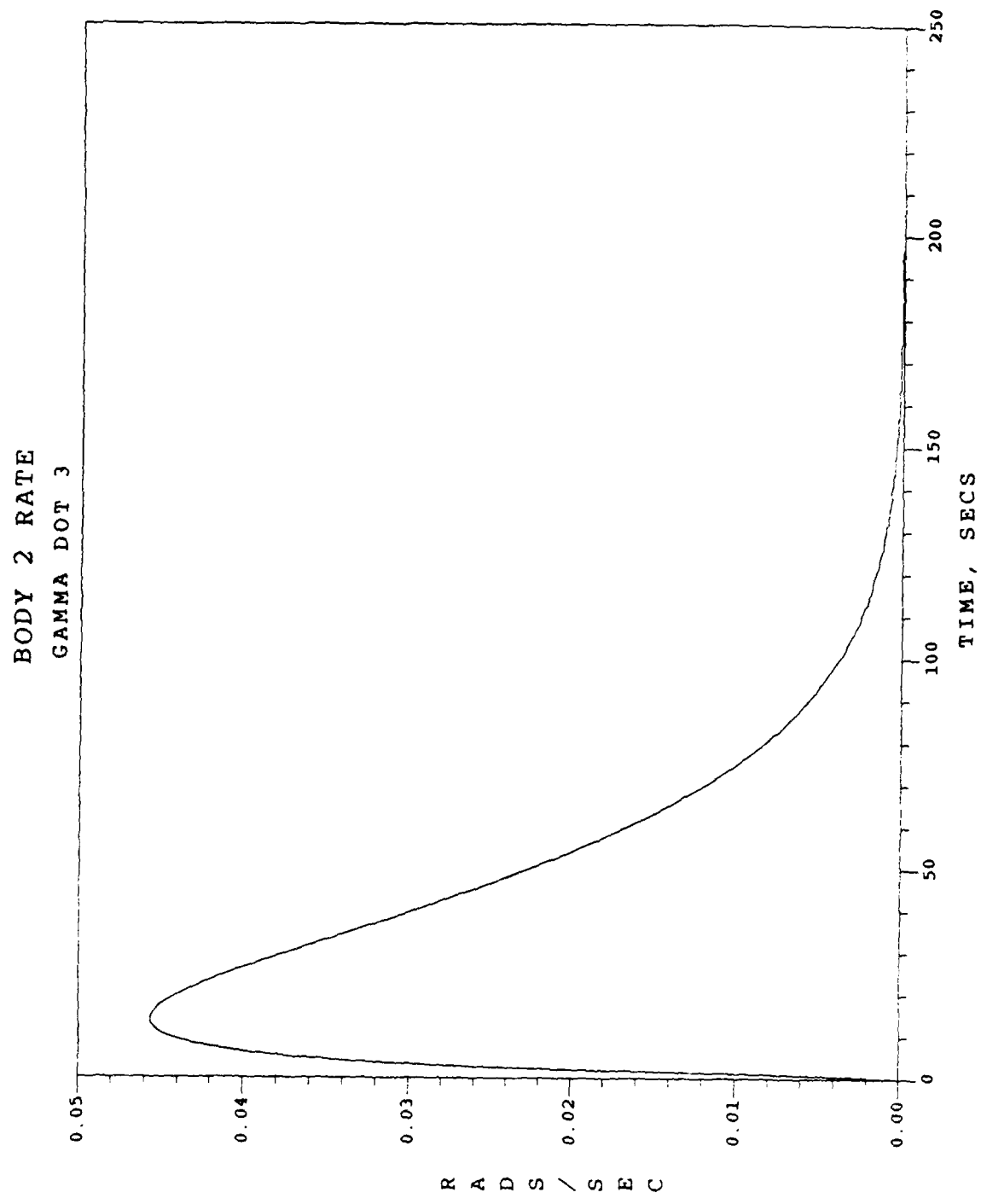


Fig. 12. Deployment Phase / Case 1  
Body 2  $\dot{\gamma}_3$  History

INTERNAL MOTOR TORQUE TG1  
(AT JOINT 1)

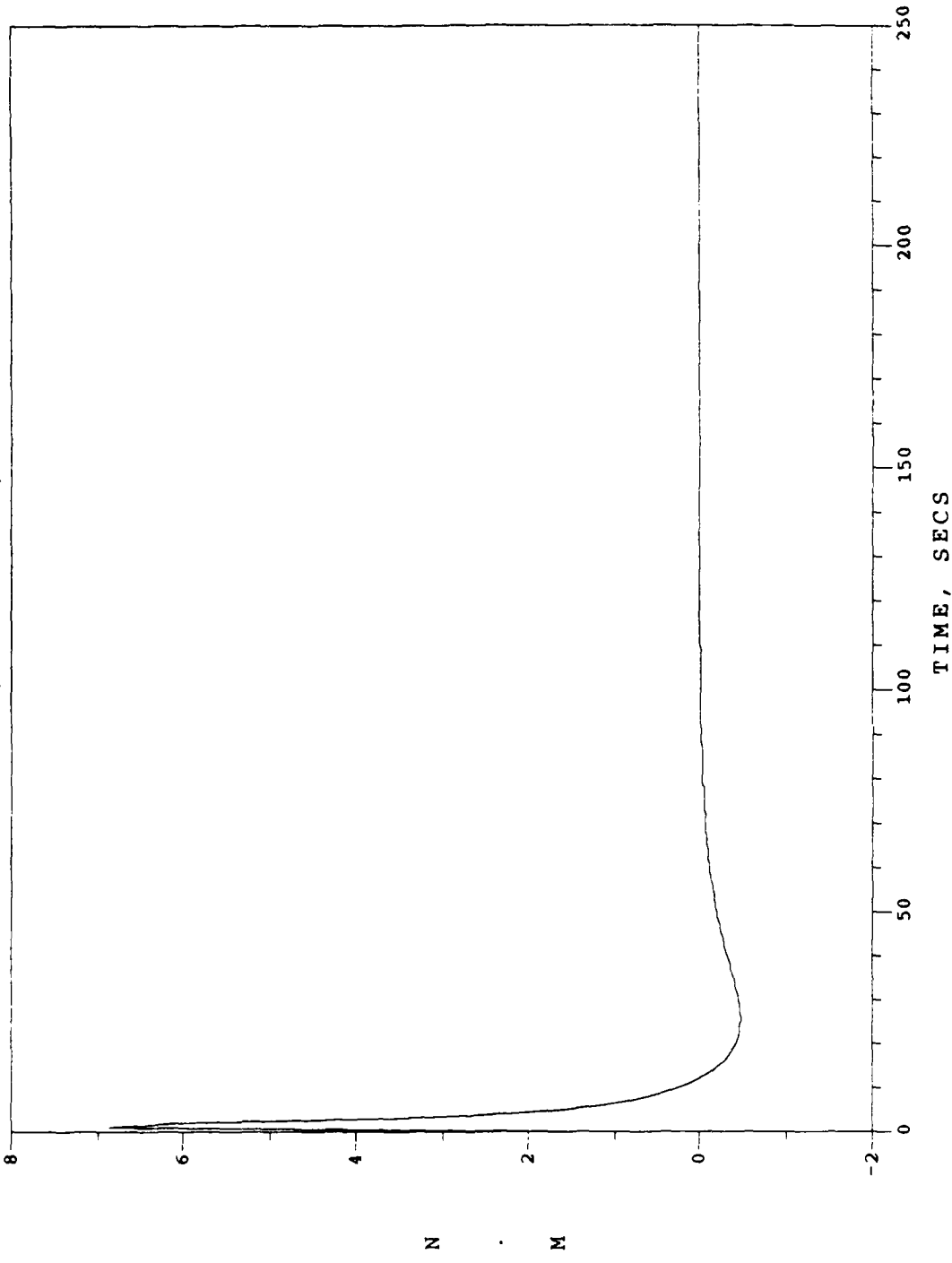


Fig. 13. Deployment Phase / Case 1  
Internal Motor Torque TG1

INTERNAL MOTOR TORQUE TG2  
(AT JOINT 1)

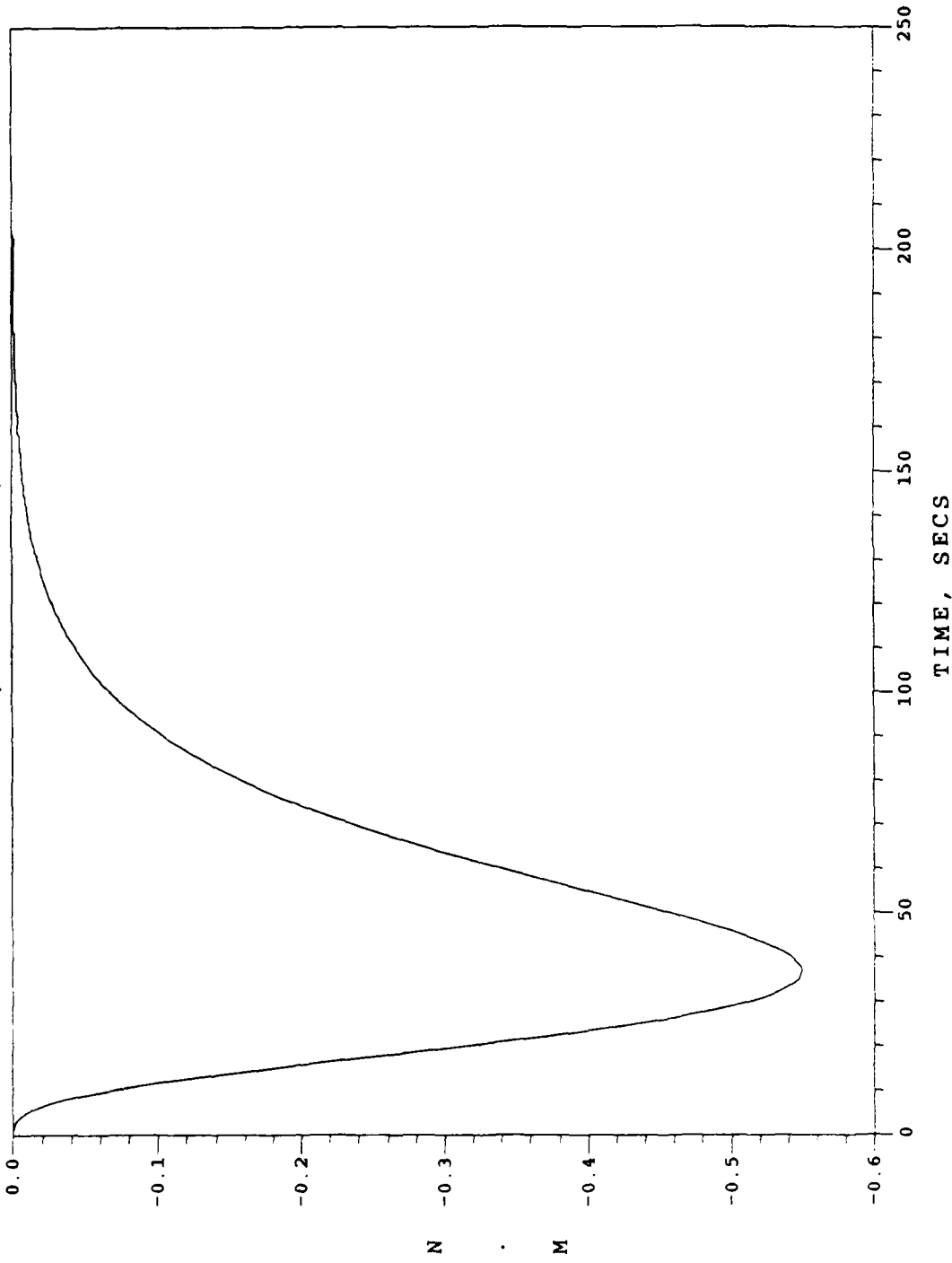


Fig. 14. Deployment Phase / Case 1  
Internal Motor Torque TG2

INTERNAL MOTOR TORQUE TG3  
(AT JOINT 2)

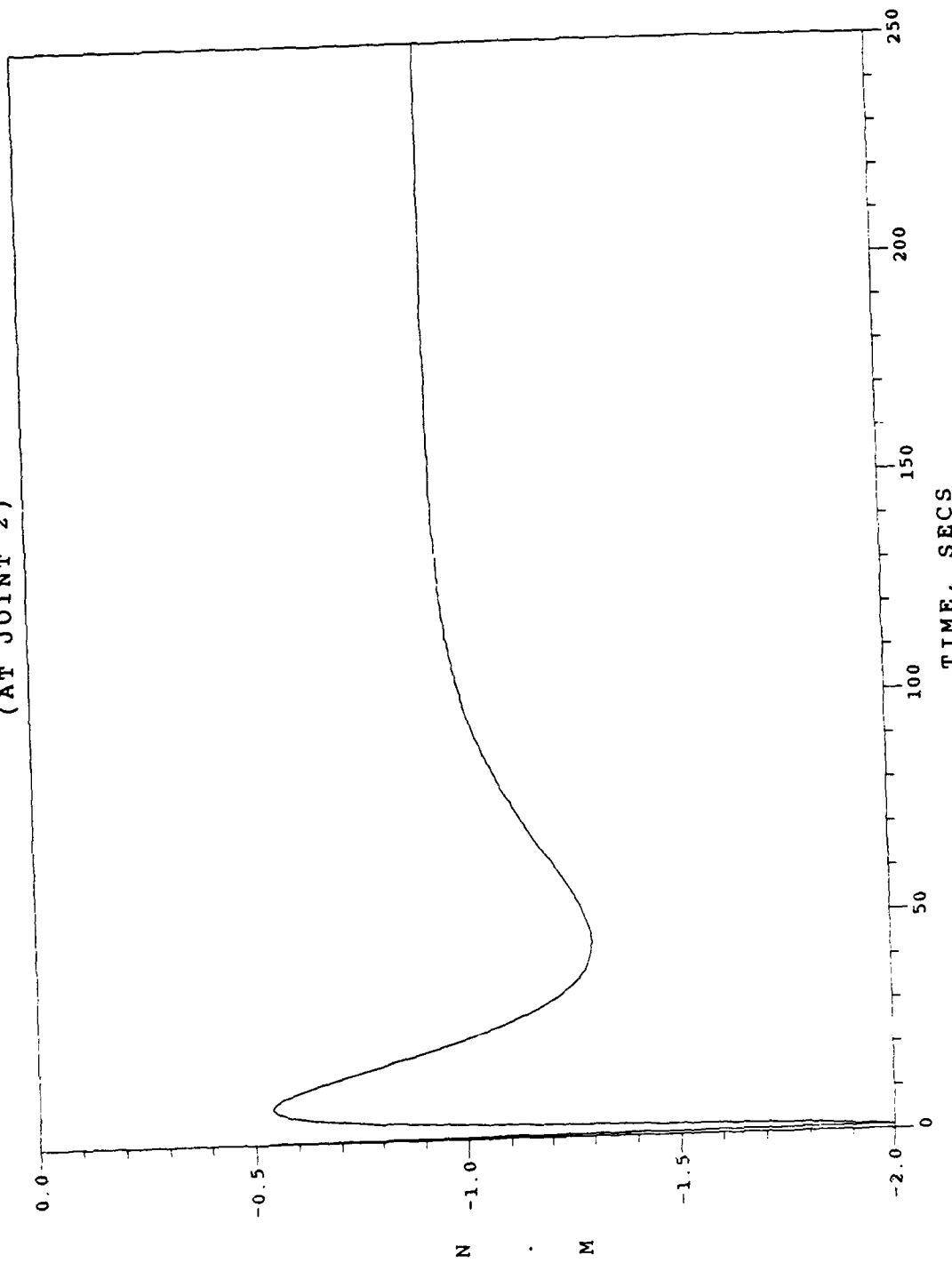


Fig. 15 Deployment Phase / Case 1  
Internal Motor Torque TG3

INTERNAL MOTOR TORQUE TG4  
(AT JOINT 3)

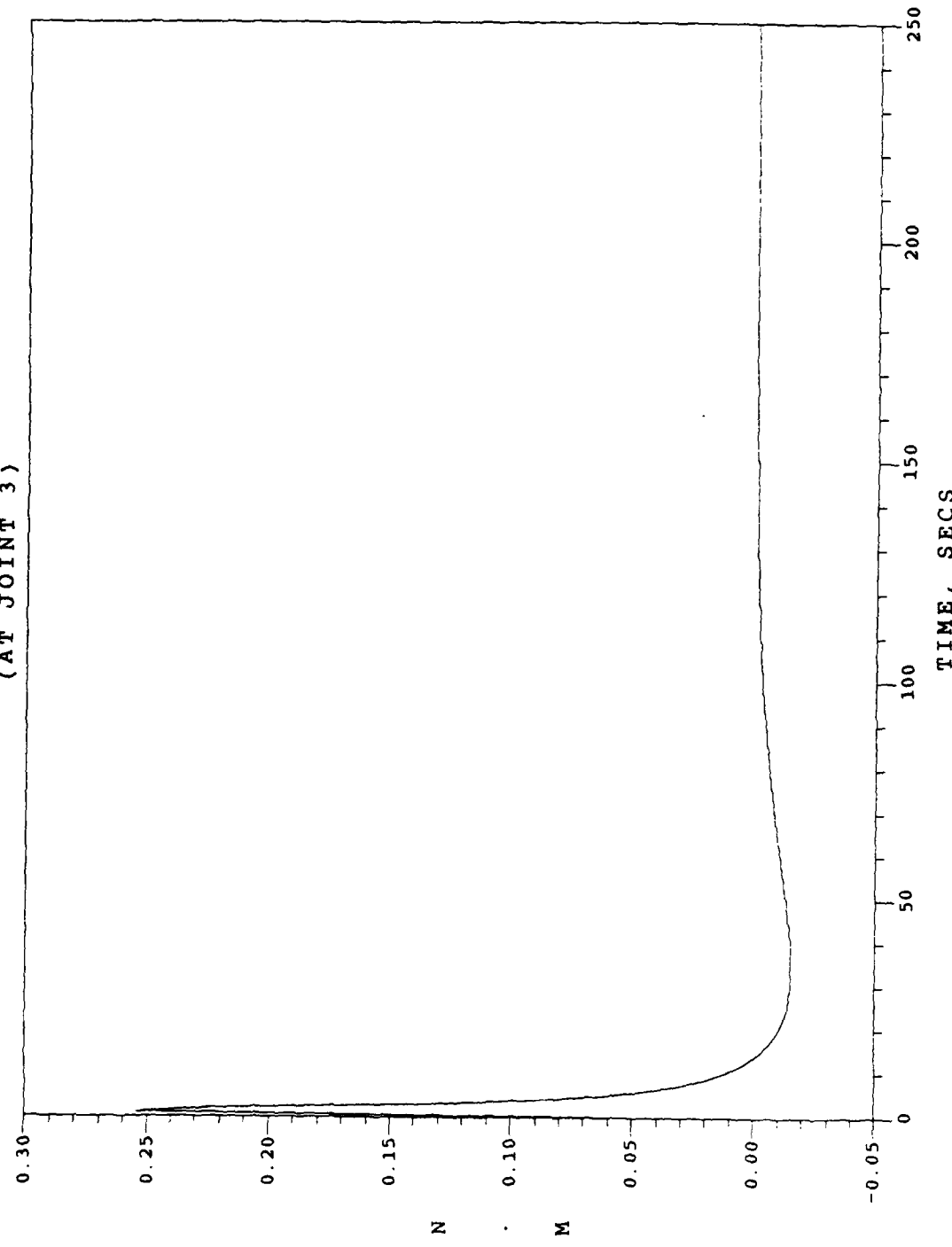


Fig. 16. Deployment Phase / Case 1  
Internal Motor Torque TG4

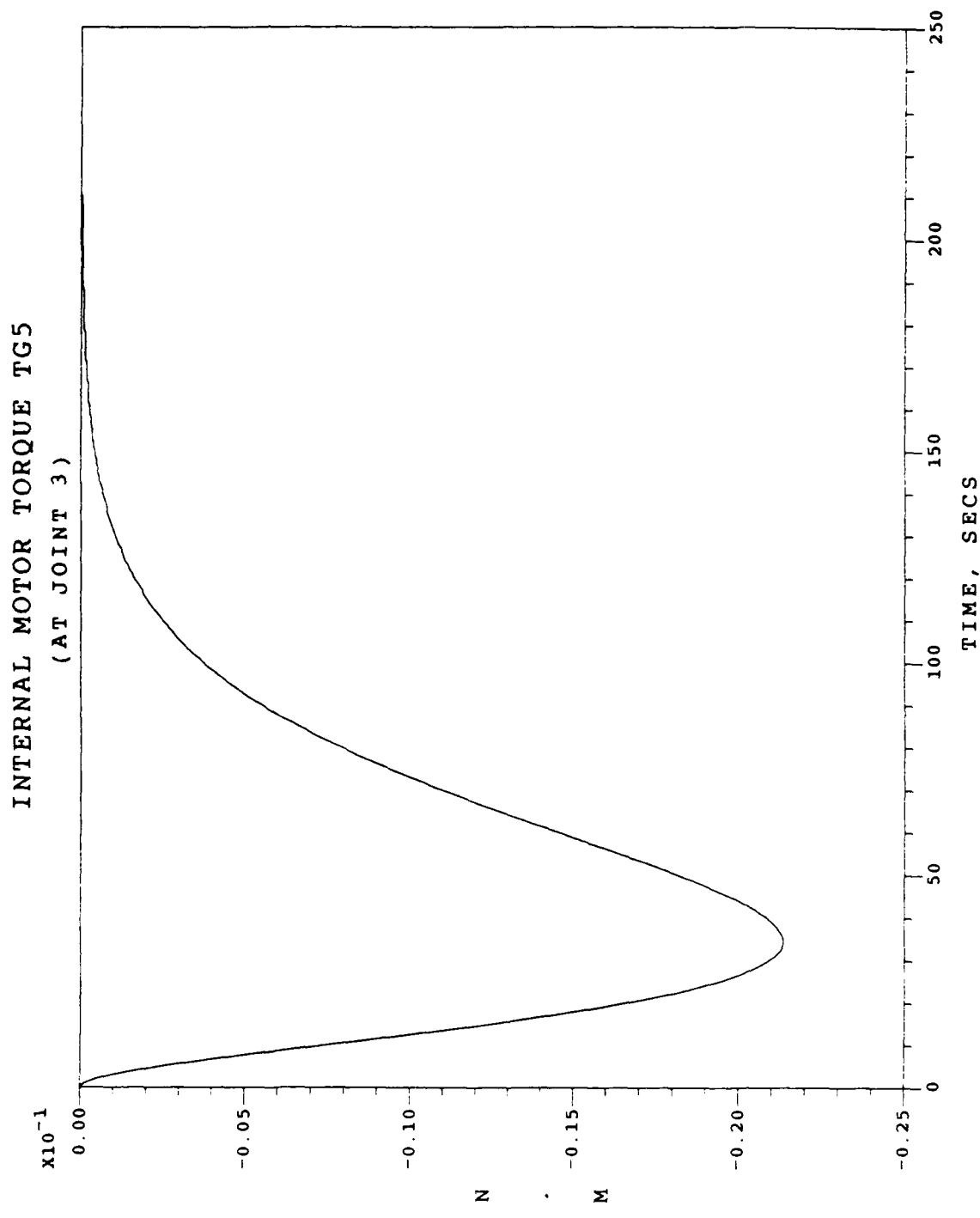


Fig. 17. Deployment Phase / Case 1  
Internal Motor Torque TG5

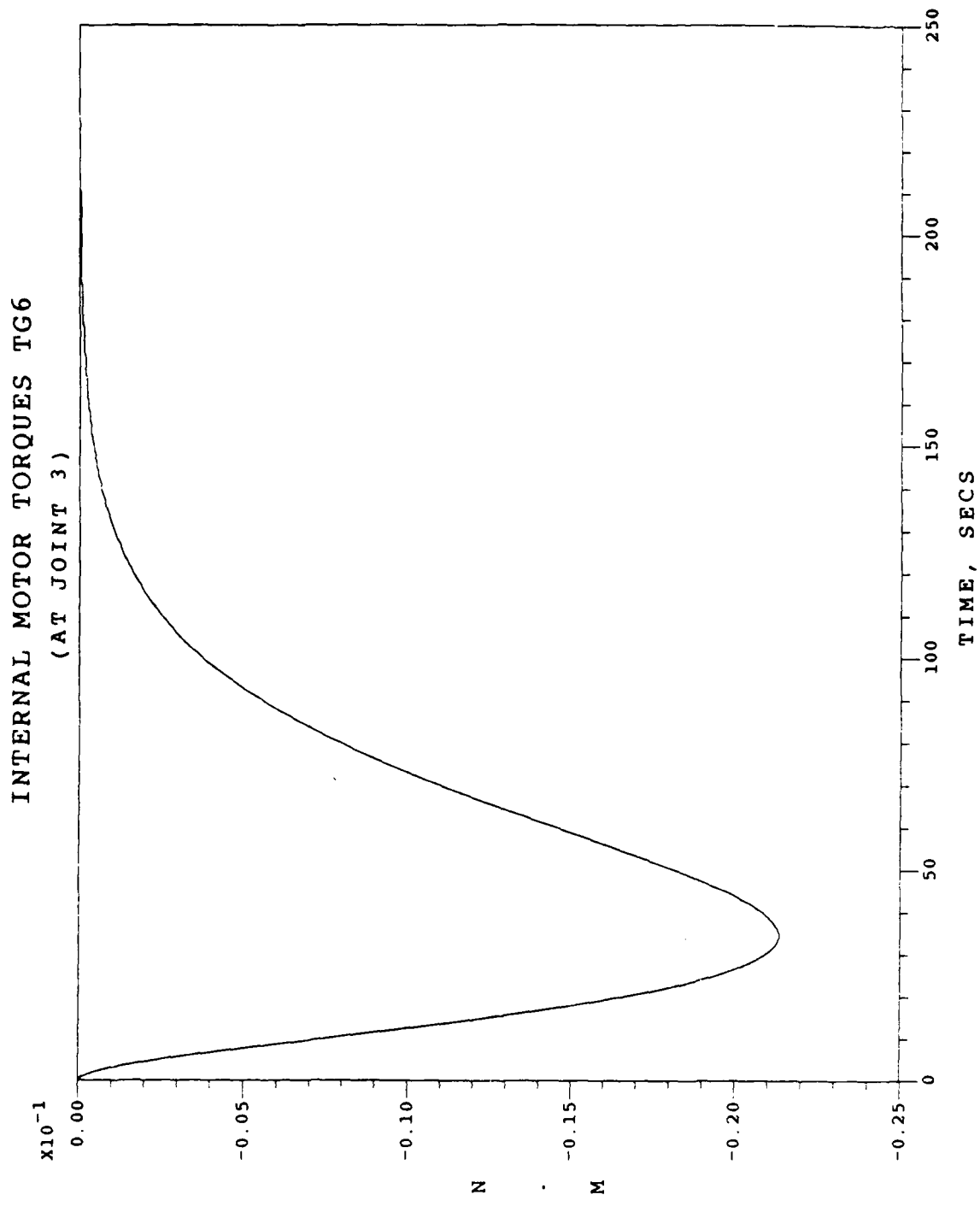


Fig. 18. Deployment Phase / Case 1  
Internal Motor Torque TG6

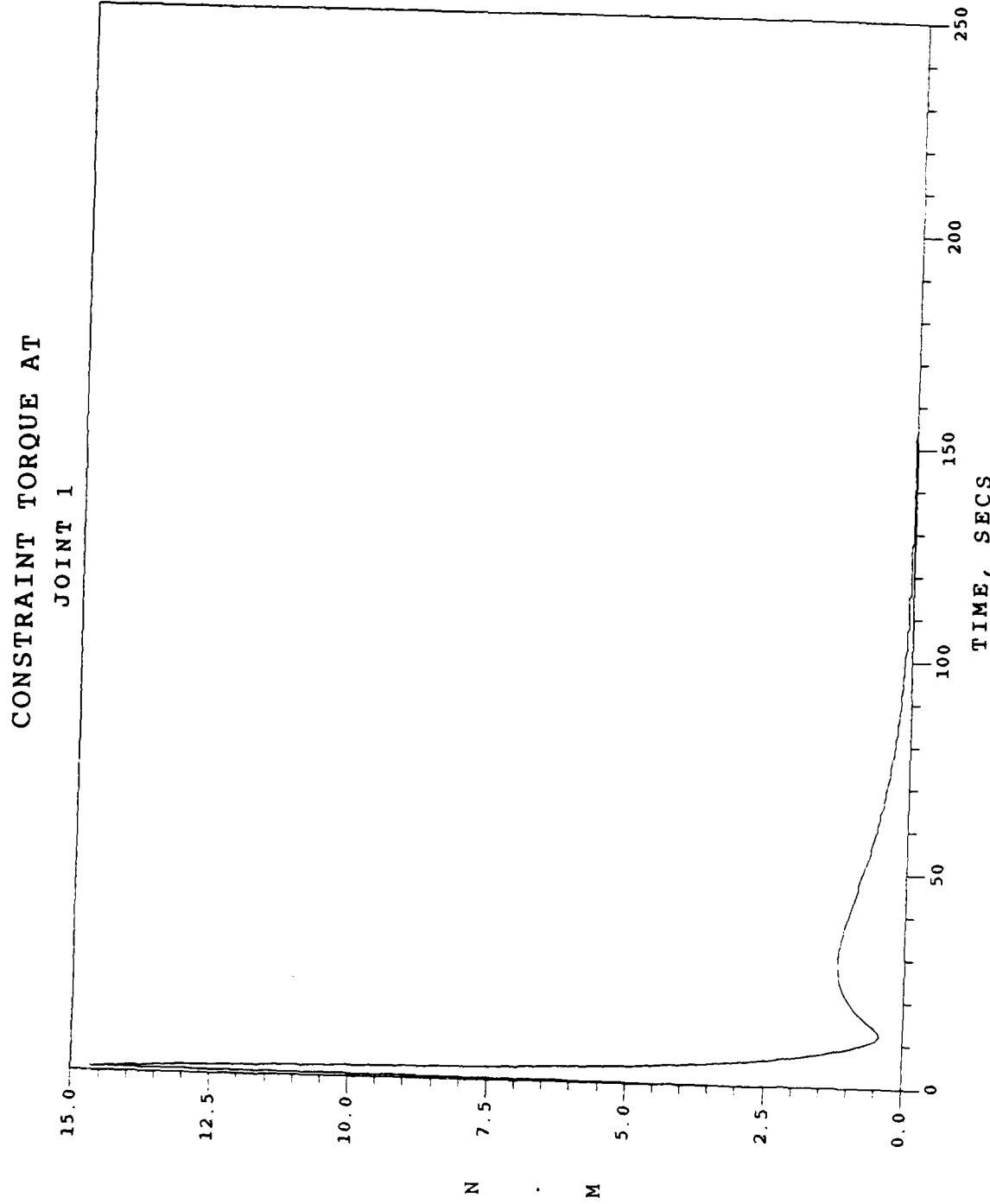


Fig. 19. Deployment Phase / Case 1  
Constraint Torque at Joint 1

CONSTRAINT TORQUE AT  
JOINT 2

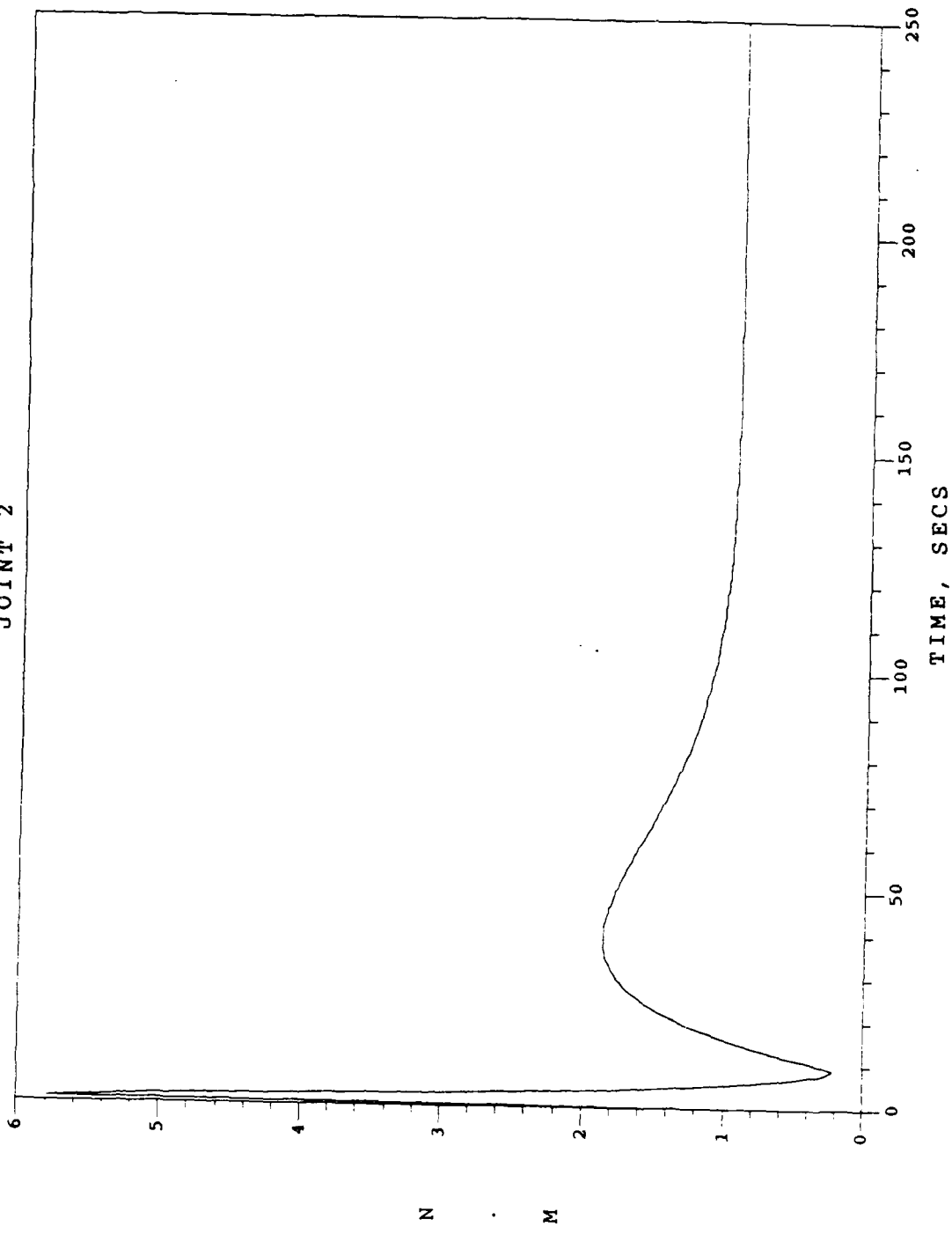


Fig. 20. Deployment Phase / Case 1  
Constraint Torque at Joint 2

CONSTRAINT TORQUE AT  
JOINT 3

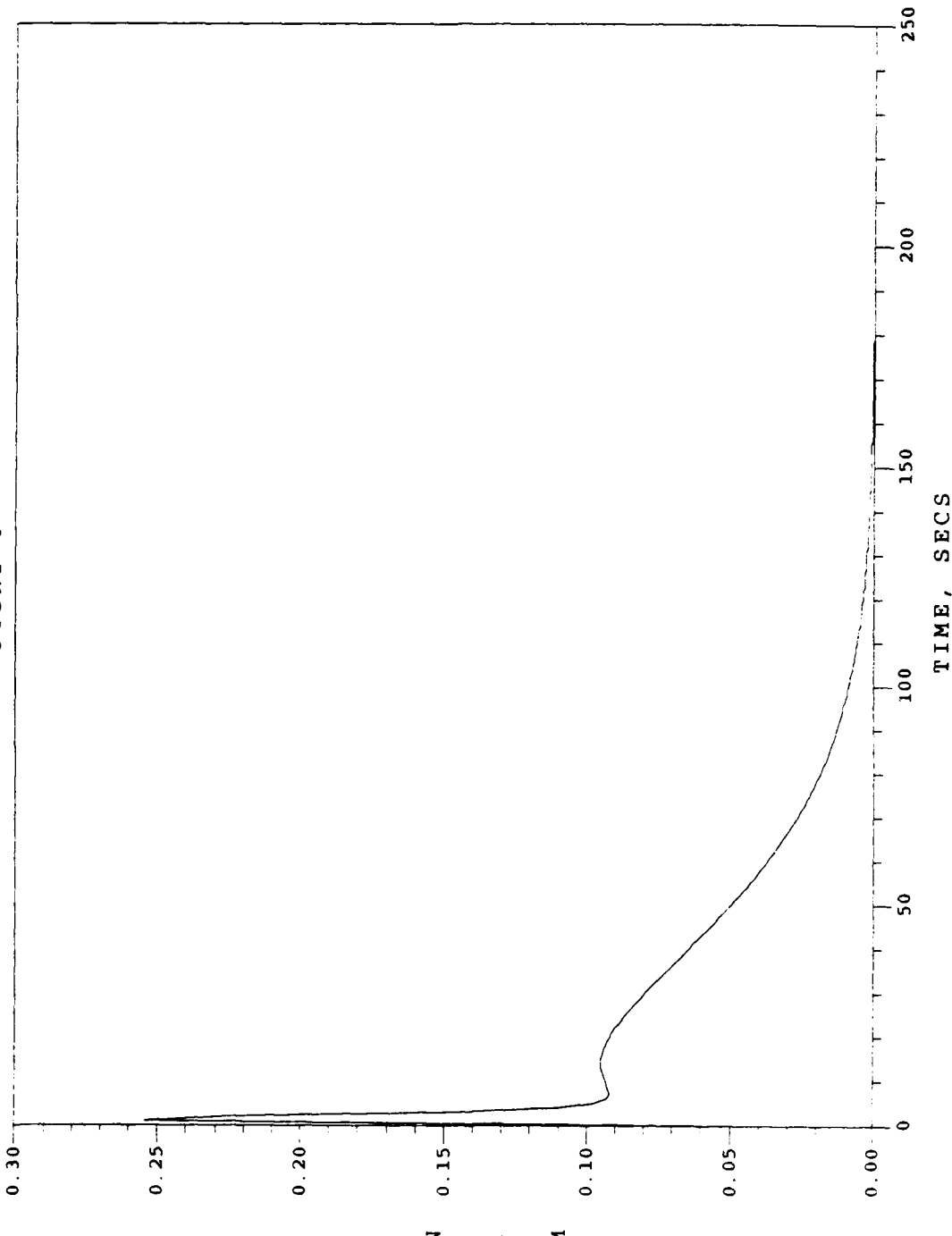


Fig. 21. Deployment Phase / Case 1  
Constraint Torque at Joint 3

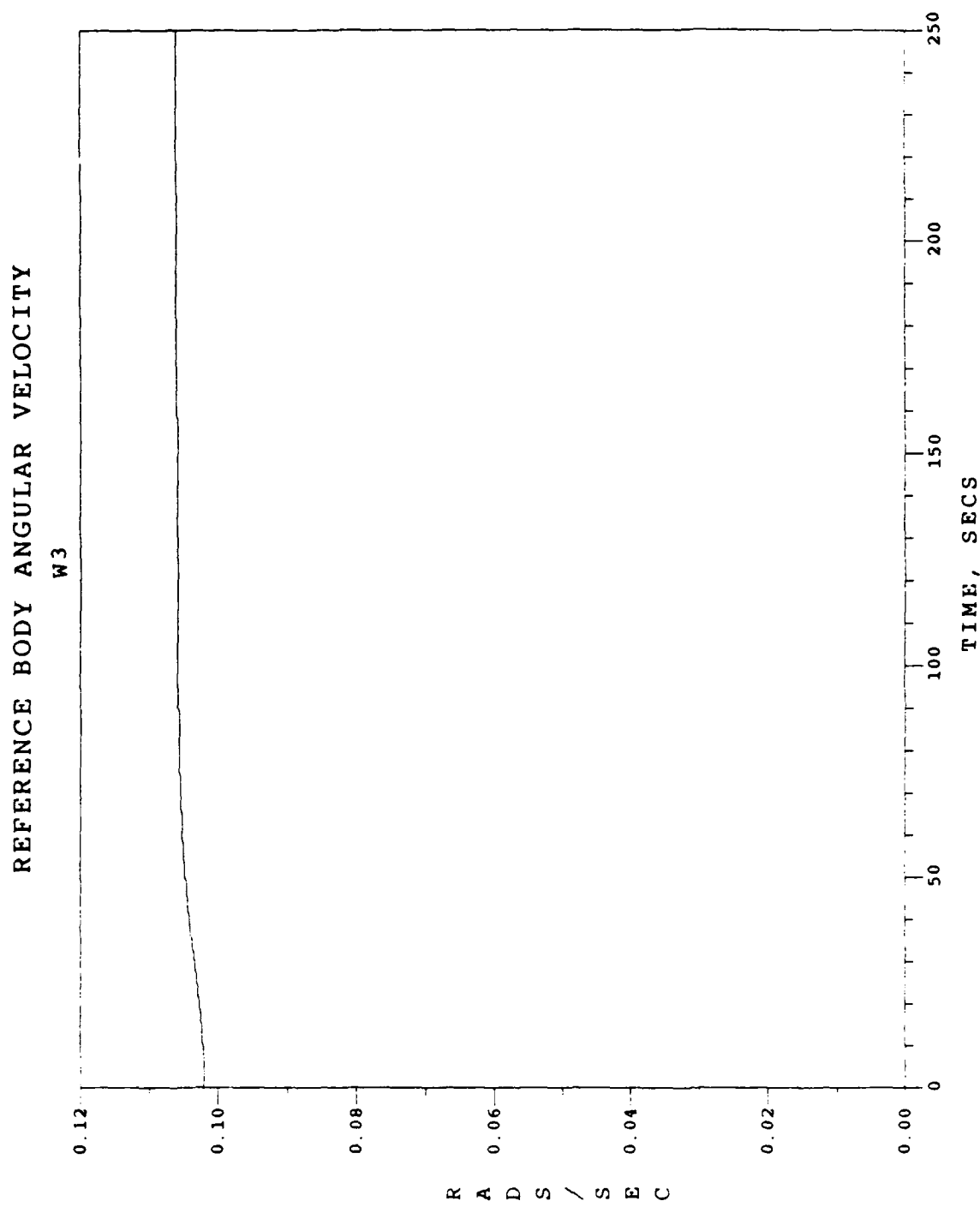


Fig. 22. Deployment Phase / Case 1  
Body 0  $\omega_{\alpha}$  History

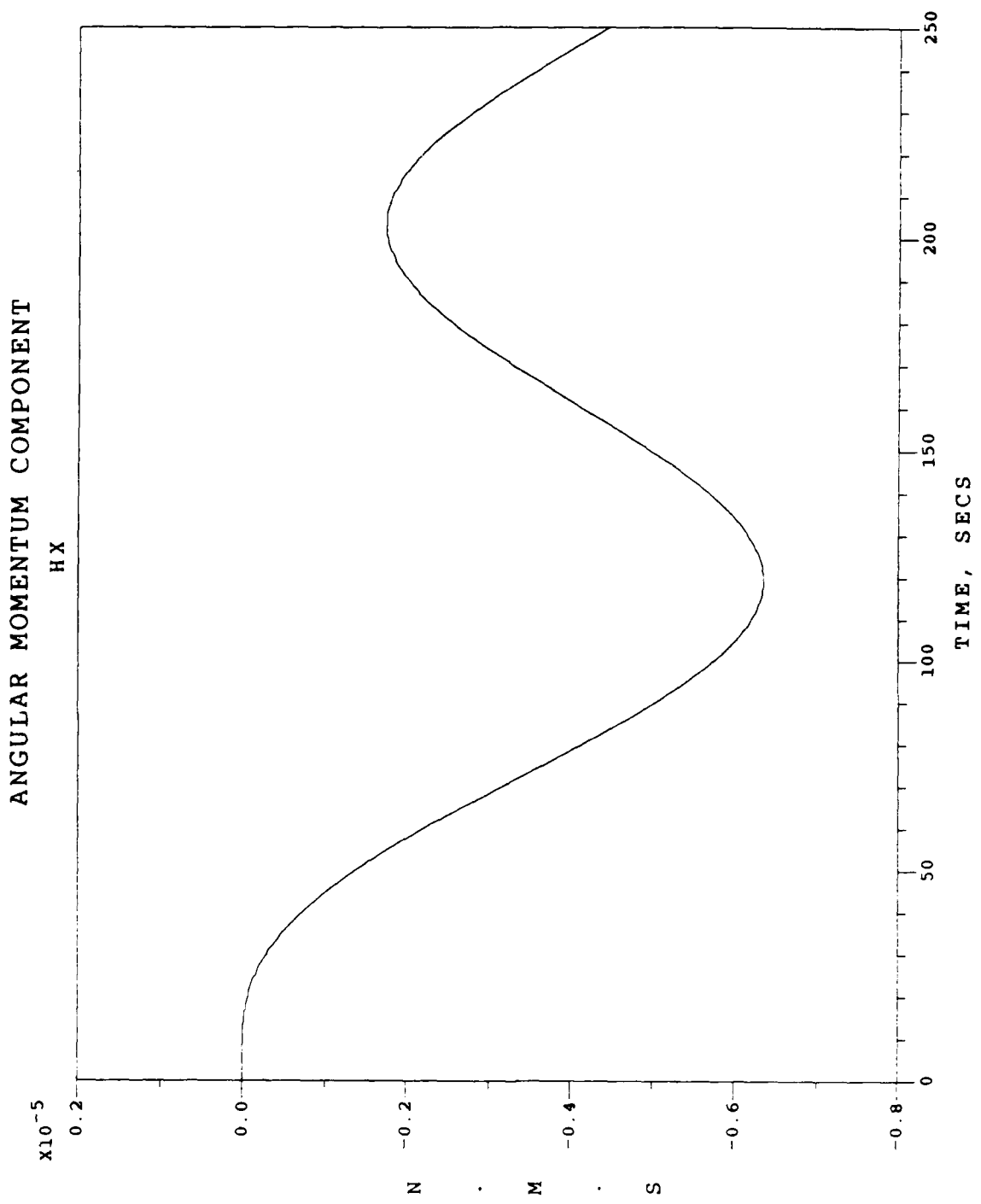


Fig. 23. Deployment Phase / Case 1  
Angular Momentum Component HX

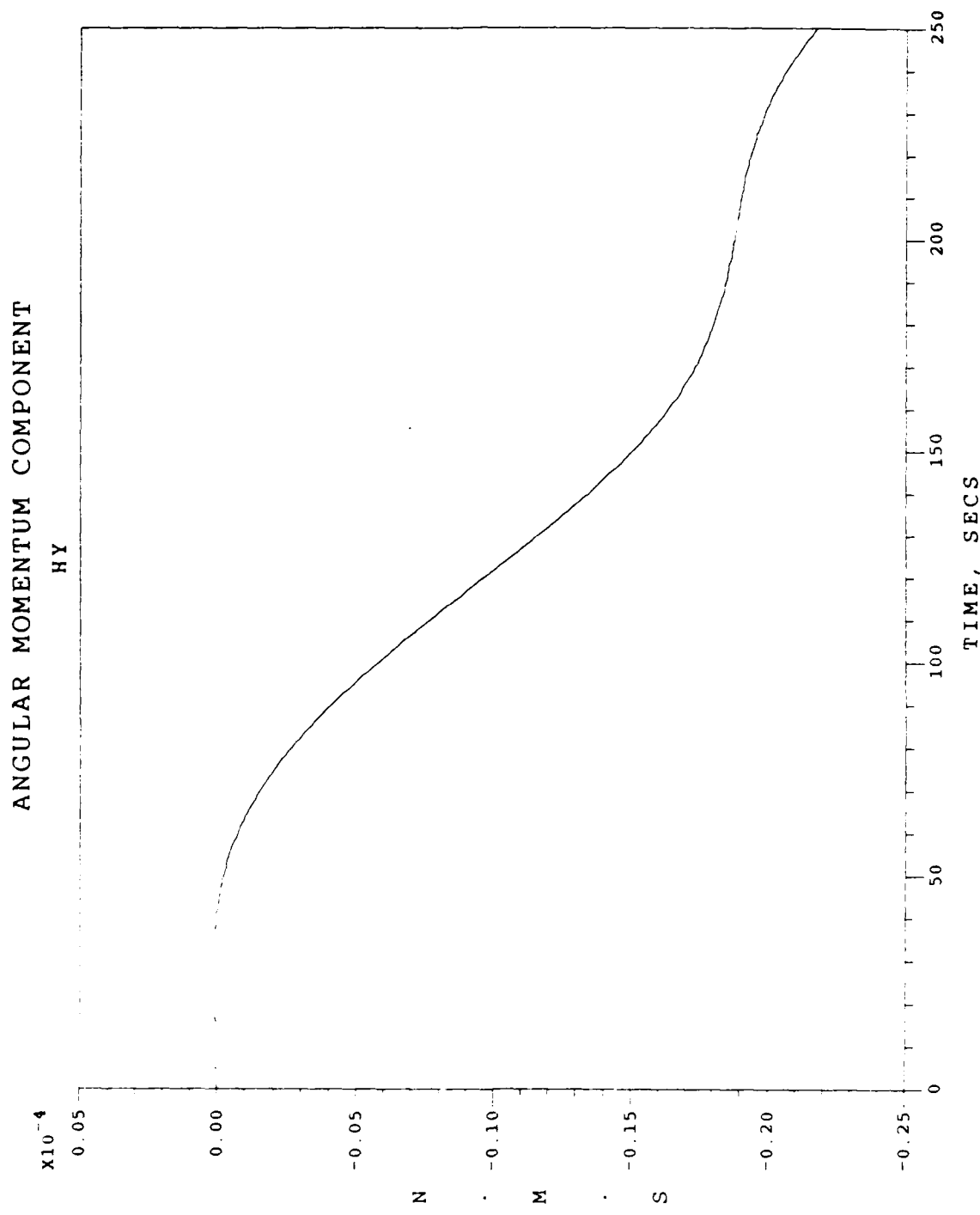


Fig. 24. Deployment Phase / Case 1  
Angular Momentum Component HY

ANGULAR MOMENTUM COMPONENT

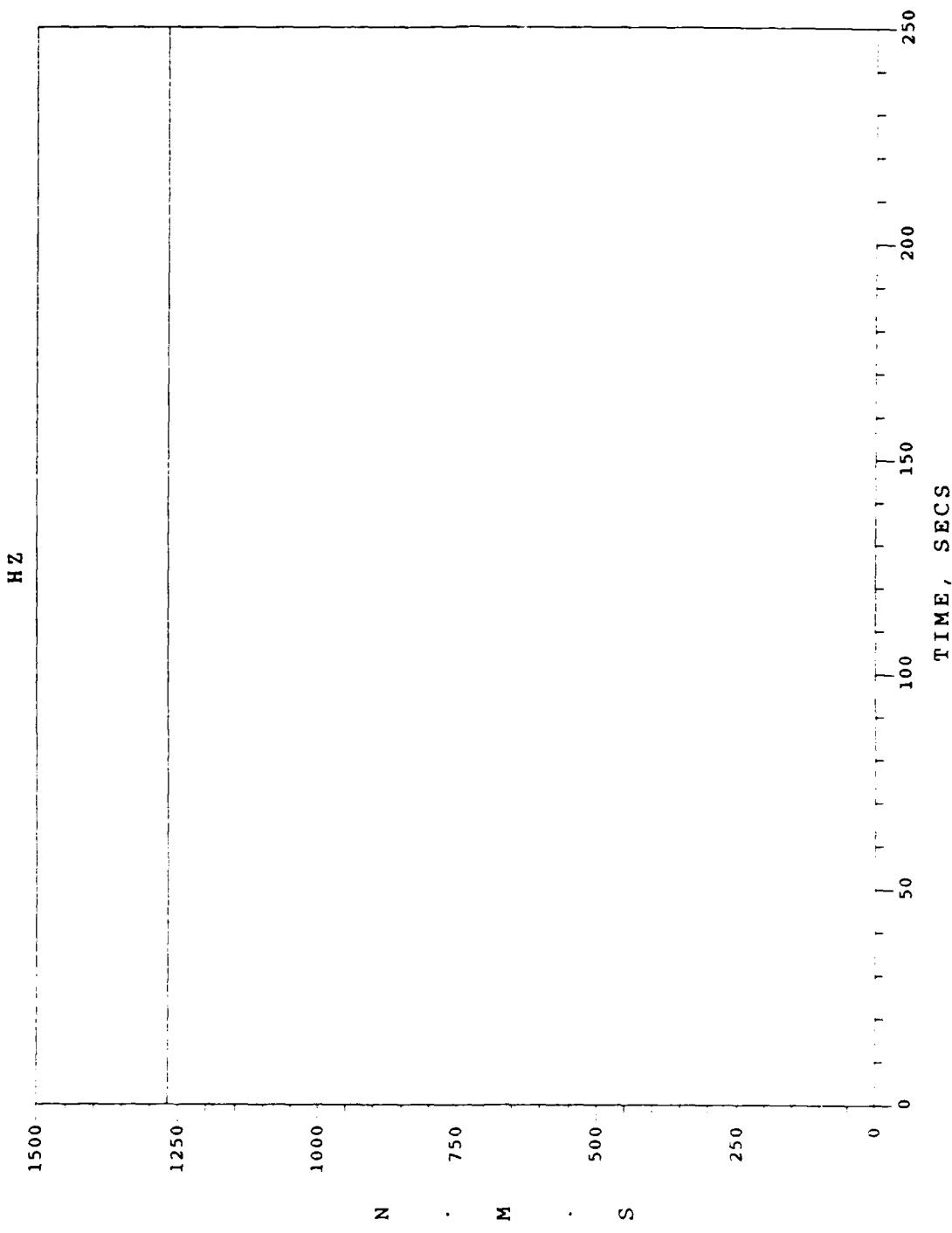


Fig. 25. Deployment Phase / Case 1  
Angular Momentum Component HZ

TOTAL SYSTEM ANGULAR MOMENTUM

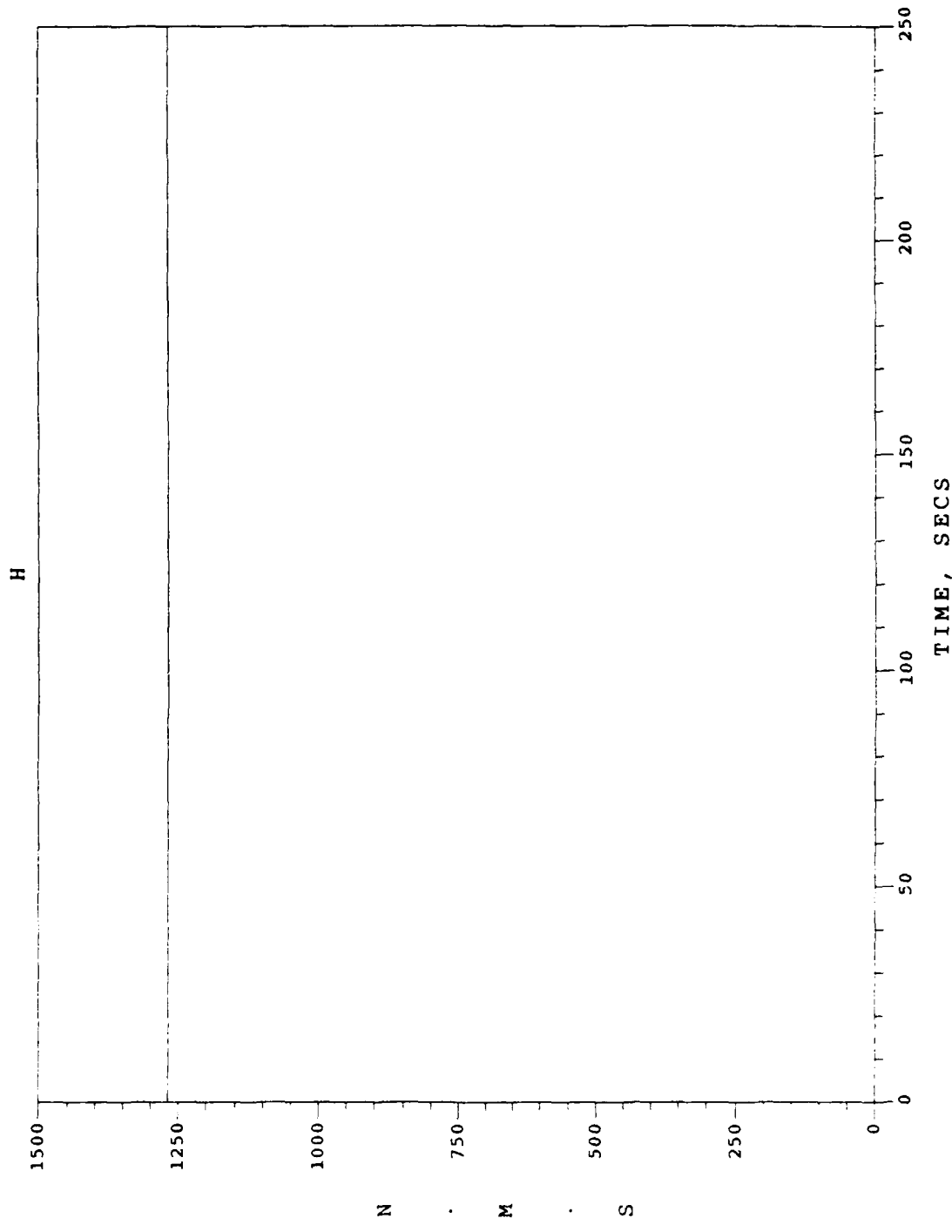


Fig. 26. Deployment Phase / Case 1  
Total System Angular Momentum

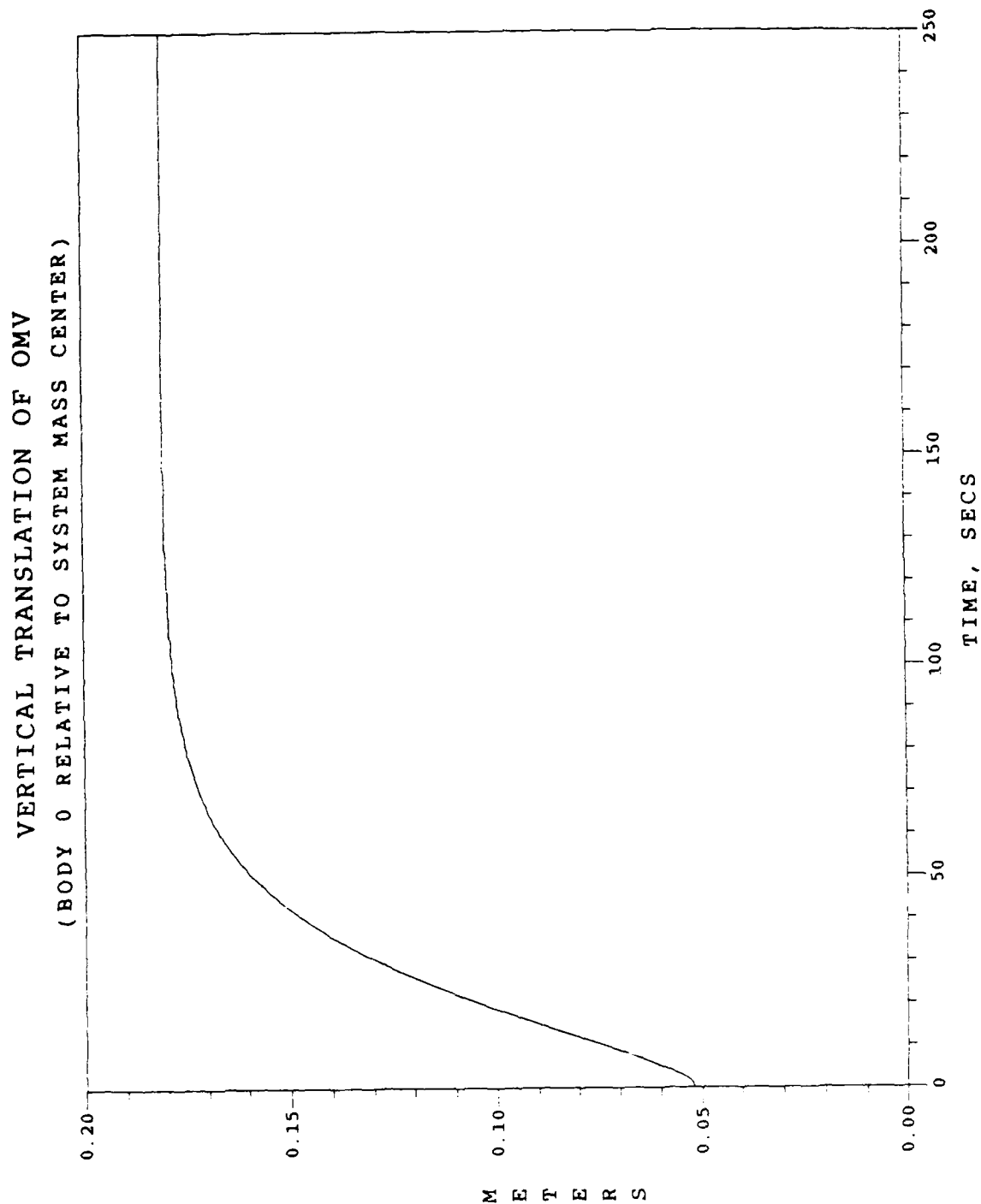


Fig. 27. Deployment Phase / Case 1  
Vertical Translation of OMV

REFERENCE BODY ANGULAR VELOCITY

W<sub>3</sub>

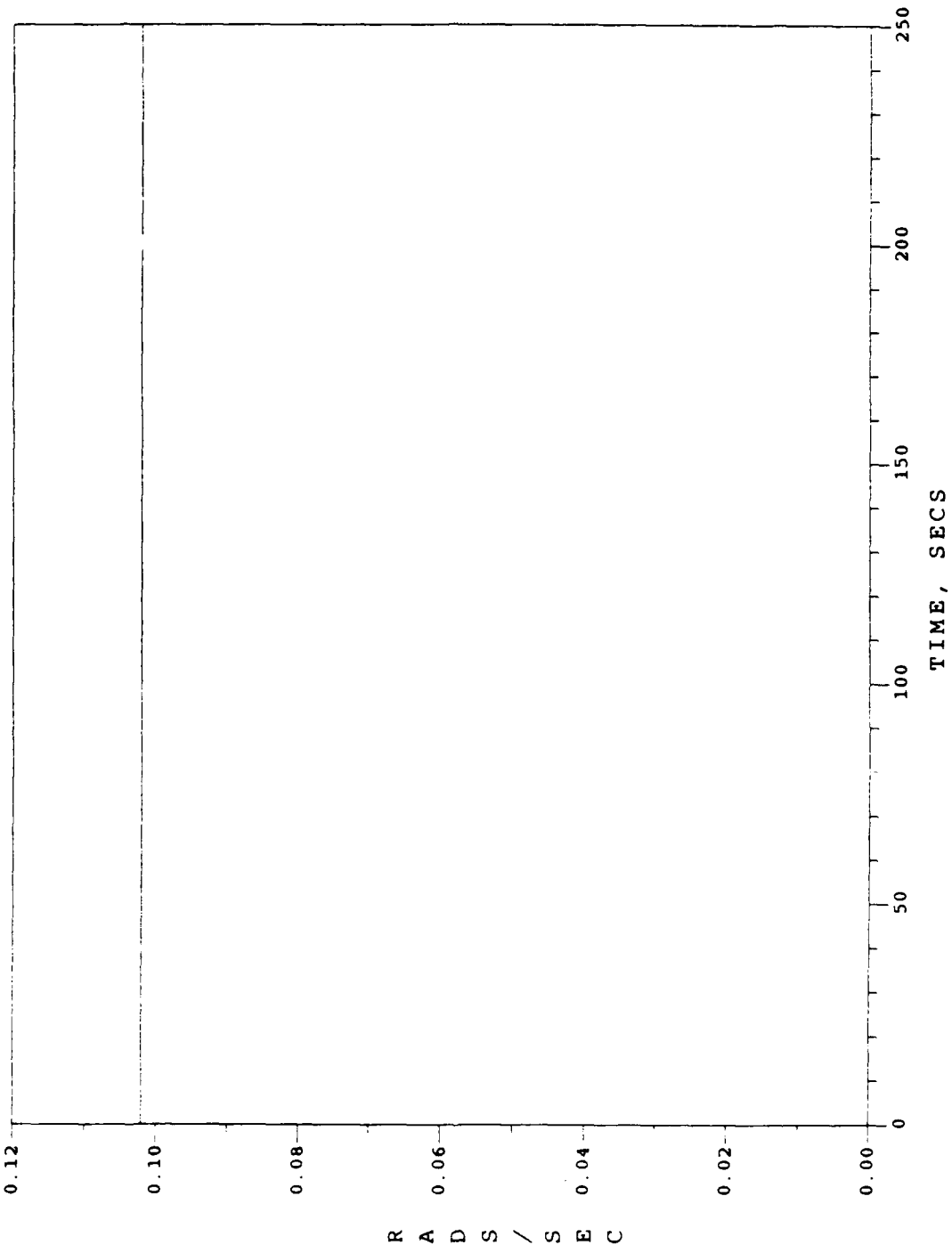


Fig. 28. Deployment Phase / Case 2  
Body 0  $\omega_{03}$  History

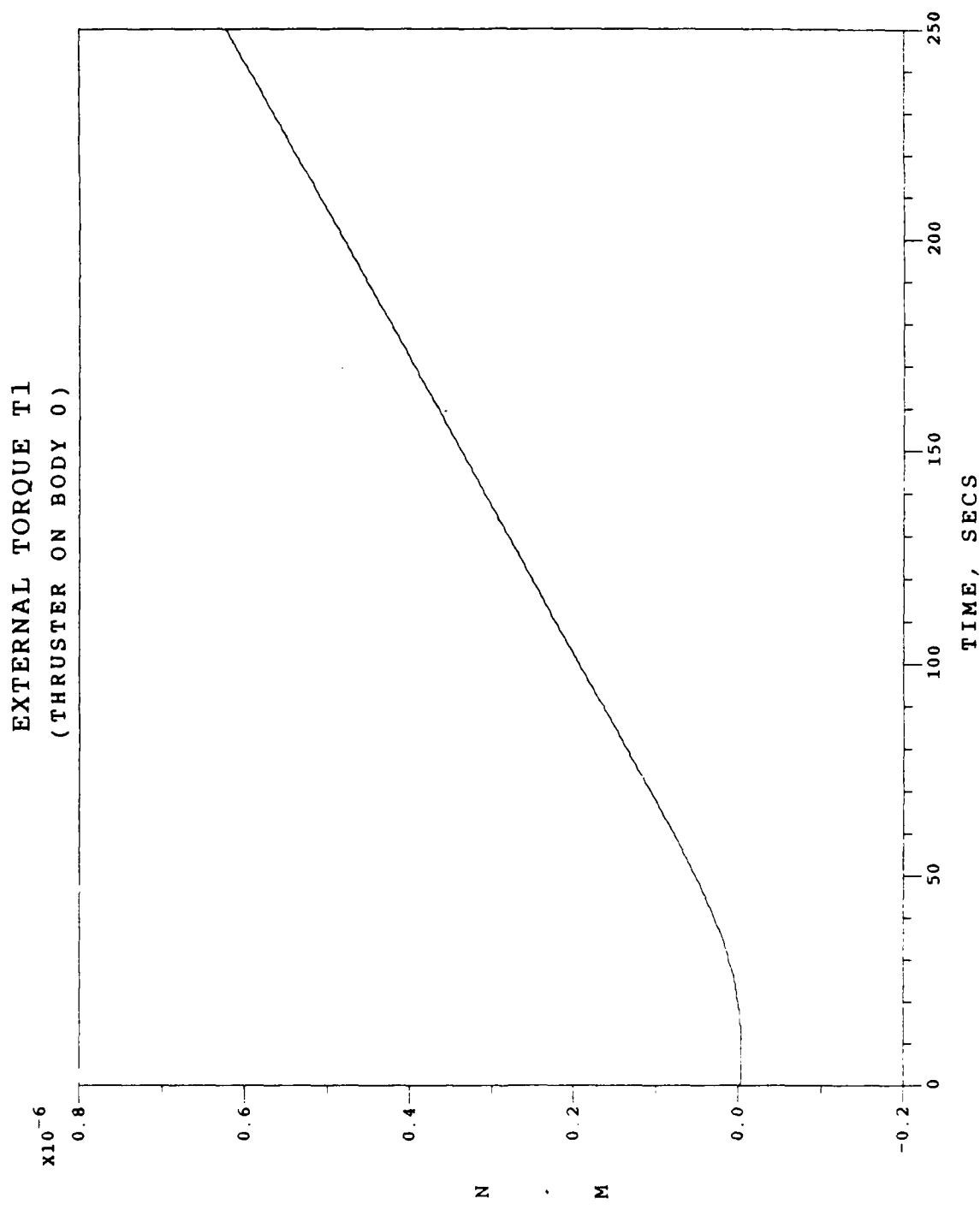
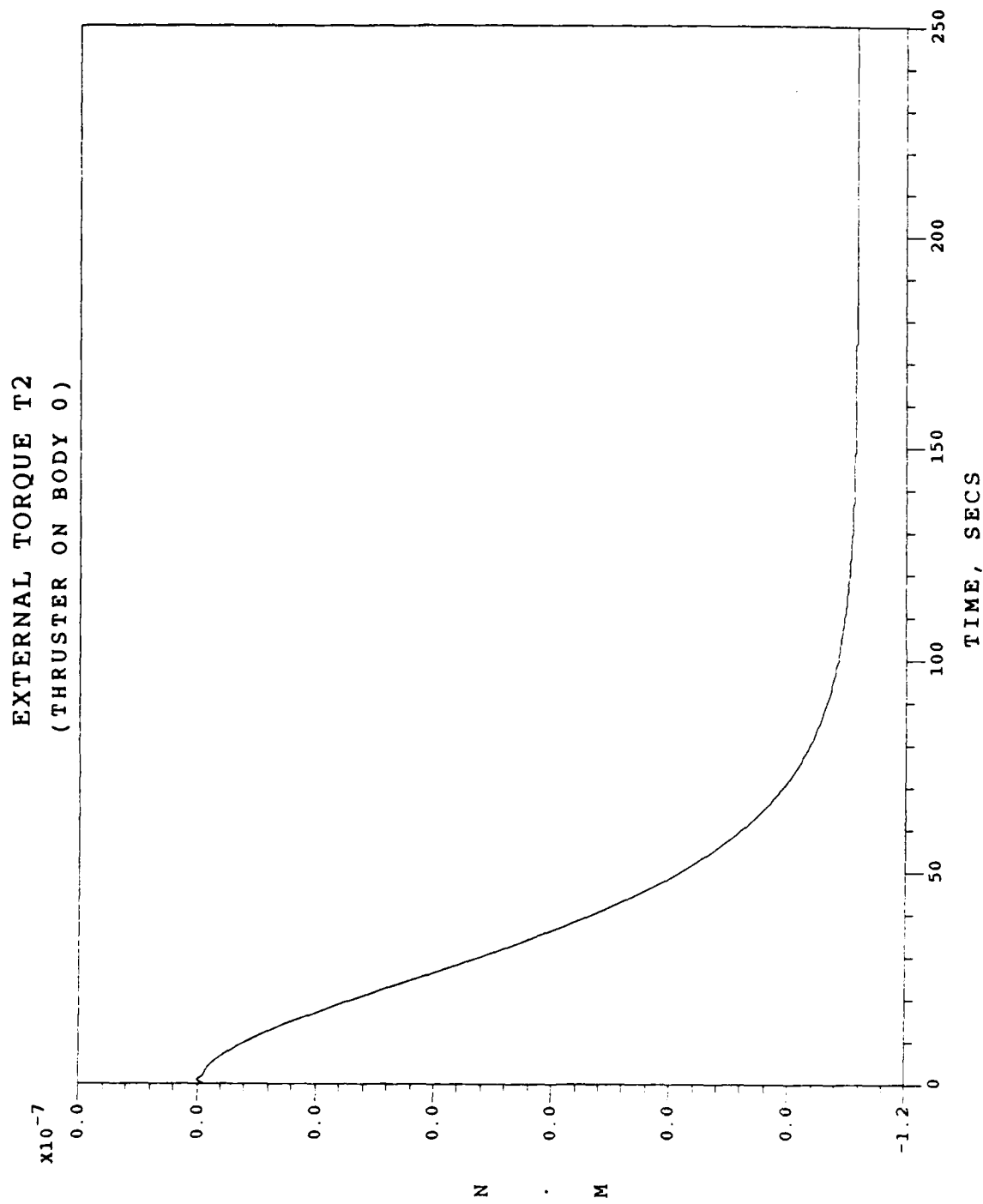


Fig. 29. Deployment Phase / Case 2  
External Torque T1



• Fig. 30. Deployment Phase / Case 2  
External Torque T2

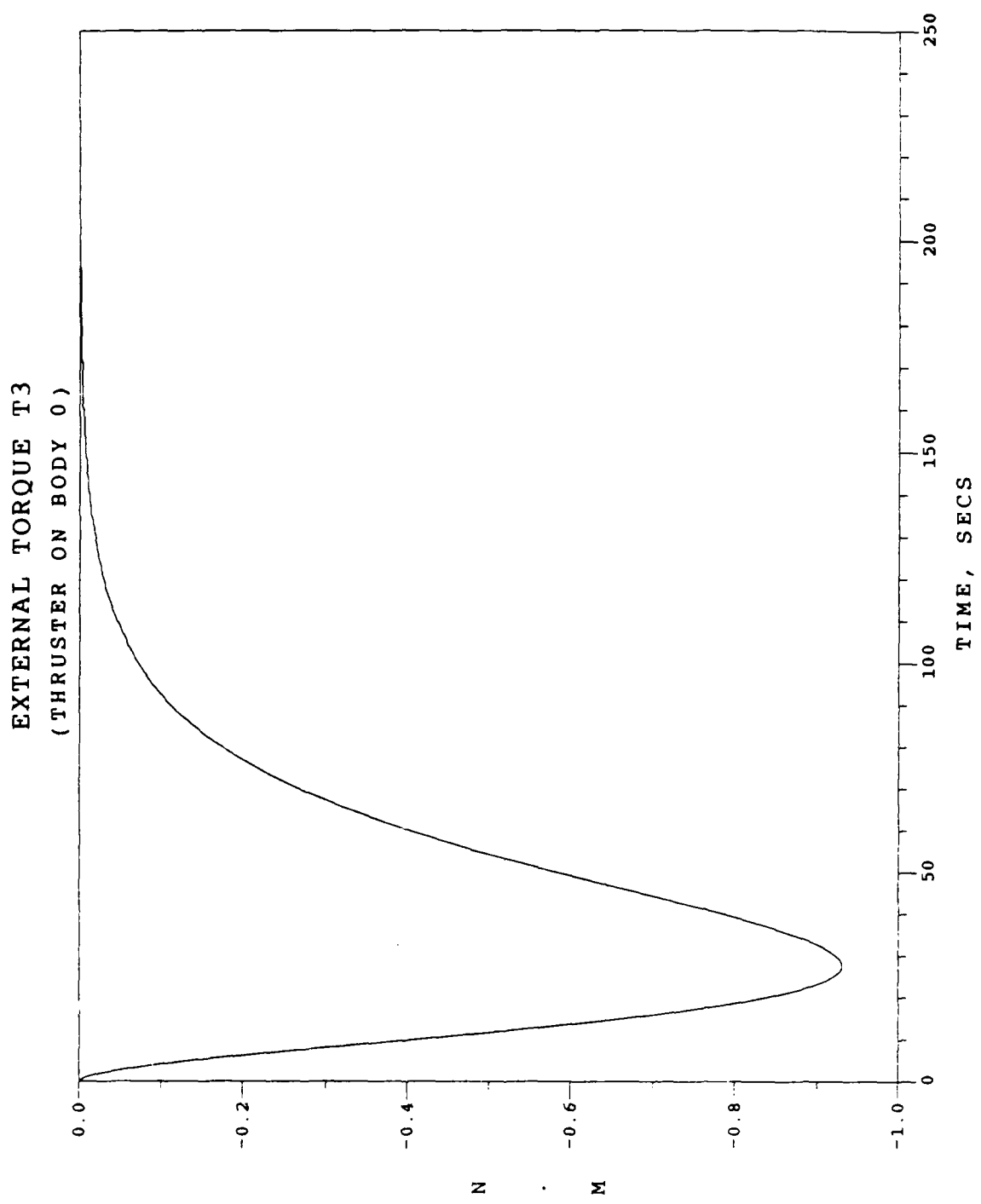


Fig. 31. Deployment Phase / Case 2  
External Torque T3

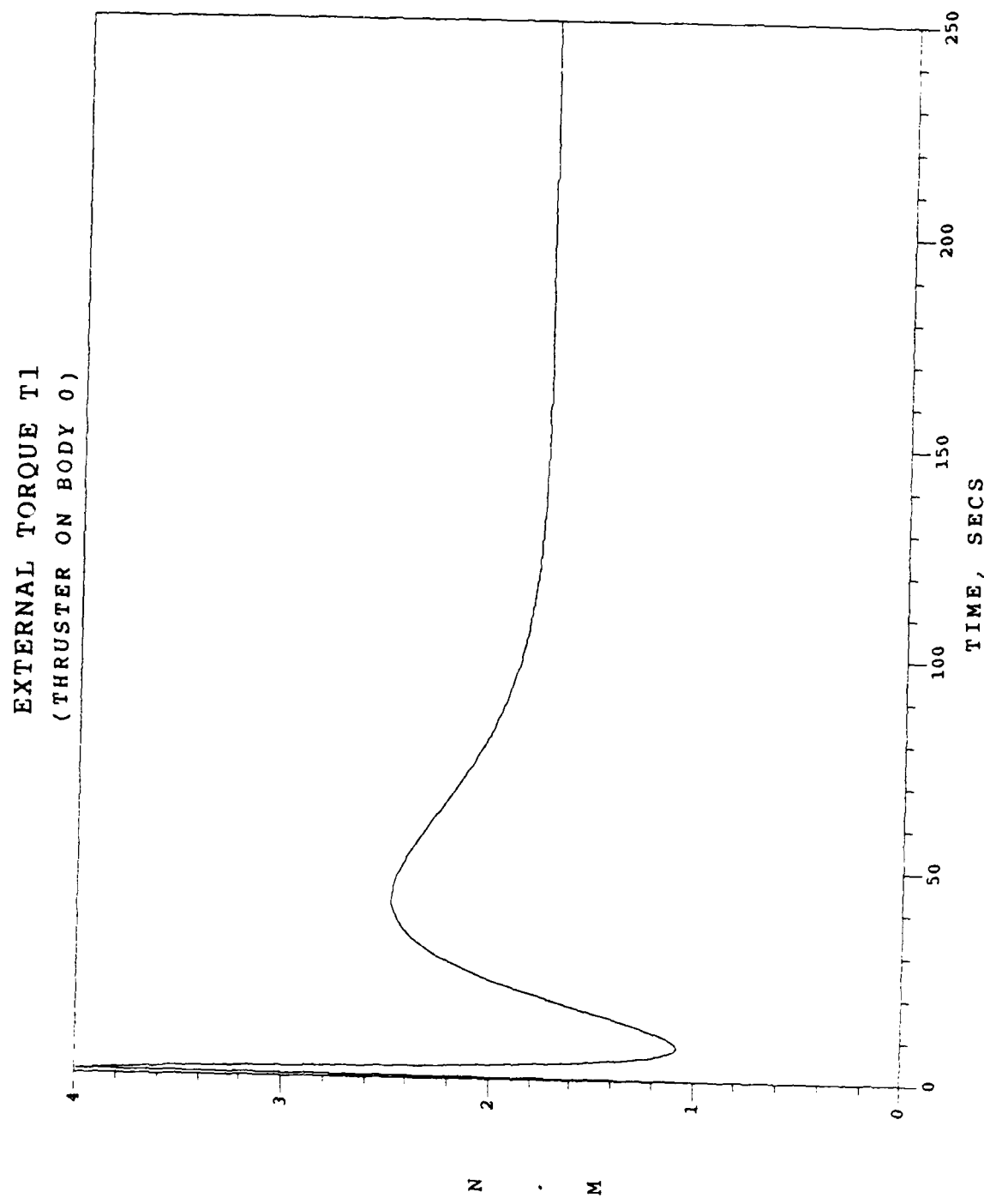


Fig. 32. Deployment Phase / Case 3  
External Torque T1

EXTERNAL TORQUE T2  
(THRUSTER ON BODY 0)

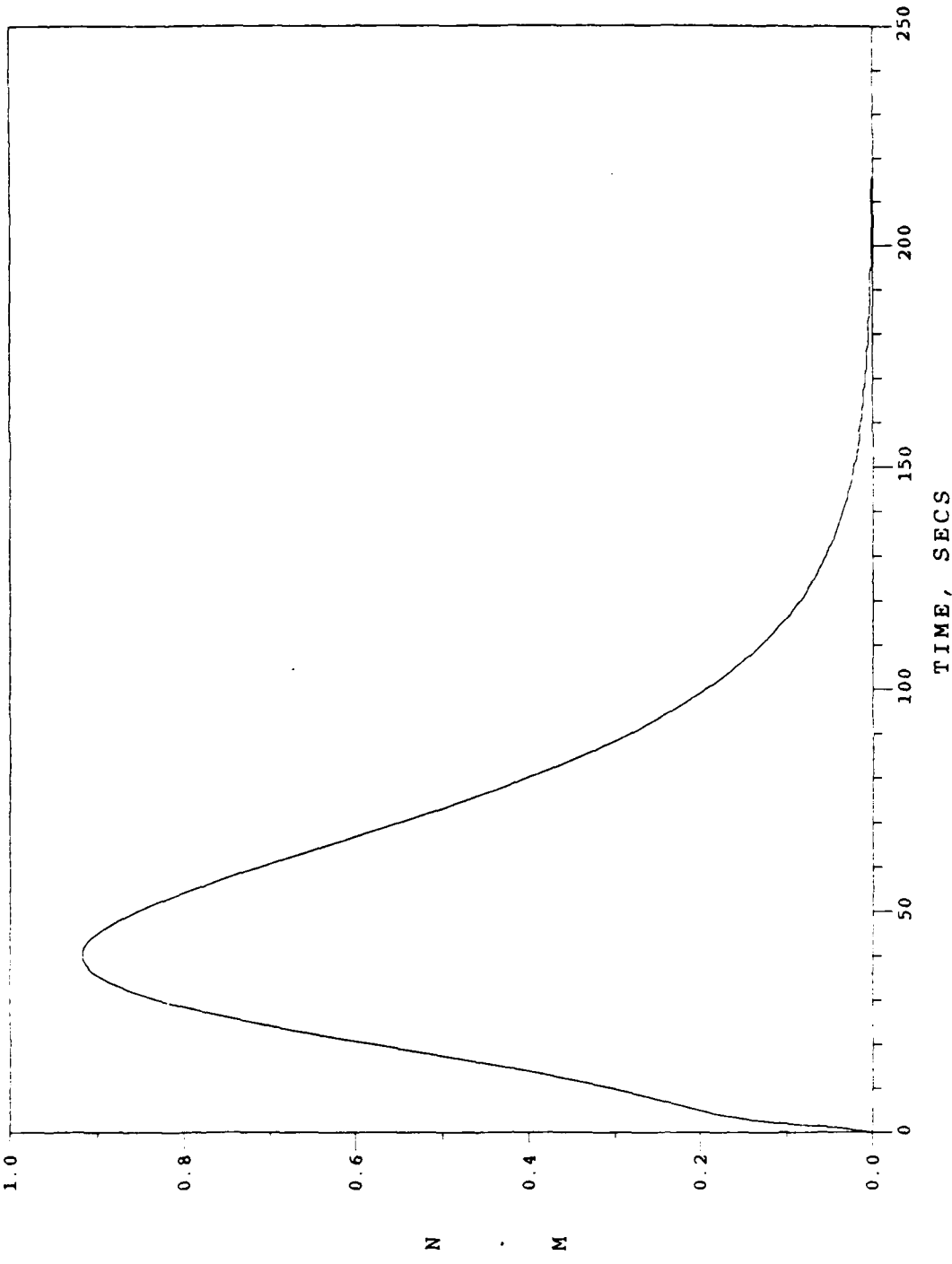


Fig. 33. Deployment Phase / Case 3  
External Torque T2

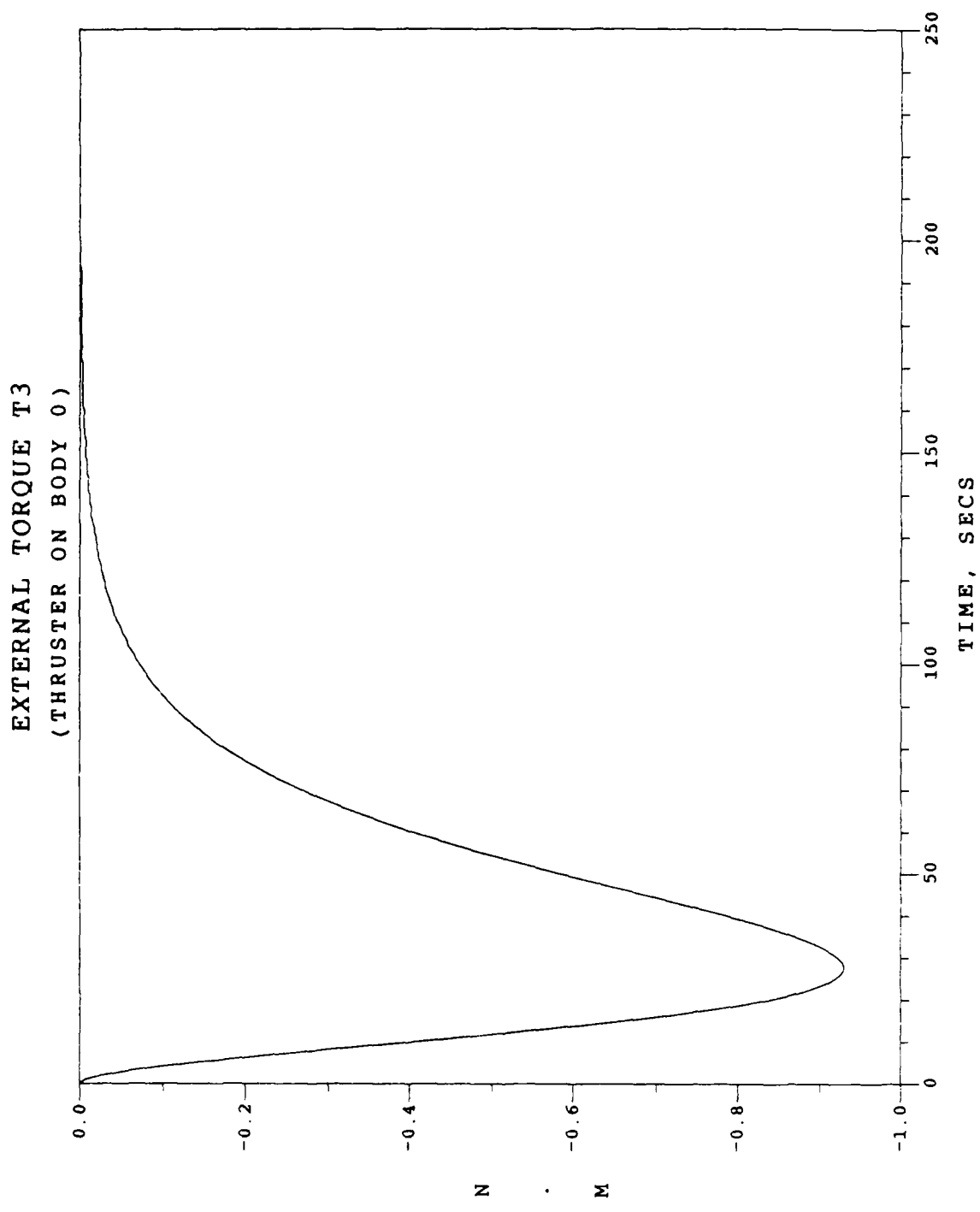


Fig. 34. Deployment Phase / Case 3  
External Torque T3

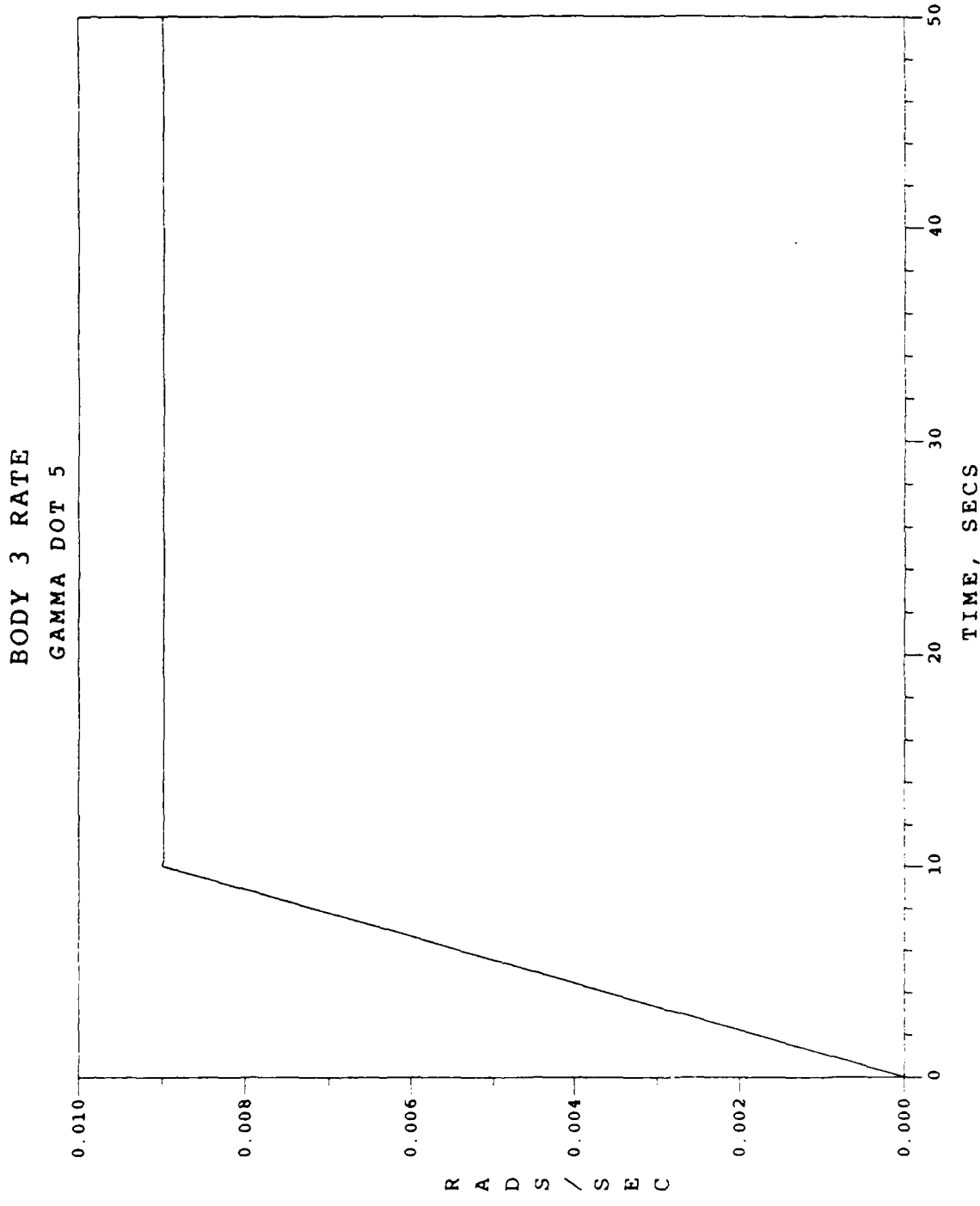


Fig. 35. Spin-up Phase / Case 4  
Body 3  $\dot{\gamma}_s$  History

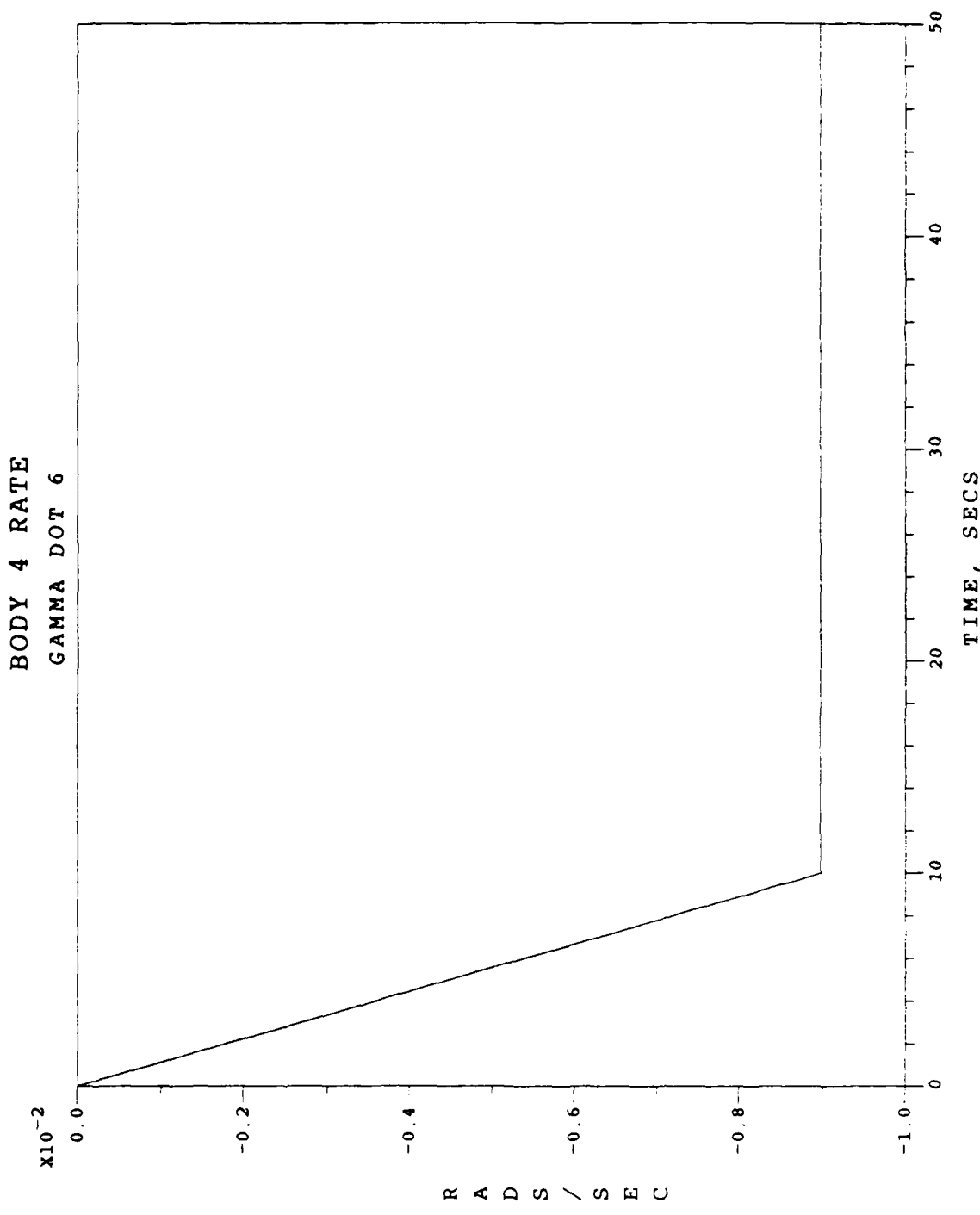


Fig. 36. Spin-up Phase / Case 4  
Body 4  $\dot{\gamma}_6$  History

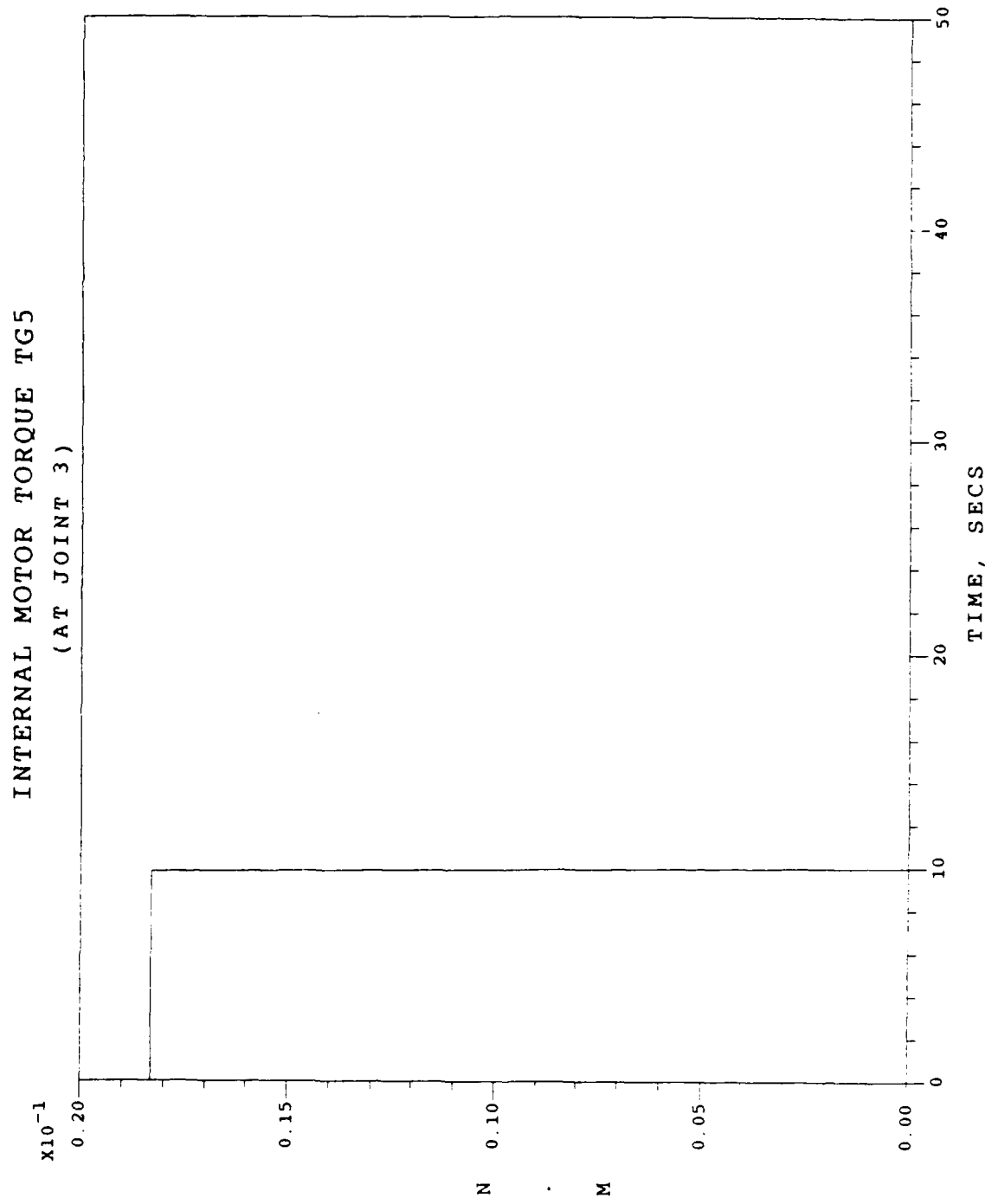


Fig. 37. Spin-up Phase / Case 4  
Internal Motor Torque TG5

INTERNAL MOTOR TORQUES TG6  
(AT JOINT 3)

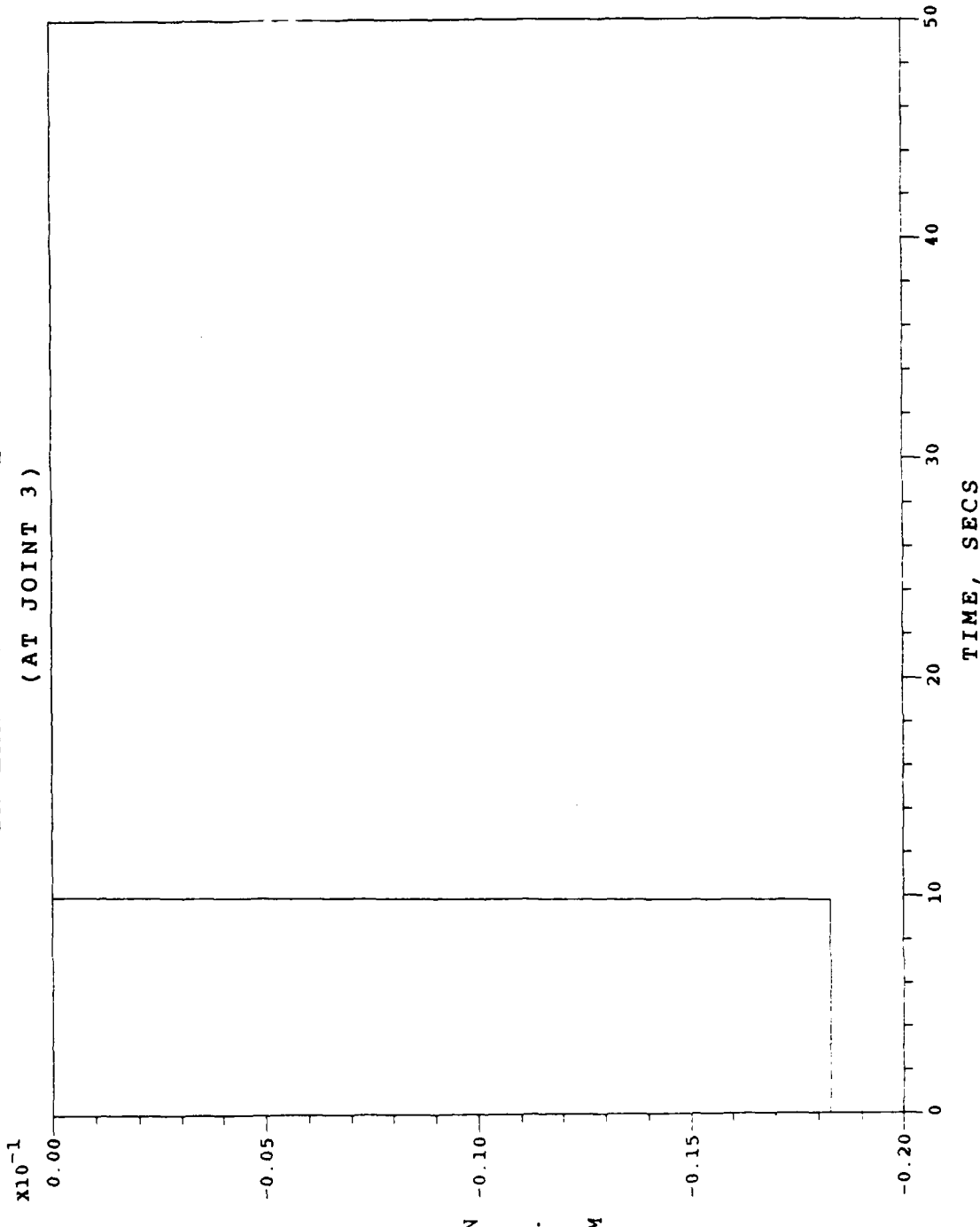


Fig. 38. Spin-up Phase / Case 4  
Internal Motor Torque TG6

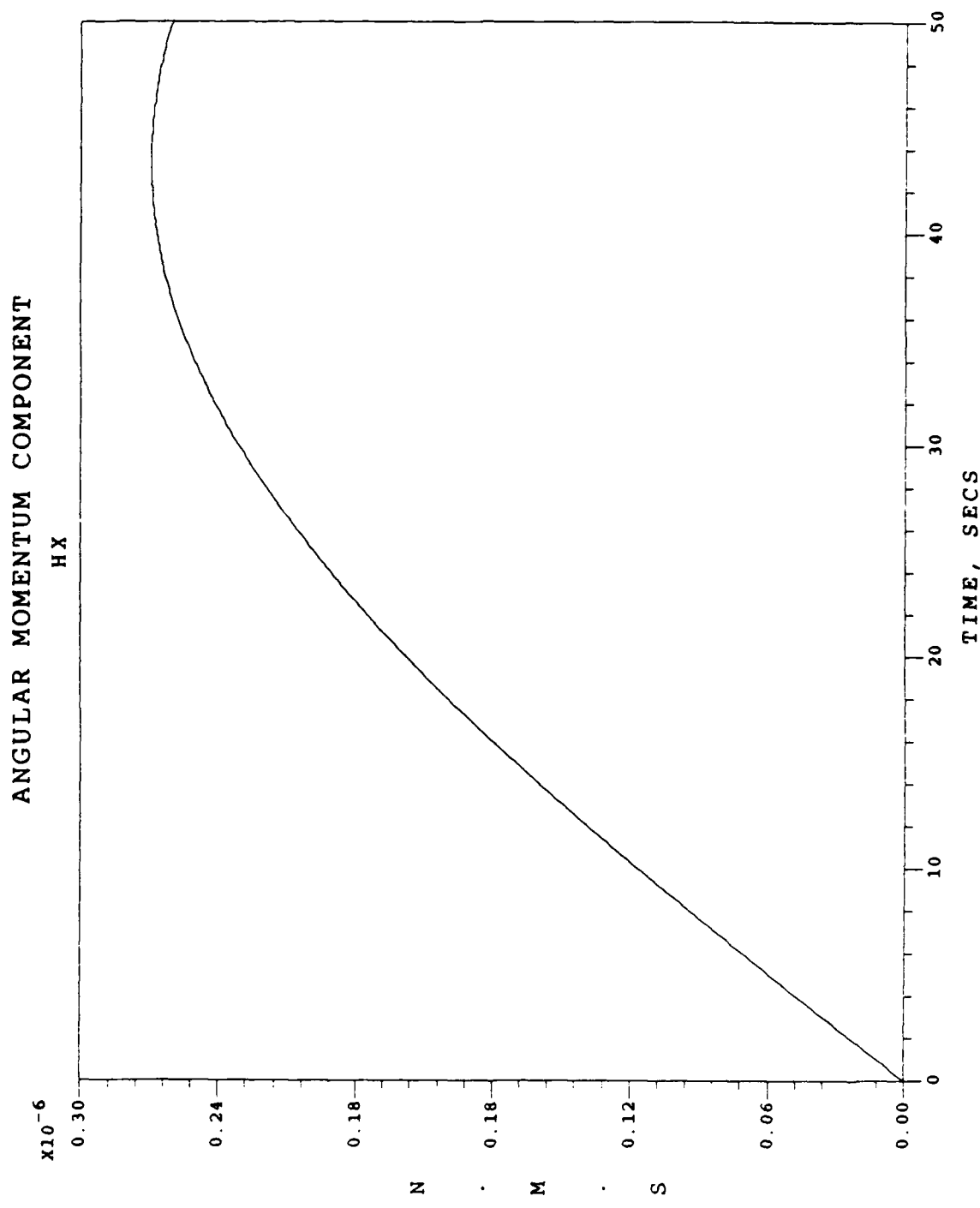


Fig. 39. Spin-up Phase / Case 4  
Angular Momentum Component HX

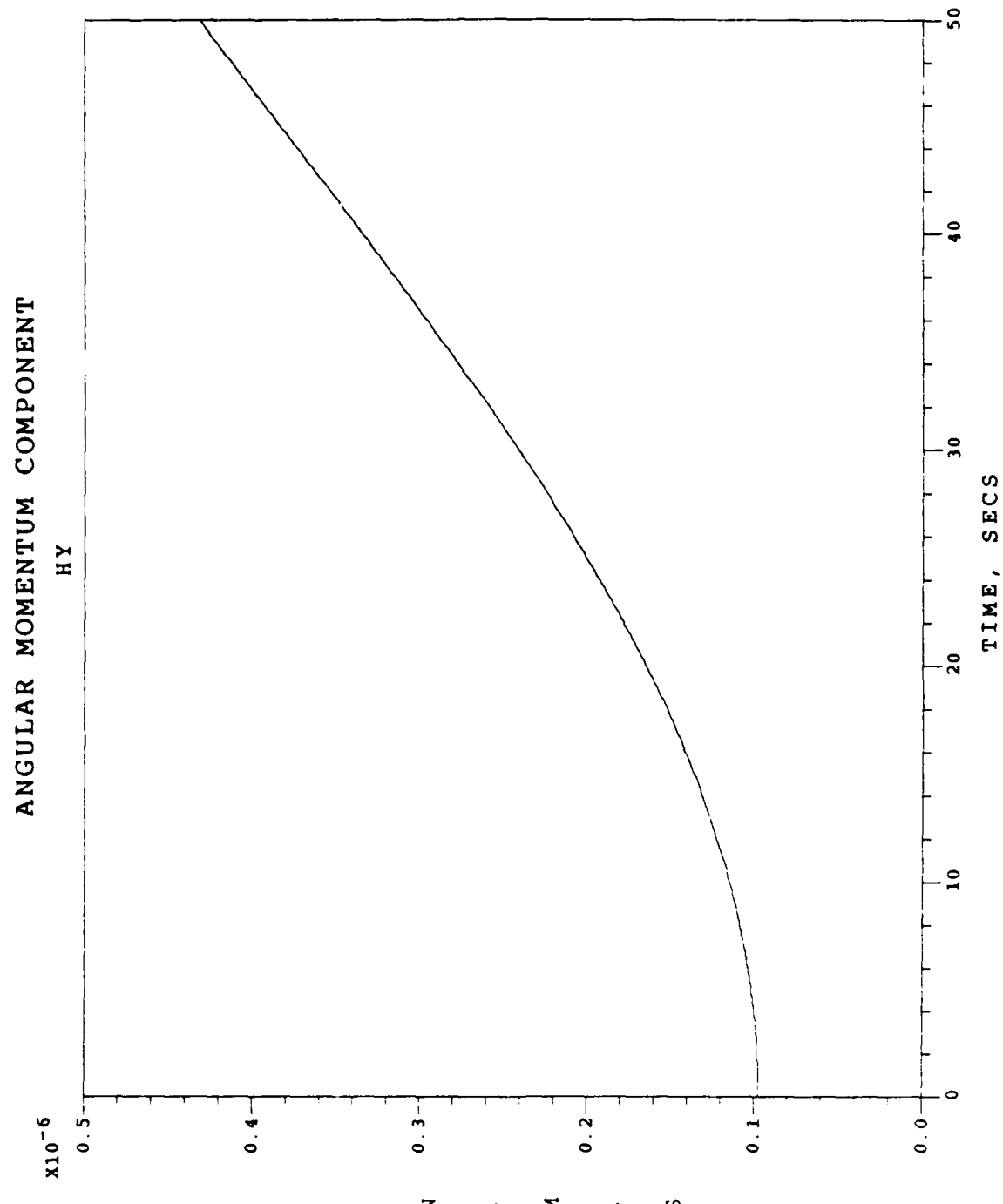


Fig. 40. Spin-up Phase / Case 4  
Angular Momentum Component HY

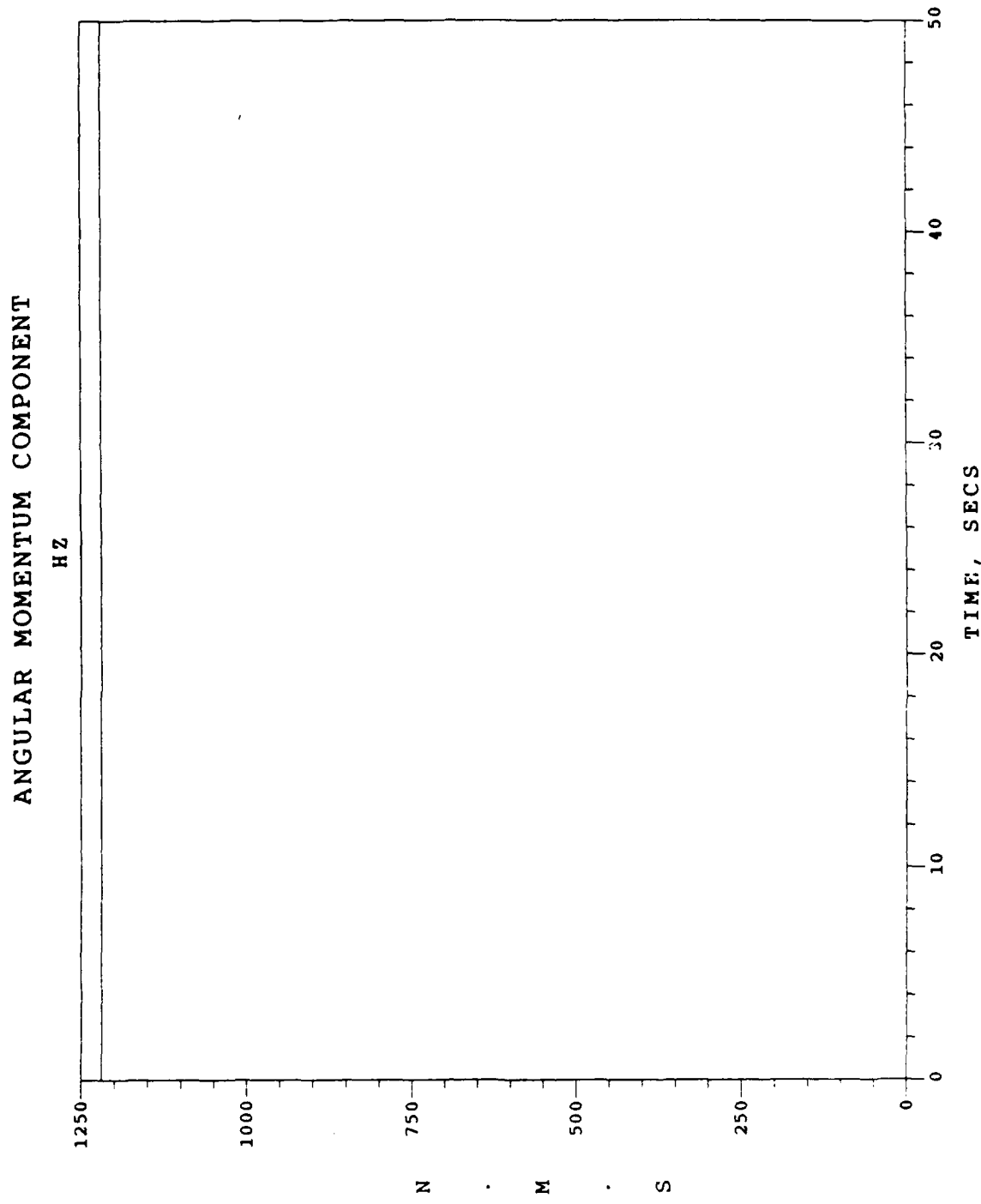


Fig. 41. Spin-up Phase / Case 4  
Angular Momentum Component HZ

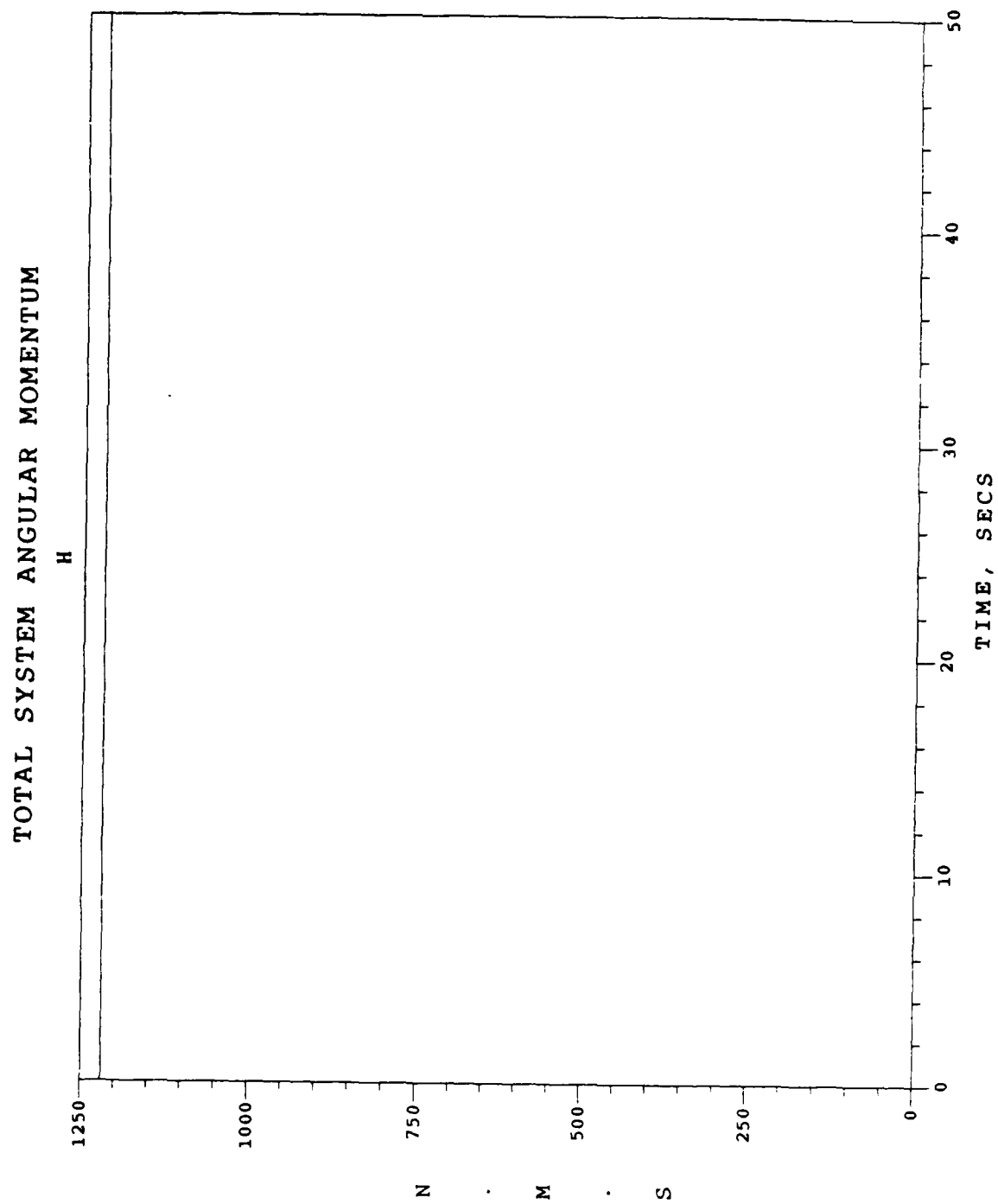


Fig. 42. Spin-up Phase / Case 4  
Total System Angular Momentum

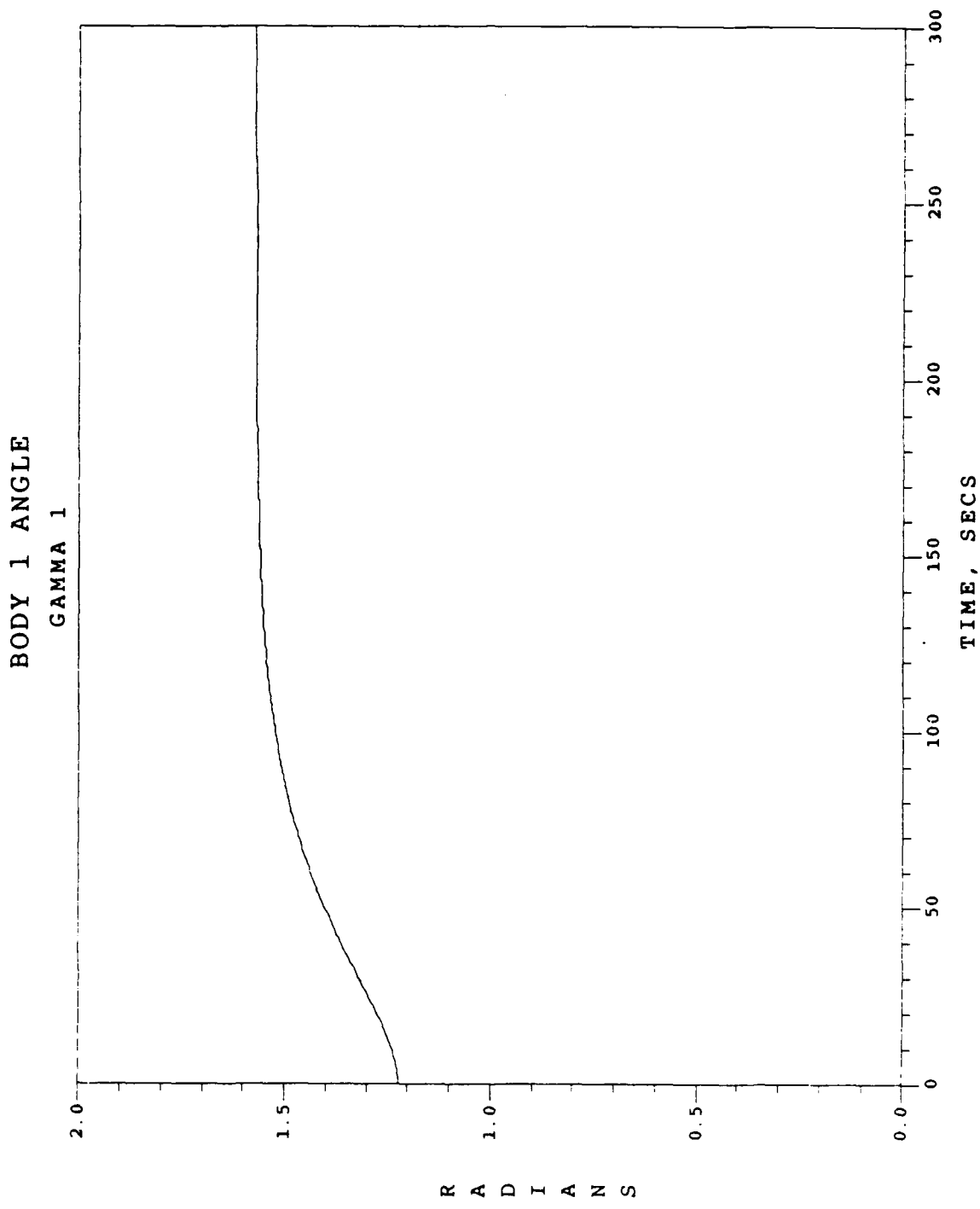


Fig. 43. Detumble/Despin Phase / Case 5  
Body 1  $\gamma_1$  History

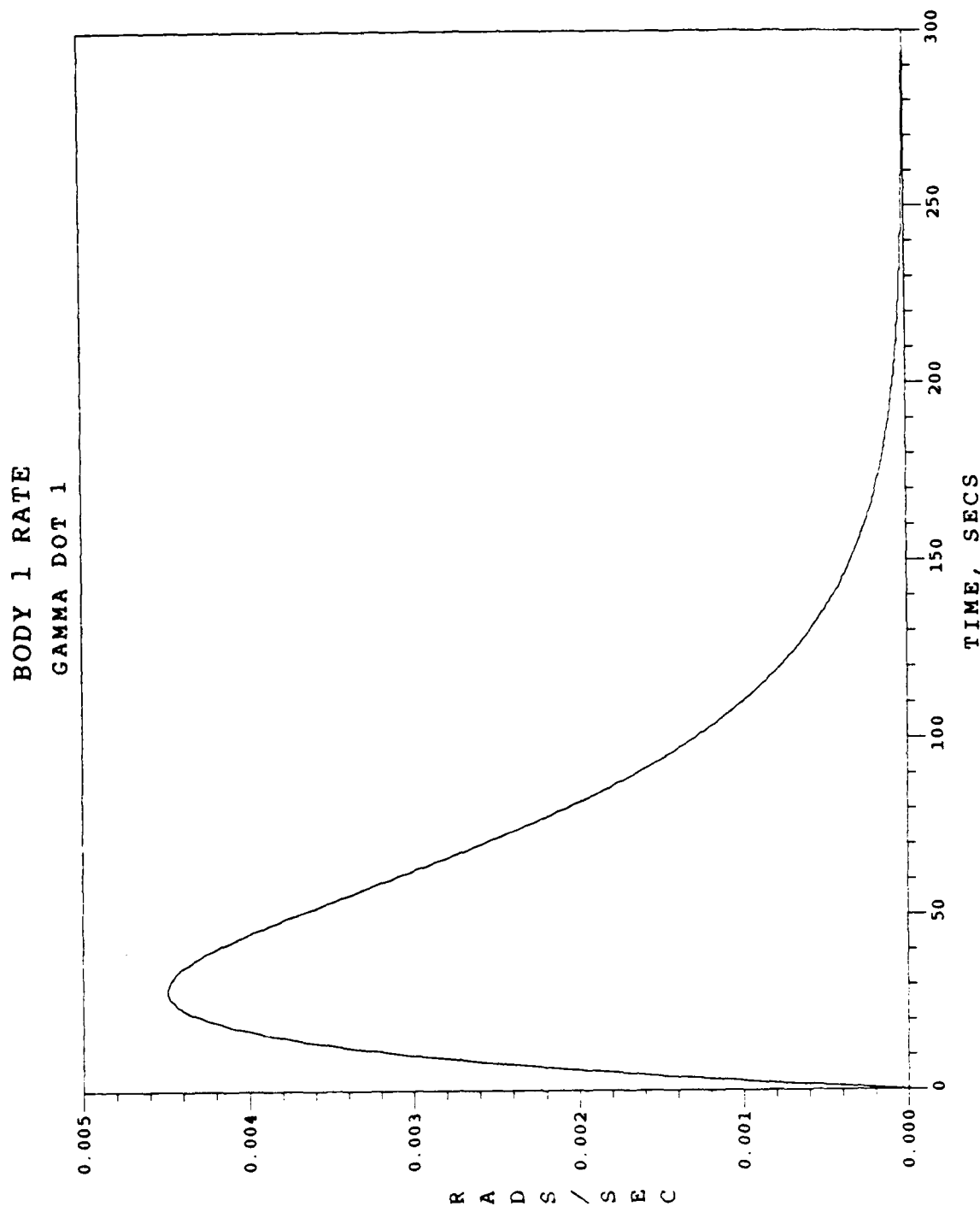


Fig. 44. Detumble/Despin Phase / Case 5  
Body 1  $\dot{\gamma}_1$  History

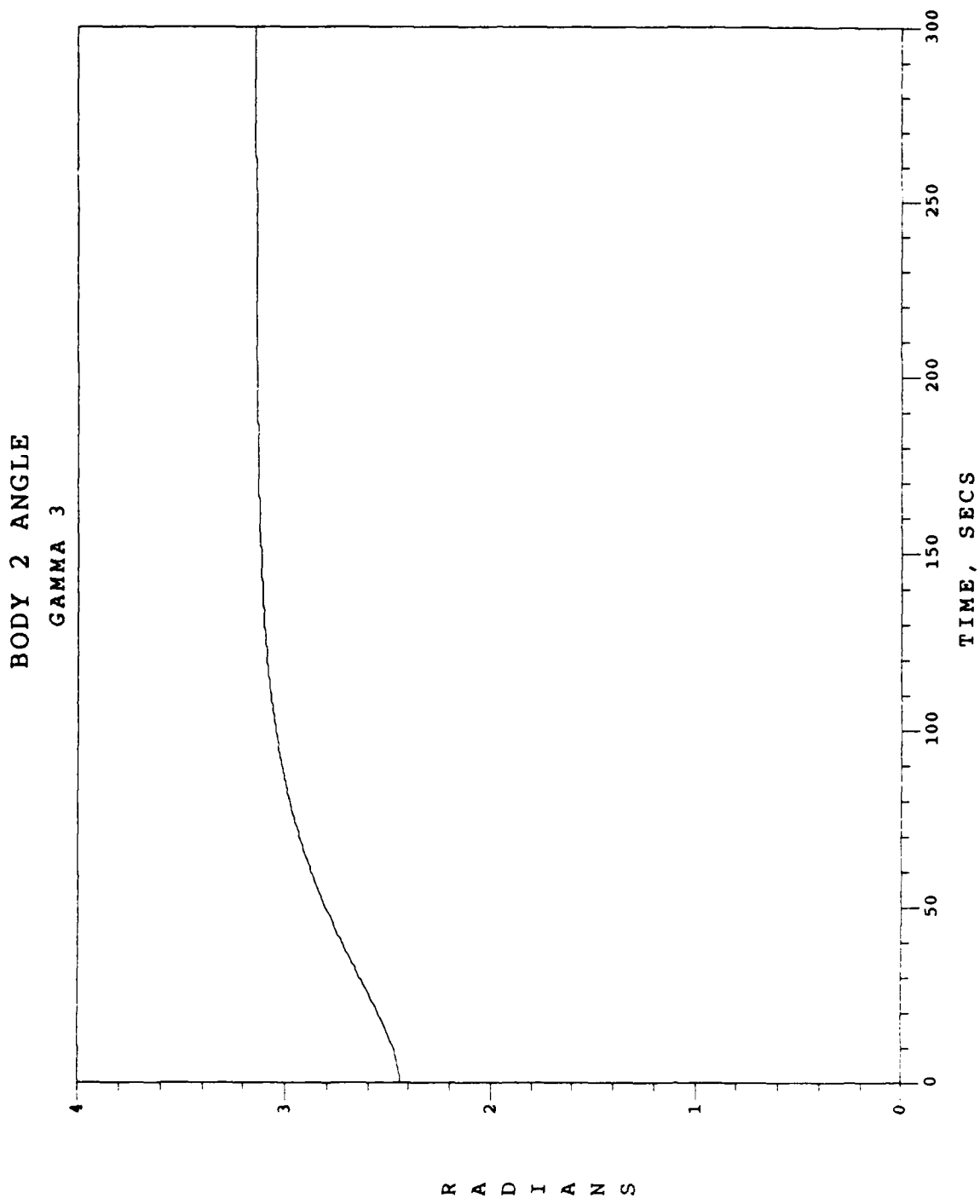


Fig. 45. Detumble/Despin Phase / Case 5  
Body 2  $\gamma_3$  History

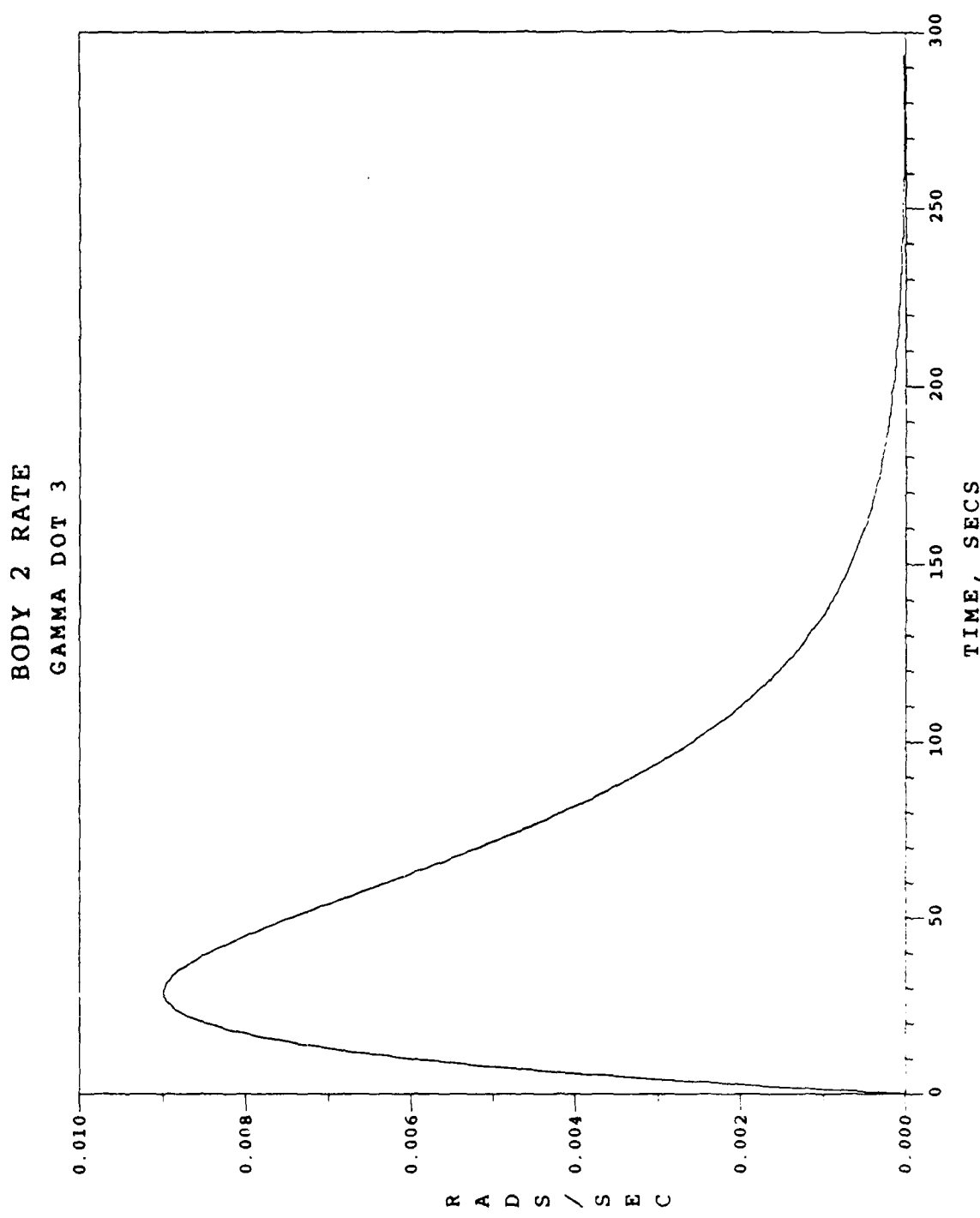


Fig. 46. Detumble/Despin Phase / Case 5  
Body 2  $\dot{\gamma}_3$  History

BODY 3 AND 4 ANGLE  
GAMMA 4

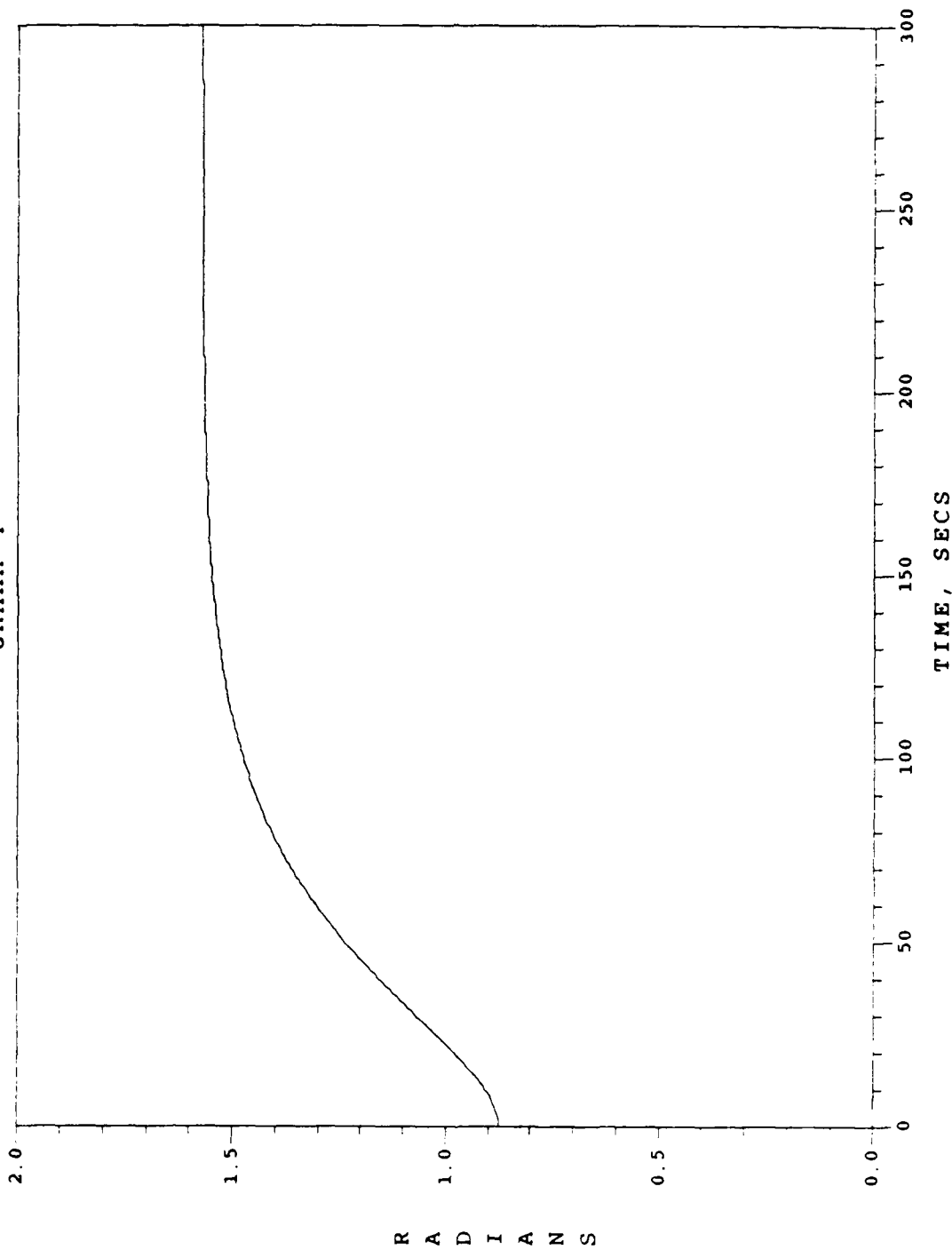


Fig. 47. Detumble/Despin Phase / Case 5  
Body 3/4  $\gamma_4$  History

BODY 3 AND 4 RATE  
GAMMA DOT 4

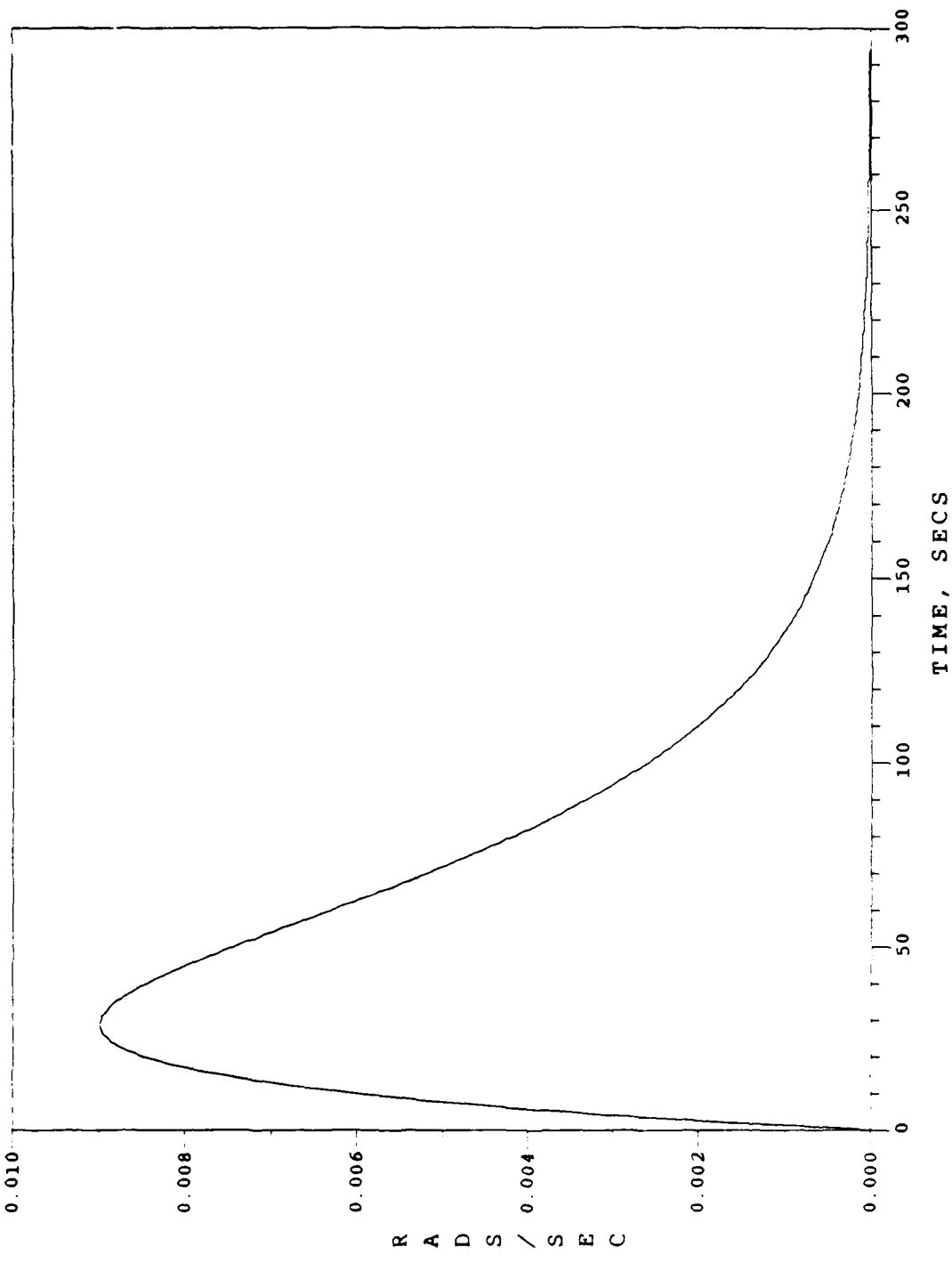


Fig. 48. Detumble/Despin Phase / Case 5  
Body 3/4  $\dot{\gamma}_4$  History

BODY 3 RATE  
GAMMA DOT 5

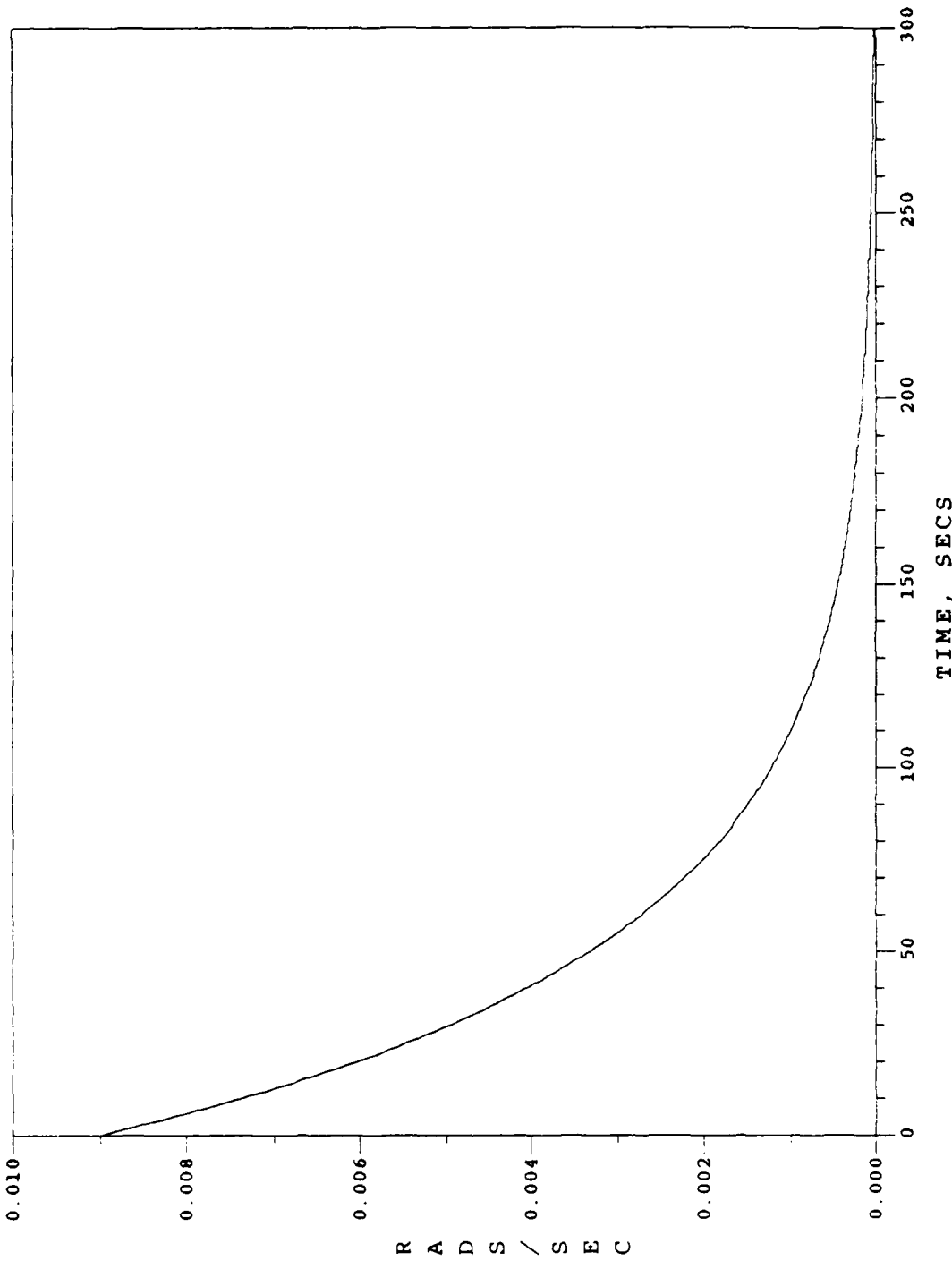


Fig. 49. Detumble/Despin Phase / Case 5  
Body 3  $\dot{\gamma}_5$  History

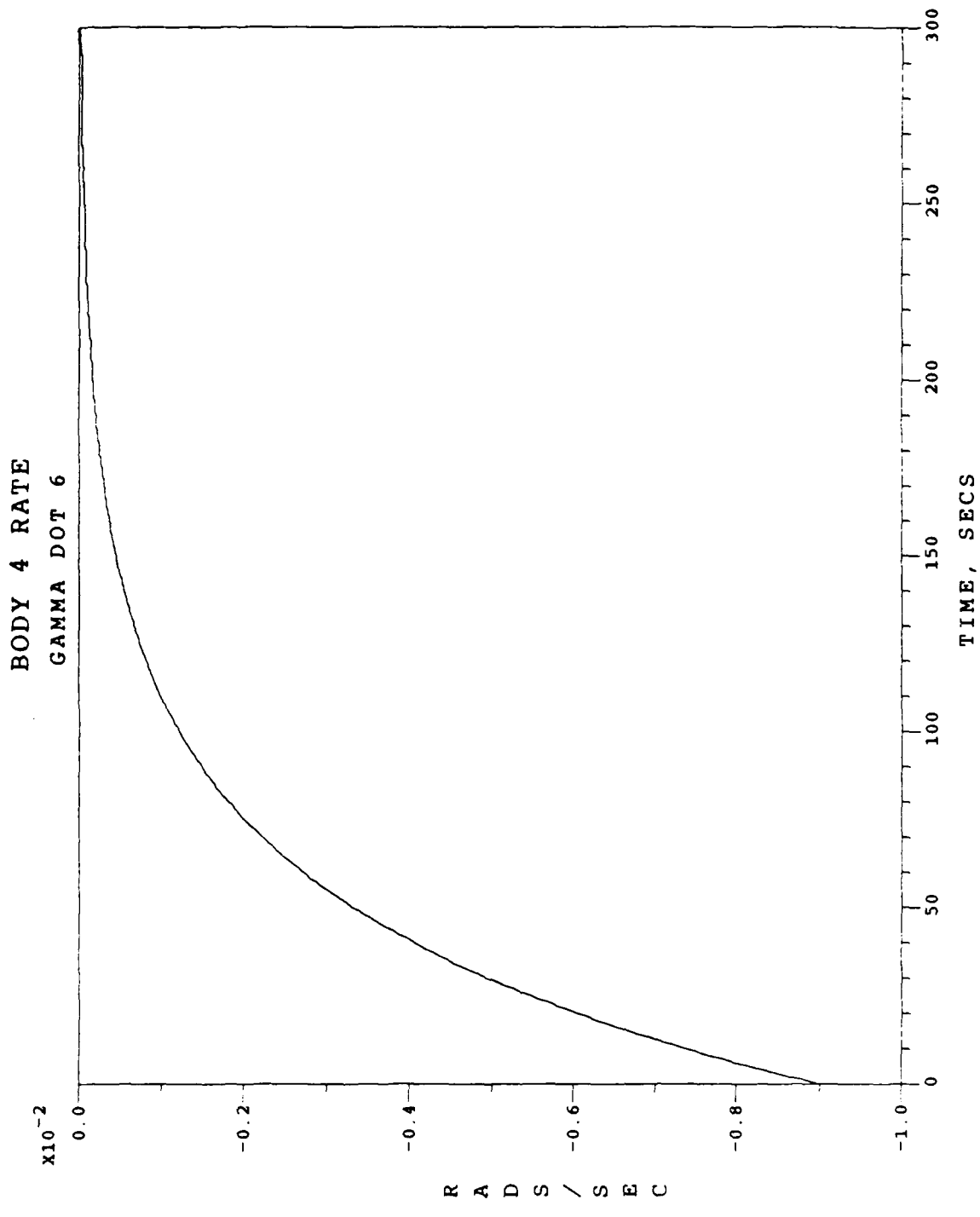


Fig. 50. Detumble/Despin Phase / Case 5  
Body 4  $\dot{\gamma}_6$  History

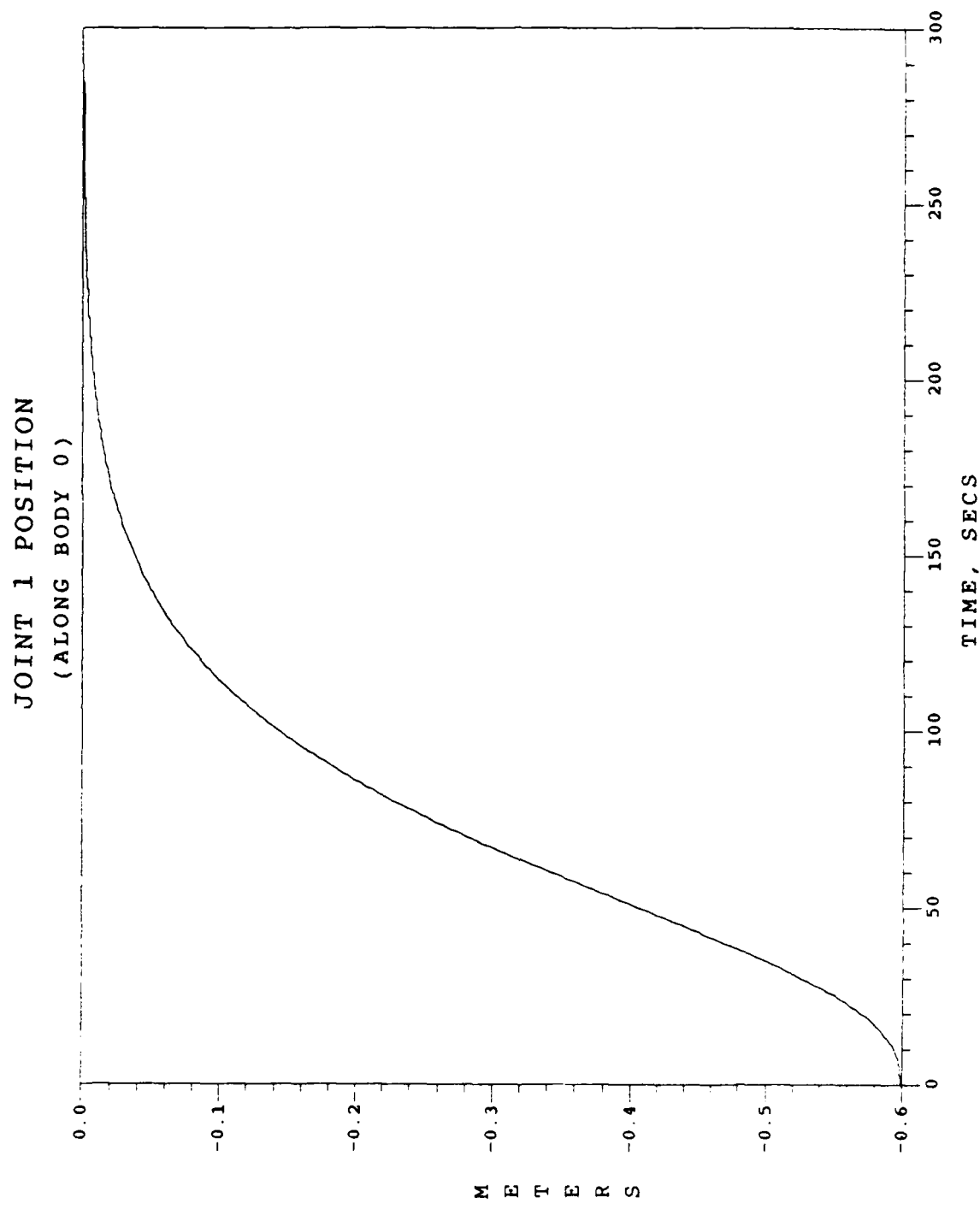


Fig. 51. Detumble/Despin Phase / Case 5  
Joint 1 Position

JOINT 1 RELATIVE VELOCITY  
(ALONG BODY 0)

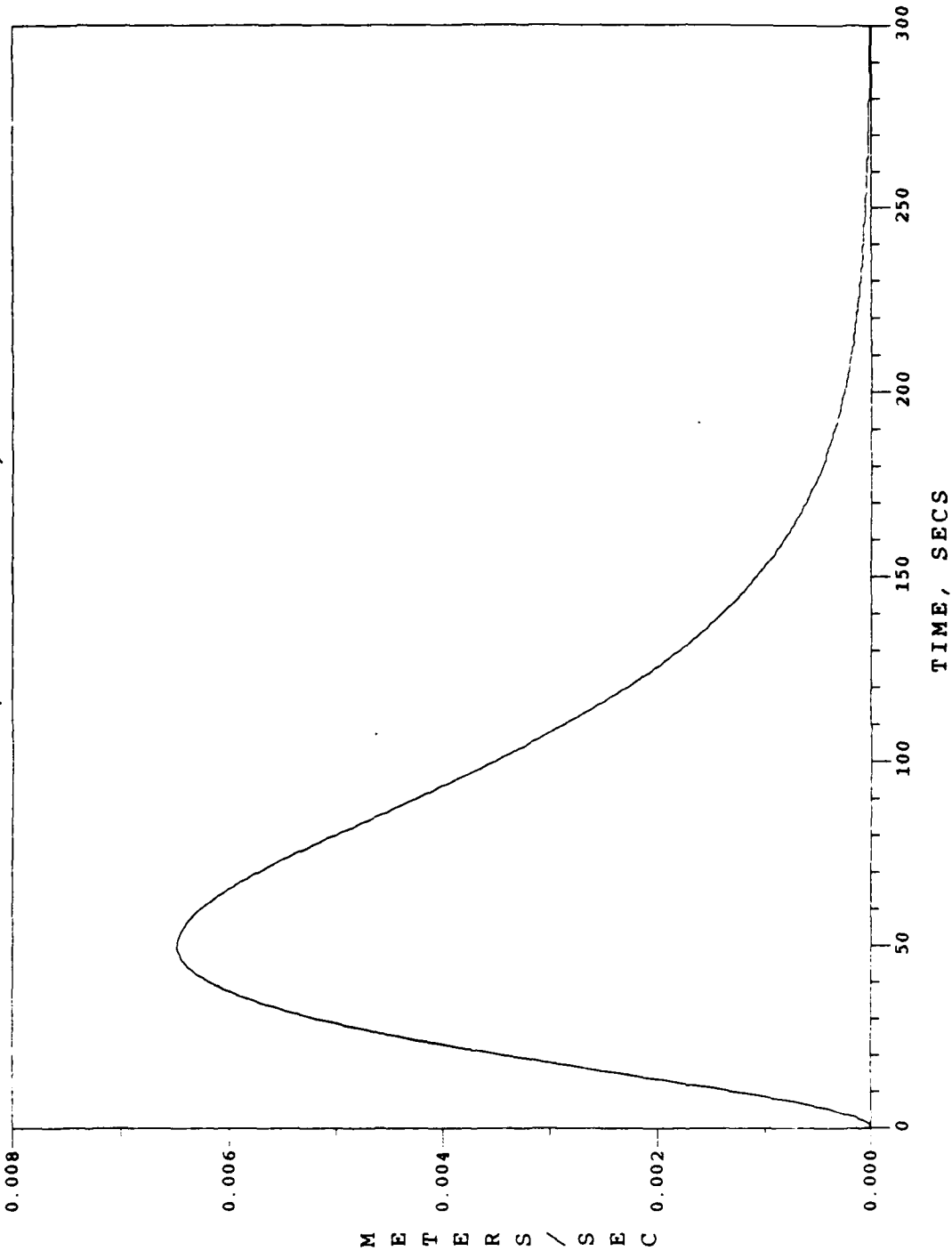


Fig. 52. Detumble/Despin Phase / Case 5  
Joint 1 Relative Velocity

JOINT 1 RELATIVE ACCELERATION  
( ALONG BODY 0 )

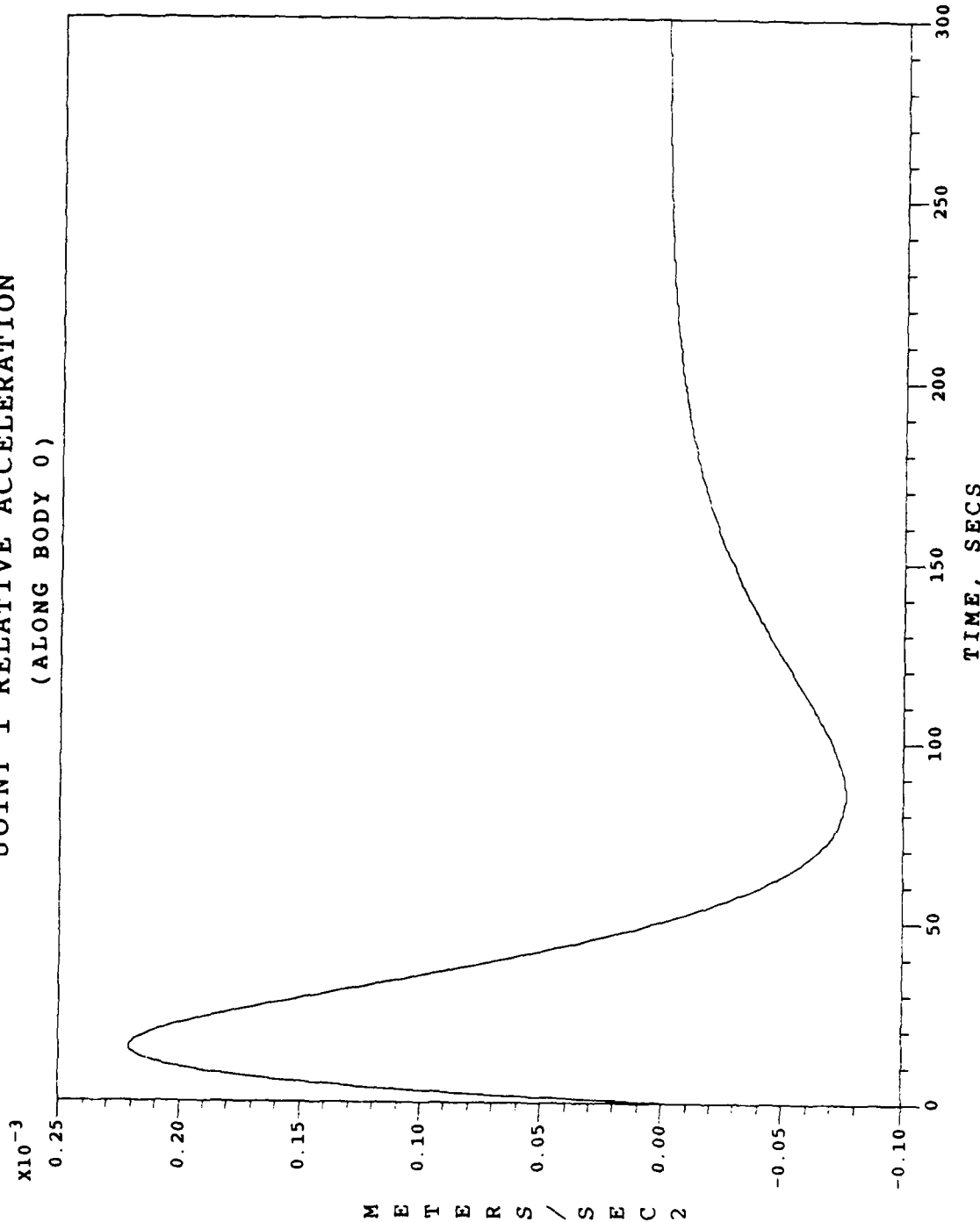


Fig. 53. Detumble/Despin Phase / Case 5  
Joint 1 Relative Acceleration

EXTERNAL TORQUE  $T_1$   
(THRUSTER ON BODY 0)

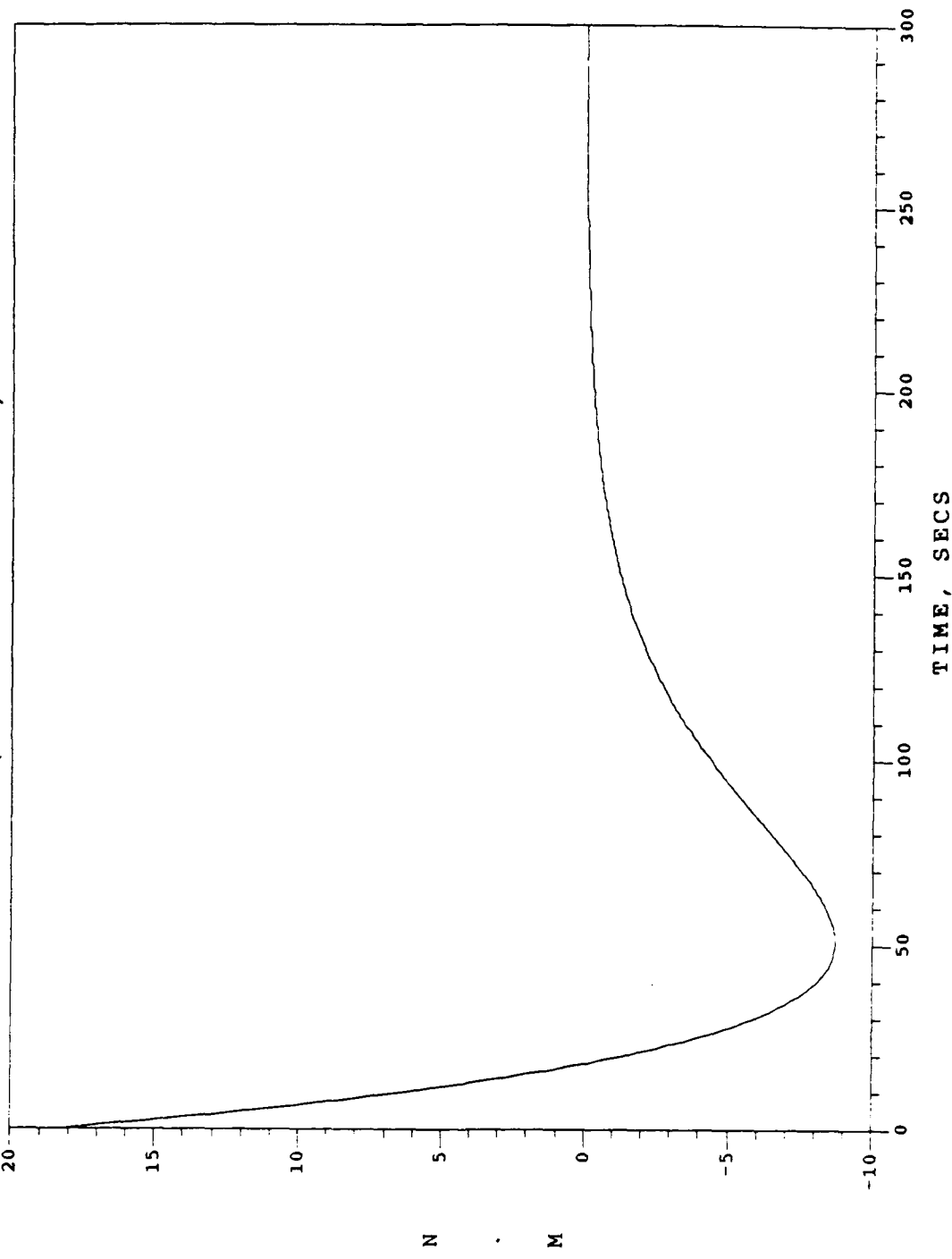
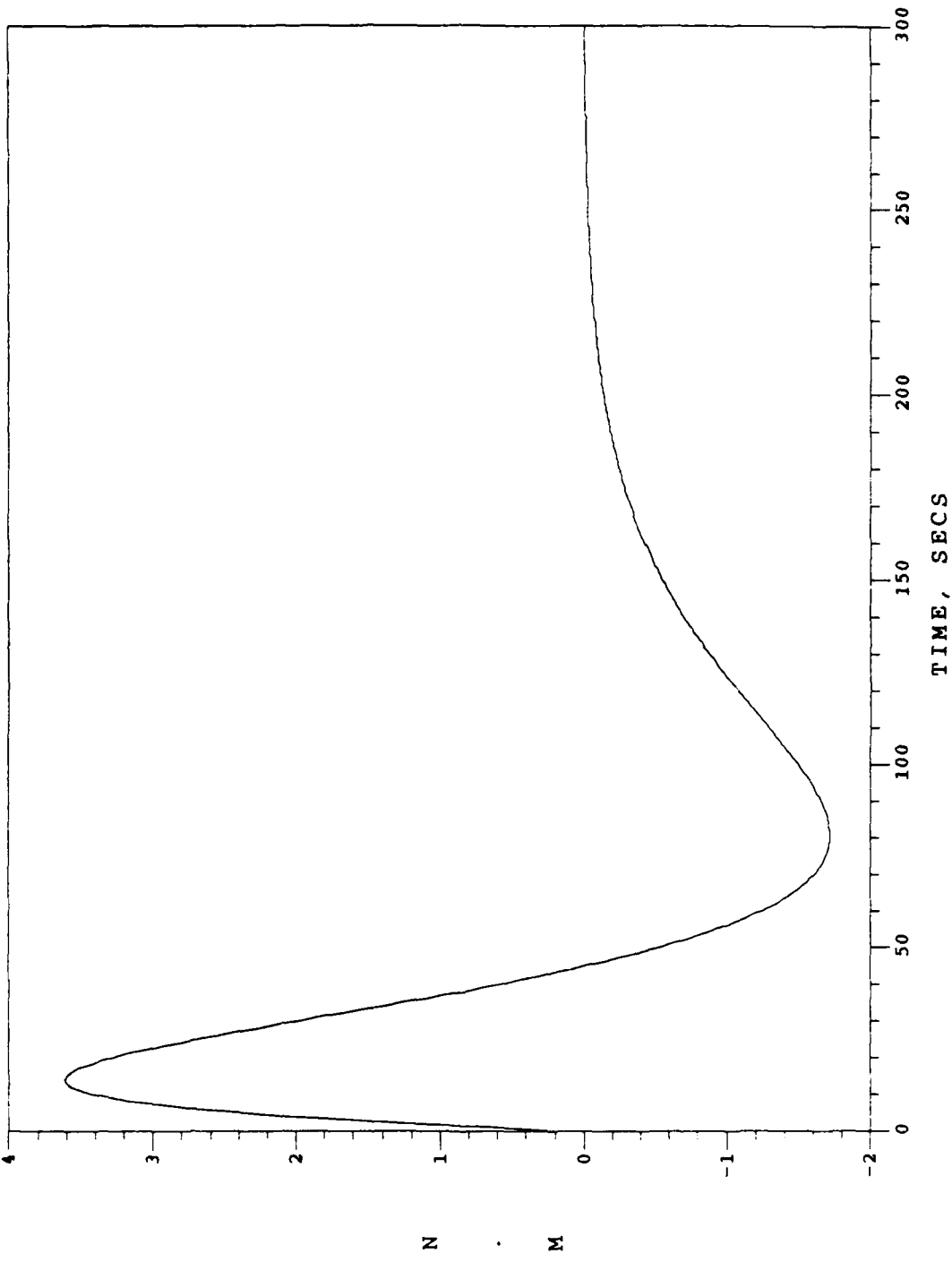


Fig. 54. Detumble/Despin Phase / Case 5  
External Torque  $T_1$

**EXTERNAL TORQUE T2  
(THRUSTER ON BODY 0)**



**Fig. 55. Detumble/Despin Phase / Case 5  
External Torque T2**

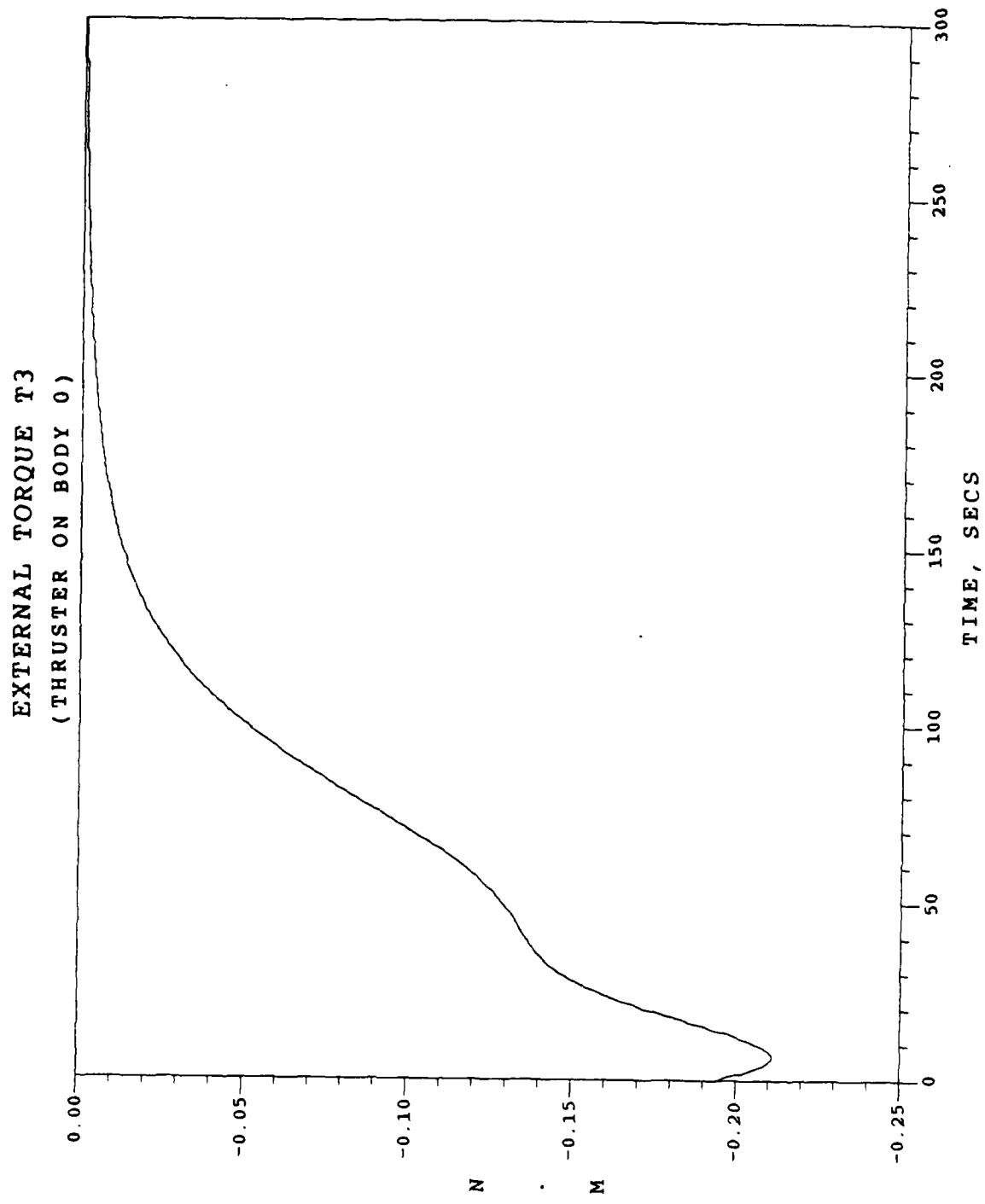


Fig. 56. Detumble/Despin Phase / Case 5  
External Torque T3

INTERNAL MOTOR TORQUE TG1  
(AT JOINT 1)

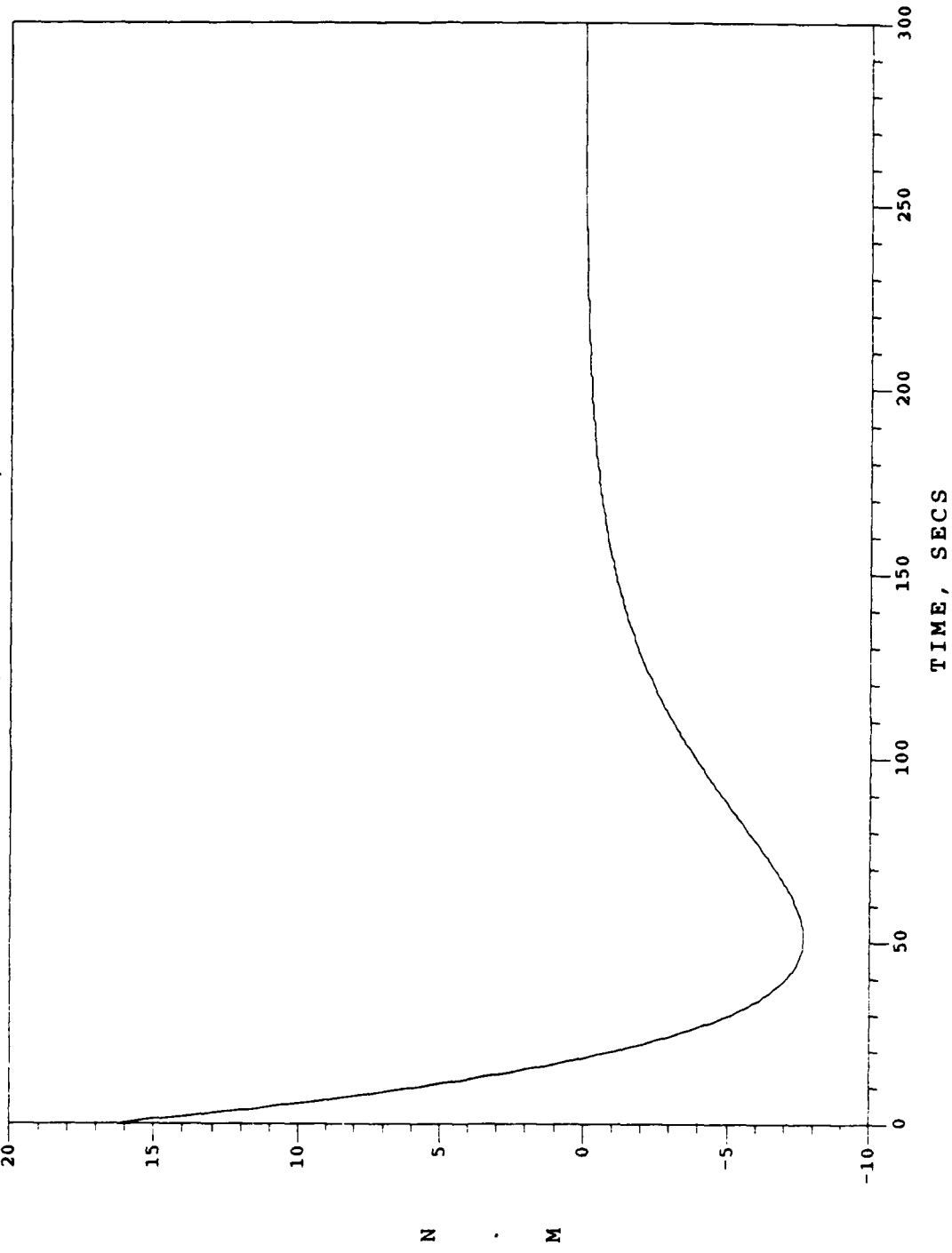


Fig. 57. Detumble/Despin Phase / Case 5  
Internal Motor Torque TG1

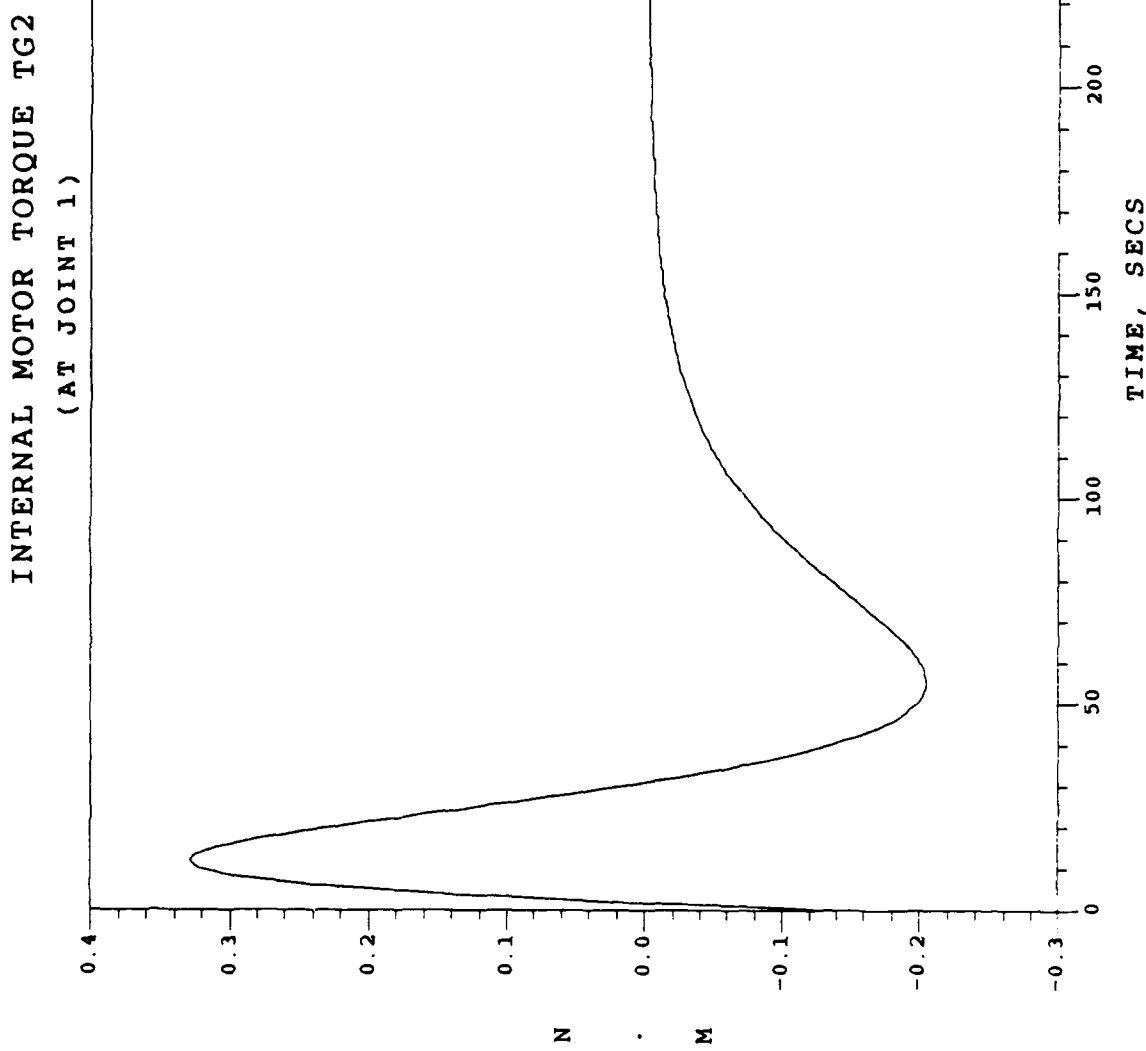


Fig. 58. Detumble/Despin Phase / Case 5  
Internal Motor Torque TG2

INTERNAL MOTOR TORQUE TG3  
(AT JOINT 2)

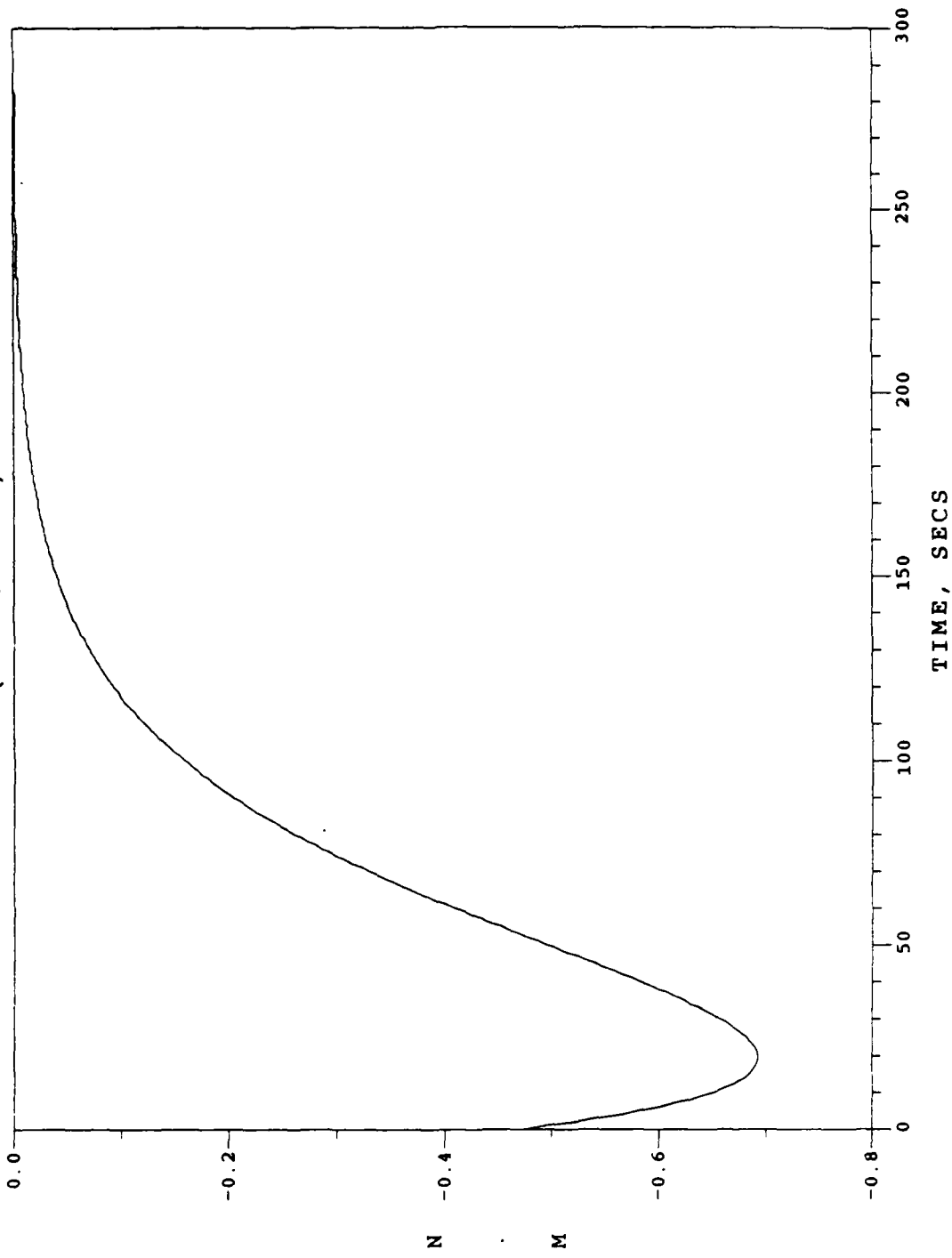


Fig. 59. Detumble/Despin Phase / Case 5  
Internal Motor Torque TG3

INTERNAL MOTOR TORQUE TG4  
(AT JOINT 3)

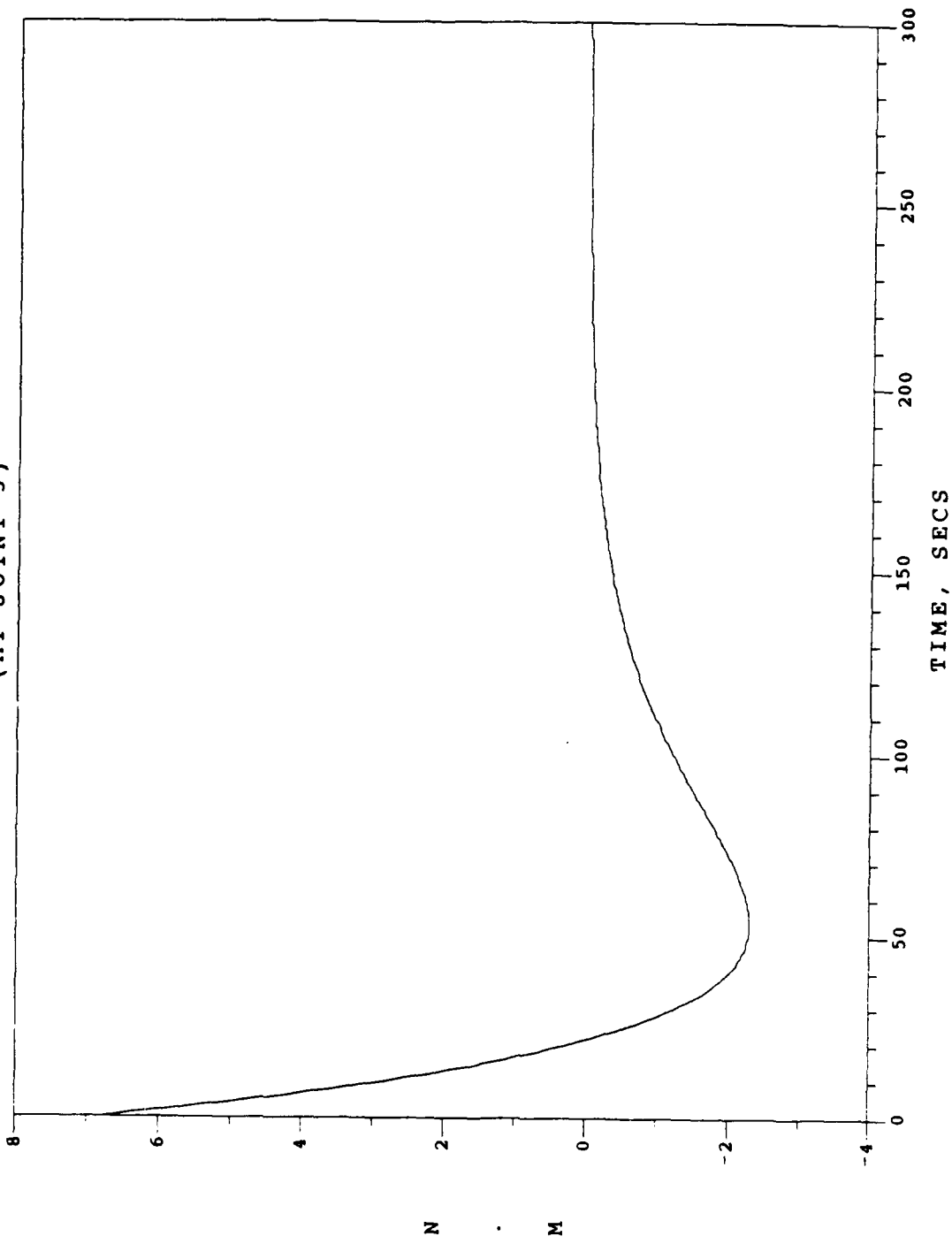


Fig. 60. Detumble/Despin Phase / Case 5  
Internal Motor Torque TG4

INTERNAL MOTOR TORQUE TG5  
(AT JOINT 3)

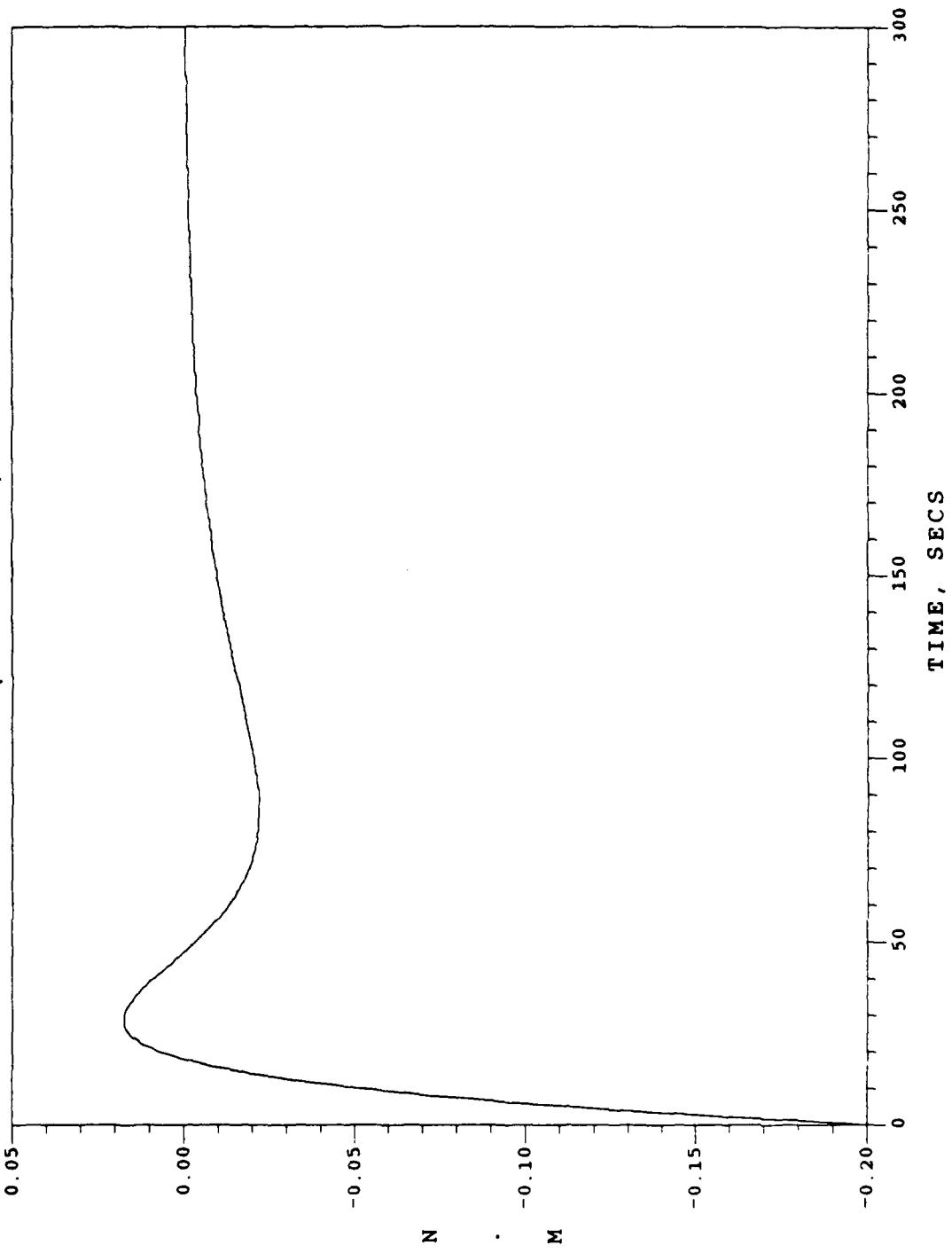


Fig. 61. Detumble/Despin Phase / Case 5  
Internal Motor Torque TG5

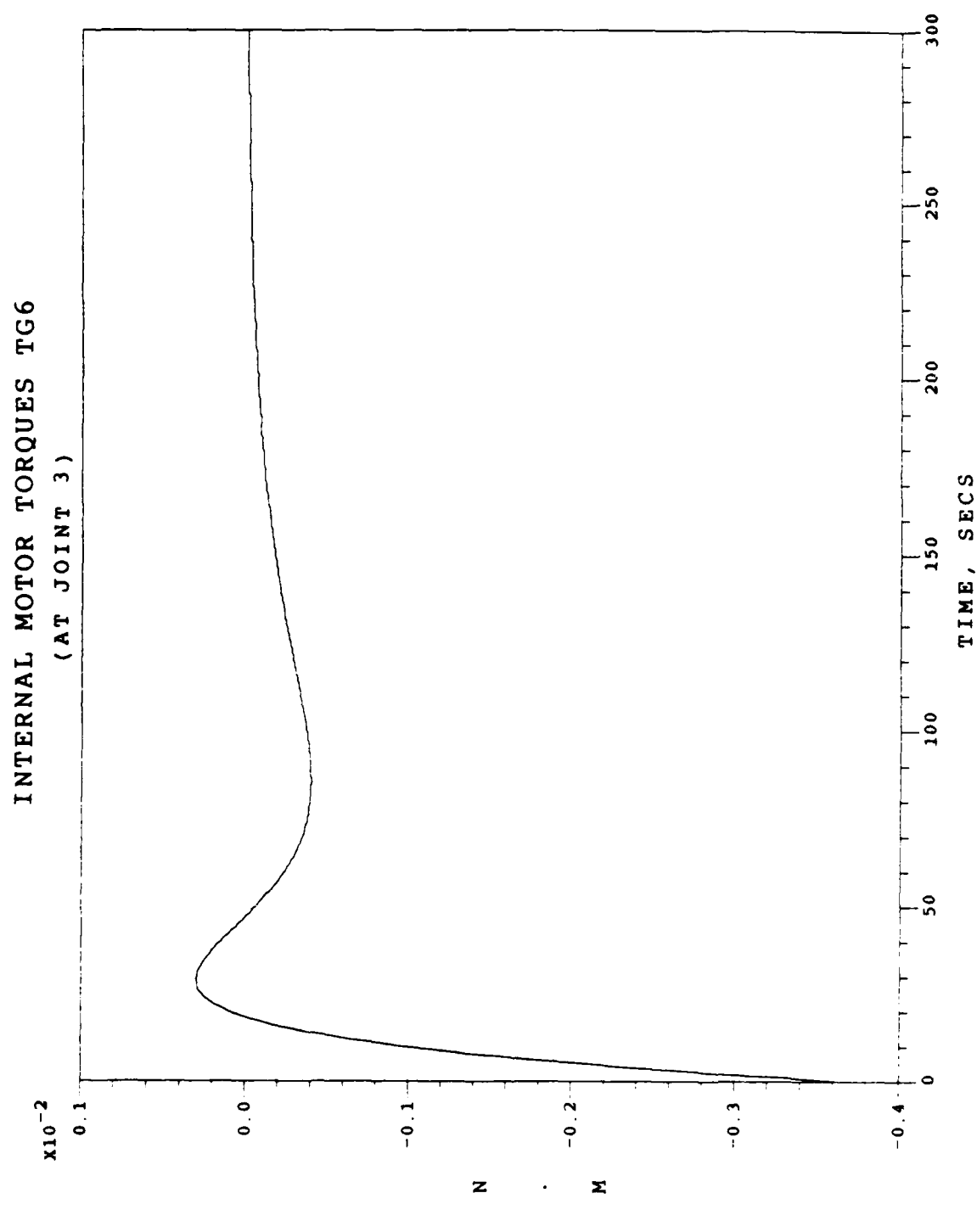


Fig. 62. Detumble/Despin Phase / Case 5  
Internal Motor Torque TG6

CONSTRAINT TORQUE AT  
JOINT 1

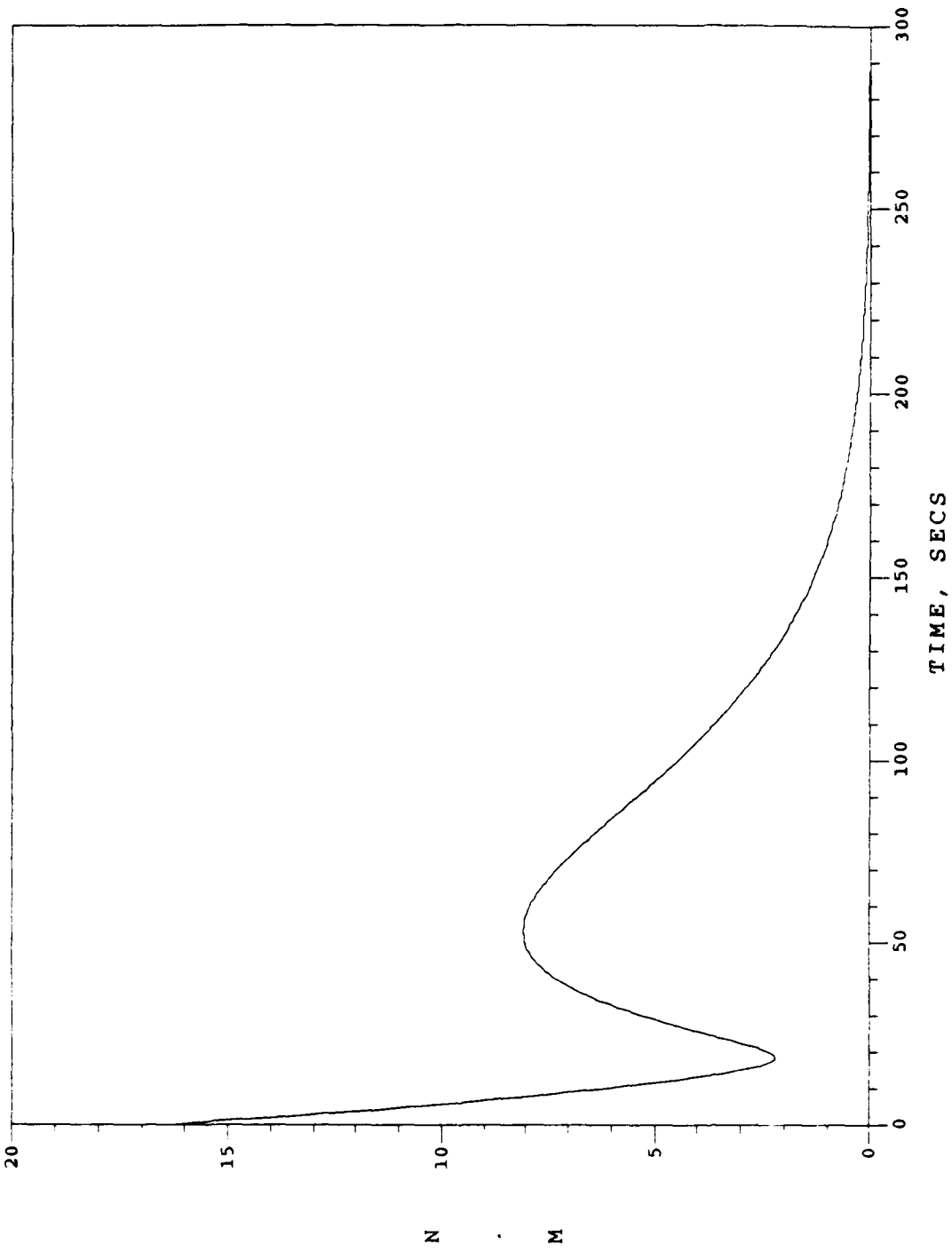


Fig. 63. Detumble/Despin Phase / Case 5  
Constraint Torque at Joint 1

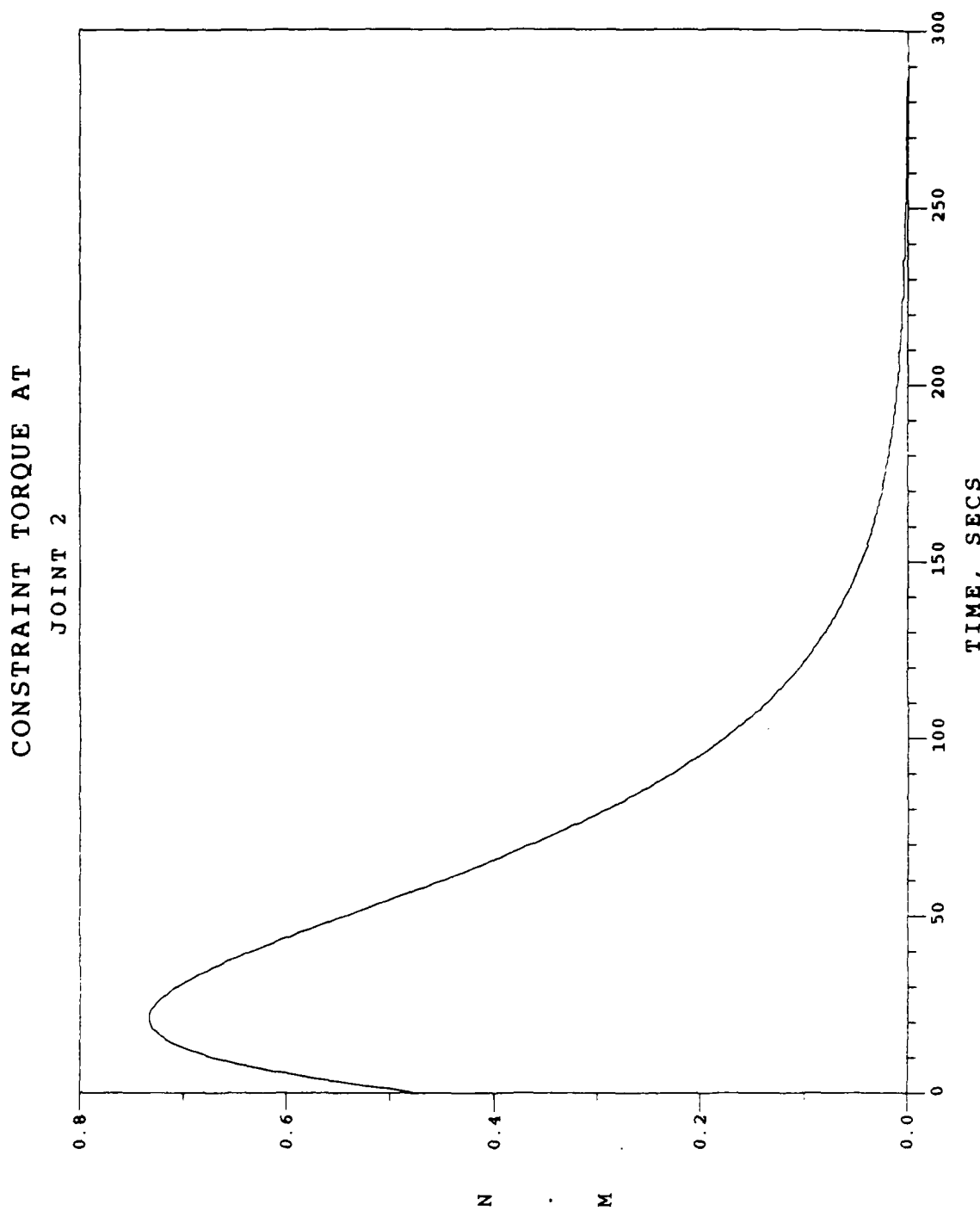


Fig. 64. Detumble/Despin Phase / Case 5  
Constraint Torque at Joint 2

CONSTRAINT TORQUE AT  
JOINT 3

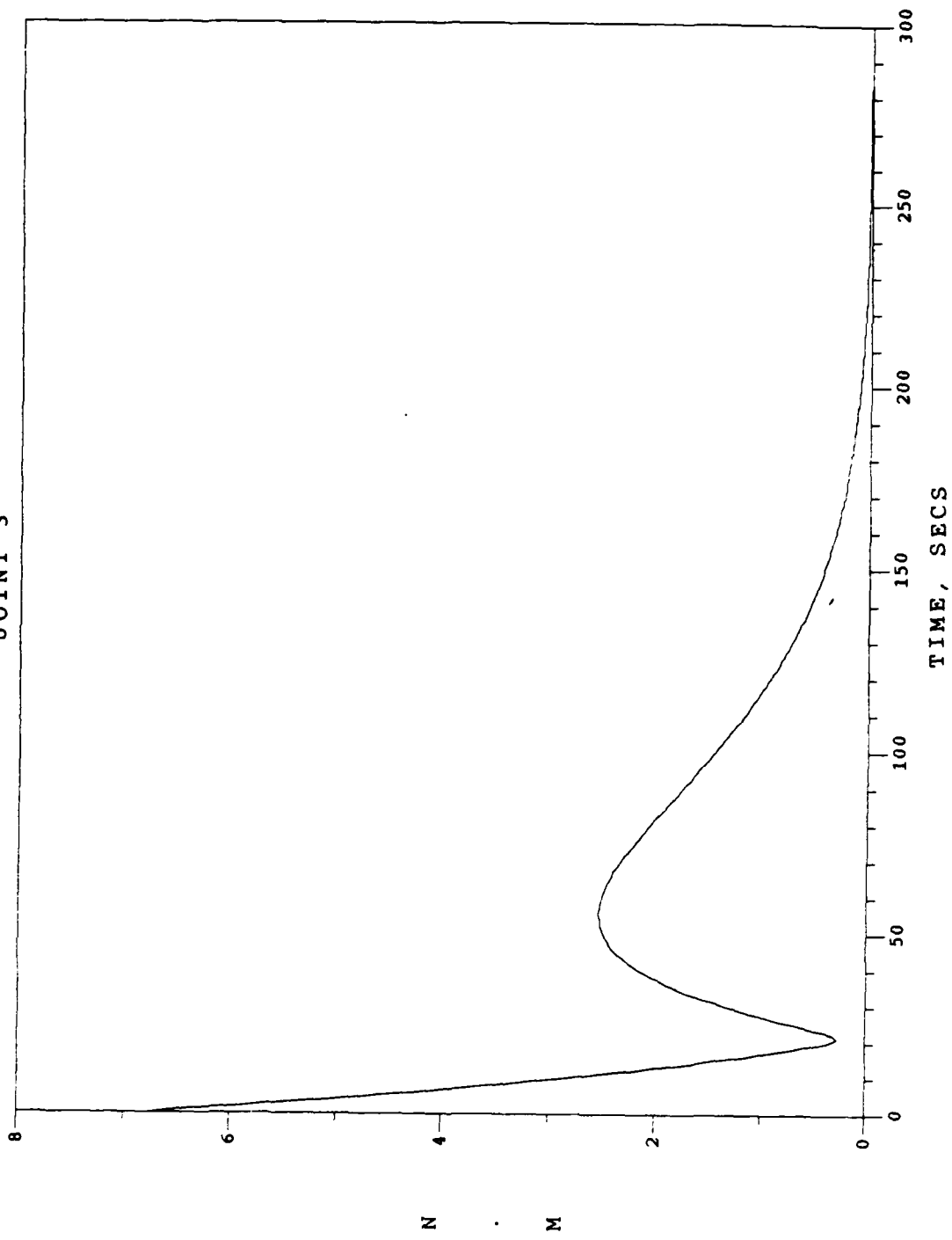


Fig. 65. Detumble/Despin Phase / Case 5  
Constraint Torque at Joint 3

CONSTRAINT FORCE AT JOINT 1  
IN Y DIRECTION - ALONG BODY 0

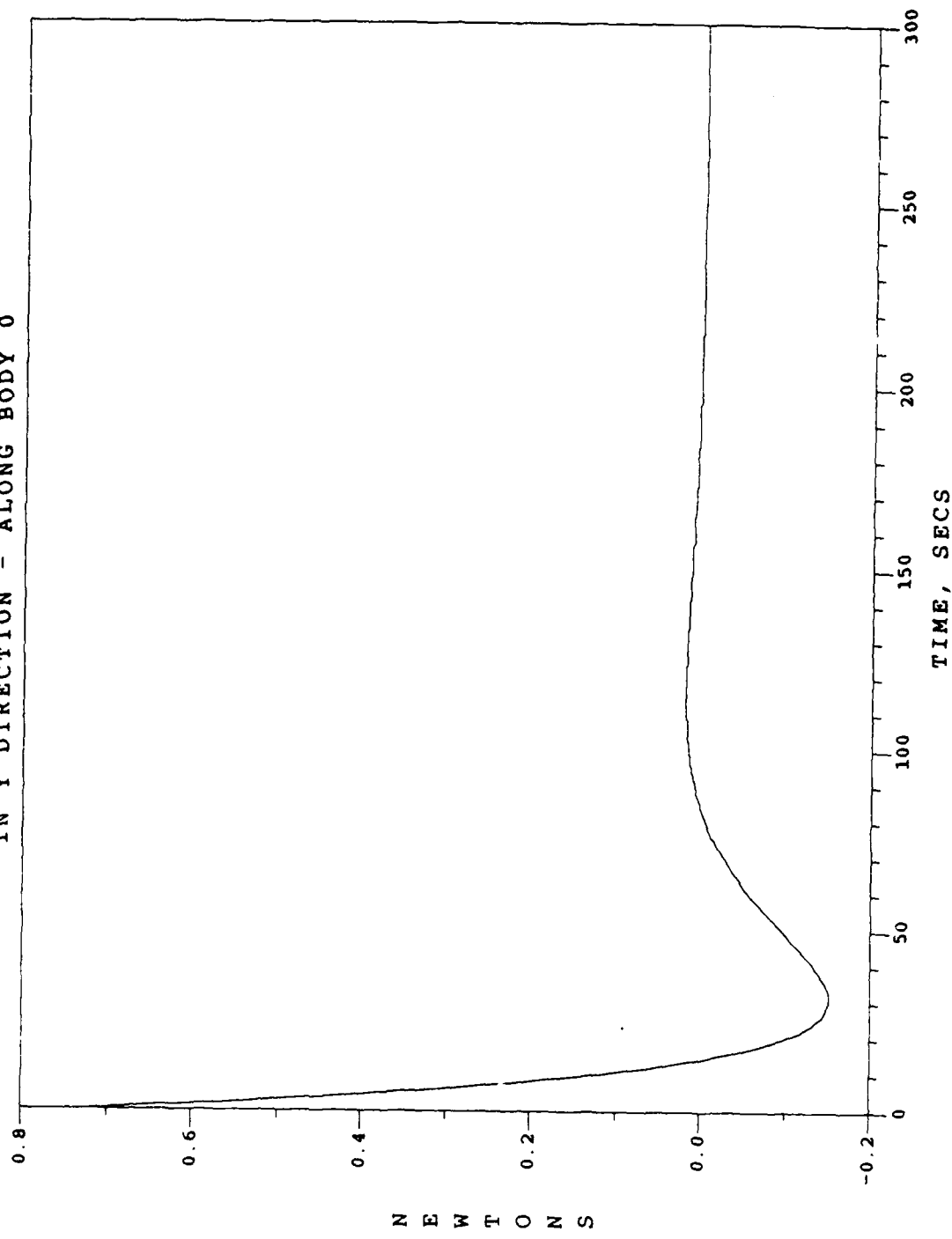


Fig. 66. Detumble/Despin Phase / Case 5  
Joint 1 Constraint Force in Y-Direction

EXTERNAL TORQUE T1  
(THRUSTER ON BODY 0)

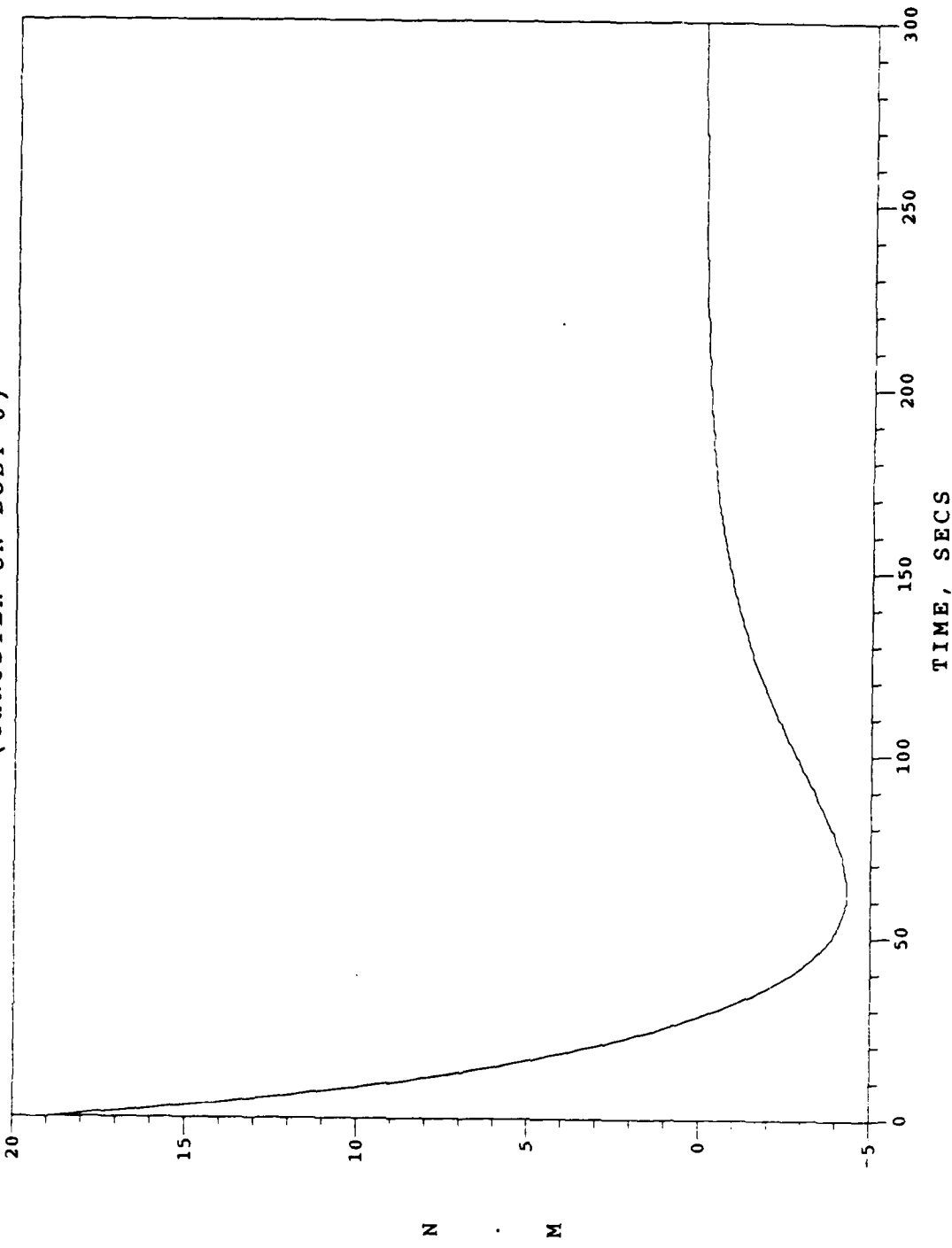


Fig. 67. Detumble/Despin Phase / Case 6  
External Torque T1

INTERNAL MOTOR TORQUE TG1  
(AT JOINT 1)

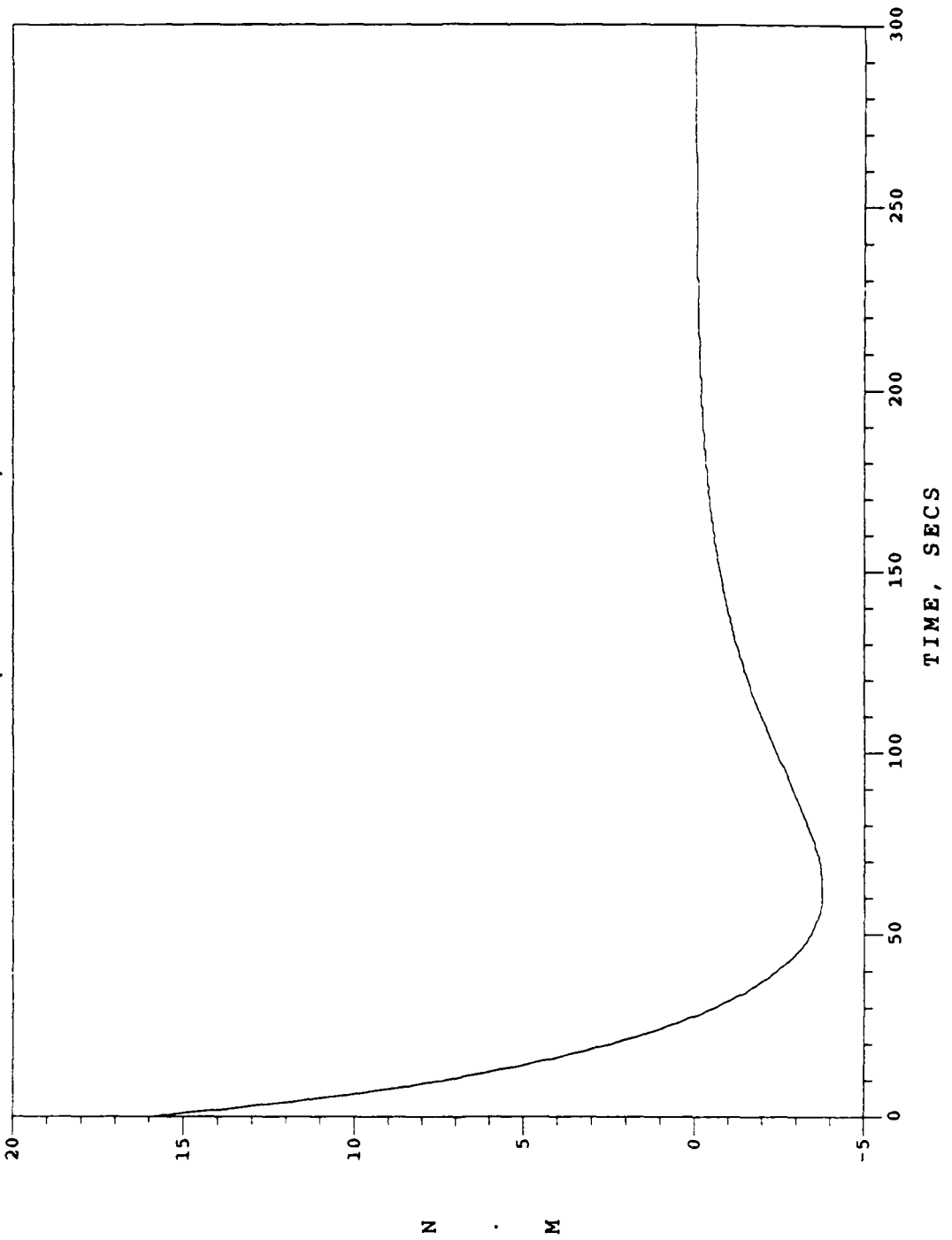


Fig. 68. Detumble/Despin Phase / Case 6  
Internal Motor Torque TG1

INTERNAL MOTOR TORQUE TG4  
(AT JOINT 3)

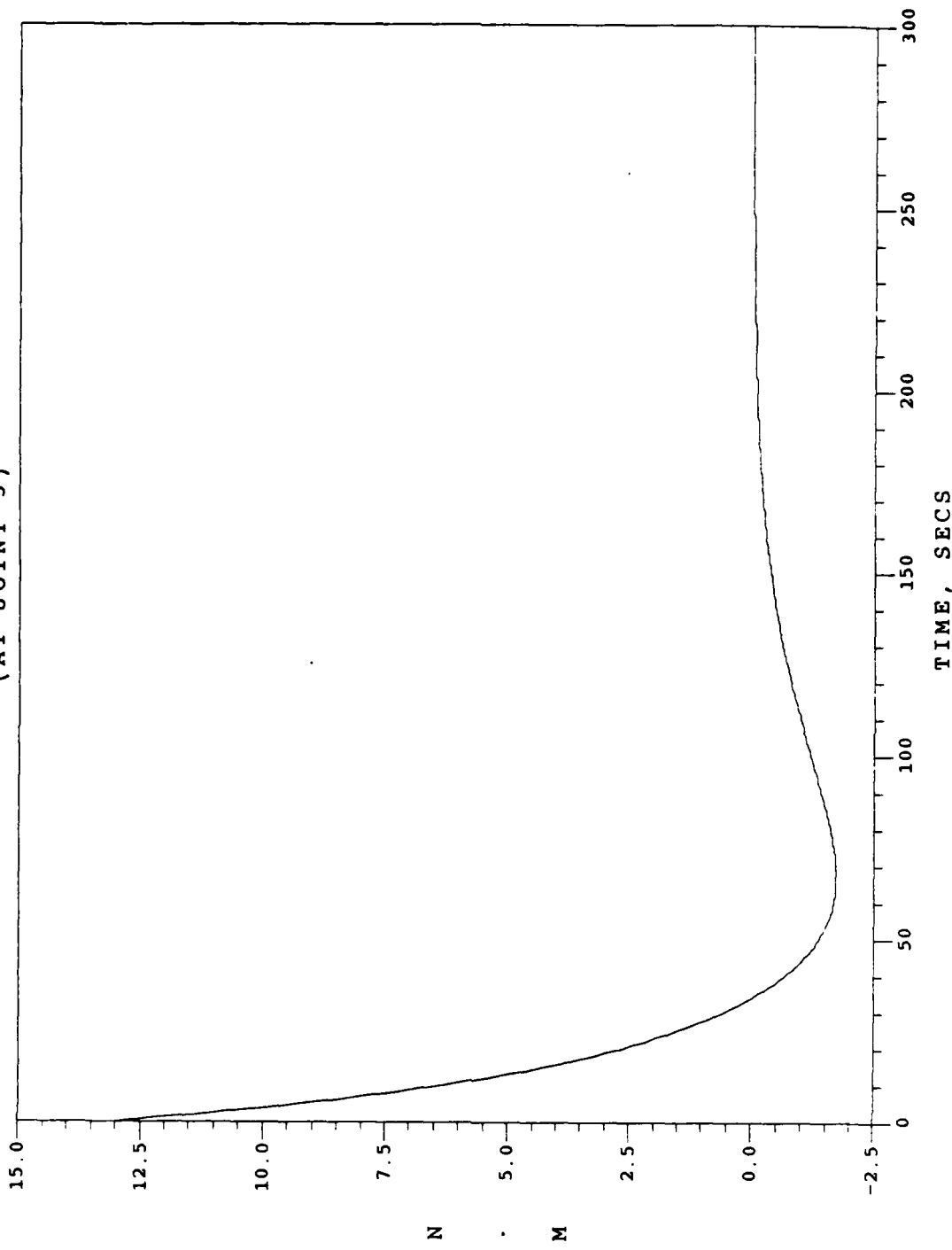


Fig. 69. Detumble/Despin Phase / Case 6  
Internal Motor Torque TG4

EXTERNAL TORQUE T1  
(THRUSTER ON BODY 0)

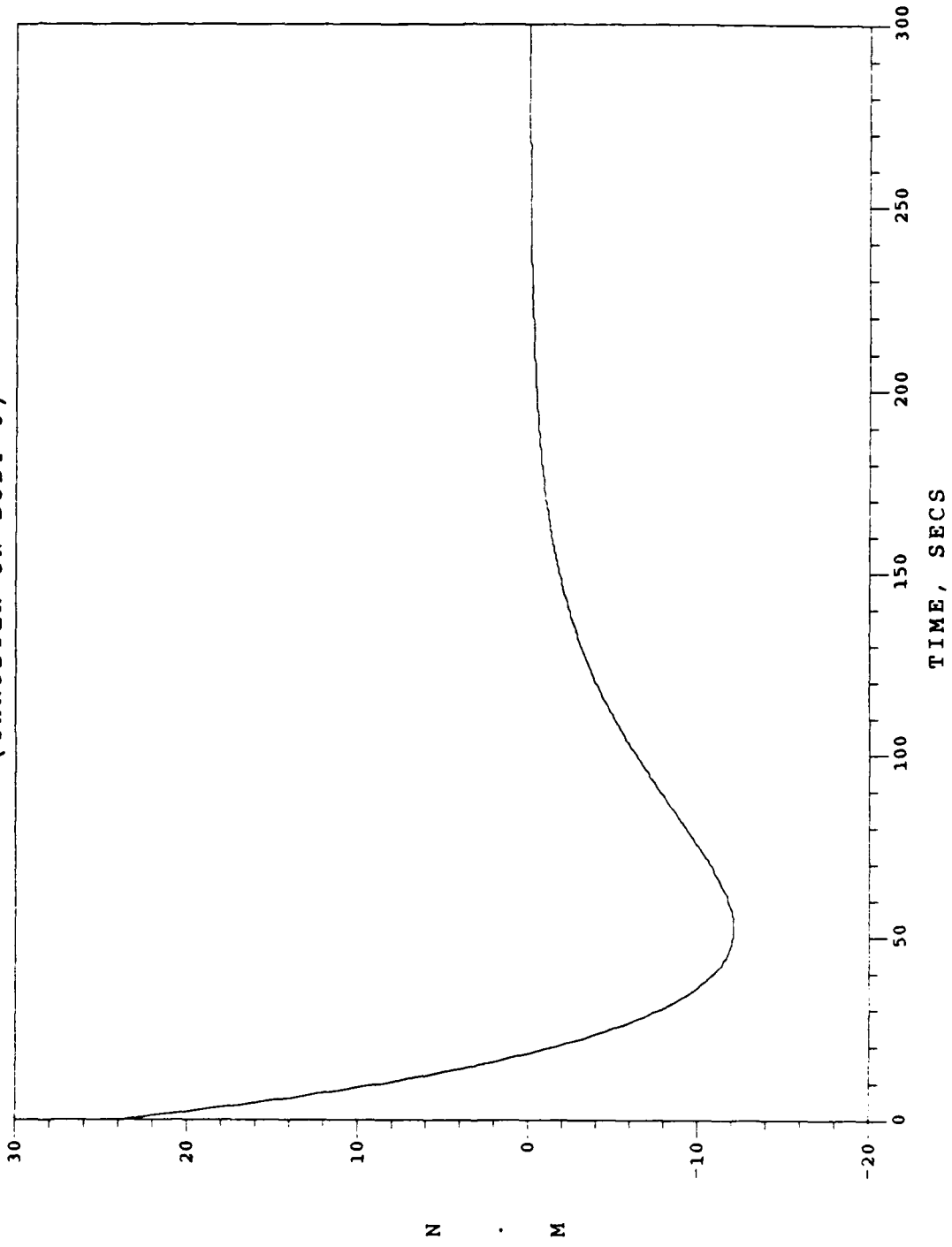


Fig. 70. Detumble/Despin Phase / Case 7  
External Torque T1

INTERNAL MOTOR TORQUE TG1  
(AT JOINT 1)

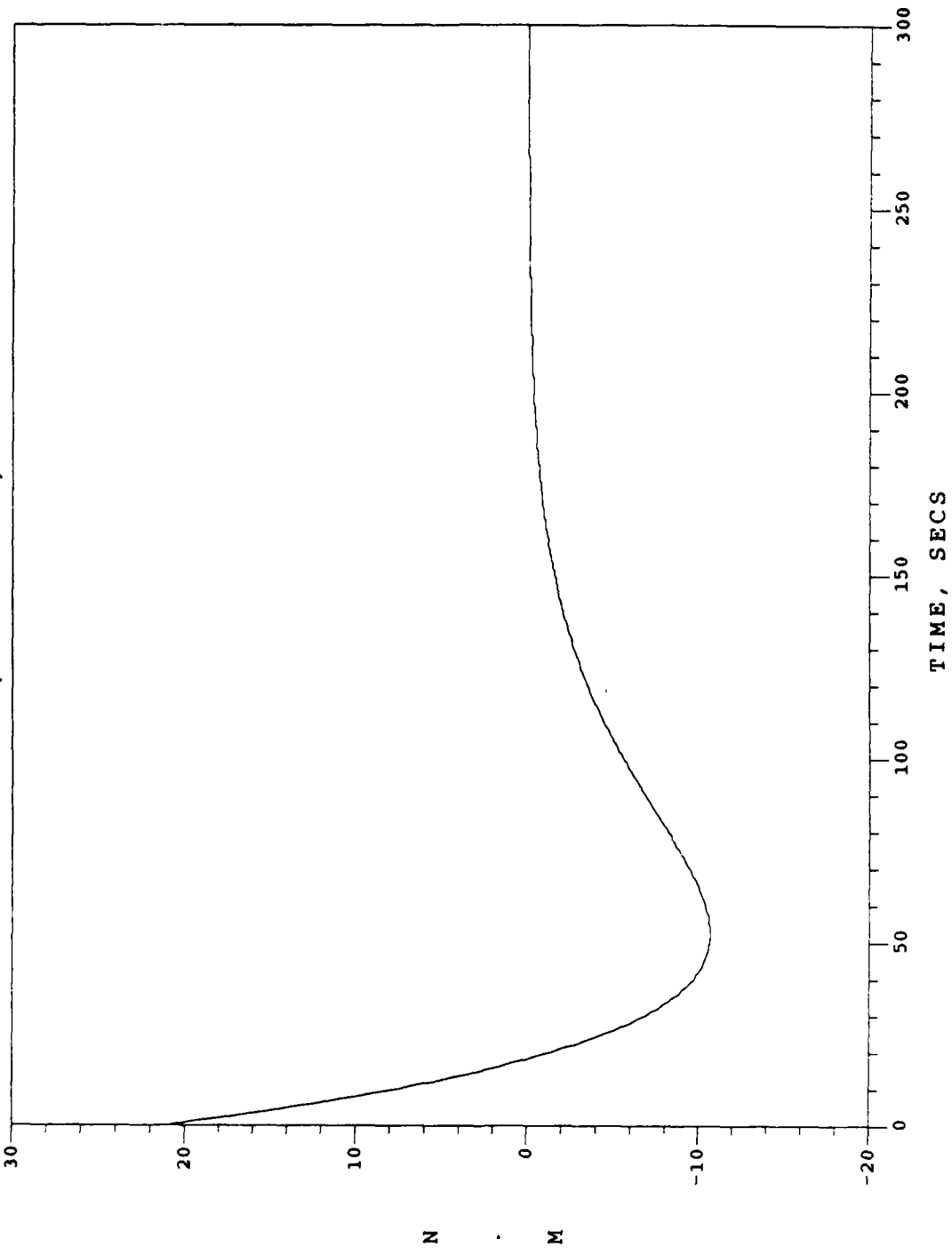


Fig. 71. Detumble/Despin Phase / Case 7  
Internal Motor Torque TG1

INTERNAL MOTOR TORQUE TG4  
(AT JOINT 3)

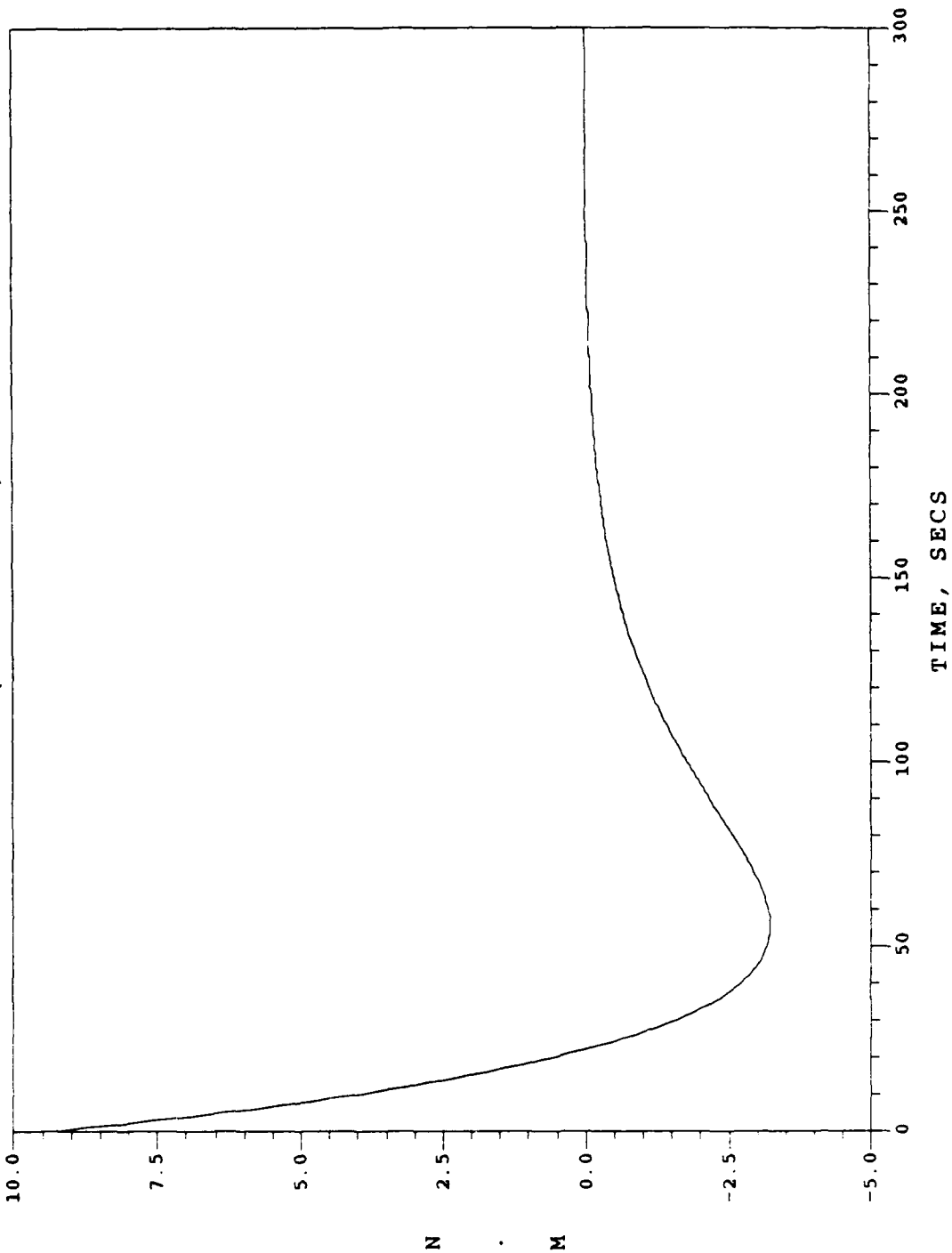


Fig. 72. Detumble/Despin Phase / Case 7  
Internal Motor Torque TG4

EXTERNAL TORQUE  $T_1$   
(THRUSTER ON BODY 0)

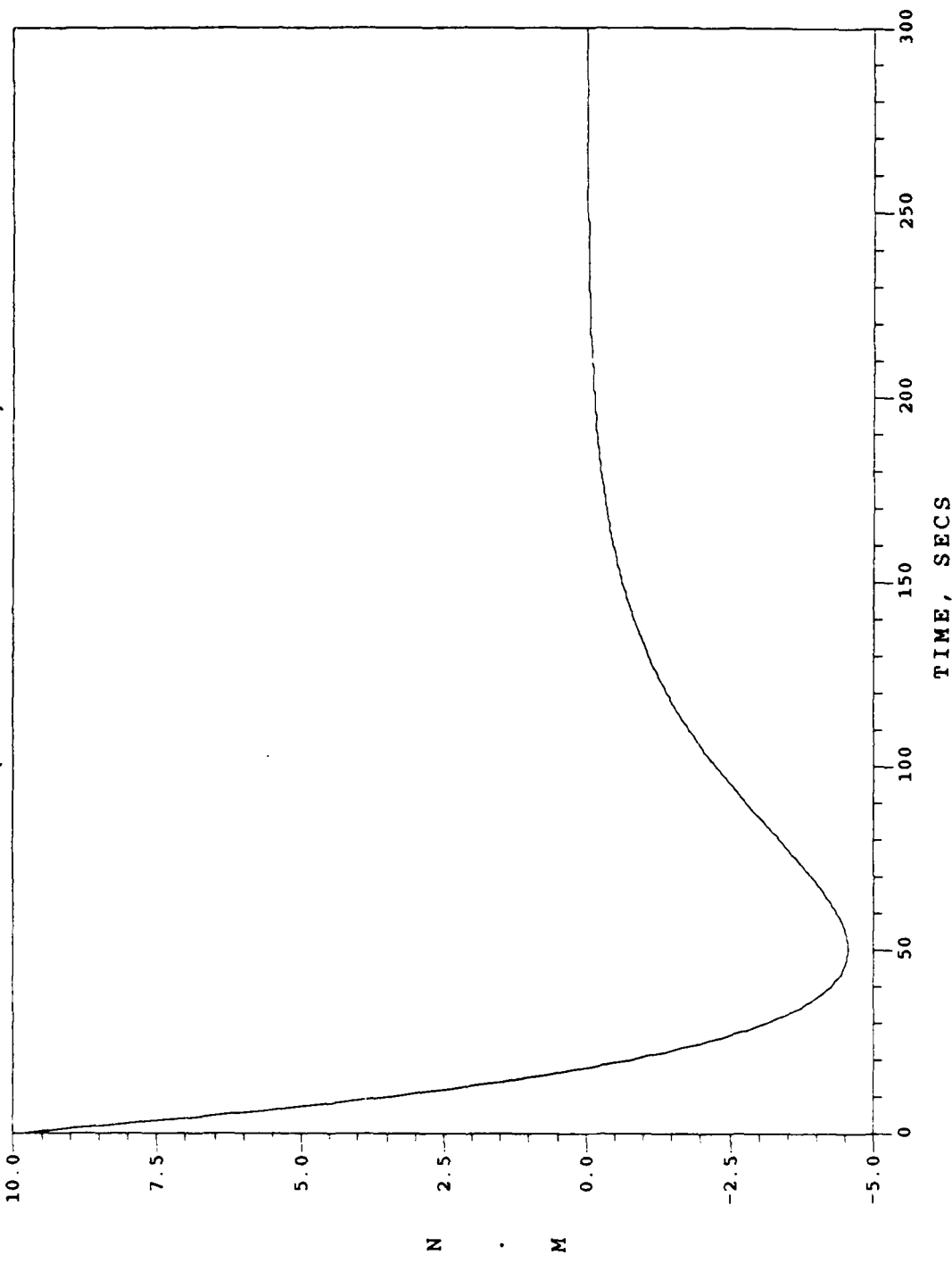


Fig. 73. Detumble/Despin Phase / Case 8  
External Torque  $T_1$

INTERNAL MOTOR TORQUE TG1  
(AT JOINT 1)

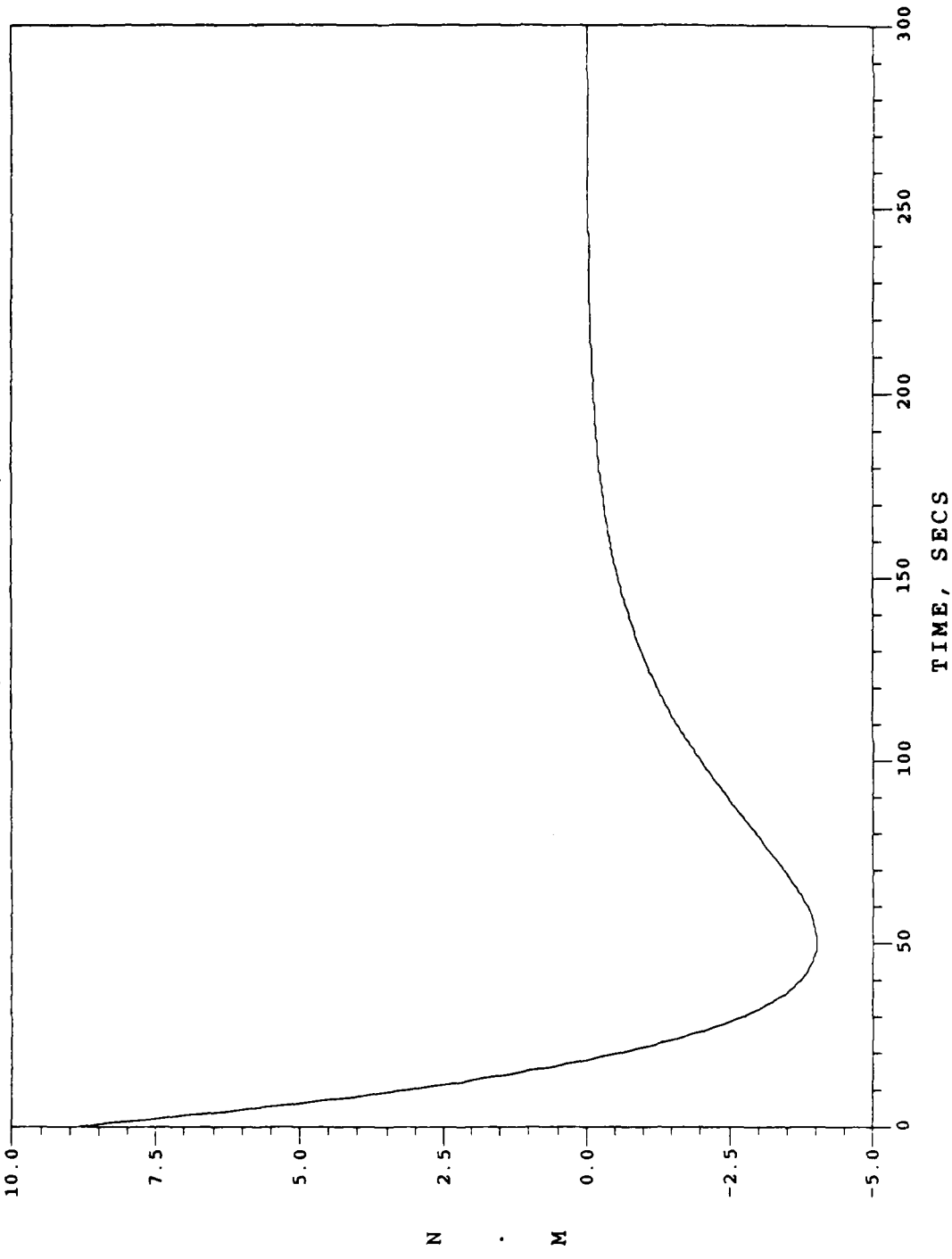


Fig. 74. Detumble/Despin Phase / Case 8  
Internal Motor Torque TG1

INTERNAL MOTOR TORQUE TG4  
( AT JOINT 3 )

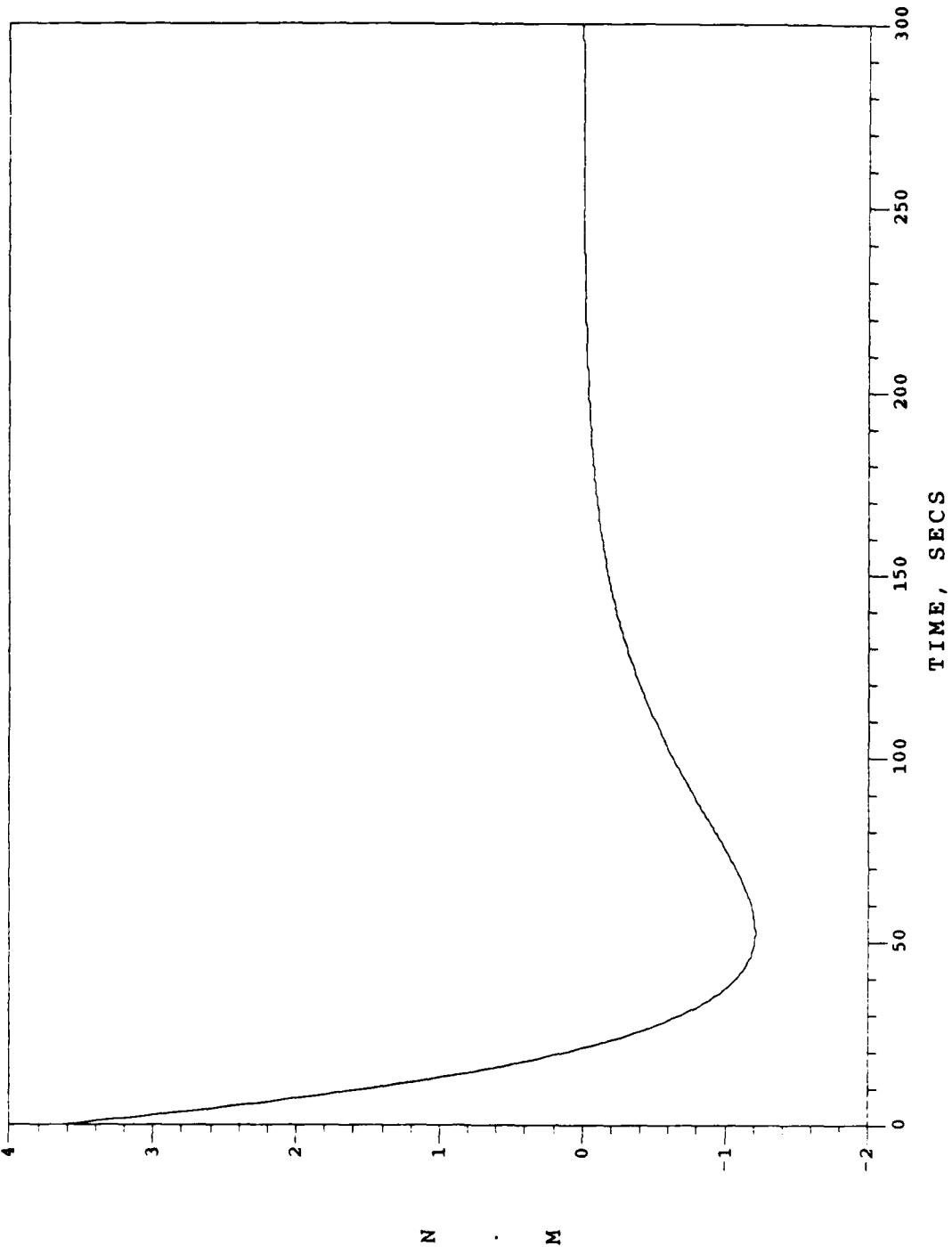


Fig. 75. Detumble/Despin Phase / Case 8  
Internal Motor Torque TG4

BODY 1 ANGLE  
GAMMA 1

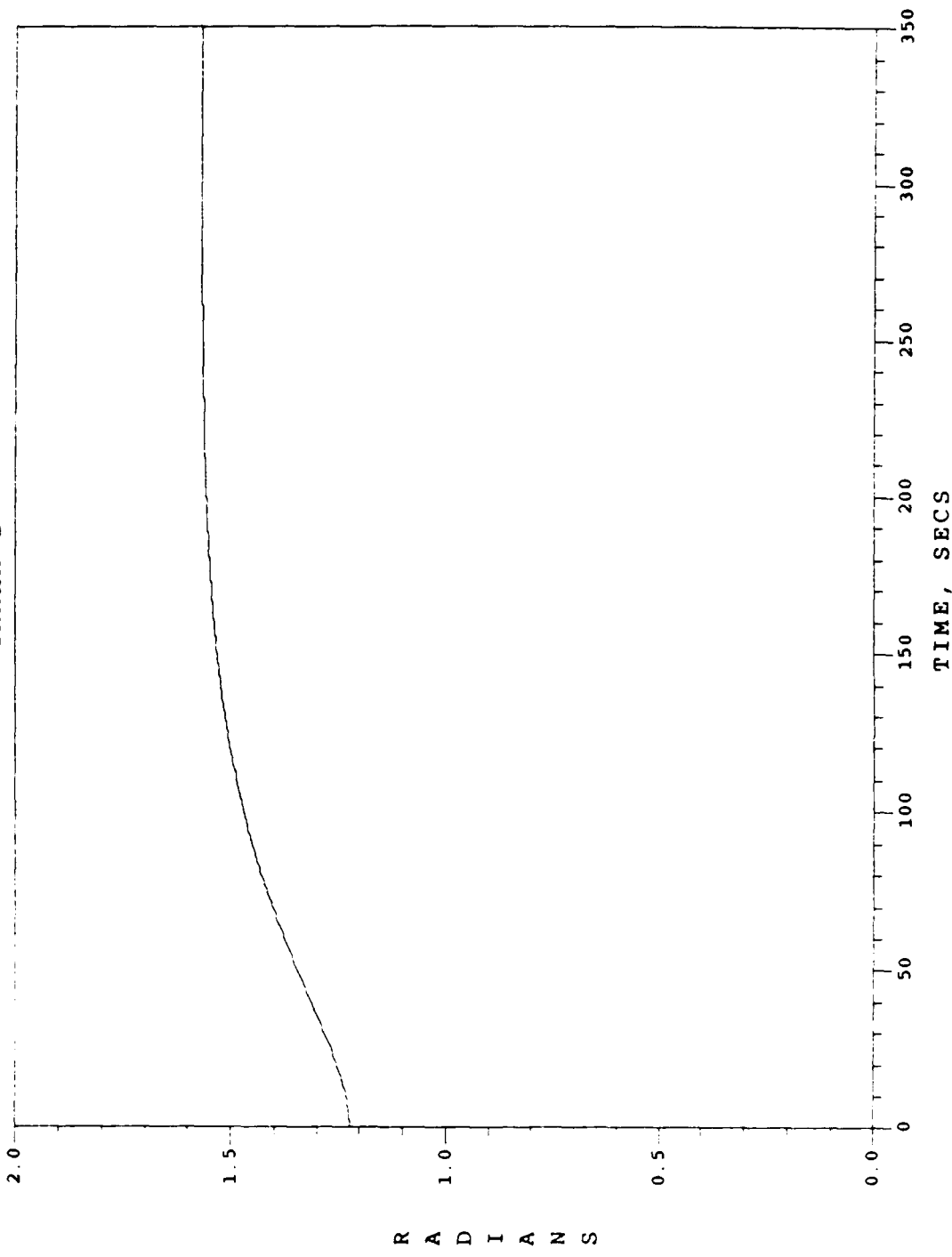


Fig. 76. Detumble/Despin Phase / Case 9  
Body 1  $\gamma_1$  History

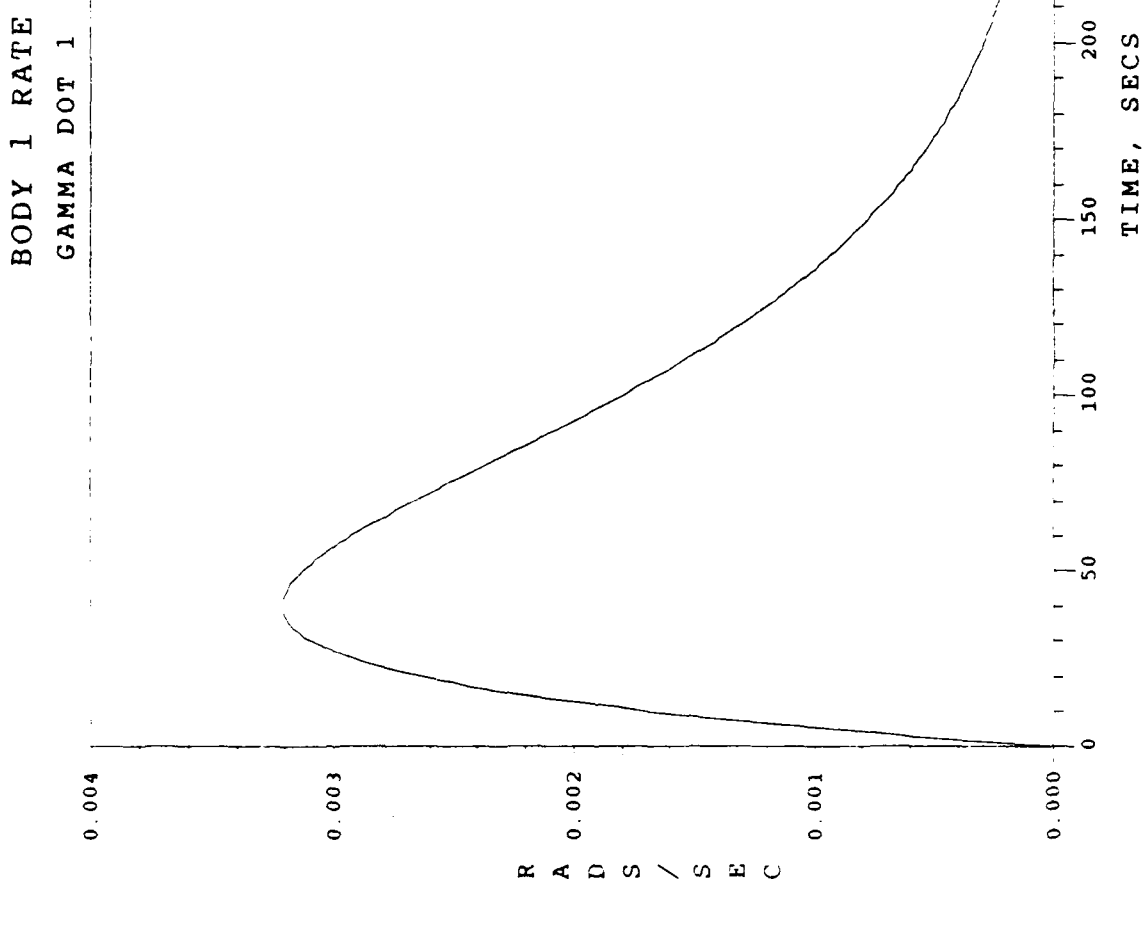


Fig. 77. Detumble/Despin Phase / Case 9  
Body 1  $\dot{\gamma}_1$  History

BODY 2 ANGLE  
GAMMA 3

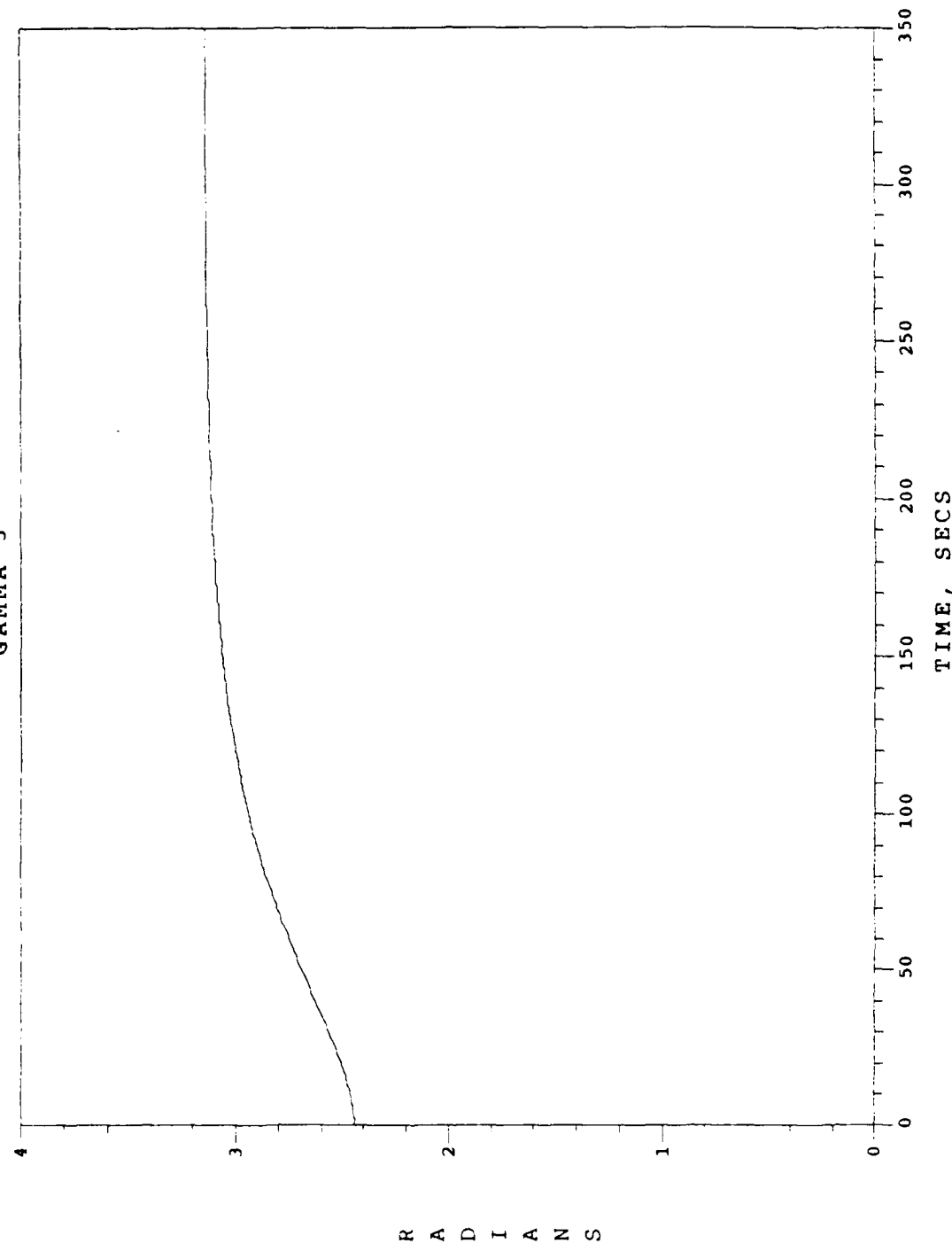


Fig. 78. Detumble/Despin Phase / Case 9  
Body 2  $\gamma_3$  History

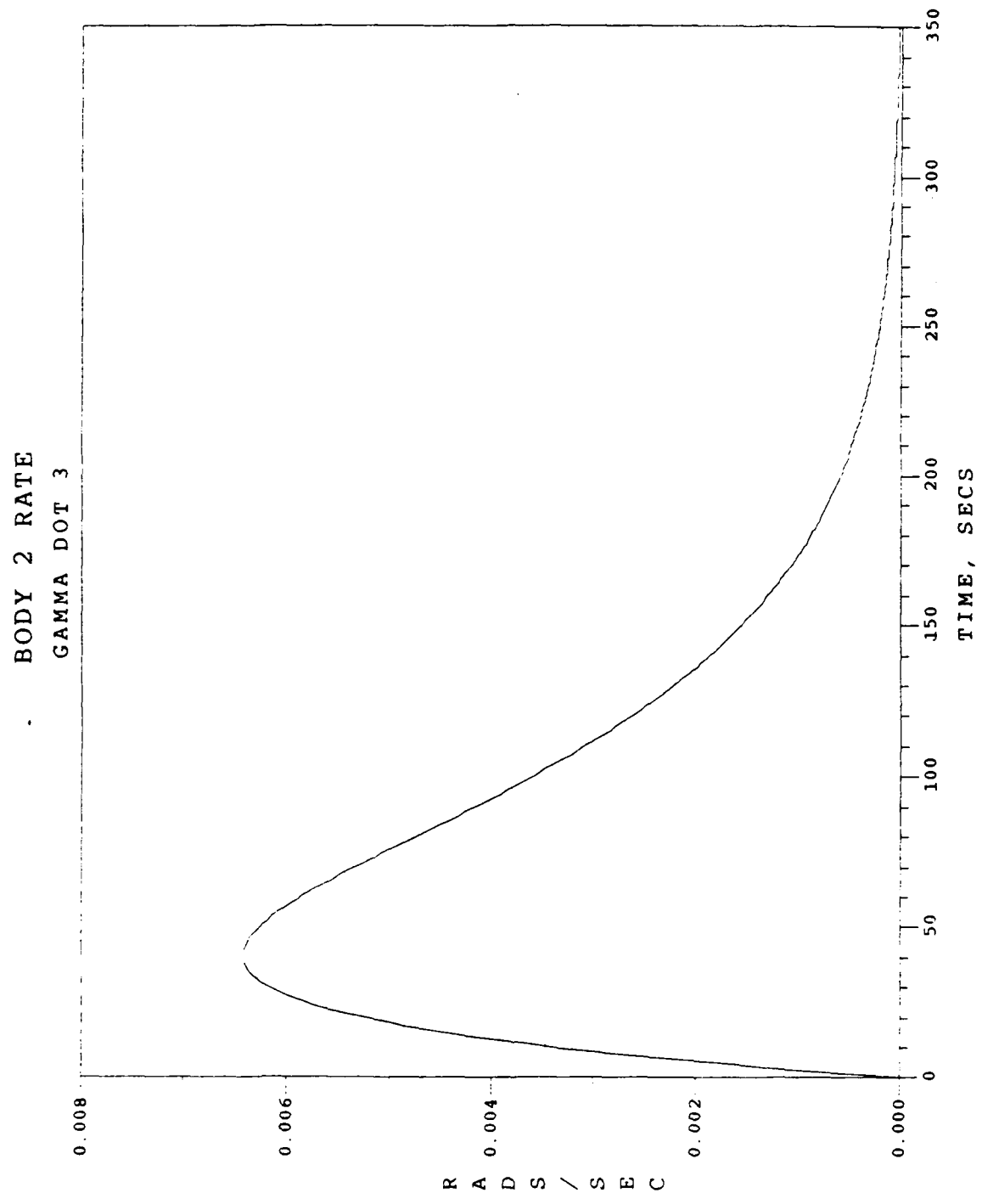


Fig. 79. Detumble/Despin Phase / Case 9  
Body 2  $\dot{\gamma}_3$  History

BODY 3 AND 4 ANGLE  
GAMMA 4

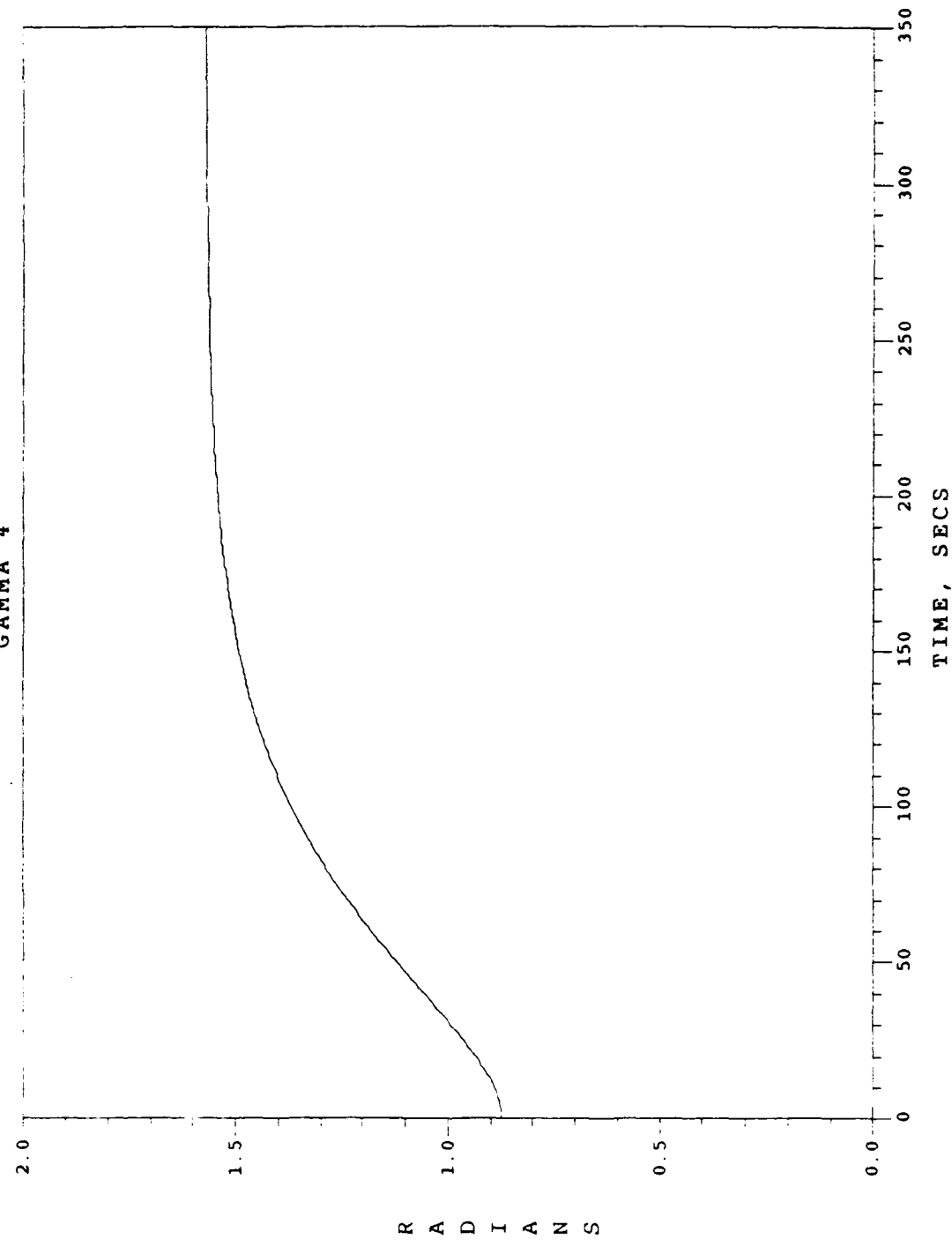


Fig. 80. Detumble/Despin Phase / Case 9  
Body 3/4  $\gamma_4$  History

BODY 3 AND 4 RATE  
GAMMA DOT 4

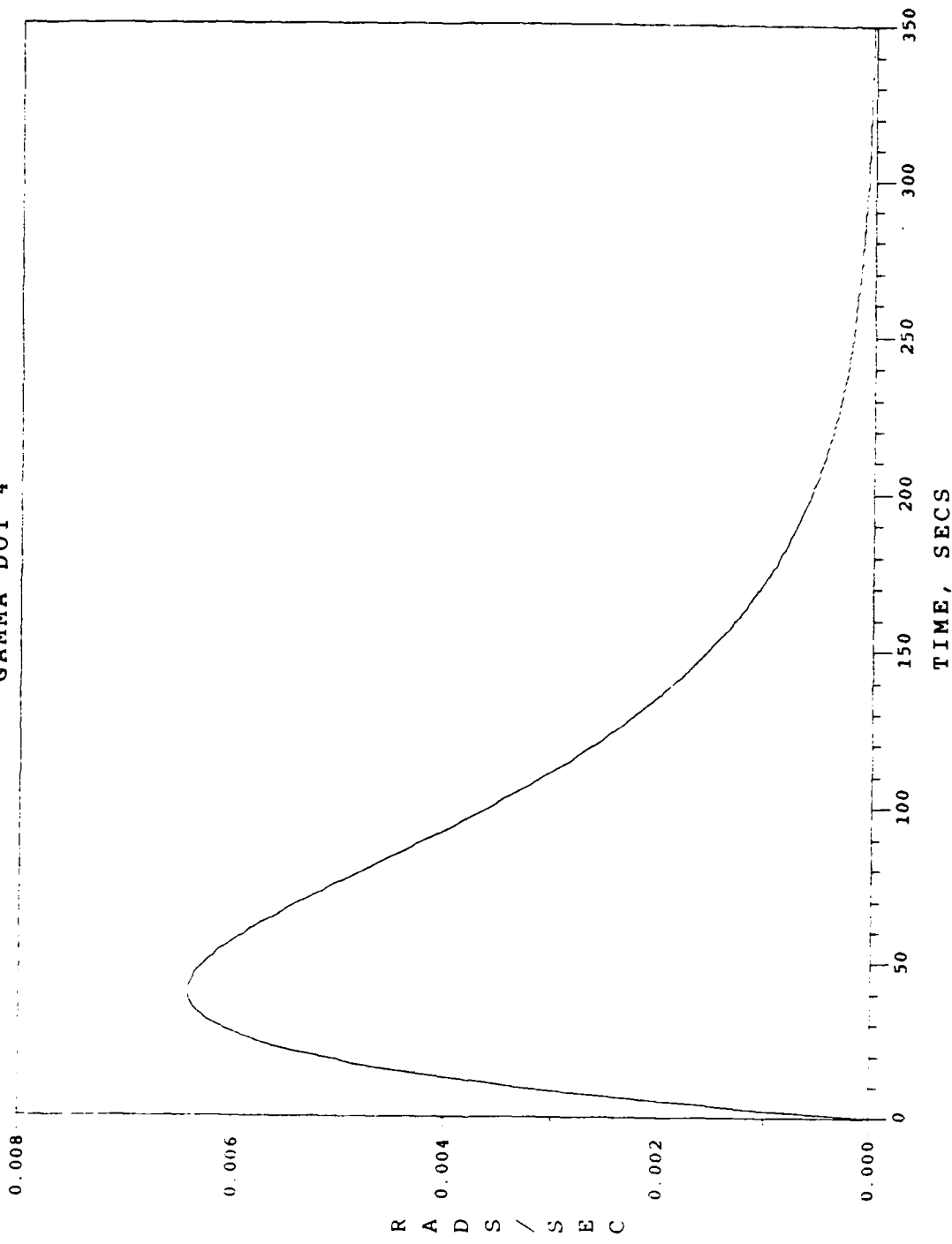


Fig. 81. Detumble/Despin Phase / Case 9  
Body 3/4  $\dot{\gamma}_4$  History

BODY 3 RATE  
GAMMA DOT 5

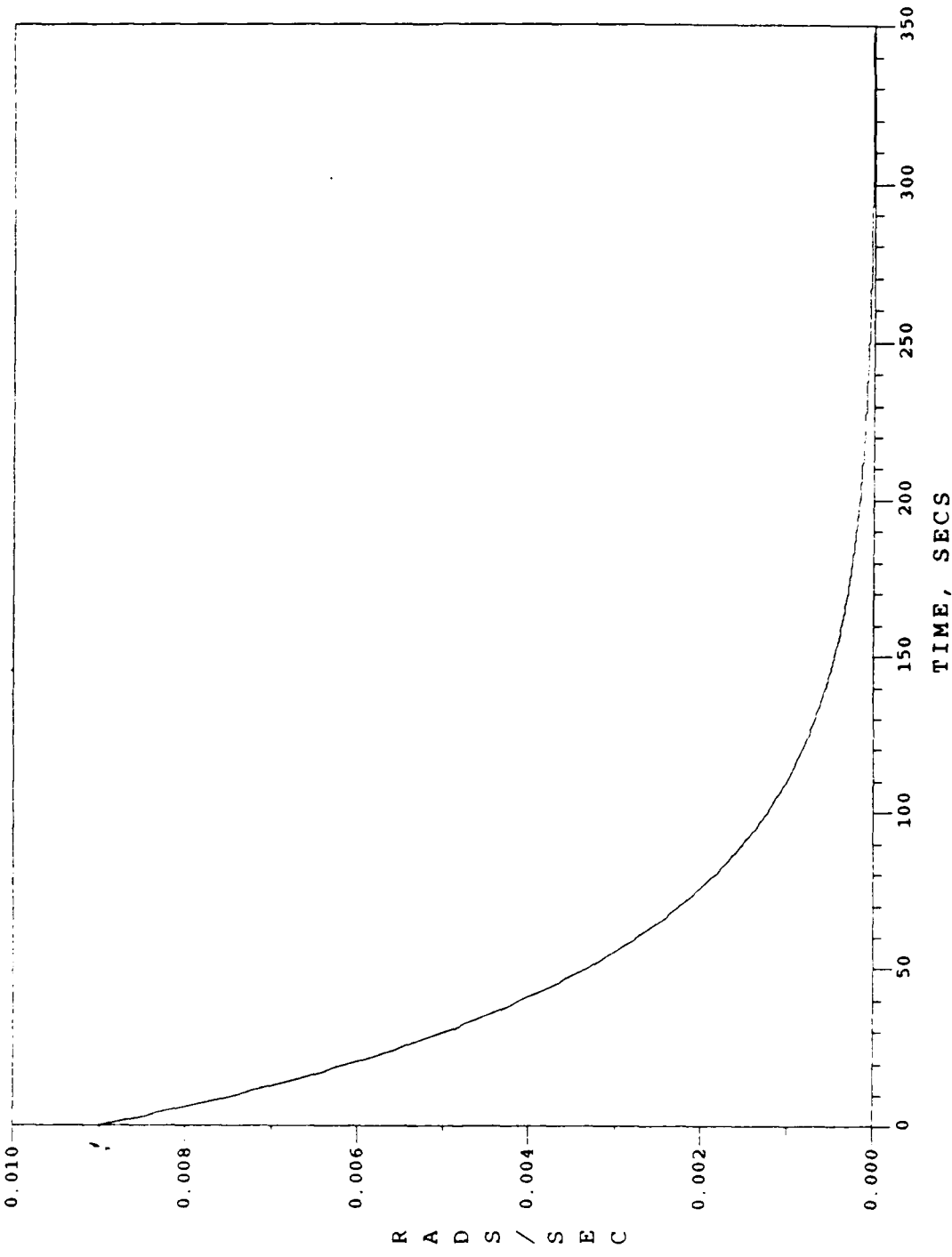


Fig. 82. Detumble/Despin Phase / Case 9  
Body 3  $\dot{\gamma}_5$  History

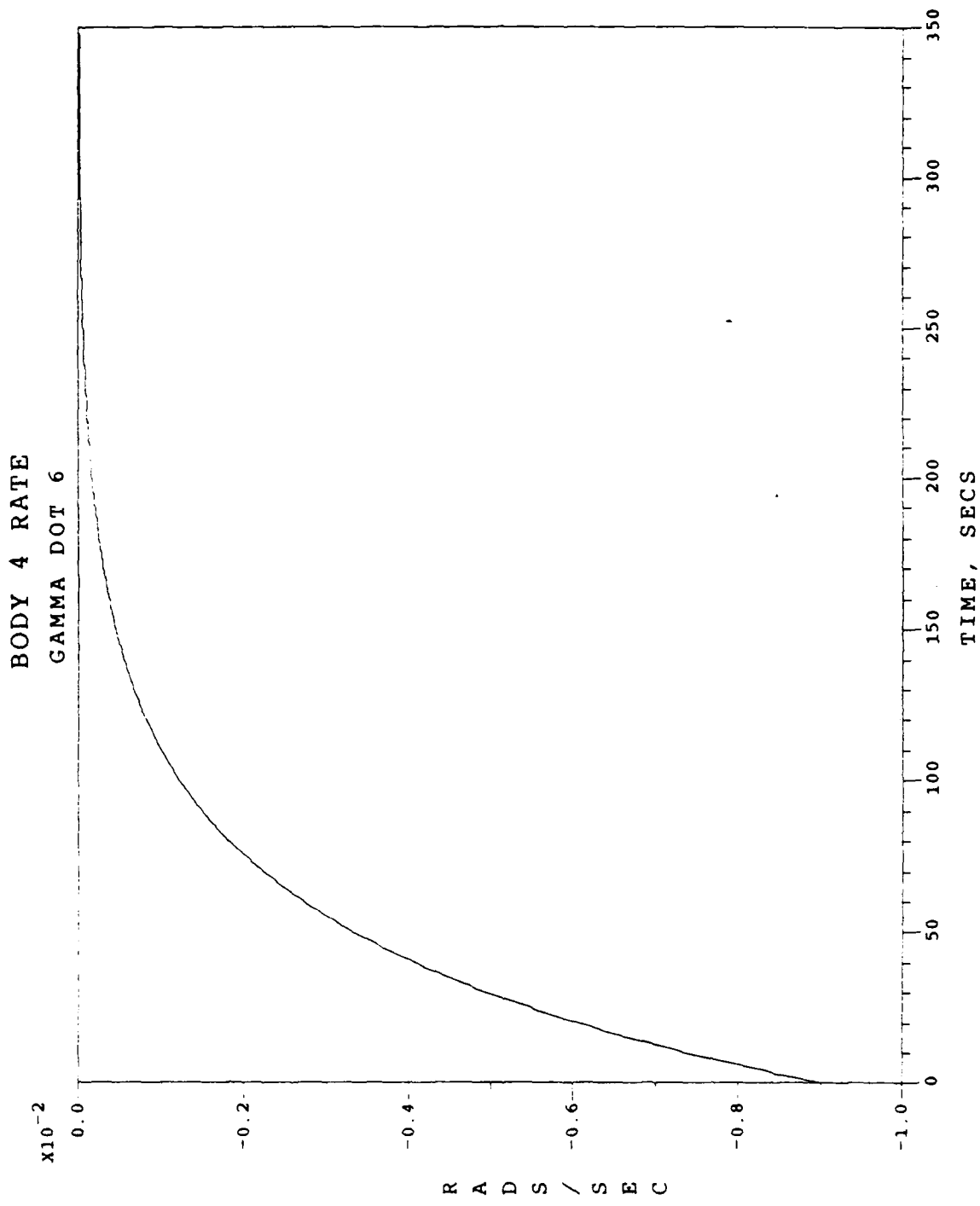


Fig. 83. Detumble/Despin Phase / Case 9  
Body 4  $\dot{\gamma}_6$  History

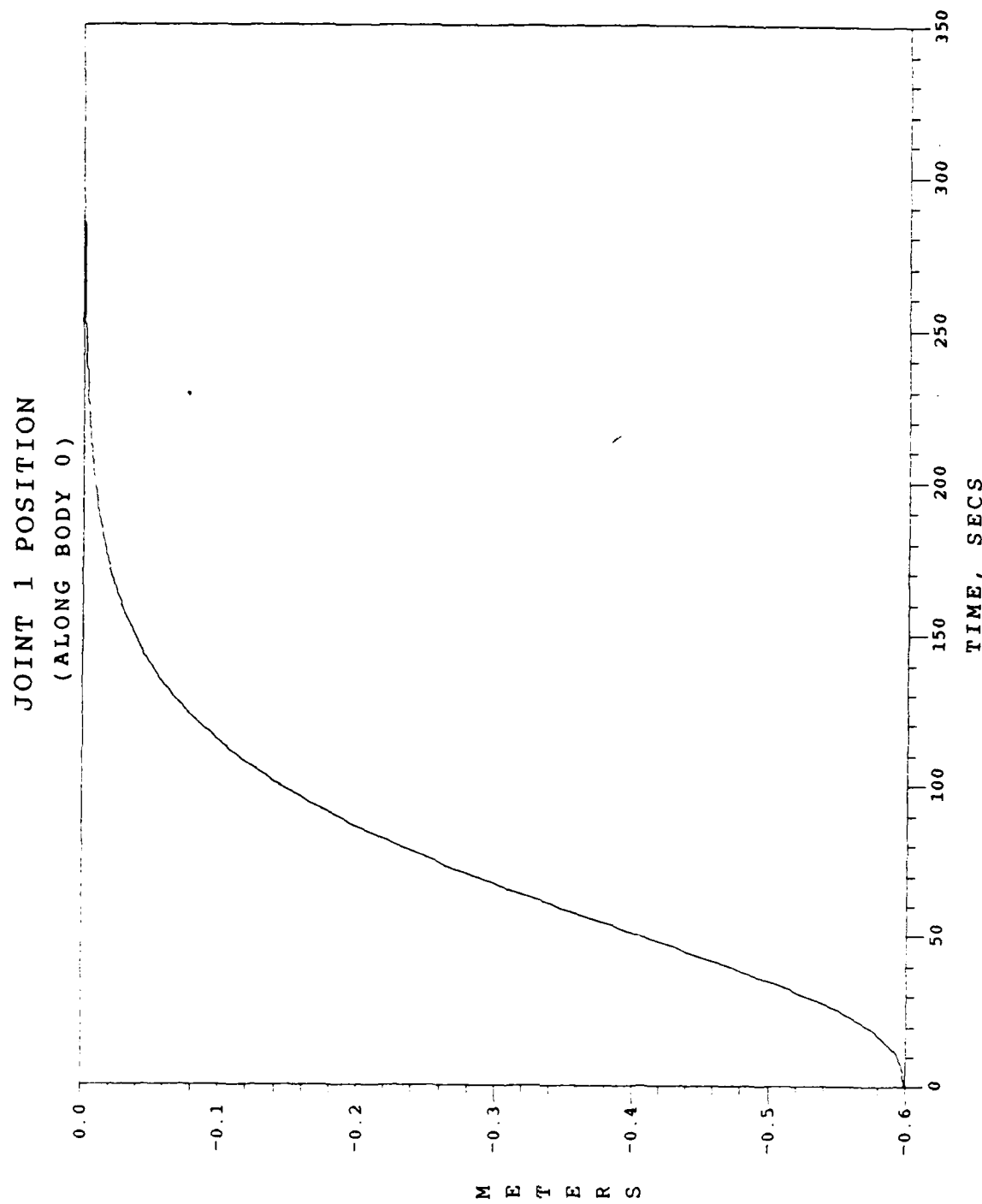


Fig. 84. Detumble/Despin Phase / Case 9  
Joint 1 Position

JOINT 1 RELATIVE VELOCITY  
(ALONG BODY 0)

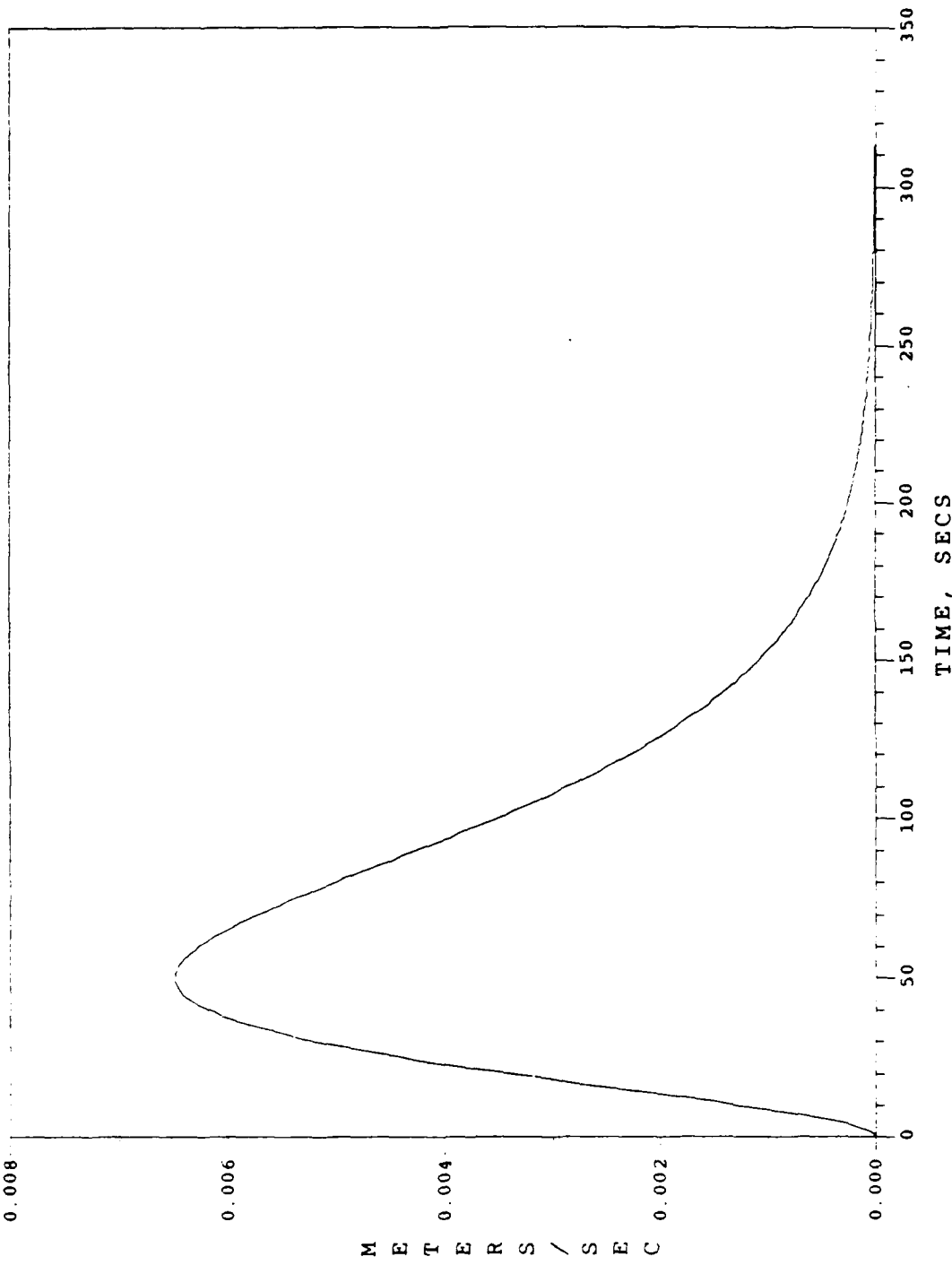


Fig. 85. Detumble/Despin Phase / Case 9  
Joint 1 Relative Velocity

JOINT 1 RELATIVE ACCELERATION  
(ALONG BODY 0)

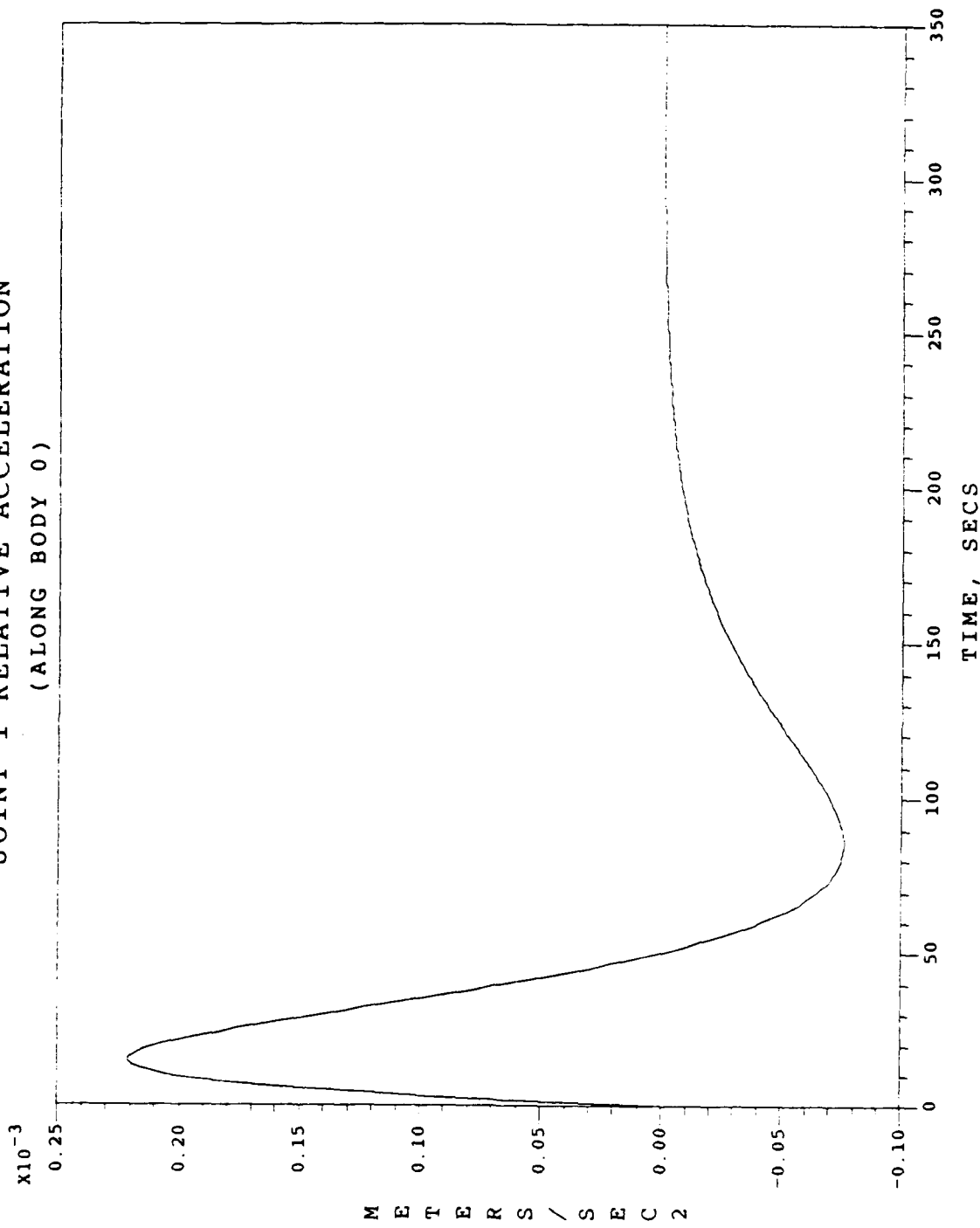


Fig. 86. Detumble/Despin Phase / Case 9  
Joint 1 Relative Acceleration

EXTERNAL TORQUE T1  
(THRUSTER ON BODY 0)

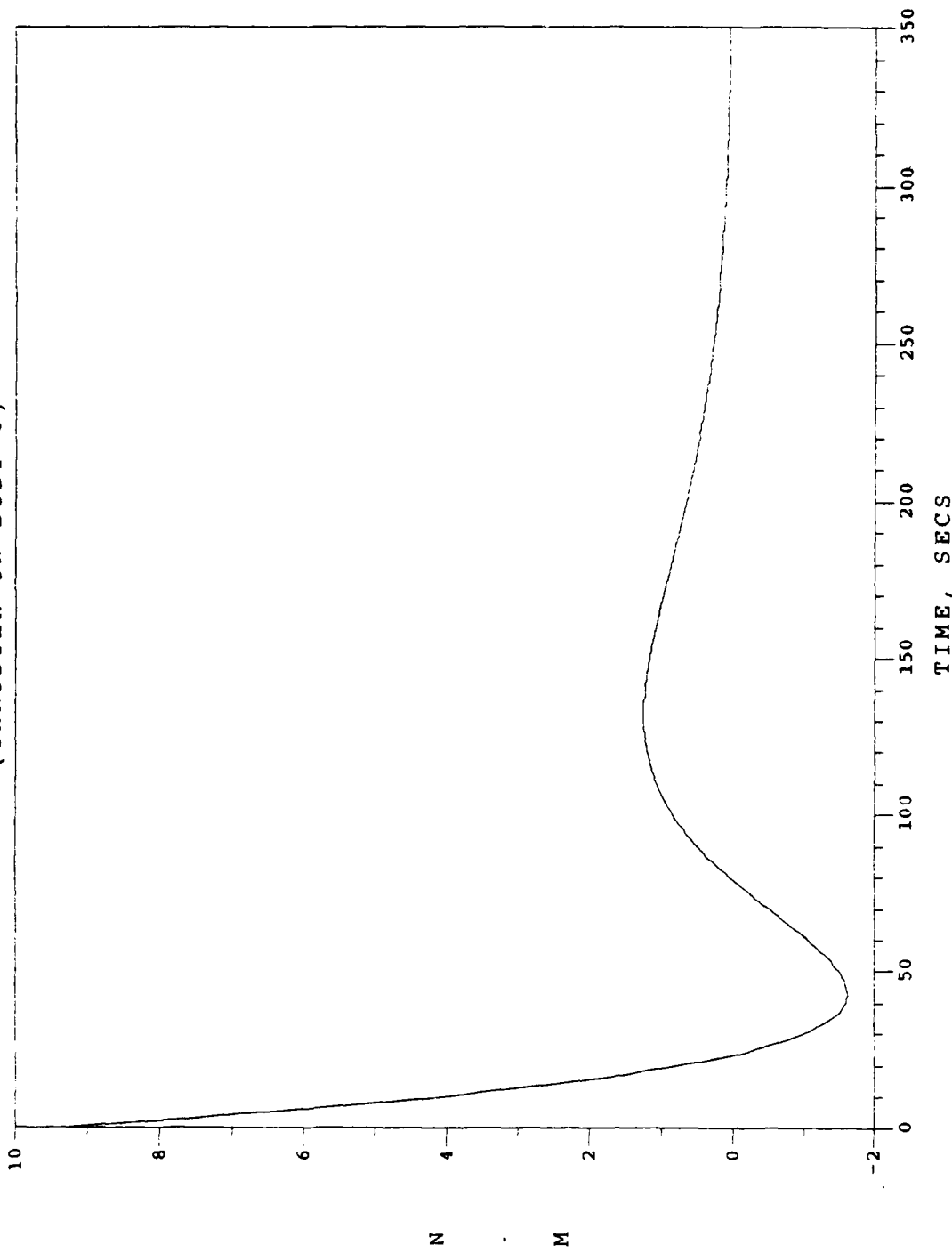


Fig. 87. Detumble/Despin Phase / Case 9  
External Torque T1

EXTERNAL TORQUE T2  
(THRUSTER ON BODY 0)

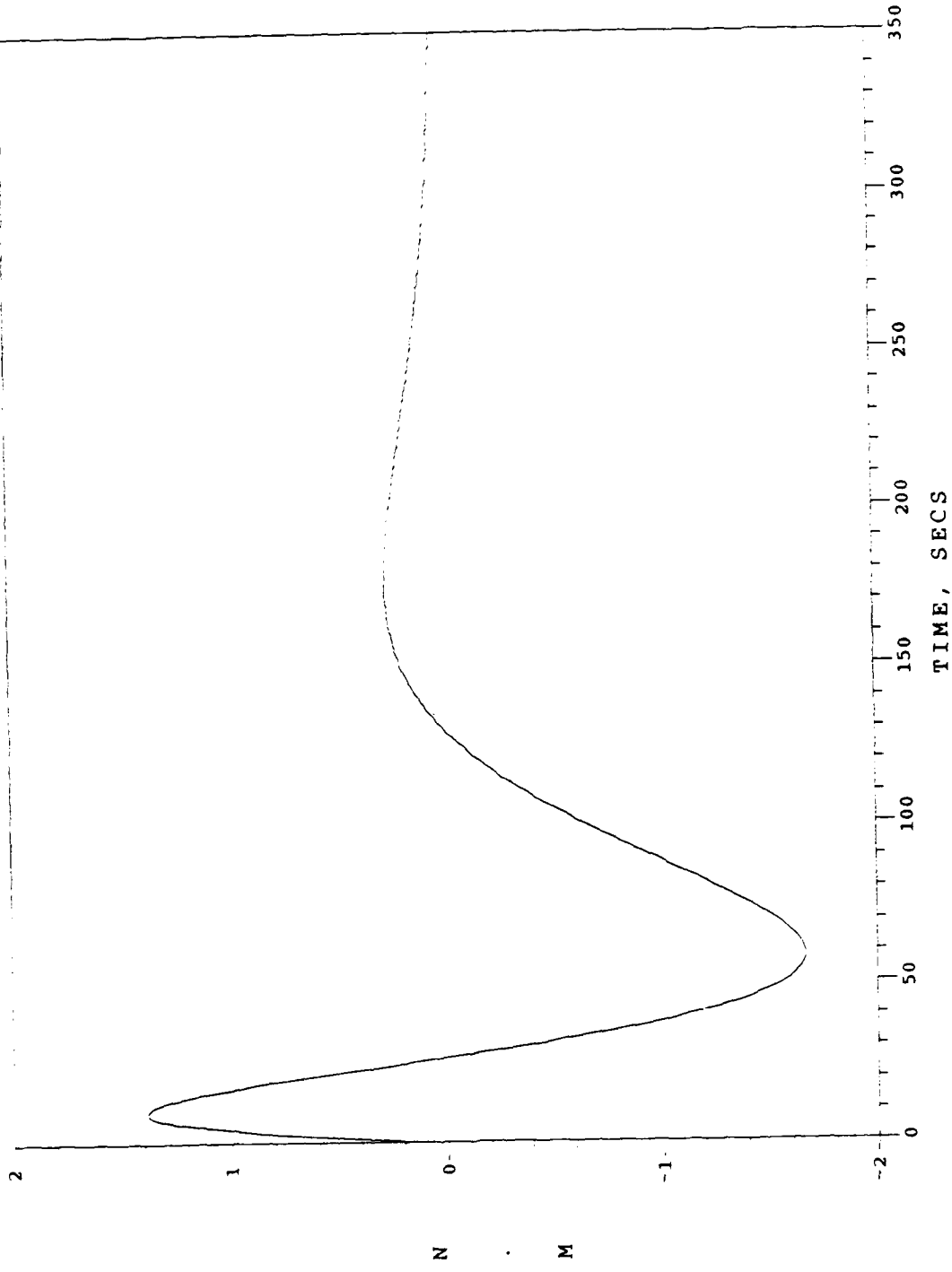


Fig. 88. Detumble/Despin Phase / Case 9  
External Torque T2

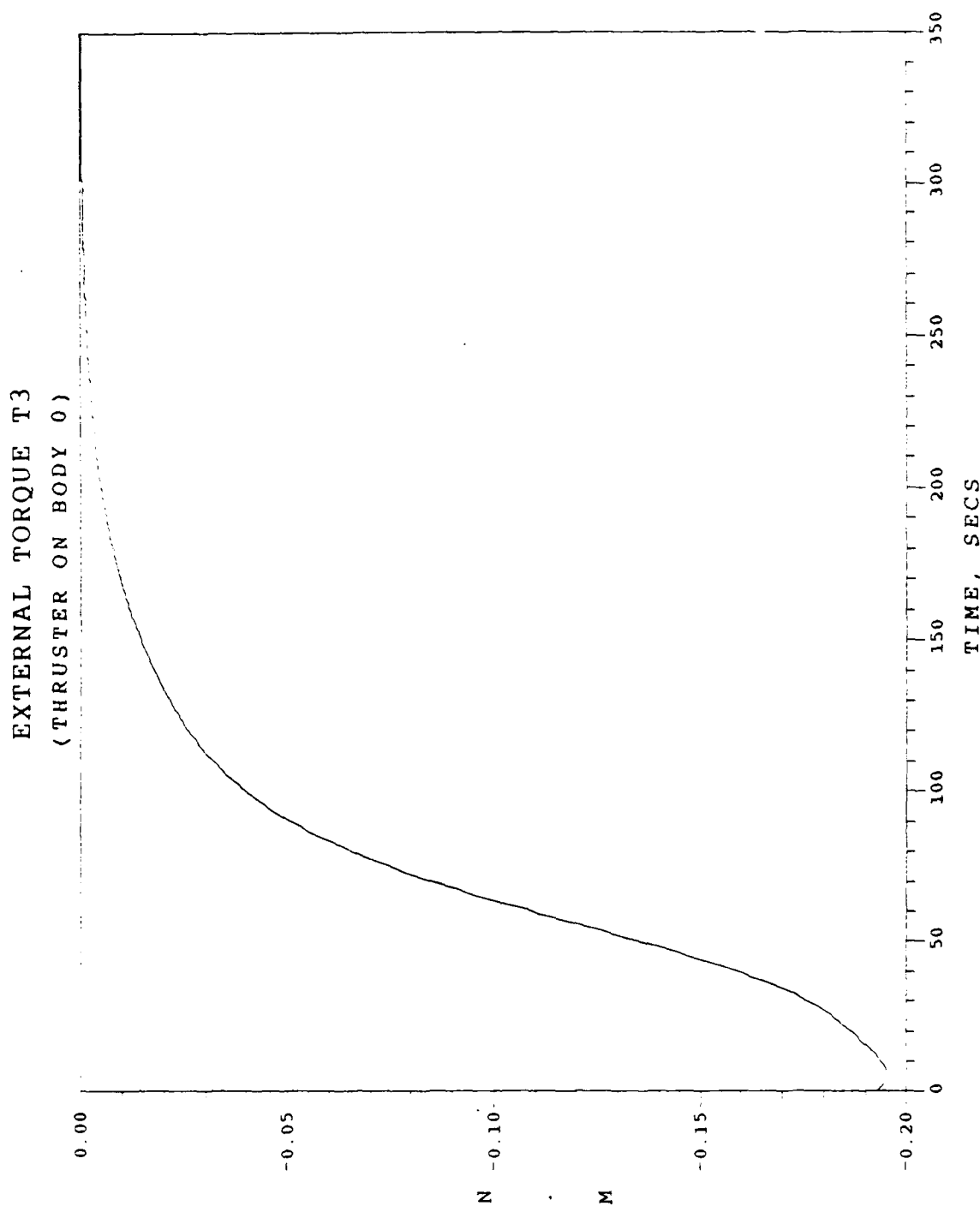


Fig. 89. Detumble/Despin Phase / Case 9  
External Torque T3

INTERNAL MOTOR TORQUE TG1  
(AT JOINT 1)

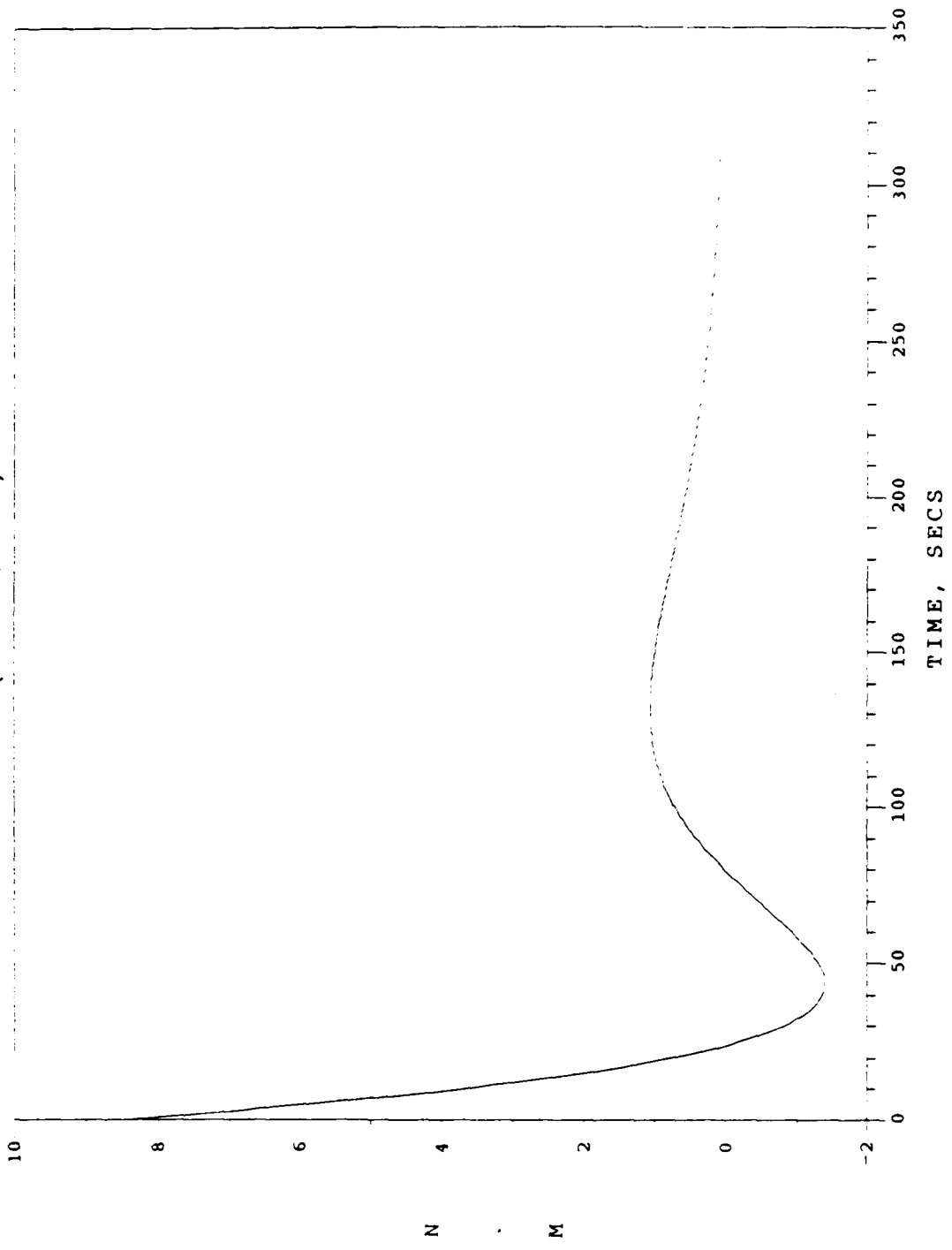


Fig. 90. Detumble/Despin Phase / Case 9  
Internal Motor Torque TG1

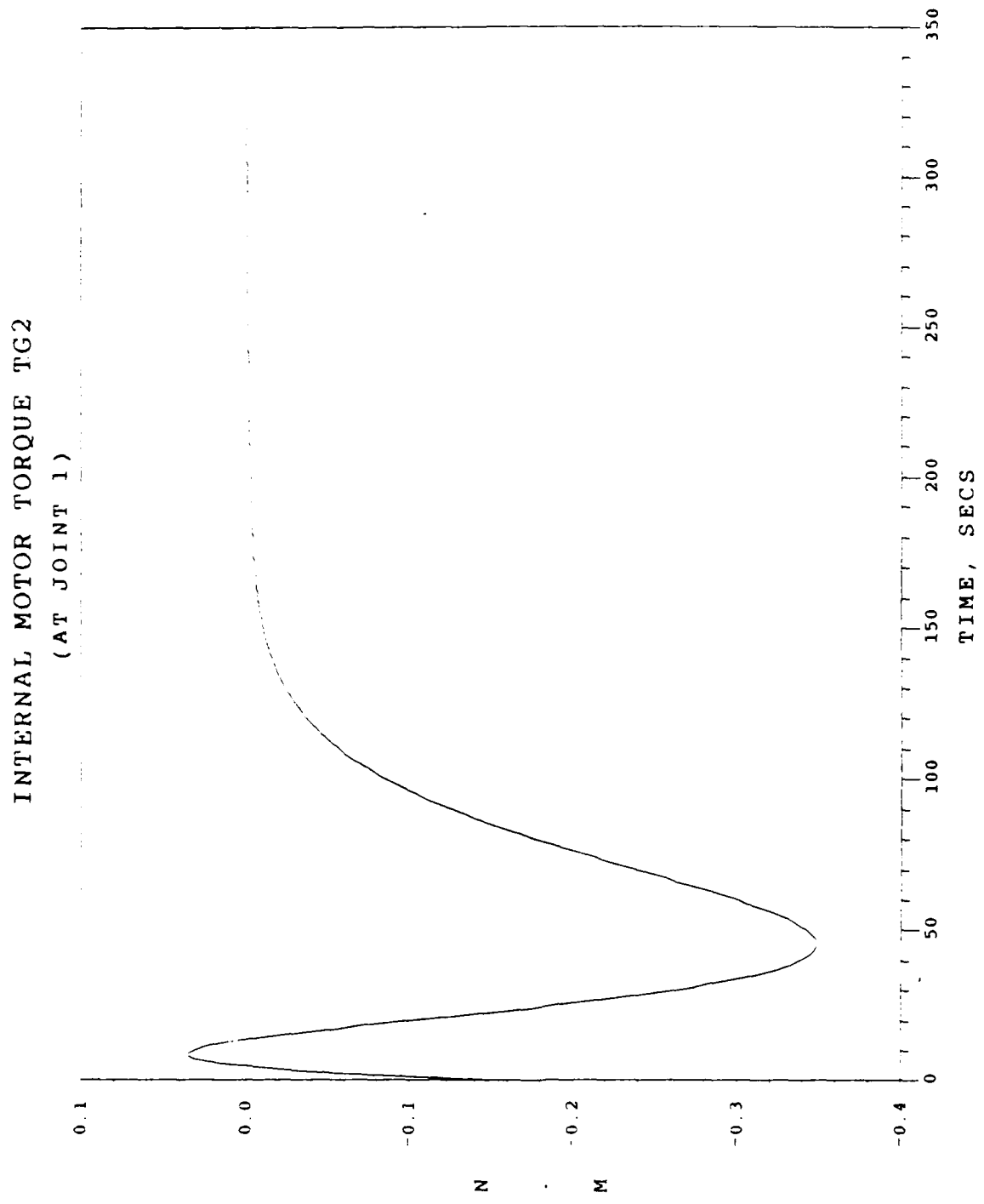


Fig. 91. Detumble/Despin Phase / Case 9  
Internal Motor Torque TG2

INTERNAL MOTOR TORQUE TG3

( AT JOINT 2 )

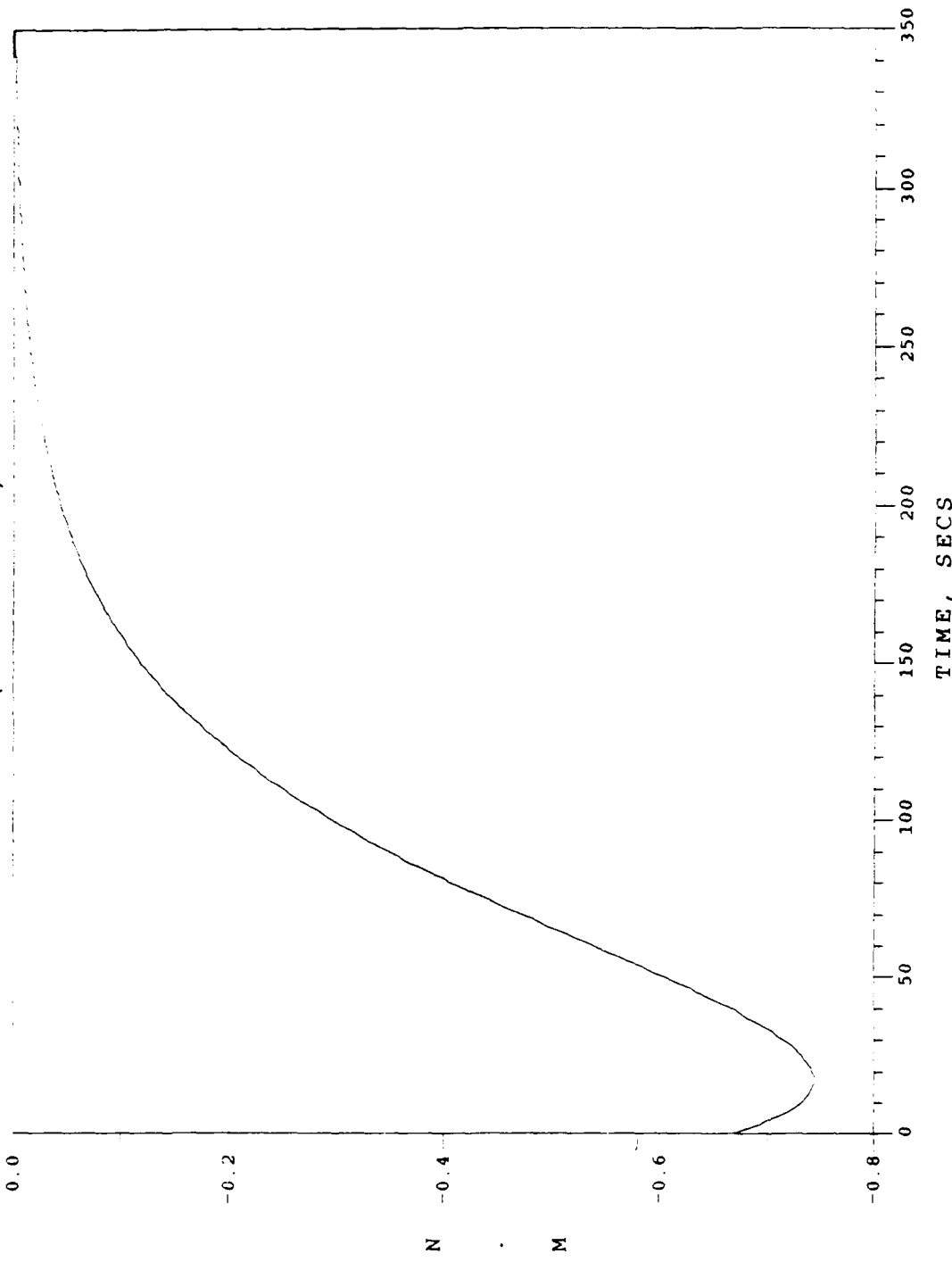


Fig. 92. Detumble/Despin Phase / Case 9  
Internal Motor Torque TG3

INTERNAL MOTOR TORQUE TG4  
( AT JOINT 3 )

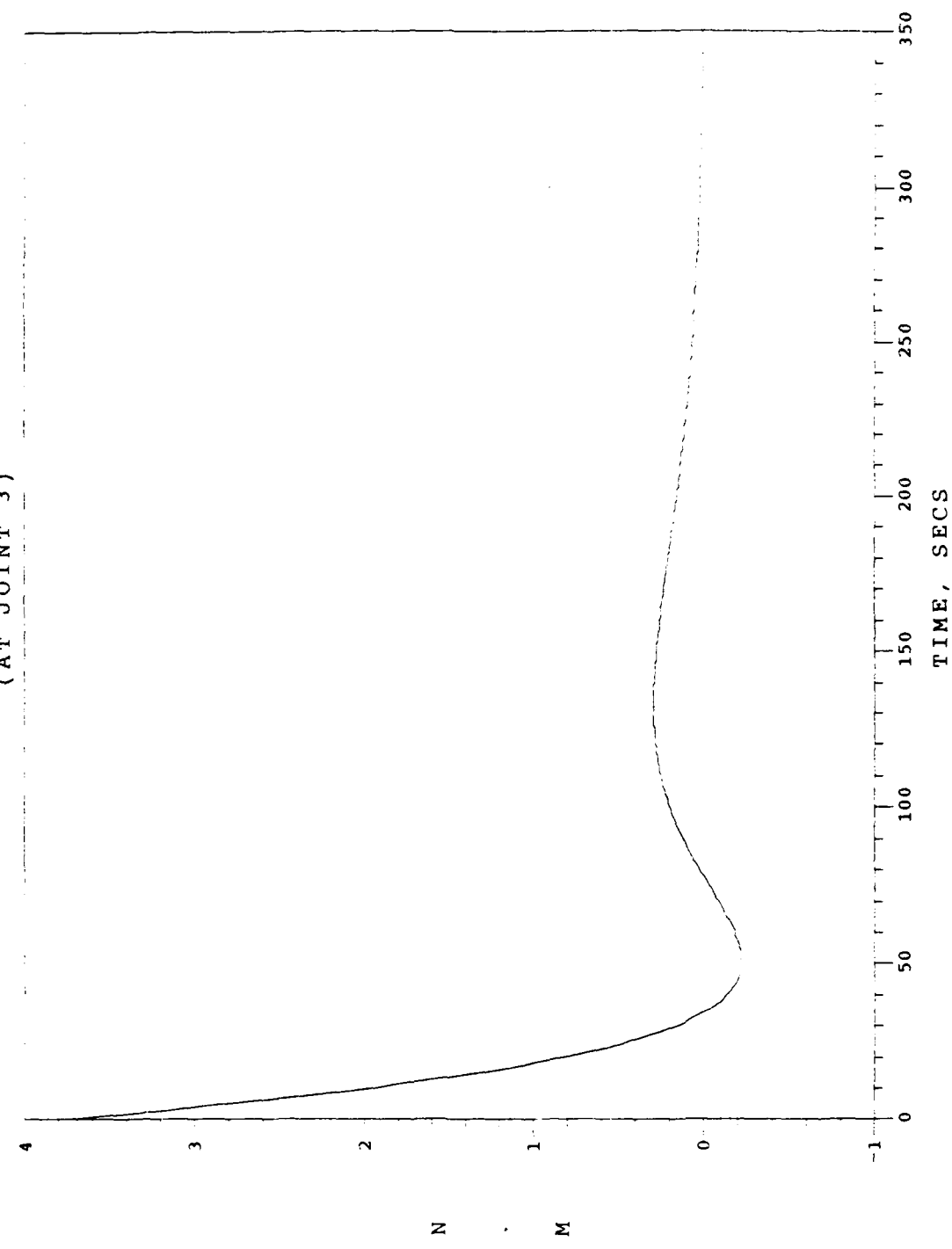


Fig. 93. Detumble/Despin Phase / Case 9  
Internal Motor Torque TG4

INTERNAL MOTOR TORQUE TG5

( AT JOINT 3 )

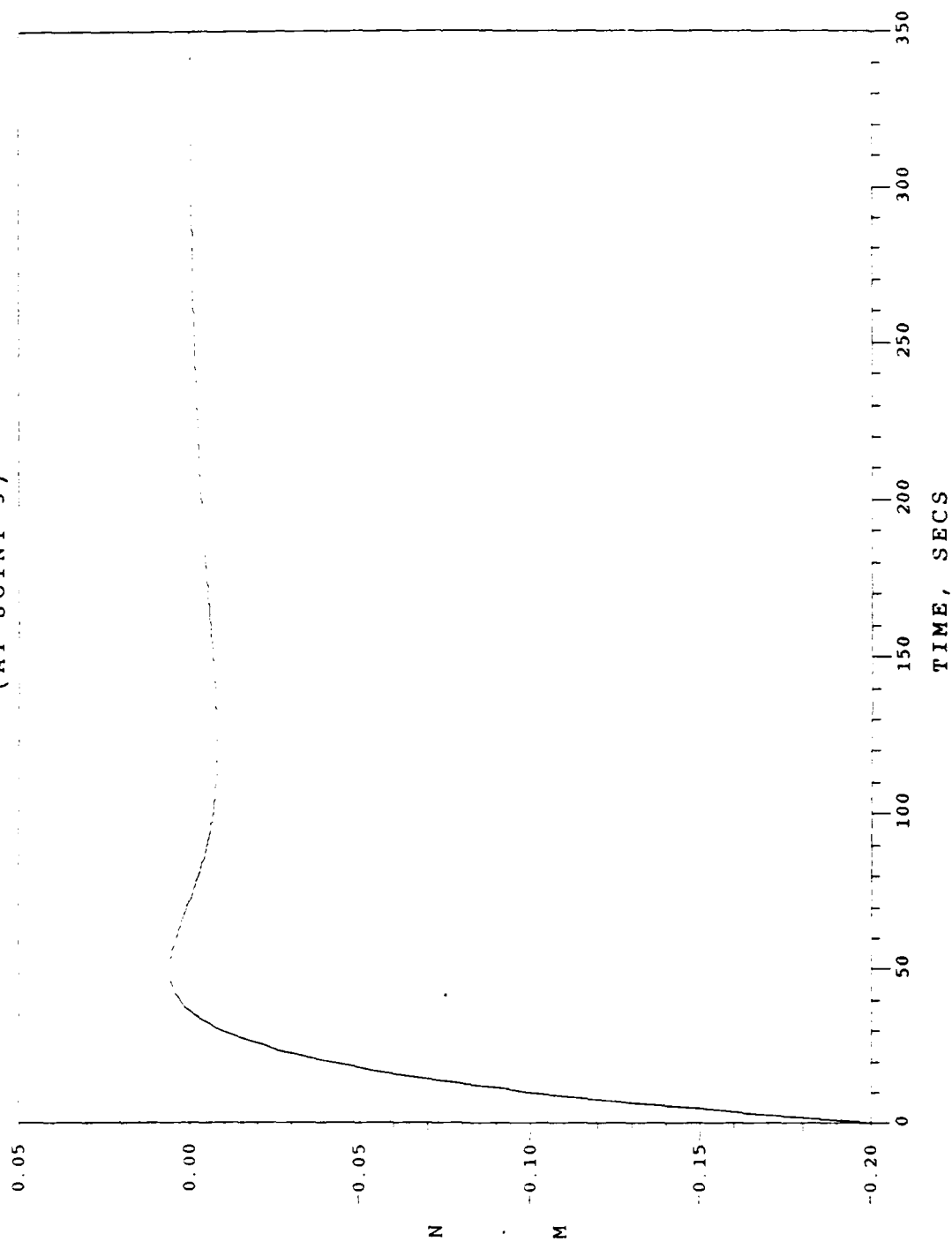


Fig. 94. Detumble/Despin Phase / Case 9  
Internal Motor Torque TG5

INTERNAL MOTOR TORQUES TG6  
( AT JOINT 3 )

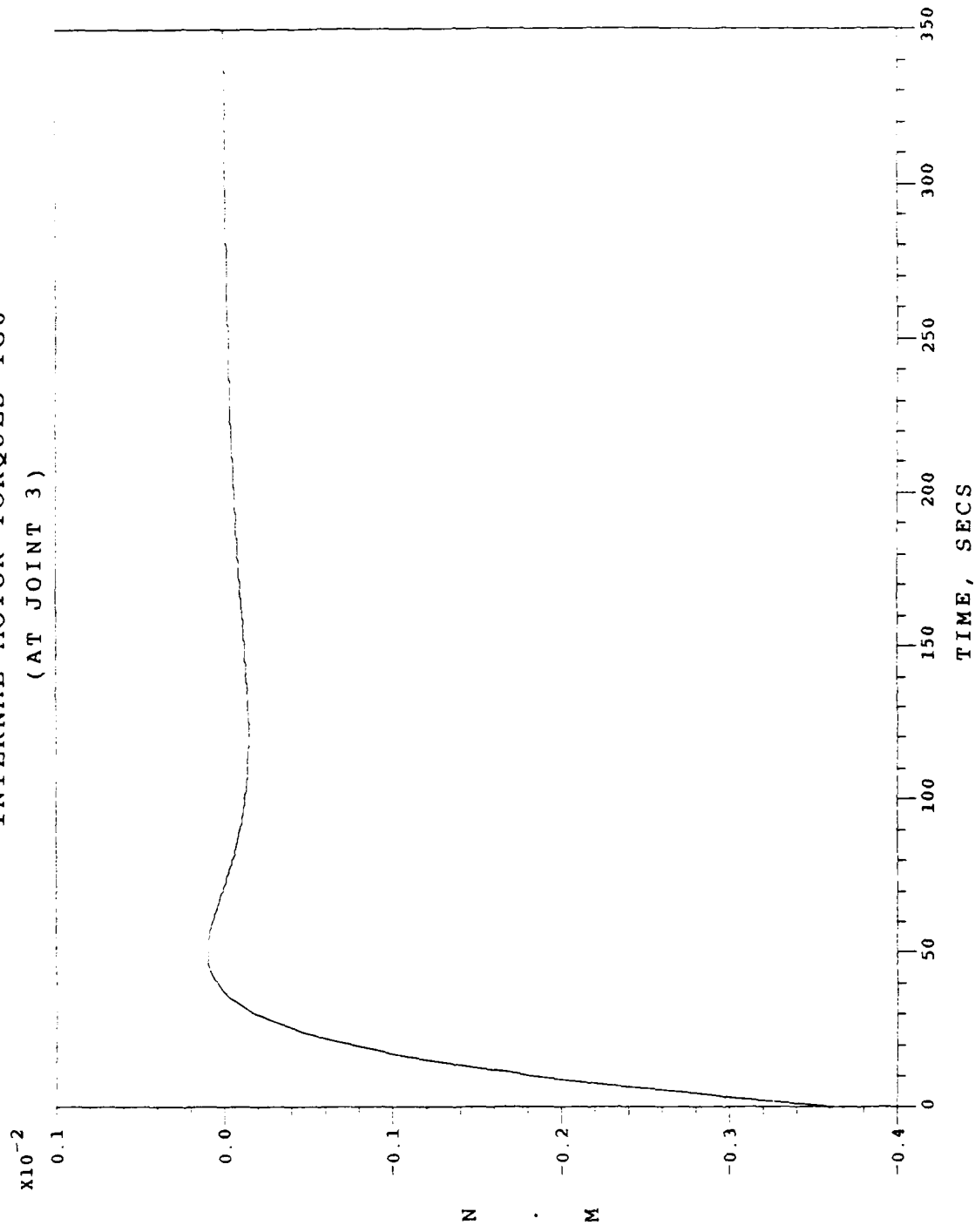


Fig. 95. Detumble/Despin Phase / Case 9  
Internal Motor Torque TG6

CONSTRAINT TORQUE AT  
JOINT 1

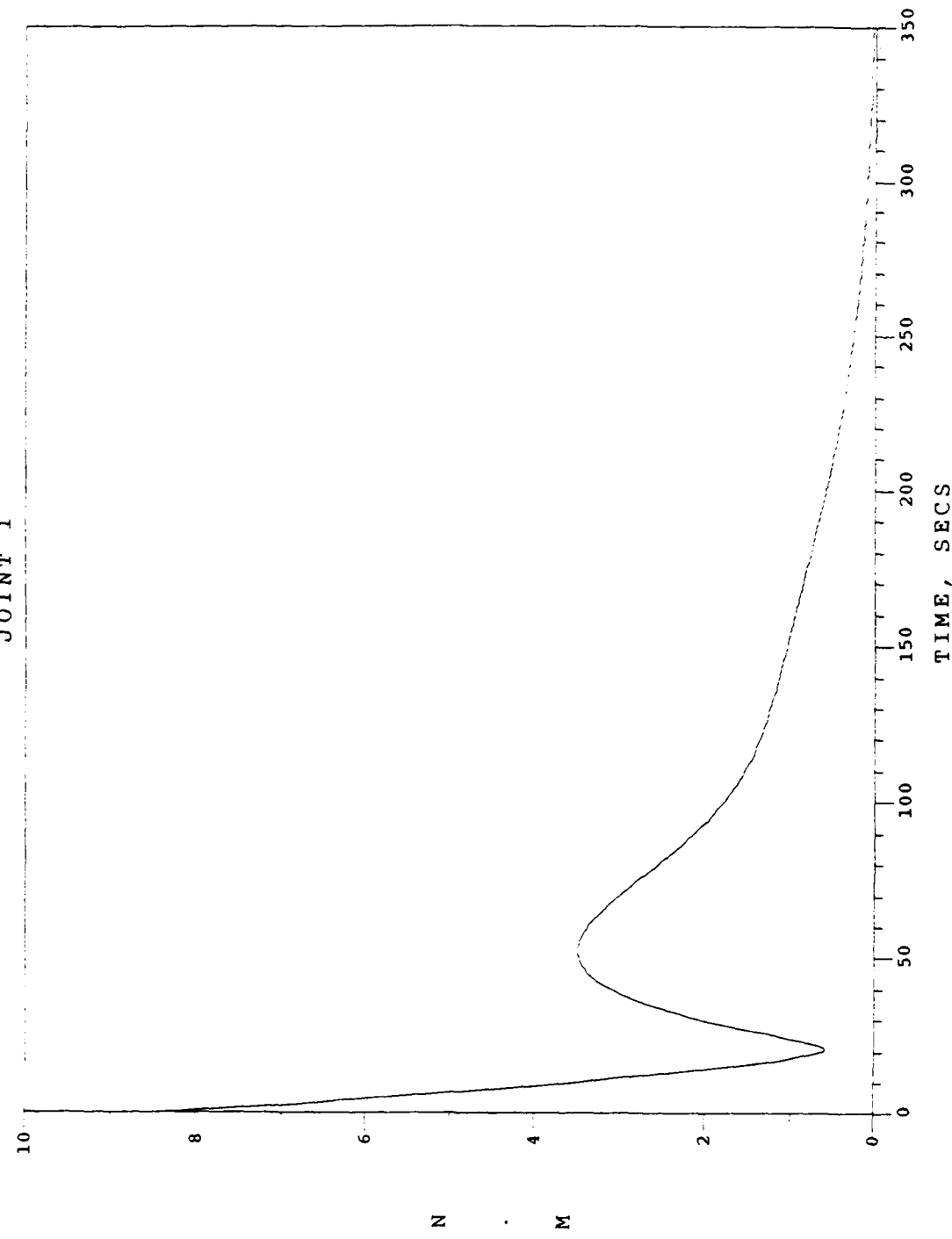


Fig. 96. Detumble/Despin Phase / Case 9  
Constraint Torque at Joint 1

CONSTRAINT TORQUE AT  
JOINT 2

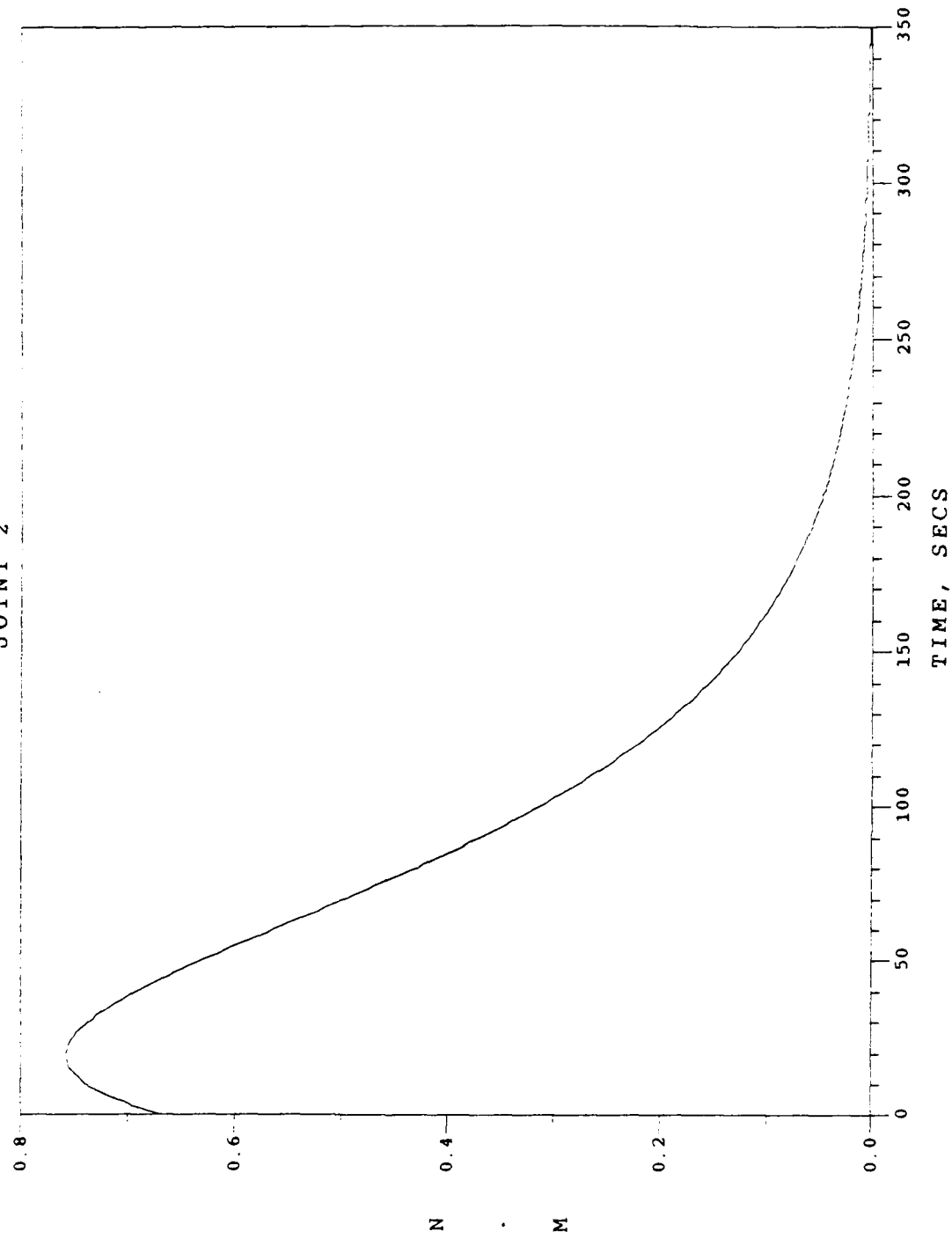


Fig. 97. Detumble/Despin Phase / Case 9  
Constraint Torque at Joint 2

CONSTRAINT TORQUE AT  
JOINT 3

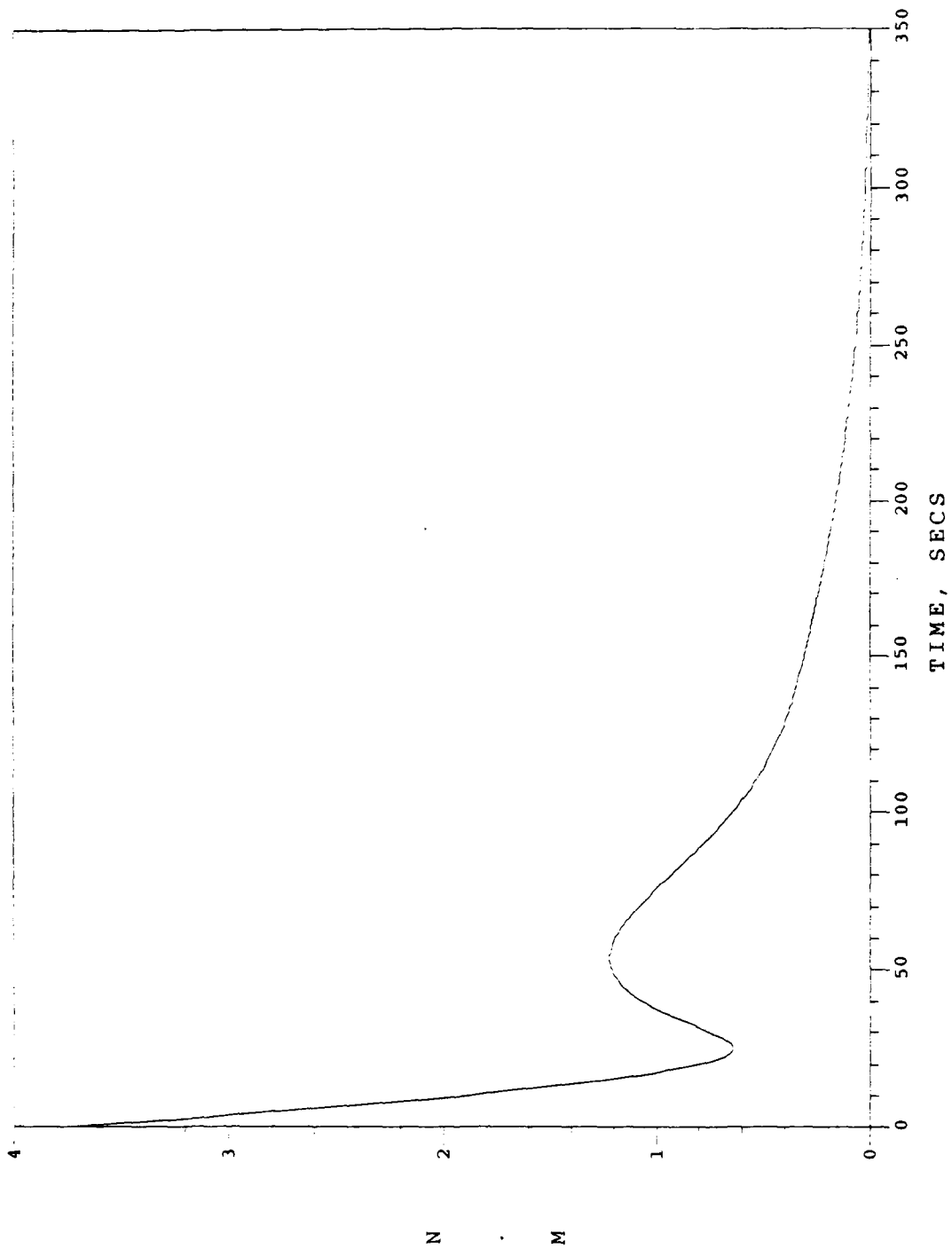


Fig. 98. Detumble/Despin Phase / Case 9  
Constraint Torque at Joint 3

CONSTRAINT FORCE AT JOINT 1  
IN Y DIRECTION - ALONG BODY 0

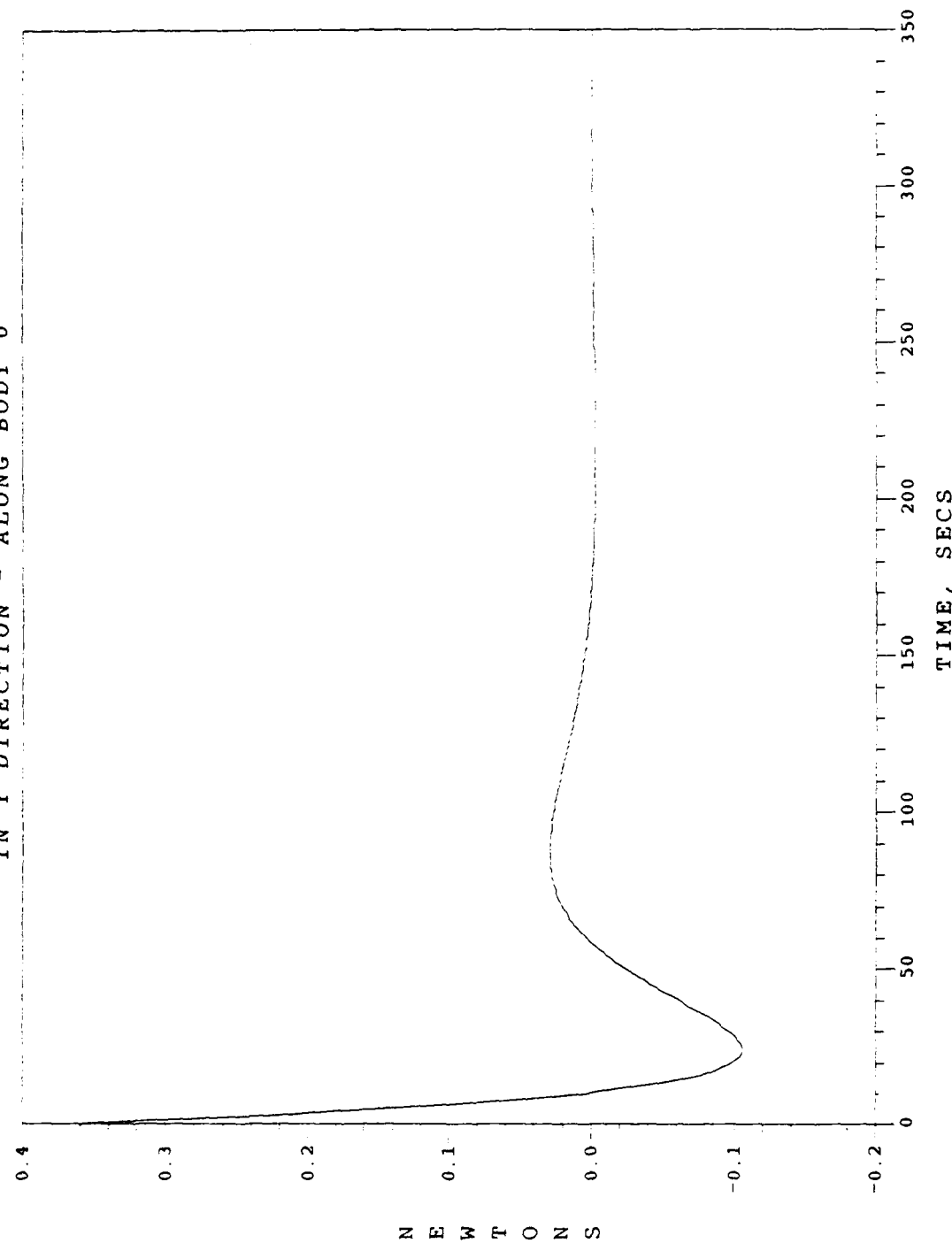


Fig. 99. Detumble/Despin Phase / Case 9  
Joint 1 Constraint Force in Y-Direction

## V. Conclusion

The equations of motion were derived for the five rigid body system used to model capture of a freely spinning and precessing axisymmetric target satellite. Control laws were formulated for each of the intended phases; deployment, spin-up, and detumble/despin. A Liapunov analysis was performed for the nonlinear feedback control required in the detumble/despin phase, in order to drive the system to a spin-stabilized state of equilibrium. A computer simulation was then used to examine each of the three phases of the capture process.

The deployment of the grappling arm and its counter-mass was successfully accomplished within an allotted 250 seconds. A sharp transient was initially observed with the TG1 motor torque at Joint 1 due to the large moment required to start the arm moving from its stored position. However, the momentary peak was less than 7 N-M and quickly leveled out. It was shown that dynamic balancing and stability could be maintained without the use of any external torques, but that the initial spin rate about the  $e_3$  axis of symmetry did not remain constant due to the conservation of angular momentum. A small application of the external T3 thruster about the  $e_3$  axis was able to alleviate this problem and keep this spin rate constant as required for capture.

The necessary external control torques to achieve deployment without utilizing the counter-mass were also shown, in order to illustrate this as a feasible alternative.

Once the grappling arm was deployed, the grappling device was spun-up for 10 seconds and its counter-mass was spun-up at an equal and opposite rate. An additional 40 seconds were allowed to elapse to observe the OMV system in a state of pure spin just prior to docking. This entire 50 second process was achieved without any external torques, and the system remained in its state of pure constant spin. The spin-up of the grappling device and the counter-mass required very small internal motor torques.

Docking was assumed to be a discrete event that initiated the detumble/despin phase. Nonlinear feedback control was immediately applied in order to detumble and despin the target. With the final selection of response values, feedback was applied for 350 seconds. All motion of the bodies was smooth as they travelled to the spin-stabilized state of equilibrium. The response values were chosen so that the movements of the bodies were coordinated with the decay of the translating joint to ensure that the composite center of

mass stayed close to the  $e_3$  axis. The most significant control torques observed were with the TG1 internal motor at Joint 1 and the external T1 thruster, both about the  $e_3$  axis. Each initially were almost 10 N-M, which is more than three times the control torques observed in the Widhalm and Conway two-body model. These higher torques can be explained by the additional mass and inertia added at Joint 1 by the grappling arm assembly and counter-mass, and by the different geometry of this problem with the grappling arm acting as a linkage between Joint 1 and the target.

Additional cases were examined in the detumble/despin process for design purposes. Quicker response times led to higher initial control torques. Reducing the length of the grappling arm had no significant effect on control magnitudes. What did have an effect on these control torques was the change in coning angles. The amount of required control torques clearly increases with increasing coning angles. Therefore, control requirements for the detumble/despin process are direct function of coning angle. It was also shown that torque requirements can be reduced by effective control of the the target's center of mass position relative to the OMV's axis of symmetry. These are all important consideration in the design of an orbital capture vehicle.

All major objectives were accomplished in this thesis. The simulation showed that a 5-body OMV using a combination of internal and external thrusters can successfully capture and detumble/despin an axisymmetric target satellite. Counter-balance masses can be effectively used in lieu of external thrusters during deployment and spin-up. The five-body system definitely adds both realism and flexibility to the original two-body model. This study gives a good indication of the dynamics and controls involved in remote orbital capture using the proposed five-body OMV model, and has hopefully paved the way for possible future studies of actual hardware design.

## **VI. Recommendations**

There are several possibilities for follow-on work with the OMV model developed in this thesis. One option would be to add an internal momentum wheel about the  $e_3$  axis to keep the OMV's spin-rate constant during deployment, without having to fire the T3 thruster. A further extension of this idea would be to add a complete set of three orthogonal momentum wheels instead of external thrusters for attitude control, as was done by Fleming (3) on the Widhalm and Conway two-body model. Another possible area of follow-on research could be to examine a wider range of targets and capture scenarios. This particular study was limited to axisymmetric target satellites only. The capture of an asymmetric target would present additional problems and requirements that would have to be examined.

### References

1. Conway, B.A., and Widhalm, J.W., "Equations of Attitude Motion for an n-Body Satellite With Moving Joints," AIAA J. of Guidance, Control, and Dynamics, Vol. 8, No.4 (July-August 1985) 537-539.
2. Conway, B.A., and Widhalm, J.W., "Optimal Continuous Control for Remote Orbital Capture," AIAA J. of Guidance, Control, and Dynamics, Vol. 9, No.2 (March-April 1986) 149-155.
3. Fleming, K.R., "The Detumbling of an Axially Symmetric Satellite With an Orbital Maneuvering Vehicle By Nonlinear Feedback Control", Masters Thesis, Air Force Institute of Technology, 1985.
4. Fletcher, H.J., Rongved, L., and Yu, E.Y., "Dynamics Analysis of a Two-Body Gravitationally Oriented Satellite," Bell System Tech. J., Vol. 42, No. 5 (1963) 2239-2266.
5. Greenwood, D.T., Principles of Dynamics. Prentice-Hall, Inc., Englewood Cliffs, NJ, 1965.
6. Hooker, W.W. "A Set of r Dynamical Attitude Equations for an Arbitrary n-Body Satellite Having r Rotational Degrees of Freedom," AIAA J., Vol. 8, No. 7 (July 1970) 1205-1207.
7. Hooker, W.W., and Margulies, G., "The Dynamical Attitude Equations for an n-Body Satellite," J. of the Astronautical Sciences, Vol. 12, No. 4 (Winter, 1965) 123-128.
8. Vidyasagar, M., Nonlinear Systems Analysis. Prentice-Hall, Inc., Englewood Cliffs, NJ, 1978.
9. Widhalm, J.W., and Conway, B.A., "Nonlinear Feedback Control for Remote Orbital Capture," AIAA J. of Guidance, Control, and Dynamics, Vol. 9, No. 6 (Nov-Dec 1986) 657-662.
10. Widhalm, J.W., "Optimal Open Loop and Nonlinear Feedback Control for Remote Orbital Capture," Ph.D. Thesis, University of Illinois at Urbana-Champaign, 1985.

Vita

Captain F. Joseph Bishop was born on [REDACTED]. He graduated from high school [REDACTED] 1980 and attended Norwich University in Northfield, Vermont. He received the degree of Bachelor of Science in Mechanical Engineering in May 1984. Upon graduation, he received a commission in the USAF through the ROTC program. He served as Chief of the Antisatellite (ASAT) Analysis Branch and later as the ASAT Deputy Test Director in the 6595th Missile Test Group, Vandenberg AFB, California. While at Vandenberg, he attended school at night and earned a Master's Degree in Systems Management from the University of Southern California. He entered the School of Engineering, Air Force Institute of Technology, in May 1987.

SECURITY CLASSIFICATION OF THIS PAGE

Form Approved  
OMB No. 0704-0188

## REPORT DOCUMENTATION PAGE

1a. REPORT SECURITY CLASSIFICATION <b>UNCLASSIFIED</b>		1b. RESTRICTIVE MARKINGS	
2a. SECURITY CLASSIFICATION AUTHORITY		3. DISTRIBUTION/AVAILABILITY OF REPORT  <b>Approved for public release; Distribution unlimited</b>	
2b. DECLASSIFICATION/DOWNGRADING SCHEDULE			
4. PERFORMING ORGANIZATION REPORT NUMBER(S)  <b>AFIT/GA/AA/88D-02</b>		5. MONITORING ORGANIZATION REPORT NUMBER(S)	
6a. NAME OF PERFORMING ORGANIZATION  <b>School of Engineering</b>	6b. OFFICE SYMBOL ( <i>If applicable</i> ) <b>AFIT/ENY</b>	7a. NAME OF MONITORING ORGANIZATION	
6c. ADDRESS (City, State, and ZIP Code)  <b>Air Force Institute of Technology (AU) Wright-Patterson AFB, OH 45433-6583</b>		7b. ADDRESS (City, State, and ZIP Code)	
8a. NAME OF FUNDING/SPONSORING ORGANIZATION	8b. OFFICE SYMBOL ( <i>If applicable</i> )	9. PROCUREMENT INSTRUMENT IDENTIFICATION NUMBER	
8c. ADDRESS (City, State, and ZIP Code)		10. SOURCE OF FUNDING NUMBERS	
		PROGRAM ELEMENT NO.	PROJECT NO.
		TASK NO.	WORK UNIT ACCESSION NO.
11. TITLE ( <i>Include Security Classification</i> )  <b>See block 19</b>			
12. PERSONAL AUTHOR(S)  <b>Bishop, F. Joseph, Capt, USAF</b>			
13a. TYPE OF REPORT  <b>MS Thesis</b>	13b. TIME COVERED  FROM _____ TO _____	14. DATE OF REPORT (Year, Month, Day)  <b>1988 December</b>	15. PAGE COUNT  <b>162</b>
16. SUPPLEMENTARY NOTATION			
17. COSATI CODES	18. SUBJECT TERMS ( <i>Continue on reverse if necessary and identify by block number</i> )  <b>satellite, dynamics, teleoperator, orbital capture, docking, detumbling, despinning, feedback control</b>		
19. ABSTRACT ( <i>Continue on reverse if necessary and identify by block number</i> )  <b>Title: REMOTE ORBITAL CAPTURE USING AN ORBITAL MANEUVERING VEHICLE EQUIPPED WITH A MULTIBODY GRAPPLING ARM ASSEMBLY</b>  <b>Thesis Advisor: Curtis H. Spenny</b>			
20. DISTRIBUTION/AVAILABILITY OF ABSTRACT <input checked="" type="checkbox"/> UNCLASSIFIED/UNLIMITED <input type="checkbox"/> SAME AS RPT. <input type="checkbox"/> DTIC USERS		21. ABSTRACT SECURITY CLASSIFICATION  <b>UNCLASSIFIED</b>	
22a. NAME OF RESPONSIBLE INDIVIDUAL  <b>Spenny, Curtis H., Assistant Professor</b>		22b. TELEPHONE ( <i>Include Area Code</i> )  <b>(513) 255-2040</b>	22c. OFFICE SYMBOL  <b>AFIT/ENY</b>

ATLANTA 30334  
Curtis H. Spenny  
12 Jan 1989

From Block 19:

The problem of detumbling and despinning a freely spinning and precessing axisymmetric target satellite using an orbital maneuvering vehicle is considered. The axisymmetric orbital maneuvering vehicle is equipped with a multibody grappling arm assembly to capture the target. Counter-masses are used to maintain dynamic balancing and stability throughout the deployment of the arm and the subsequent spin-up of the grappling device prior to docking. The five-body system is modeled using Eulerian-based equations of motion developed by Hooker and Margulies. Open-loop control laws are formulated to deploy the grappling arm assembly and spin-up the grappling device using internal motor torques. A Liapunov technique is applied to derive a nonlinear feedback control law that drives the docked system to a final spin-stabilized state of equilibrium. External thrusters are used to maintain the absolute motion of the system during this process. Variations in grappling length, target coning angle, and response times are examined for design purposes. State and control histories are presented and the results from this five-body model are compared with the Widhalm and Conway two-body study. The simulation indicates that the required control magnitudes are higher for the five-body model but are still quite reasonable. The addition of the grappling arm assembly adds both realism and flexibility to the capture process.

*These, (and) —*